

---

# Comparison of the 1981 INEL Dispersion Data With Results From a Number of Different Models

---

Prepared by W. S. Lewellen, R. I. Sykes, S. F. Parker

Aeronautical Research Associates of Princeton, Inc.

Prepared for  
U.S. Nuclear Regulatory  
Commission

8505310421 850531  
PDR NUREG  
CR-4159 R PDR

## NOTICE

This report was prepared as an account of work sponsored by an agency of the United States Government. Neither the United States Government nor any agency thereof, or any of their employees, makes any warranty, expressed or implied, or assumes any legal liability of responsibility for any third party's use, or the results of such use, of any information, apparatus, product or process disclosed in this report, or represents that its use by such third party would not infringe privately owned rights.

## NOTICE

### Availability of Reference Materials Cited in NRC Publications

Most documents cited in NRC publications will be available from one of the following sources:

1. The NRC Public Document Room, 1717 H Street, N.W.  
Washington, DC 20555
2. The Superintendent of Documents, U.S. Government Printing Office, Post Office Box 37082,  
Washington, DC 20013-7982
3. The National Technical Information Service, Springfield, VA 22161

Although the listing that follows represents the majority of documents cited in NRC publications, it is not intended to be exhaustive.

Referenced documents available for inspection and copying for a fee from the NRC Public Document Room include NRC correspondence and internal NRC memoranda; NRC Office of Inspection and Enforcement bulletins, circulars, information notices, inspection and investigation notices; Licensee Event Reports; vendor reports and correspondence; Commission papers; and applicant and licensee documents and correspondence.

The following documents in the NUREG series are available for purchase from the NRC/GPO Sales Program: formal NRC staff and contractor reports, NRC-sponsored conference proceedings, and NRC booklets and brochures. Also available are Regulatory Guides, NRC regulations in the *Code of Federal Regulations*, and *Nuclear Regulatory Commission Issuances*.

Documents available from the National Technical Information Service include NUREG series reports and technical reports prepared by other federal agencies and reports prepared by the Atomic Energy Commission, forerunner agency to the Nuclear Regulatory Commission.

Documents available from public and special technical libraries include all open literature items, such as books, journal and periodical articles, and transactions. *Federal Register* notices, federal and state legislation, and congressional reports can usually be obtained from these libraries.

Documents such as theses, dissertations, foreign reports and translations, and non NRC conference proceedings are available for purchase from the organization sponsoring the publication cited.

Single copies of NRC draft reports are available free, to the extent of supply, upon written request to the Division of Technical Information and Document Control, U.S. Nuclear Regulatory Commission, Washington, DC 20555.

Copies of industry codes and standards used in a substantive manner in the NRC regulatory process are maintained at the NRC Library, 7920 Norfolk Avenue, Bethesda, Maryland, and are available there for reference use by the public. Codes and standards are usually copyrighted and may be purchased from the originating organization or, if they are American National Standards, from the American National Standards Institute, 1430 Broadway, New York, NY 10018.



---

# Comparison of the 1981 INEL Dispersion Data With Results From a Number of Different Models

---

Manuscript Completed: January 1985  
Date Published: May 1985

Prepared by  
W. S. Lewellen, R. I. Sykes, S. F. Parker

Aeronautical Research Associates of Princeton, Inc.  
50 Washington Road  
P. O. Box 2229  
Princeton, NJ 08540

Prepared for  
Division of Radiation Programs and Earth Sciences  
Office of Nuclear Regulatory Research  
U.S. Nuclear Regulatory Commission  
Washington, D.C. 20555  
NRC FIN B0446

## ABSTRACT

The results from simulations by 12 different dispersion models are compared with observations from an extensive field experiment conducted by the Nuclear Regulatory Commission at the Idaho National Engineering Laboratory in July, 1981. Comparisons were made on the bases of hourly  $\text{SF}_6$  samples taken at the surface, out to approximately 10 km from the 46 m release tower, both during and following 7 different 8-hour releases. Comparisons are also made for total integrated doses collected out to approximately 40 km. Three classes of models are used. Within the limited range appropriate for Class A models this data comparison shows that neither the puff models or the transport and diffusion models agree with the data any better than the simple Gaussian plume models. The puff and transport and diffusion models do show a slight edge in performance in comparison with the total dose over the extended range approximate for class B models. The best model results for the hourly samples show approximately 40% calculated within a factor of two when a  $15^\circ$  uncertainty in plume position is permitted and it is assumed that higher data samples may occur at stations between the actual sample sites. This is increased to 60% for the 12 hour integrated dose and 70% for the total integrated dose when the same performance measure is used. None of the models reproduce the observed patchy dose patterns. This patchiness is consistent with the discussion of the inherent uncertainty associated with time averaged plume observations contained in our companion reports on the scientific critique of available models.

## Table of Contents

I.	Introduction . . . . .	1
II.	Review of the Dispersion Data. . . . .	4
2.1	Available Data	
2.1.1	Surface Wind Network, MESONET . . . . .	4
2.1.2	Radar-Tracked Pilot Balloons, RABALS. . . . .	5
2.1.3	Meteorological Tower Measurements . . . . .	5
2.1.4	Supplementary Meteorological Data . . . . .	6
2.1.5	Surface SF6 Measurements. . . . .	6
2.1.6	ALPHA-1 Lidar Data. . . . .	7
2.2	Test Cases	
III.	Individual Model Results	
3.1	Gaussian Plume Models	
3.1.1	ISC . . . . .	11
3.1.2	TEM . . . . .	13
3.1.3	GP. . . . .	13
3.2	Puff Models	
3.2.1	MESOT MODEL . . . . .	14
3.2.2	MESOI . . . . .	15
3.2.3	MESODIFF. . . . .	15
3.2.4	ARL-Puff. . . . .	15
3.2.5	MESOI . . . . .	16
3.3	TRANSPORT and Diffusion Models	
3.3.1	PATRIC. . . . .	17
3.3.2	MATHEW/ADPIC. . . . .	17
3.3.3	IMPACT. . . . .	17
3.3.4	SPLITPUFF . . . . .	18
IV.	Intermodel Comparisons	
4.1	Twelve Hour Total Dose on the Fine Mesh. . . . .	31
4.2	Hourly Dose on the Fine Mesh . . . . .	41
4.3	Total Integrated Dose on the Coarse Mesh . . . . .	50
4.4	Lidar Plume Cross Section. . . . .	51
V.	Real Time Tests of the ARAC System . . . . .	64

VI. Concluding Remarks . . . . .	.81
References . . . . .	.83
Appendices	
A. Review of Data Used for the Model Tests. . . . .	A-1
B. Model Results for Integrated Dose. . . . .	B-1
C. Analysis of the Lidar Data . . . . .	C-1

## LIST OF FIGURES

- 2. 1) July, 1981, INEL Field Experiment; Surface Wind Tower and RABAL Locations.
- 2. 2) Sampler Locations
- 3. 1-3. 4) Sample Hourly Dose Predictions for Select Hours as given by ISC, TEM, GP and MESOT.
- 3. 5-3. 8) Sample Hourly Dose Predictions for Select Hours as given by MESOI, MESODIF, ARL-PUFF and MESOT.
- 3. 9-3.12) Sample Hourly Dose Predictions for Select Hours as given by PATRIC, MATHEW/ADPIC, IMPACT and SPLIT-PUFF.
- 4. 1-4. 8) Different Performance Measures of the Comparison Between the Observed 12 hour dose and the Model Predictions.
- 4. 9-4.16) Different Performance Measures of the Comparison Between the Observed Hourly Doses and the Model Predictions.
- 4.17-4.23) Different Performance Measures of the Comparison Between the Total Integrated Dose for each of 3 Tests and the Model Predictions.
- 4.24-4.25) Comparison Between Plume Spreads as Observed by the LIDAR and Model Predictions.
- 5. 1-5. 2) Selected Dose Calculations Provided by the ARAC Real Time Model Prediction.
- 5. 3-5.14) Different Comparisons Between Observations and Predictions made by ARAC, ISC, TEM and MESOT.
- A. 1-A.42) Field Data for the Individual Tests

B. 1-B.41) Model Predictions for the Individual Tests

C. 1-C. 9) Detailed Analysis of Lidar Data



## FOREWORD

This report is one of a series of reports documenting the results of a coordinated program established by the Office of Nuclear Regulatory Research to assess available capabilities for estimating atmospheric dispersion. The objective of this research effort is to provide an assessment of atmospheric dispersion models that may be used in the emergency preparedness decision-making process. This program should provide some basis for selection and design of computerized emergency response systems, along with estimates of accuracies expected from such atmospheric dispersion models.

The conclusions expressed in this particular document are based on the data from the (1981) INEL Field Experiment. They represent the findings of the authors for this data set, and have been peer reviewed. However, the Model Evaluation Project is ongoing, with results from the SEADEx Experiment presently under study. Therefore, these results can be considered final for the INEL study, but preliminary for the Model Evaluation Program as a whole. It is the opinion of the authors that the results of this study represent a significant body of work, and are worthy of publication at this stage. However, as these results are based solely on the INEL study, final model performance rankings may change with the inclusion of information from additional data collection efforts.

#### ACKNOWLEDGEMENTS

We wish to thank Frank Kornegay and his colleagues at Oak Ridge National Laboratory for their technical assistance and for calculating the results for five of the models (ISC, TEM, MESOI, MESODIF, and IMPACT) shown in this report. We also wish to thank Robert Abbey and Robert Kornasiewicz of the NRC for the technical monitoring of this work.

## I. Introduction

As a part of a general study to evaluate the ability of a number of dispersion models to satisfy the Nuclear Regulatory Commission's requirement for emergency response models, an extensive field experiment was carried out at INEL in July 1981. Results from seven days' observations are compared with the results of a number of these models in this report. The Nuclear Regulatory Commission has established the requirement for two classes of predictive capabilities reflecting the requirements for two emergency planning zones. A class A model, designed to predict plume exposure within 10 miles of the site, must be able to produce initial estimates of atmospheric dispersion within 15 minutes of any incident. The class B model, designed for the prediction of relative concentrations and deposition within an ingestion zone which extends out 50 miles from the site, should provide estimates within 45 minutes.

An initial screening of candidate models based on a scientific critique of available dispersion models is made in a separate report (Lewellen et al., 1983). As a result of this analysis, three types of models were chosen for detailed comparison with field observations. These three types are: 1) gaussian plume with straight line trajectory; 2) gaussian puff with spatially and temporally varying winds; and 3) more sophisticated transport and diffusion models. The initial expectation is that the first type is a candidate for class A models only and that the third type is a candidate for class B only. The puff models are attractive candidates for both class A and class B use.

Most past field tests of atmospheric dispersion have been designed primarily as tests of diffusion with the mean wind fixed. Such tests leave out the contribution of spatially and temporally varying transport winds to dispersion. This effect is likely to be very important, probably even the dominant effect, in predicting dispersion for emergency planning at real sites. This test involves data from field experiment which was specifically designed to obtain data to evaluate models for the emergency response application (Dickson, Start and Cate, 1981). A fine grid network close to a

release tower was combined with a coarse grid extending out approximately 100 km. The goal was to observe the complete surface concentration patterns resulting from a few hours' release under various meteorological conditions. Section II gives a brief description of the data available from this field program with a more complete presentation of the data in Appendix A.

Section III provides a review of the results of 12 model calculations for this data set. A large part of these model results are plotted in detail in Appendix B for direct qualitative comparison with the data in Appendix A. Section IV provides the detailed results of intermodel comparisons using a pattern test developed specifically for this emergency response application (Lewellen, Sykes, and Oliver, 1981). The pattern test provides for a quantitative measure of how the discrepancies between model predicted surface dose and observed dose is influenced by a given uncertainty in the predicted plume position. Since discrepancies between observations and predictions may be due either to incorrect predictions of the plume concentrations or to incorrect predictions of the plume location, the pattern test measures the improvement in agreement between measured and predicted concentrations as the plume is shifted through a given angle. Emergency planners do not need to know the exact concentration distribution resulting from a given emission, since they are not likely to know the emissions very accurately. They are more interested in knowing with what level of confidence it is possible to specify the approximate position of the plume and its approximate concentration. The pattern test is designed to give this answer. It will provide the fraction of the experimental observations which are predicted within a given factor for a given spatial uncertainty.

As a part of this evaluation exercise, real time tests were carried out on the ARAC system. Lawrence Livermore Laboratory was notified of the time and conditions of the tracer release on these two days. Their model predictions were transmitted to the NRC emergency response center in Washington, D.C. Evaluation of the accuracy of these predictions are included in Section V.

All of the model performances were considerably poorer on this test than on previous tests designed to measure diffusion under near ideal conditions. The data do not show the impact of well defined plumes; but rather a more broken patchy pattern supposedly due to the changing meteorological conditions. None of the models reproduce this same patchy structure. The more sophisticated models do not show a significant advantage over the simpler models. More work is required to determine what part of this result is due to an inherent variability in atmospheric dispersion and what part to model deficiencies.

The importance of this variability to the estimates of concentrations of material following an accident at an operating reactor is to increase the areas of concern. If the codes to be used in emergency response display the variability shown in this study, then the accuracy, plus the variability of the results, are both of interest to the decision maker. Studies conducted in conjunction with these analyses, (Lewellen, et al, 1983), convincingly indicate that the atmospheric motions responsible for the variability noted in this study are beyond the capabilities of any presently-available code. This finding will affect greatly the accuracy and useability of emergency-response models.

## II. Review of the Dispersion Data

### 2.1. Available Data

Meteorological data of several types were available for incorporation into the numerical model predictions. The three principal sources were the surface wind station network (MESONET), radar-tracked pilot balloons (RABAL's), and high frequency turbulence measurements from an instrumented tower close to the tracer release point. In addition to these data, radio-sonde ascents were made every 3 hours to determine the mixing depth and temperature structure of the atmosphere; tetroons were released at various heights giving estimates of air parcel trajectories; and subjective estimates of stability based on visual observation were also made.

The SF<sub>6</sub> tracer gas was released from a six inch diameter pipe at a height of 46m. Release rates for the first tests were about 200lbs/hrs, but this was increased to 400lbs/hrs for later tests. An oil fog was released through the same pipe as the SF<sub>6</sub>; this provided the flow visualizations for photographic records, and also the tracer for the ALPHA-1 lidar system.

Tracer data was obtained from two sources: fixed bag samplers on the ground, and airborne lidar measurements of the plume.

#### 2.1.1. Surface wind network, MESONET

INEL has established an extensive network of surface wind stations throughout the Snake River plain shown in Figure 2.1. The network contains some 30 anemometers at heights generally between 15 m and 30 m above the ground, which telemeter their measured wind at 6 minute intervals into a central station where they are recorded on magnetic tape. For the model predictions, 22 stations were used to determine the wind field; the remaining stations were too far from the region of interest.



A major problem in this and any study dealing with data comparisons is the choice of the techniques used to replace missing data values. For those codes capable of incorporating data from a number of stations, the interpolation schemes of the codes were assumed to adequately replace the missing data points. For the single-point codes, the choice of replacement data is of greater importance. In this study, any hour where data from the release point was unavailable, data from the nearest operational station were used. This replacement is assumed to be representative of the techniques that would be employed by an operator at a reactor faced with a similar dilemma. In periods of interesting meteorology, such as the development or decay of an up-valley flow, the choice of replacement data could be critical, but the nearest operational station, regardless of location with respect to the wind shift line, was chosen for consistency.

#### 2.1.2. Radar-tracked pilot balloons, RABAL's

During the INEL field experiment, several tracking radars were employed at different sites to obtain vertical profiles of mean wind. For these preliminary comparisons, results from three positions were available; one radar was located at the tracer release point, a second roughly 30 km to the Northeast, and the third about 20 km to the Southeast. Pilot balloons were released every 30 minutes at the radar sites, and provide a reasonably accurate measurement of the vertical wind structure. It should be noted that the measurement is a very short time average (it takes about 1 minute for the balloon to rise through 200 m); thus the profile has a resolution of 200 m in the vertical, and is subject to variation when large-scale turbulent eddies are present.

#### 2.1.3. Meteorological tower measurements

Detailed measurements of turbulence structure were made using fast response anemometry at heights of 15 m and 45 m on the instrumented tower at the source release point. Mean wind, mean temperature, and

turbulent Reynolds stresses were recorded, although the system was not working for a large portion of test 5. None of the models is capable of utilizing such detailed turbulent information, but the measurements were used to help decide the atmospheric stability, and also to provide horizontal velocity fluctuation information which was used to calculate horizontal spread rates in some of the models.

#### 2.1.4. Supplementary meteorological data

At intervals of about 3 hours, radio-sondes were released by PNL to obtain the vertical temperature structure of the atmosphere. The radio-sondes were released from three locations, namely the Fire Station 3 km north of the release point, at Howe 25 km north, and at the Diversion Dam 10 km southwest of the release point. The temperature profiles were used to determine the mixed layer depth in conjunction with visual observations.

Tetroons were also released from the source point throughout the tracer release period. The tetroons were set to follow the wind at the mid-level of the estimated mixing layer. These neutrally buoyant balloons can be tracked by radar out to distances on the order of 100 km, and are useful in giving trajectory information. However, it should be noted that the level of the tetroon must be preset according to some estimate of the average tracer plume height. In a deep, well-mixed boundary layer the exact height will not be crucial, but in a stable layer with strong wind shears it is difficult to ensure that the tetroon is at the same level as the plume.

#### 2.1.5. Surface SF<sub>6</sub> measurements

The principal data on tracer dispersion came from two networks of bag samplers, as described by Dickson et al.(1981). The first network is on a small scale, and sampler locations are shown in Figure 2.2. Each sampler contained twelve 1 liter bags with an inlet manifold which was switched each hour, so that a 1 hour sample was collected in

each bag consecutively. The second network is also shown in Figure 2.2, and consists of single 20 liter bags over a larger region. These samplers collected air over a period of 24-36 hours from the start of each release, and therefore provide a total dose measure for each test. The smallest detectable concentration of SF<sub>6</sub> in the bags is around 2 ppt., so that the minimum measurable dose depends linearly on the sample time.

#### 2.1.6. ALPHA-1 LIDAR data

In addition to surface concentration data, the airborne ALPHA-1 lidar system (Uthe et al., 1980) was used to obtain cross sections of the plume. The data is limited in that multiple passes are necessary at each cross section to obtain a meaningful time-average of the plume. However, the lidar data is our only quantitative information on the vertical structure of the plume, and can provide measures of the horizontal and vertical spread.

#### 2.2. Test Cases

Tests were run on nine different days in July, 1981. Data from the last seven tests are presented in some detail in Appendix A. The first two tests have been treated as shakedown tests. A brief narrative of tests three thru nine is included.

A cursory inspection of the observed surface patterns show them to generally exhibit a rather high degree of patchiness. It is relatively clear that any model will have difficulty in reproducing such patterns as those shown in Figs. A16 and A17. However, such highly scattered results are quite consistent with our discussion of inherent plume variability contained in Section 3 of Lewellen, et.al. (1983). A small source emitting into a thick turbulent boundary layer should produce a highly variable plume unless the observations are averaged over a time much longer than the turbulent time scale.

July 1981 INEL Field Experiment  
Surface Wind Tower and RABAL Locations

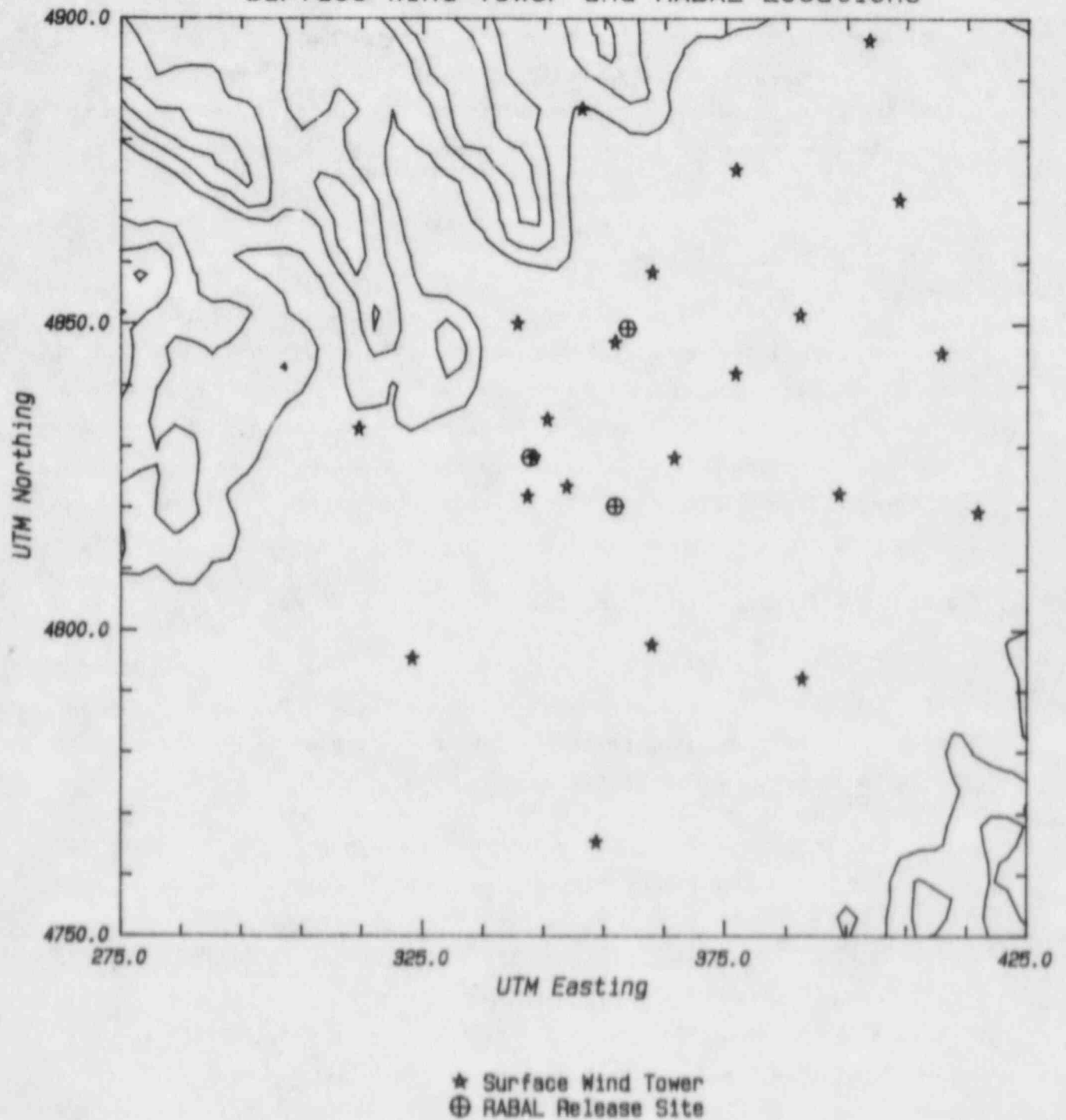


FIGURE 2.1

July 1981 INEL Field Experiment  
Sampler Locations

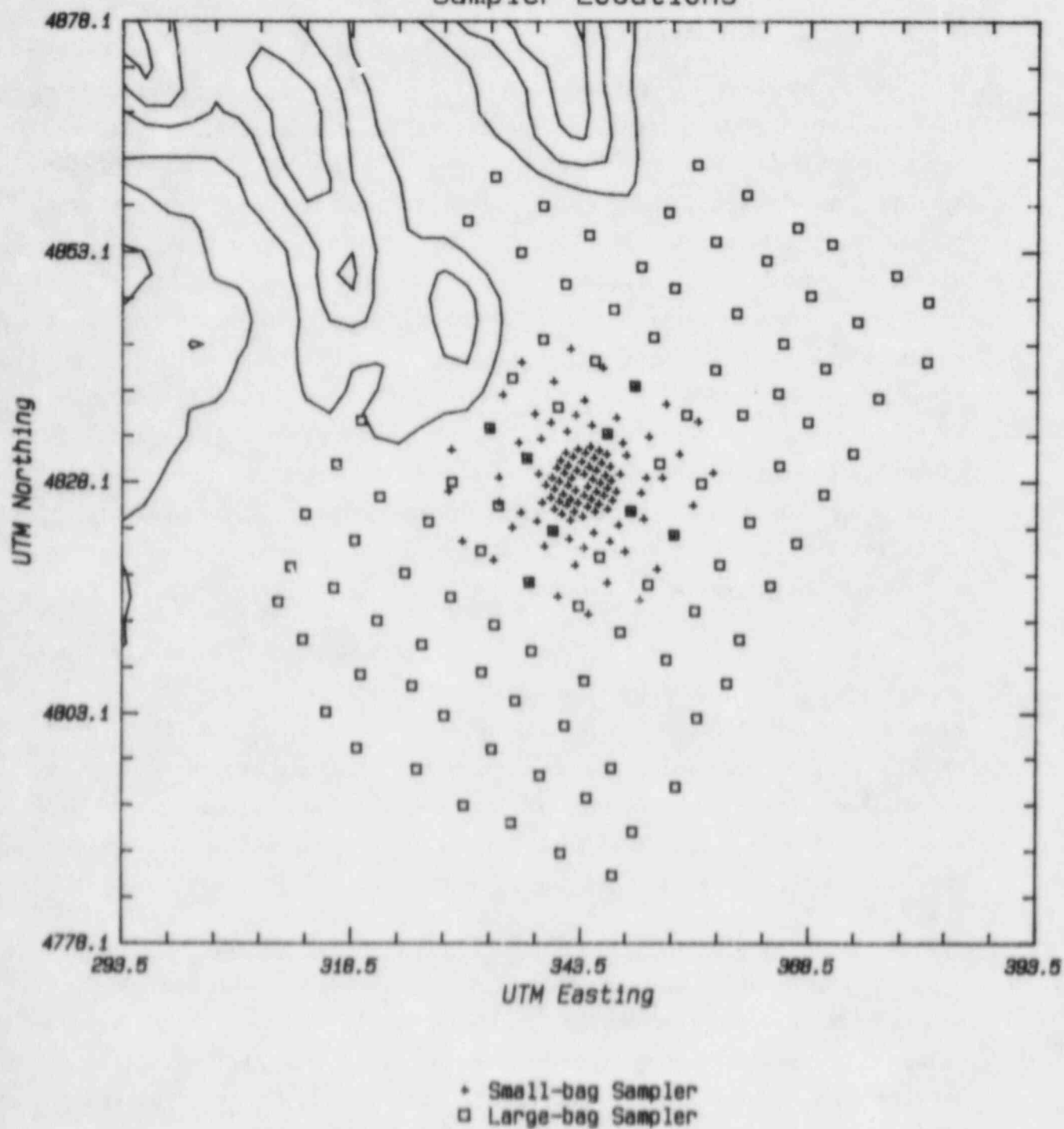


FIGURE 2.2

### III. Individual Model Results

#### 3.1. Gaussian Plume Models

We first look at the results of the simplest type models. As described in our report critiquing the available dispersion models, the input requirements to drive these models are minimal. For the two specific models considered, ISC and TEM, all that is required is a wind speed, wind direction, stability class, mixing layer height and emissions rate. We have added a third model, which we call GP, to see if there is any advantage evident from this data of using specific measurements of horizontal wind variance in predicting the horizontal plume dispersion. Codes selected for study were chosen to represent the types of models currently available and used by the utilities. Although the codes do not incorporate all options that might be used on some other codes, they do span the range of models likely to be utilized by utilities for emergency response, and should be a representative sample of the currently-available codes.

The models have all been run on two different grid systems, a fine grid with 1 km spacing over a domain of 40 x 40 km, and a coarse grid with 2.5 km spacing over a domain of 100 x 100 km. The fine grid results will be used primarily to compare with the hourly tracer samples while the coarse grid is used to compare with the total integrated samples. It is also interesting to look at the difference in the predicted patterns due only to the resolution of the grid used with the model.

In order not to inundate the reader with plots, only four of the hourly predictions are shown here for each model. These hours have been chosen to exemplify four quite different meteorological conditions. Results of all the hourly comparisons are included in the results of Section IV. The total of the 12 hourly predictions and the total integrated dose for each of seven tests for each model are included in Appendix B.



As should be expected, these Gaussian plume models yield well defined surface plumes for the hourly results exhibited in Figs. 3.1 to 3.4. Nature is not near so well organized, as exhibited in Fig. A.3. Even after averaging over 12 individual hourly distributions this difference is clearly in evidence when comparing the corresponding figures for 12 hour doses in Appendices A and B. This class of models may be expected to perform more poorly in comparison with the total integrated dose which extends much further from the release point. This is certainly borne out in a qualitative comparison of the corresponding total dose figures in Appendices A and B. However, as noted in Appendix A part of this poor comparison may be due to a relatively large uncertainty in the validity of the total dose data for all but the last three cases. The tetroon puff model (MT) results have been included on Figures 3.1 to save space; these results will be discussed with the other puff models.

#### 3.1.1. ISC (IS)

Figure 3.1 shows the predicted surface concentration for the fourth hour of test three (0300-0400, July 19, 1981). There is no apparent correlation between ISC's predicted plume for this hour and the observations shown in Figure A.4. The observations show the plume impacting at several points all around the source point, while ISC predicts a narrow plume off to the northeast. The varied pattern appears to be due to the combination of sharp vertical gradients in the wind, light and variable winds at the surface, and the remnants from the previous three hours of the plume.

Figure 3.2 shows the predicted surface concentration for the third hour of test five, i.e., 0700-0800, July 23, 1981. The wind at the source was from the North at this time, so we have a plume extending out of the domain to the south. There is not much agreement with the observed data, shown in Figure A.15 which indicates a strong impact to the West. There is observational evidence of material being transported to the south, but only for about 10 km. This is because the winds are

light (roughly  $1-2 \text{ ms}^{-1}$ ), while the Gaussian model makes the steady-state assumption that material has travelled out infinitely far along the wind vector.

Figure 3.3 shows the predicted surface concentration for the fourth hour of test six (2000-2100, July 25, 1981). In this case there is recognizable agreement between the prediction and the observations (Fig. A.21). The maxima occur close to the same positions and are almost within a factor of two of each other. The tail of the observed plume bends to the south but this certainly provides better agreement between the model predictions and observations than either of the preceding two cases.

Figure 3.4 shows the second hour from test seven, i.e., 1400-1500, July 27, 1981. In this case we have a wider plume, due to the greater instability, directed towards the North-Northeast. The observations, Figure A.27 are actually in reasonably good agreement. There is a maximum close to the source, with the 1 ppm.-sec. contour covering a similar region in the two figures. The 0.3 ppm.-sec. in the data meanders a little to the Northeast and off the edge of the measurement grid, but has a similar width to the predicted plume. The error in direction is about  $30^\circ$ . There is an isolated maximum of 0.1 ppm.-sec. situated 10 km east of the source, but this is not predicted by the simple Gaussian plume.

The 12 hour integrated doses for cases three thru nine on the fine (1 km) grid are shown in Appendix B, Figures B.1 thru B.21. Note that the Gaussian plume calculation is complete after 8 hours, since there is no predicted surface concentration after the release has stopped. Thus, the 8 hour dose is the total dose for these models. The total dose can be seen to be made up of individual plumes with the wind passing thru marked shifts in direction for many of the cases. For example, Figure B.7 for case five should be compared with the observations in Figure A.18 which is the 12 hour dose in the small-bag samplers.

Statistical comparisons between the model results and observations will be discussed in Section IV.

### 3.1.2. TEM (TE)

The TEM results are similar to the ISC results since they both use the same winds. However, the spread of the plume is significantly larger in TEM, and the surface doses are correspondingly lower than ISC. This wider spread does at least go in the right direction to make TEM agree a little more with the data than does ISC.

### 3.1.3. GP

In this model, the horizontal spread rate is based on the measured  $\sigma_\theta$ , i.e., the r.m.s. fluctuation in wind direction. This yields a somewhat larger spread rate for Figure 3.1 but a spread midway between ISC and TEM for the other three hours. The largest difference shown for the four hours of Figures 3.1 to 3.4 is the fact that an opposite wind direction is used for GP for the hour shown of test three. This is possible because the 46 meter wind from the met tower was used for GP while the network wind closest to the release point was used for ISC and TEM.

This model generally produces a more diffuse plume than the standard two models due to its dependence on measured  $\sigma_\theta$ . It will be seen in Section IV that this model proved somewhat more accurate than the other two Gaussian plume models. Part of this advantage may be traceable to its use of somewhat different winds. The 46m winds were likely to be more representative than the MESONET winds since they are actually at the release point, and were not missing as often during the test periods as the MESONET data.

### 3.2. Puff Models

In general, the results from the puff models for the same four hours shown in Figures 3.5-3.8 provide more realistic looking plumes than the Gaussian plume results, since they are able to take some account of the changes in wind speed and direction. As we showed in the previous section, the plume models are forced to predict a plume which stretches infinitely far in the direction of the wind for each hour. This is clearly in error when the wind is very light and does not persist for very long. The puff model results below can be contrasted with the plume results, and demonstrate the limited transport particularly for the early stages of test 5. In spite of these potential advantages the qualitative hour comparisons shown here do not indicate a clear realization of these performance advantages.

The other major feature which should provide more accurate results is the ability to keep track of the pollutant after the release has ended. The plume models switch off when the release ends, and therefore miss any wind shifts after the release. The puff models are able to account for this in the total dose calculation.

#### 3.2.1. MESOT (MT)

This nonstandard model which takes the observed tetraon trajectories and applies the MESOI diffusion algorithms was added to help diagnose the test results. Results for the four hours considered here are included in Figures 3.1 to 3.4. The results are quite different from the previous steady state plume results but in general are not any closer to the data observations. In fact, except for the test five hour shown, the tetraon puff model tends to yield results inferior to the steady state plume results. The limited number of tetraon trajectories available is unable to provide a clear indication of plume position on this limited fine mesh grid. This is particularly noticeable for the hour chosen from test six. During this particular hour, there is no tetraon anywhere on the fine mesh. For purposes of

obtaining the 12 hour total dose, emissions during such a period are added to the closest time. Comparison of the integrated doses predicted by MT in Appendix B with the observations of Appendix A show that it does provide for more qualitative agreement than is evident for the Gaussian plume results.

### 3.2.2. MESOI (MI)

Only the last two of these four hours shown tend to display any qualitative agreement between the data and the model predictions. Even in these relatively well behaved cases MESOI tends to overpredict the maximum surface impact. This tendency to overpredict, as a result of placing the emission at the surface rather than its true value of 46 meters, is particularly noticeable in Figures 3.5 and 3.6. The same effect is also quite evident in the 12 hour integrated doses of Appendix B, but is not so evident in the total dose on the larger grid.

### 3.2.3. MESODIF (MD)

The main differences between the MESOI and MESODIF models are in the horizontal diffusion calculation, and the winds used to transport the puffs. MESODIF uses the 6-minute averaged winds while MESOI uses hourly averaged winds with linear interpolation between hours. About the only difference this produces for the hour shown in Figure 3.5 is a reduction in the peak value

However, for the next two hours shown in Figures 3.6 and 3.7 Mesodif actually records a higher peak value than MESOI. The second hour of test 7, Figure 3.8, is very similar to the MESOI result, and both are in qualitative agreement with the observations for this hour shown in Figure A.27. However, neither are as accurate as the Gaussian plume model results of Figure 3.4.

### 3.2.4. ARL-Puff (AL)

This model shows much more diffuse patterns for Figures 3.5 and 3.6

but much narrower plumes for Figures 3.7 and 3.8. This is a direct result of the use of a constant horizontal spread rate of 1m/sec. In the first two light wind cases the puff sits on the grid and continues to expand while for the last two relatively strong wind cases the puff is swept off the grid before it has much chance to expand. In spite of this very crude parameterization of the horizontal diffusion, this model produces peak surface concentration which are closer to the observations than the previous puff models in every case but the test six hour where MESOI is somewhat closer. The relatively high diffusion for the light wind cases also tends to make the integrated doses appear in better qualitative agreement with the observations as may be observed by comparing the corresponding figures in Appendix A and B.

#### 3.2.5. MESQJ (MJ)

MESQJ is a modified version of MESOI which accounts for an elevated source and uses the 6-minute winds like MESODIF. These differences are sufficient to make the results from MESQJ and MESOI quite different. For the first hour shown in Figure 3.5 the vertical diffusion for this nocturnal hour is so small that the maximum value is now significantly underpredicted. The overprediction remains for the hour from test five shown in Figure 3.6. The improvements in the pattern test results are extremely marginal. MESQJ performs best for the test six hour and shows little difference from MESOI in the unstable case seven hour.

### 3.3. Transport and Diffusion Models

The models in this section use more detailed information about the wind field. Most of the models use a three-dimensional wind field to move the tracer, and can therefore account for winds in different directions at different heights. This is the major advantage over the simple puff models which only use the surface winds to transport the tracer. Some of the models also attempt to take some account of terrain



features and steer the flow around large hills. However, their ability to account for terrain effects cannot be assessed from the present data since none of the samplers were located in the regions of high terrain.

These models should not be expected to show large performance advantage on the short-range fine mesh used in Figures 3.9-3.12 and they do not. They should have their best relative advantage on the extended grid used for the total dose calculation.

#### 3.3.1. PATRIC (PA)

PATRIC results continue the overprediction of the surface impact for the first hour common to all the models except MESOJ. In fact, PATRIC seriously overpredicts the peak surface impact for all four hours shown. Of course, part of this problem may be due to the difficulty of actually registering the maximum surface impact within a fixed network of surface samplers. The models will be given the benefit of this doubt in one of the statistical comparisons shown in the next chapter.

#### 3.3.2. MATHEW/ADPIC (AD)

The results for MATHEW/ADPIC shown for these four hours are quite similar to the PATRIC results. The inclusion of terrain is probably responsible for the slightly higher surface impact for Figures 3.9 and 3.10. The biggest difference for the two model results should occur on the larger grid used for the total dose calculations. Appendix B shows the major difference between the two results are higher peak values predicted for MATHEW/ADPIC. Only test eight, Figure B.38 produces a result in the opposite direction.

#### 3.3.3. IMPACT (IM)

IMPACT also shows results similar to PATRIC. It shows somewhat better performance in Figure 3.11 and perhaps somewhat poorer in Figure 3.12 but qualitatively at least there is little basis to chose one over

the other. This similarity extends to the total dose patterns shown in Appendix B. Probably the largest qualitative differences are for cases three and seven shown in Figures B.24 and B.35. In case three PATRIC, shows more plume impact in the southwest while for case seven, it is IMPACT which shows some of the plume in the southwest.

#### 3.3.4. SPLITPUFF (SP)

The SPLITPUFF model differs from the previous puff models in that puffs are allowed to split and move at different rates in response to the vertical wind structure. The results presented in this section were obtained with three layers within the "mixed-layer", and an outer region above the boundary layer. The winds in each of the four levels were obtained from the velocity profile measurements. On the assumption that the transport and diffusion models should outperform the puff models of the last section, then this model is included to see how much of this performance difference can be made up by a puff model which can correctly handle the effects of wind shear.

Since the other transport and diffusion models show no obvious advantage over the simpler puff models, SPLITPUFF is not expected to either.

July 1981 INEL Field Experiment : Test 3  
 Model Predictions : Surface Dose for 0300 - 0400

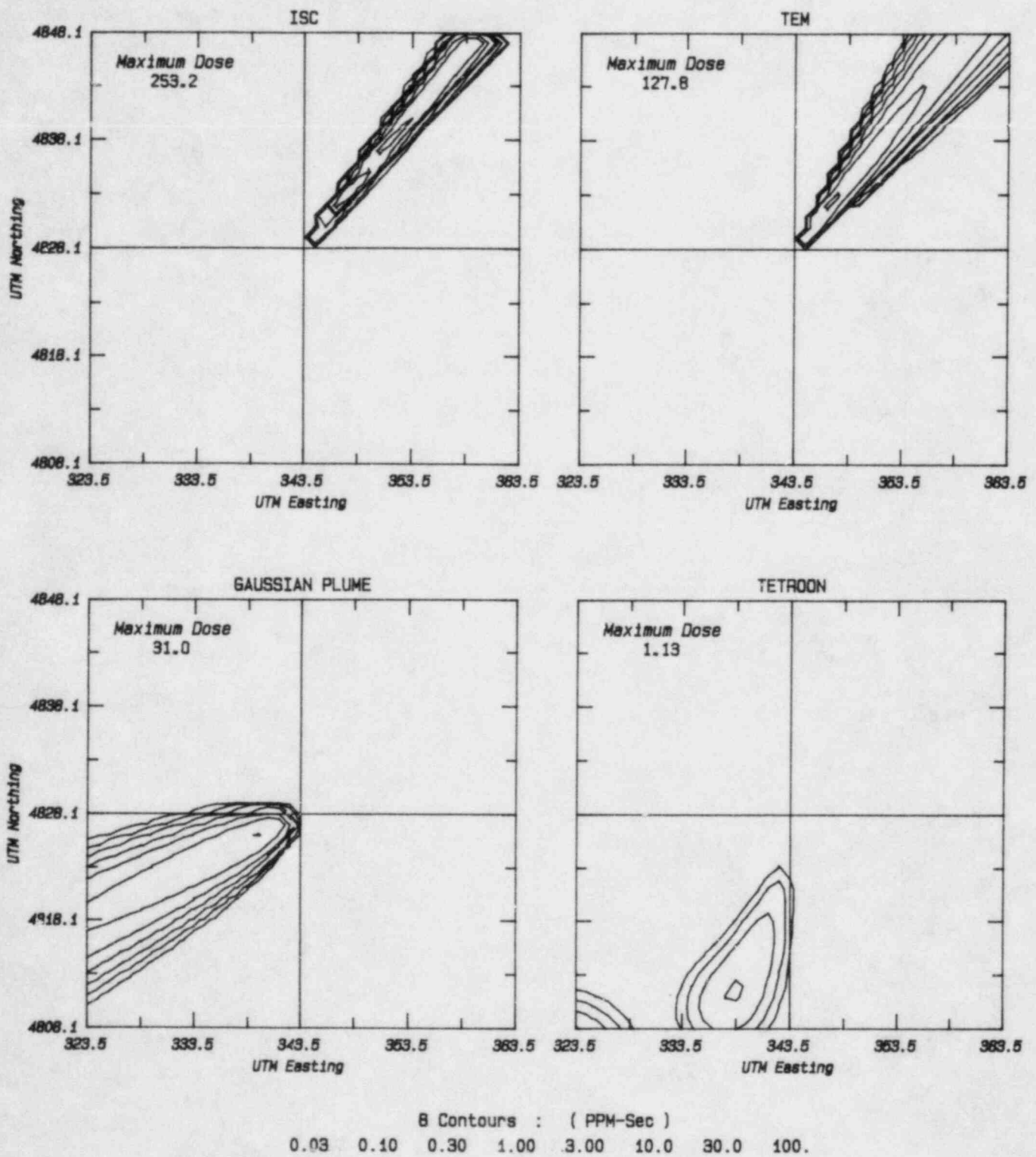


Figure 3.1

July 1981 INEL Field Experiment : Test 5  
 Model Predictions : Surface Dose for 0700 - 0800

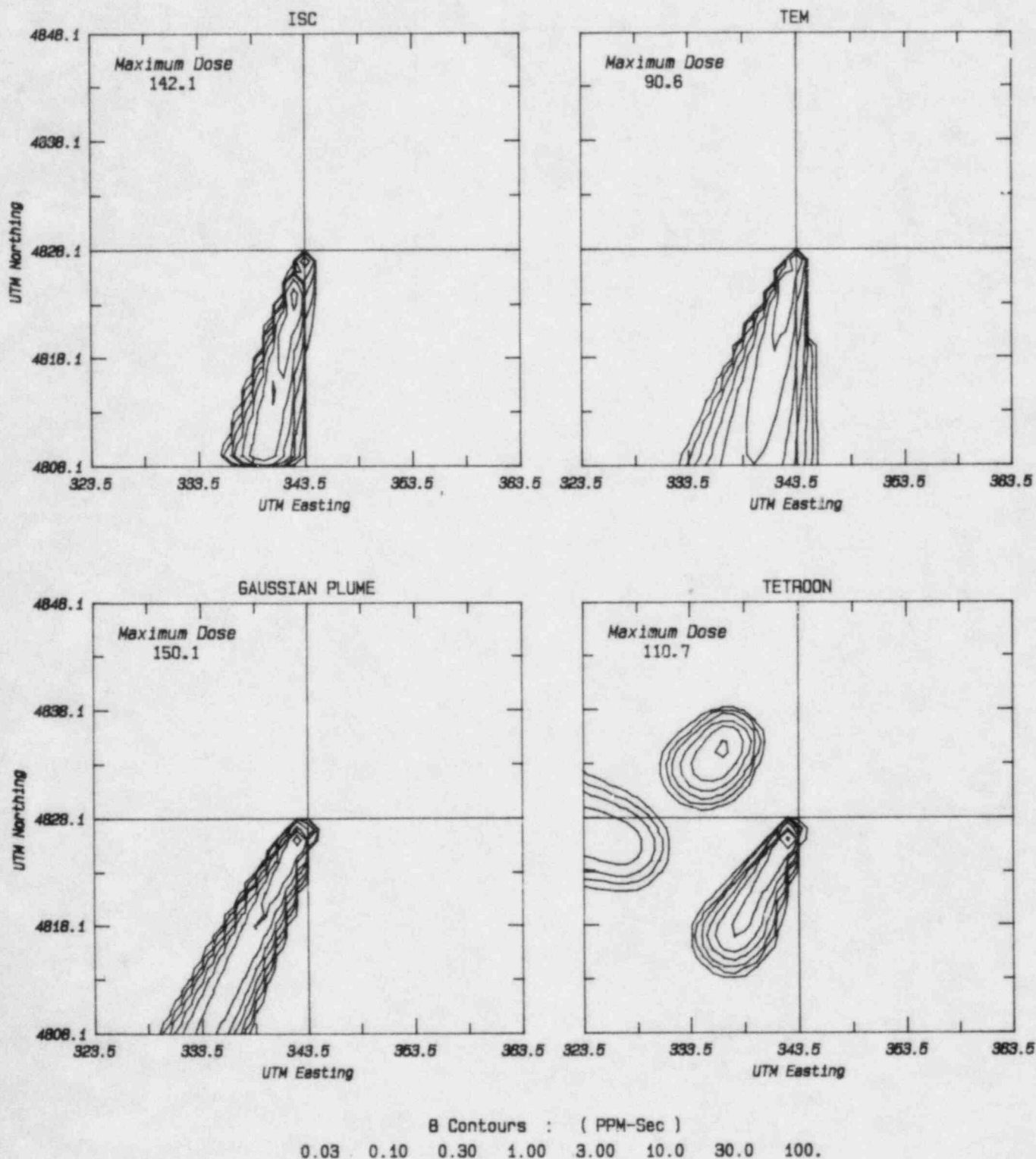


Figure 3.2

July 1981 INEL Field Experiment : Test 6  
 Model Predictions : Surface Dose for 2000 - 2100

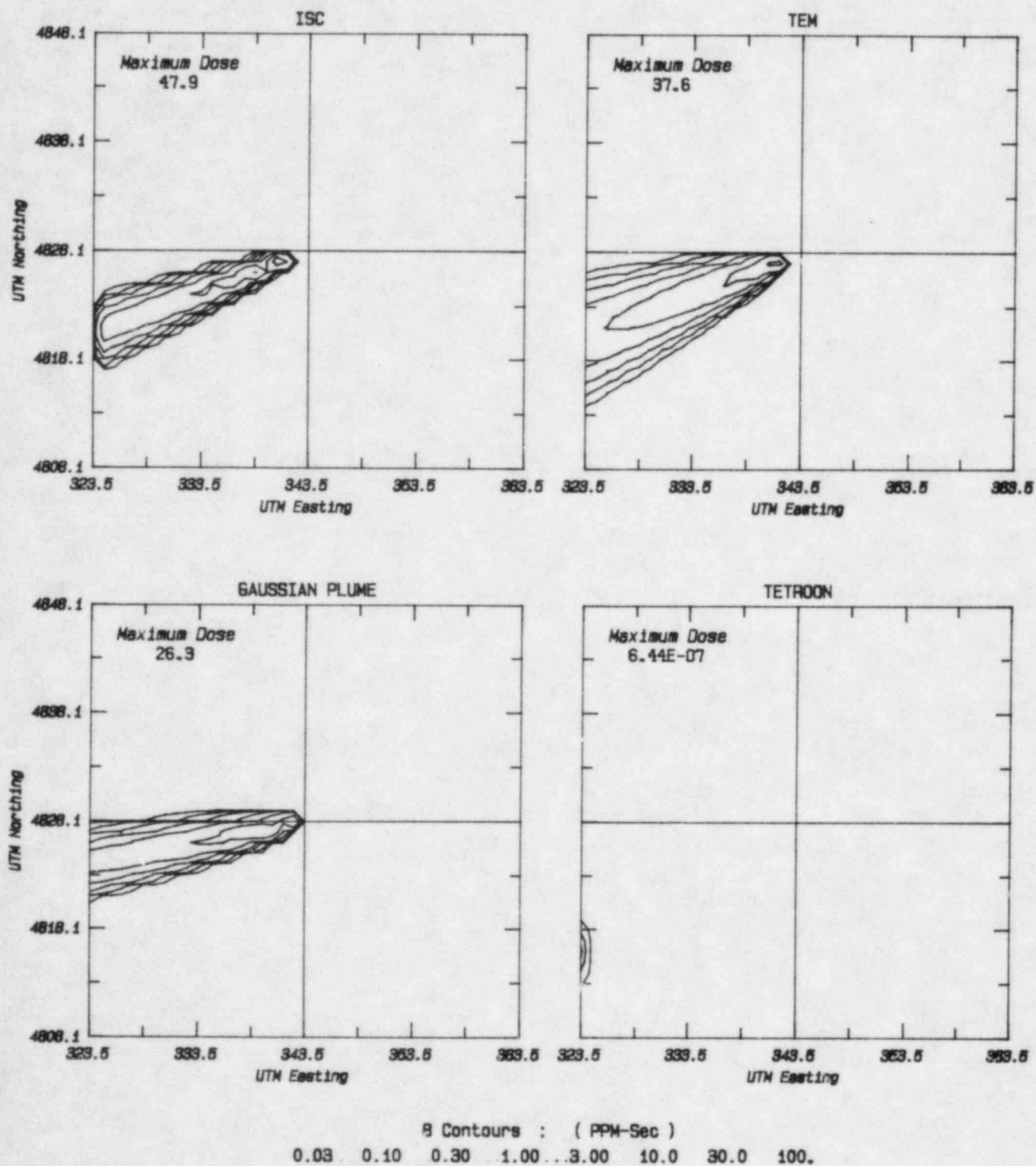


Figure 3.3

July 1981 INEL Field Experiment : Test 7  
 Model Predictions : Surface Dose for 1400 - 1500

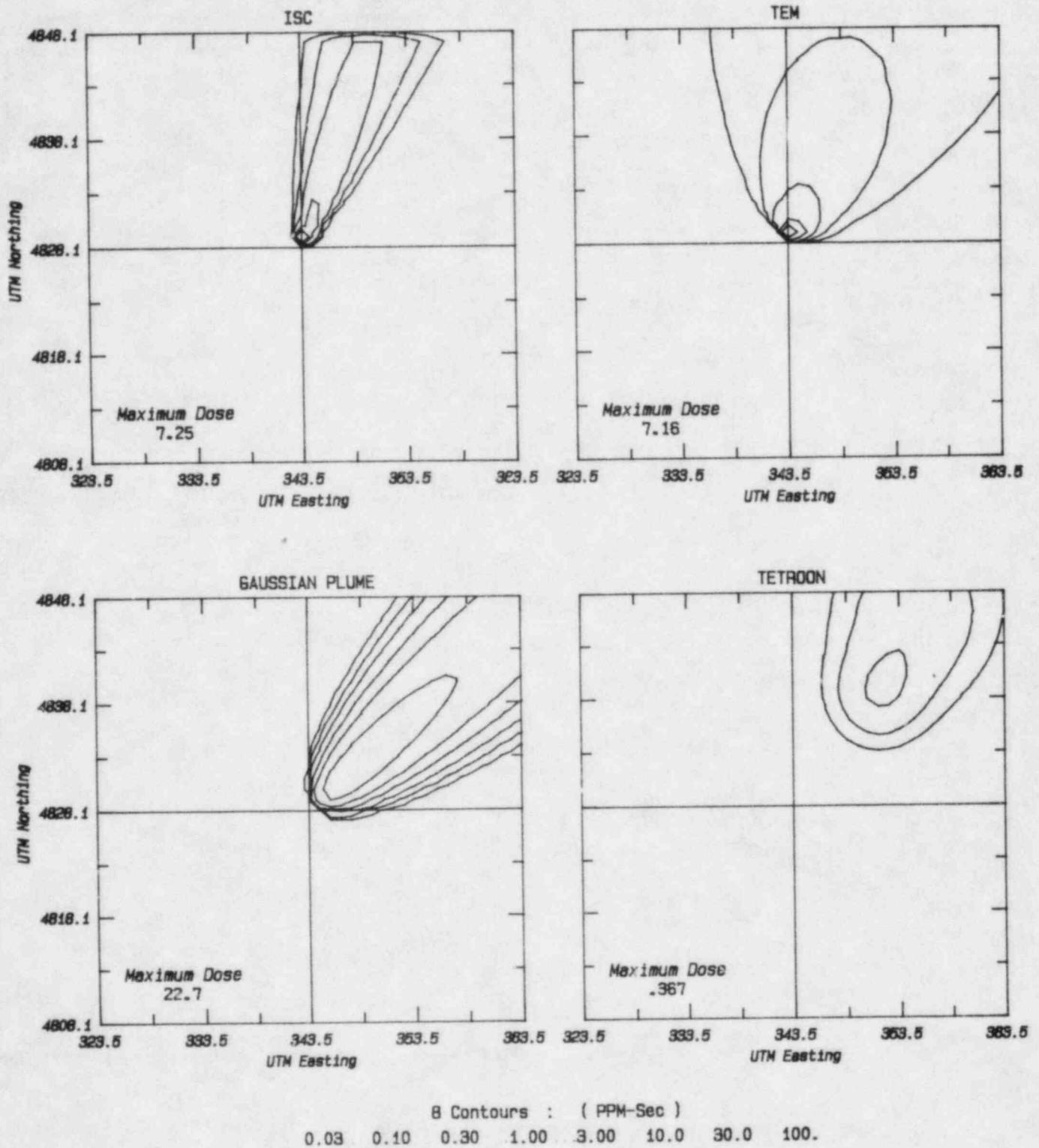


Figure 3.4



July 1981 INEL Field Experiment : Test 3  
Model Predictions : Surface Dose for 0300 - 0400

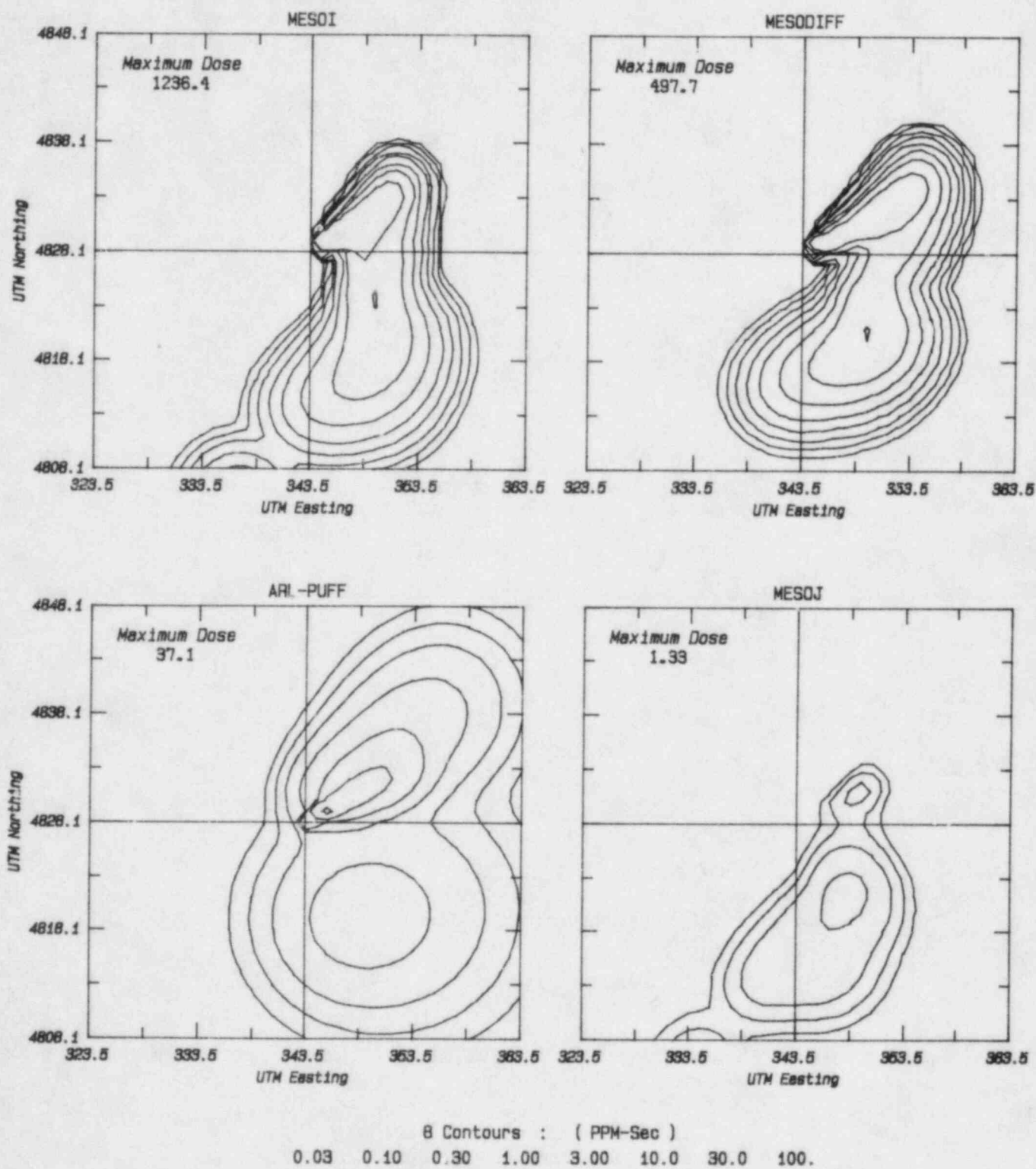


Figure 3.5



July 1981 INEL Field Experiment : Test 5  
 Model Predictions : Surface Dose for 0700 - 0800

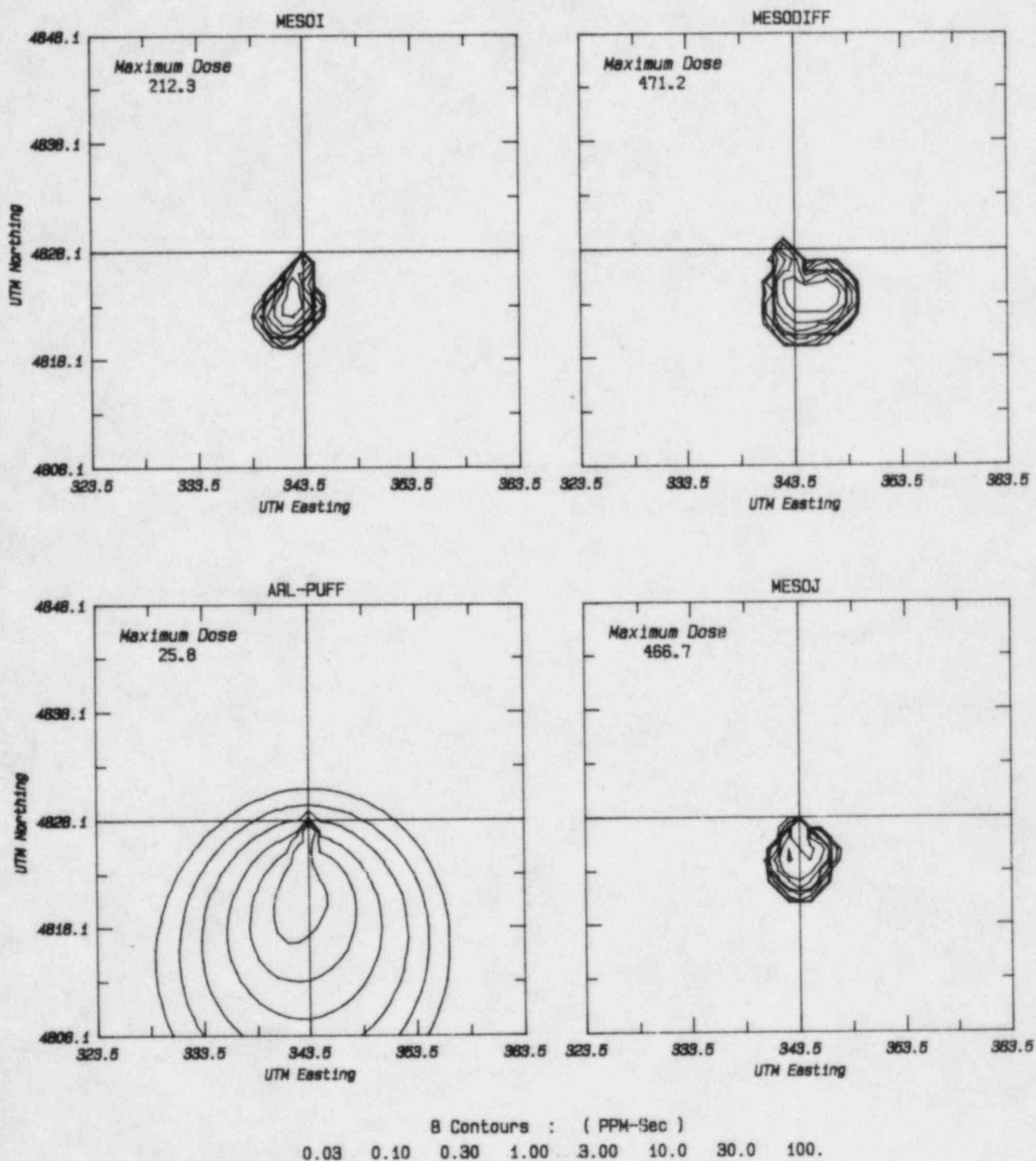


Figure 3.6

July 1981 INEL Field Experiment : Test 6  
 Model Predictions : Surface Dose for 2000 - 2100

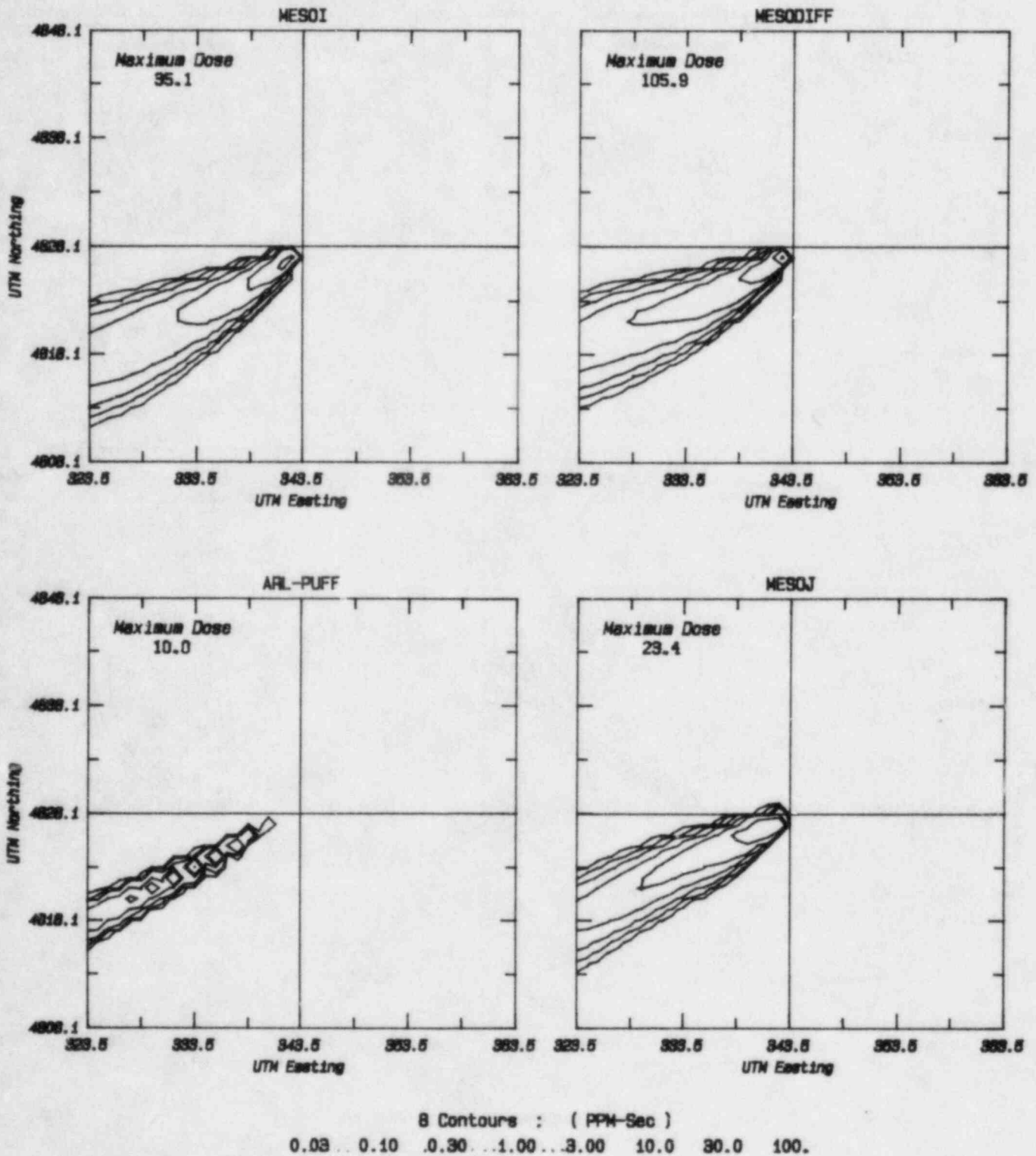


Figure 3.7

July 1981 INEL Field Experiment : Test 7  
 Model Predictions : Surface Dose for 1400 - 1500

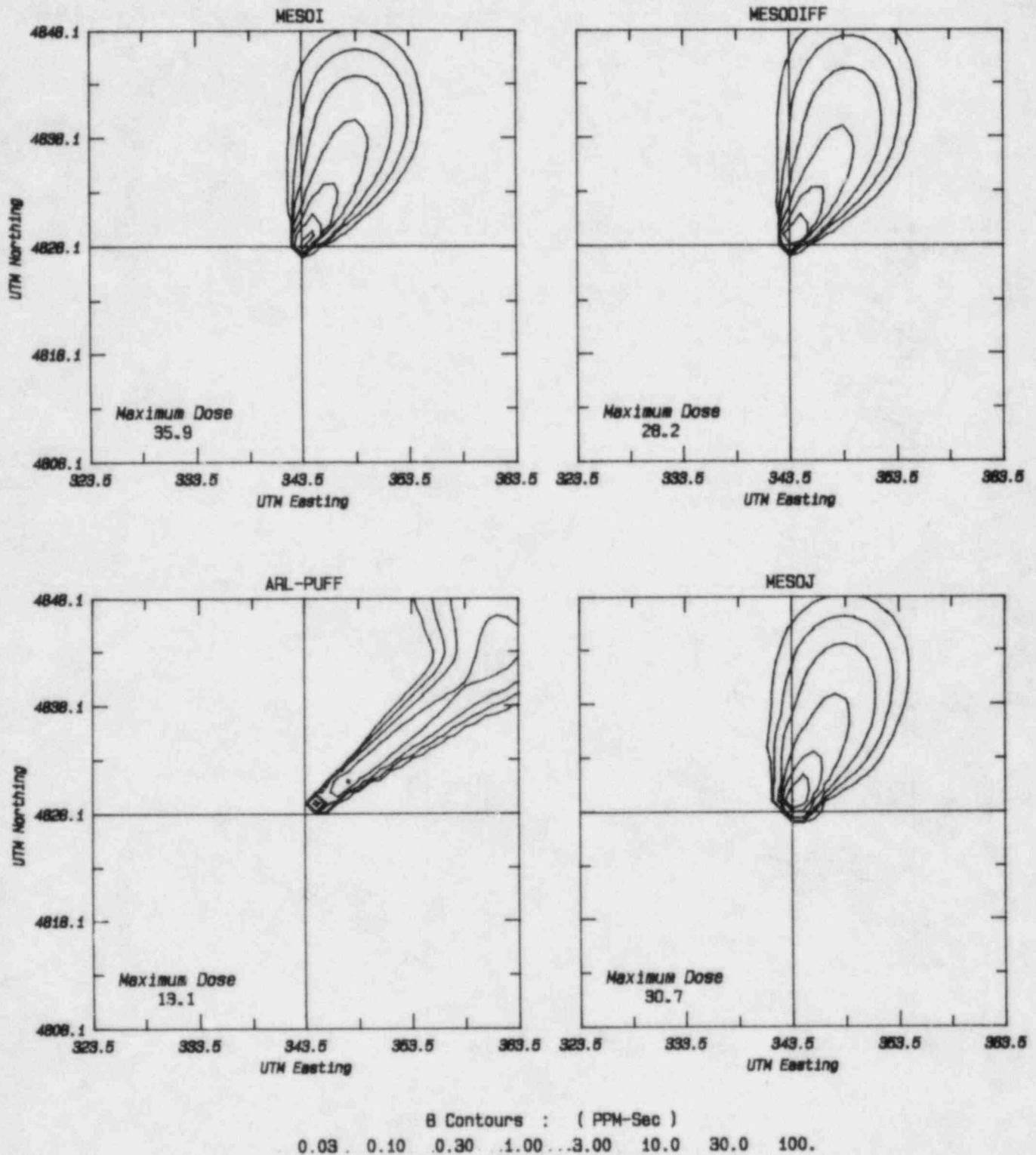
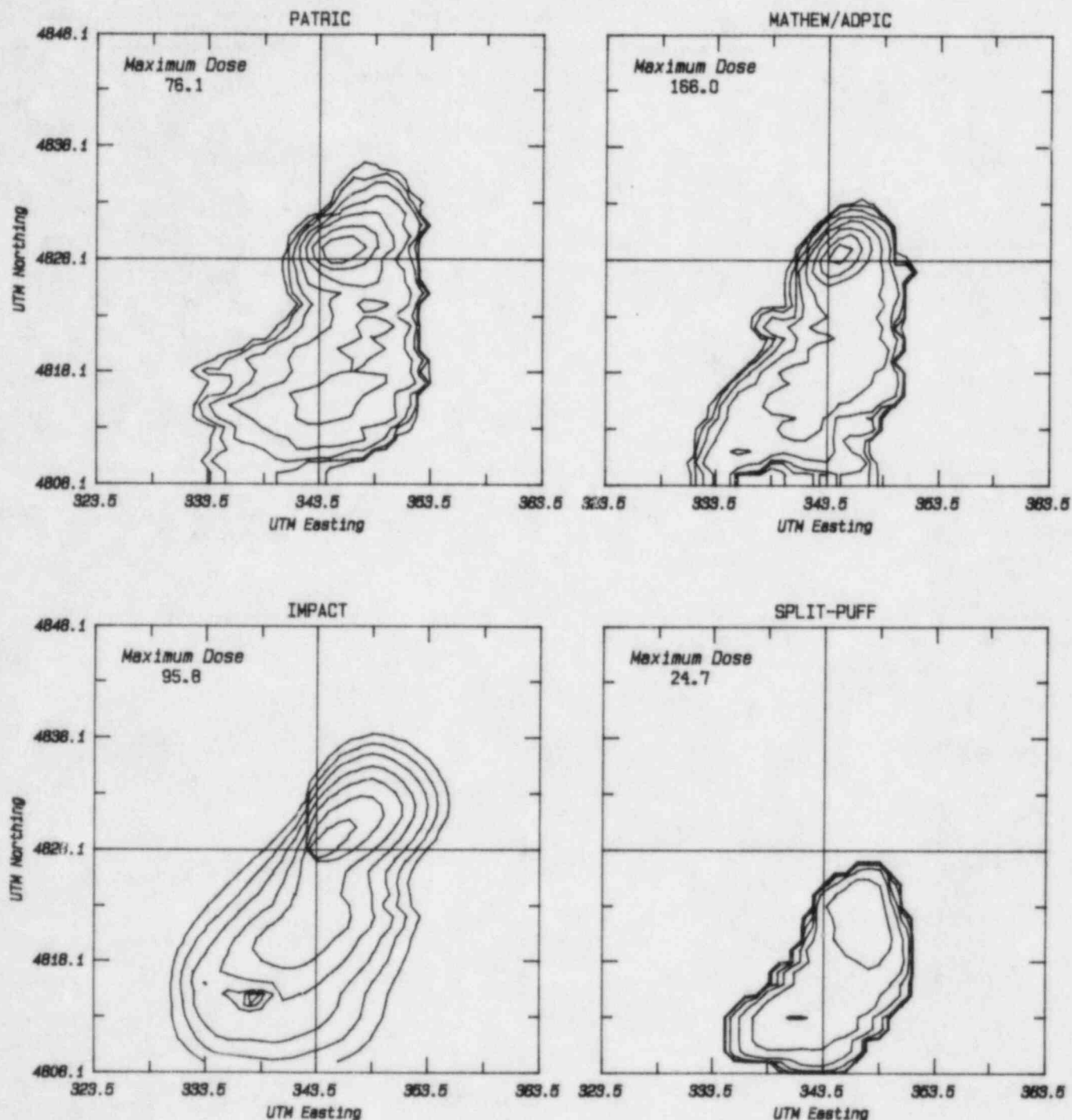


Figure 3.8

July 1981 INEL Field Experiment : Test 3  
 Model Predictions : Surface Dose for 0300 - 0400



B Contours : ( PPM-Sec )  
 0.03 0.10 0.30 1.00 3.00 10.0 30.0 100.

Figure 3.9

July 1981 INEL Field Experiment : Test 5  
 Model Predictions : Surface Dose for 0700 - 0800

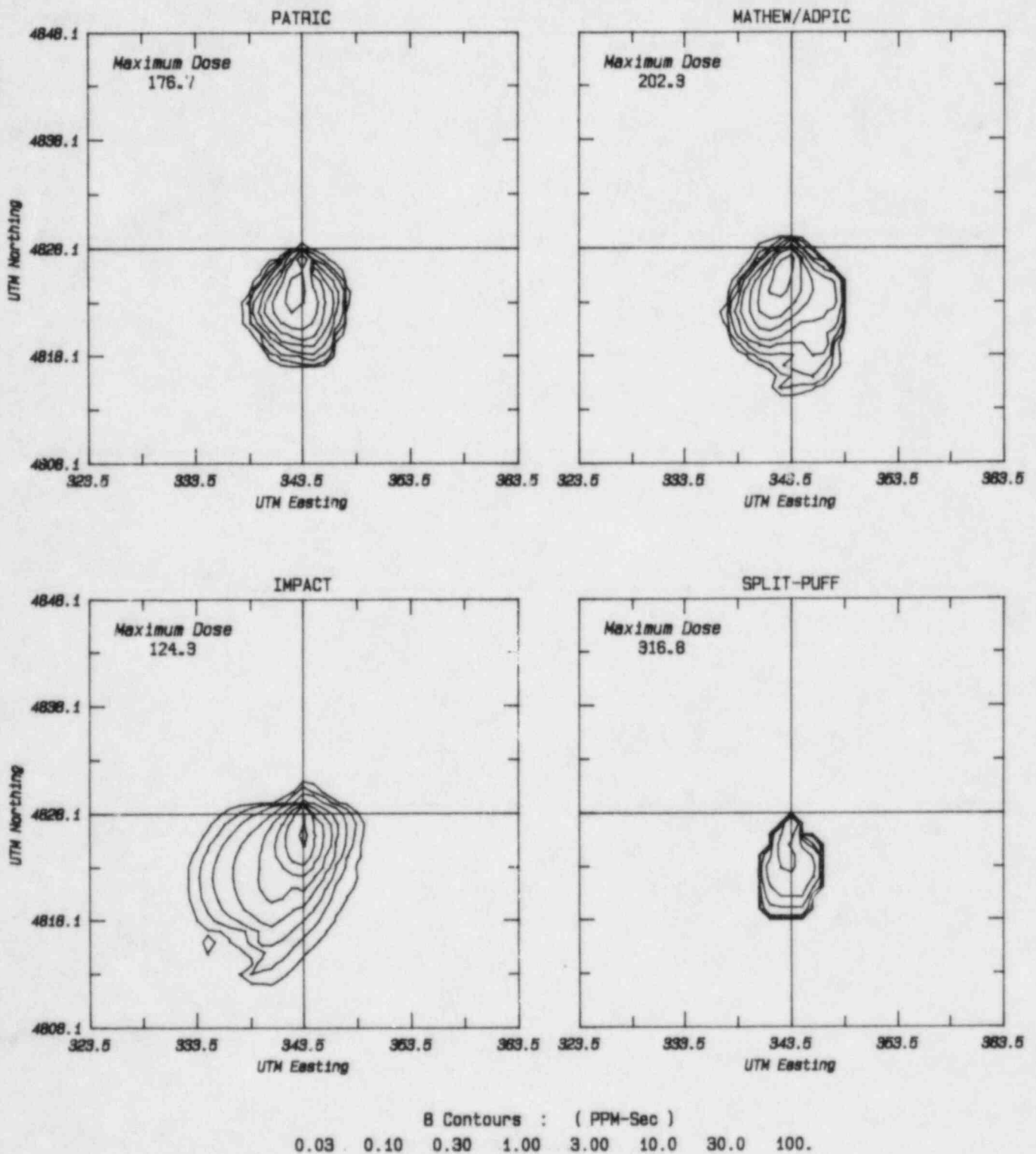


Figure 3.10

July 1981 INEL Field Experiment : Test 6  
Model Predictions : Surface Dose for 2000 - 2100

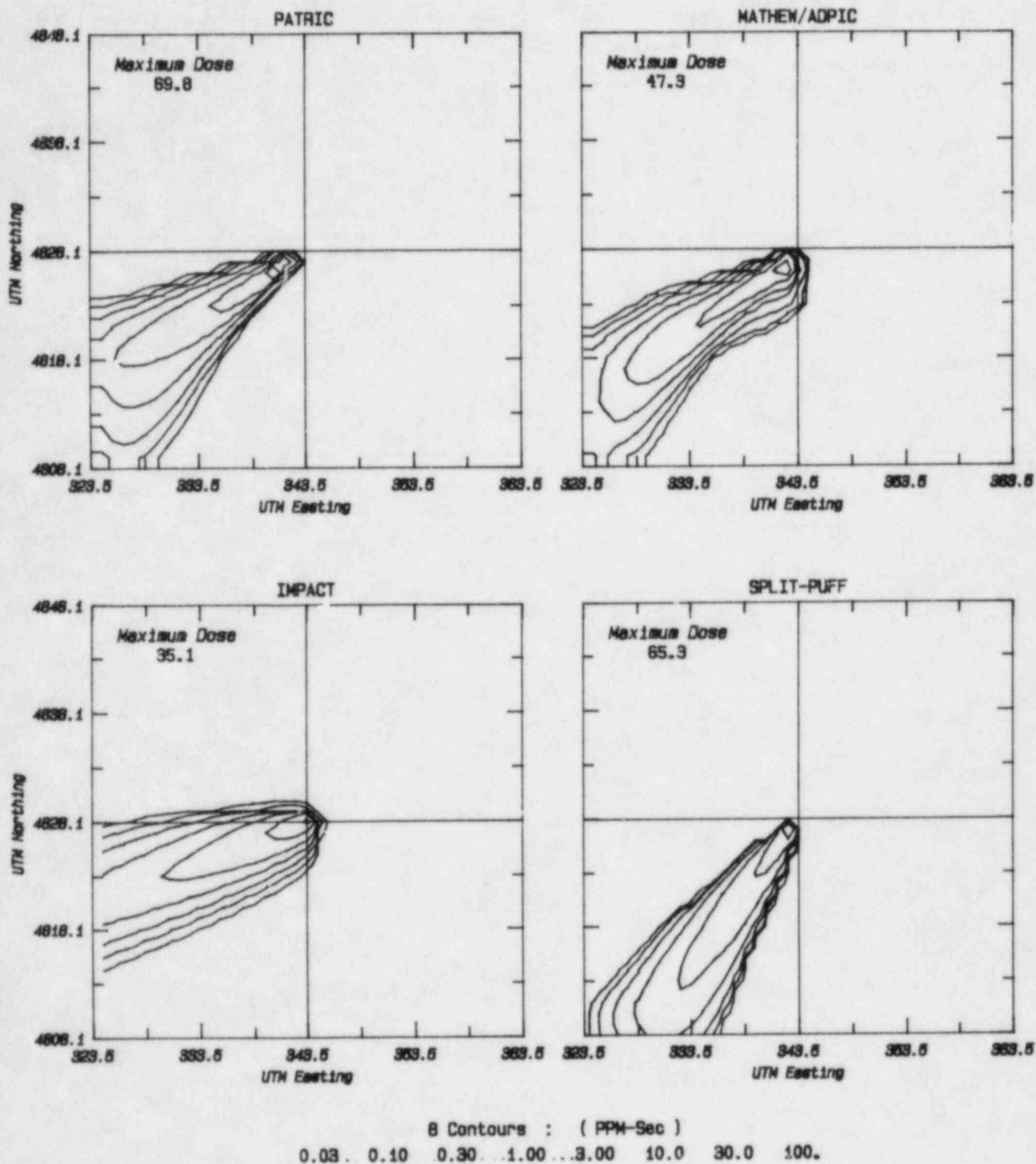
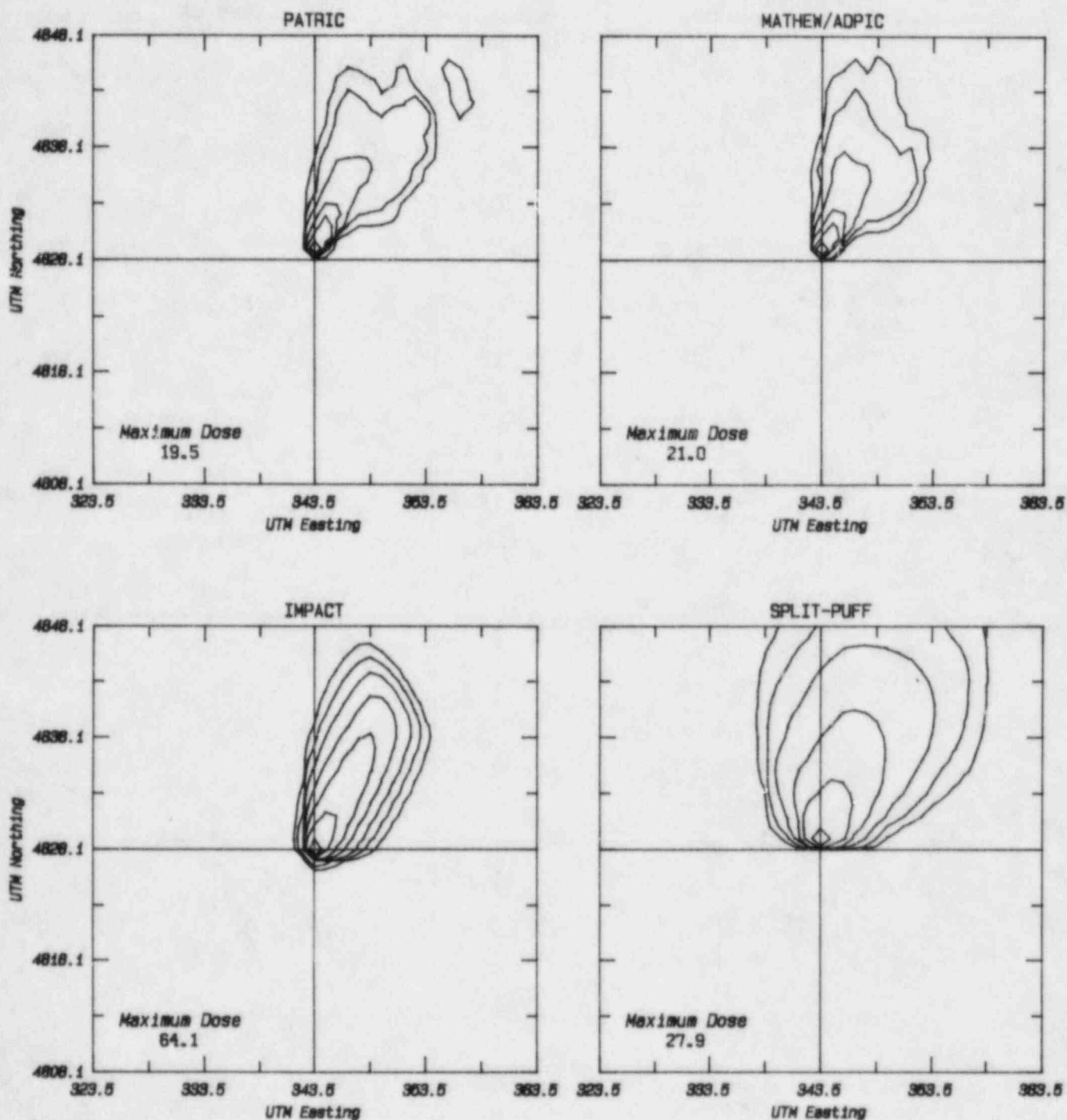


Figure 3.11



July 1981 INEL Field Experiment : Test 7  
 Model Predictions : Surface Dose for 1400 - 1500



8 Contours : ( PPM-Sec )  
 0.03 . 0.10 . 0.30 . 1.00 . 3.00 . 10.0 . 30.0 . 100.

Figure 3.12

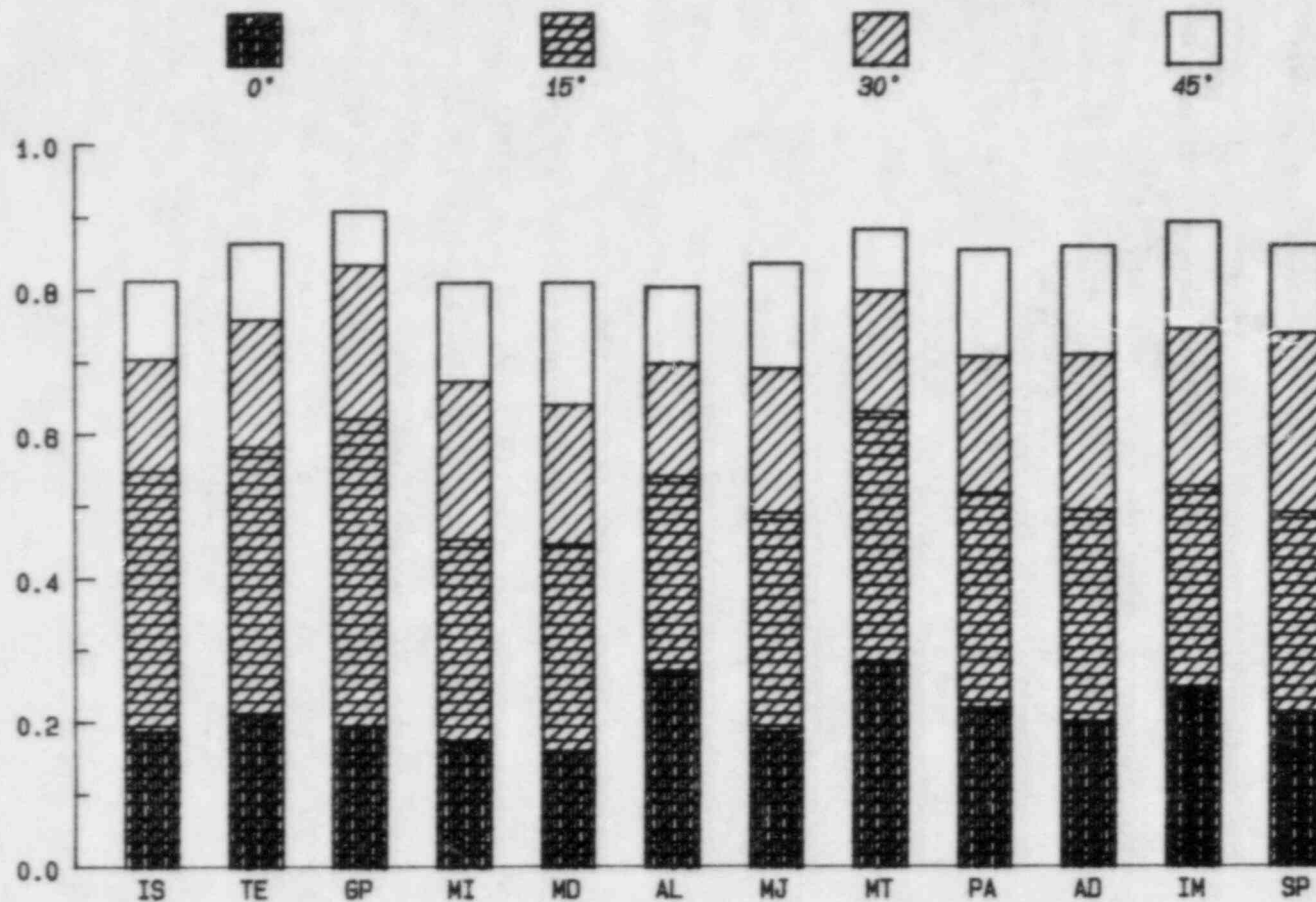


#### IV. Intermodel Comparisons

The model results are compared with the data in a relatively large number of ways in order to provide as clear a picture as possible of the relative accuracy of the different measures. Our basic comparison is the pattern test described by Lewellen, Sykes and Oliver, (1980). This provides a consistent means of seeing how much the comparison between observations and model is influenced by shifts in model pattern positions. The measures of accuracy chosen for intermodel comparisons here are % within a factor of two, % within a specified absolute increment, root mean square error, and the correlation coefficient. The first two are chosen because they provide easy interpretation, while the last two are preferred by statisticians. The model shift in position is compared in two ways. For comparisons labelled as "data value" the comparison is between any specific data value and the model prediction which is closest to that data value within the area designated by the angular increment. For comparisons labelled as "max data value" the comparison is centered about any specific sampler site but the comparison is between the maximum observation and the maximum model result within the area designated by the angular increment. Both measures are the same at  $\Delta\theta=0^\circ$ . The first approach gives the model the greatest possible benefit of any uncertainty in predicted position, while the second approaches the standard paired-in-time-only result at large values of  $\Delta\theta$ . The greatest discrepancy between the two measures will occur when the model predicts results significantly greater than any observations. If one believes that the data network has correctly captured the maximum surface impact then this second measure provides a truer measure of the model accuracy.

##### 4.1 12 Hour Total Dose on the Fine Mesh

Figure 4.1 shows that the models correctly predict only about 20% of the data within a factor of two and no significant improvement is seen for the more complex models. Considerably more favorable comparisons are obtained as the uncertainty in the model prediction position is allowed



Tests 3 Thru 9  
12 Hour Total Dose : Percent within a factor of 2 : (Data Value)

Figure 4.1

to increase. Roughly 70% of the data points are predicted within a factor of two by some model value within an area surrounding the data point defined by the  $30^\circ$  increment. The reader should perhaps be reminded that the area around the data point extends a distance  $\pm r\Delta\theta$  in the radial direction, where  $r$  is the distance between the source and the sampling point, as well as the same distance in the angular direction.

The performance measure is somewhat influenced by the treatment of the background noise. A background value of  $4 \times 10^{-2}$  ppm-sec has been added to both the data and the model prediction for the comparison of Figure 4.1. Alternatively, if all of the comparisons which have both data and model result below the noise level are excluded then the % within a factor of two appears as in Figure 4.2. The biggest difference is seen for the precise zero degrees comparison. The average 20% is reduced to more like 15%. We have chosen to use the former measure which depends upon the addition of the background value for the rest of our comparisons.

Figure 4.3 shows the percent of the model predictions that are within an absolute dimensional value of 1 ppm-sec of the observed data. It is seen that roughly half of the data values are within this value which is 25 times the background noise level. It should perhaps be noted that the highest 12 hour dose observed was 95 ppm-sec for test six. Again there is relatively little model-to-model performance variation. The greatest difference between models shows up in the statistical measures of Figures 4.4 and 4.5. Both the correlation coefficient and the root mean square errors are much worse for Mesodif and MESOI than for the other models. What is perhaps most surprising is that the steady state plume models actually out perform the more sophisticated models. This is particularly true for the new GP model.

The three comparisons made in Figures 4.1, 4.4 and 4.5 are repeated in Figures 4.6 to 4.8 but with the comparisons based on the maximum data value and the maximum model predictions within the compared areas. Remember that this yields the same comparison for the zero degrees, but

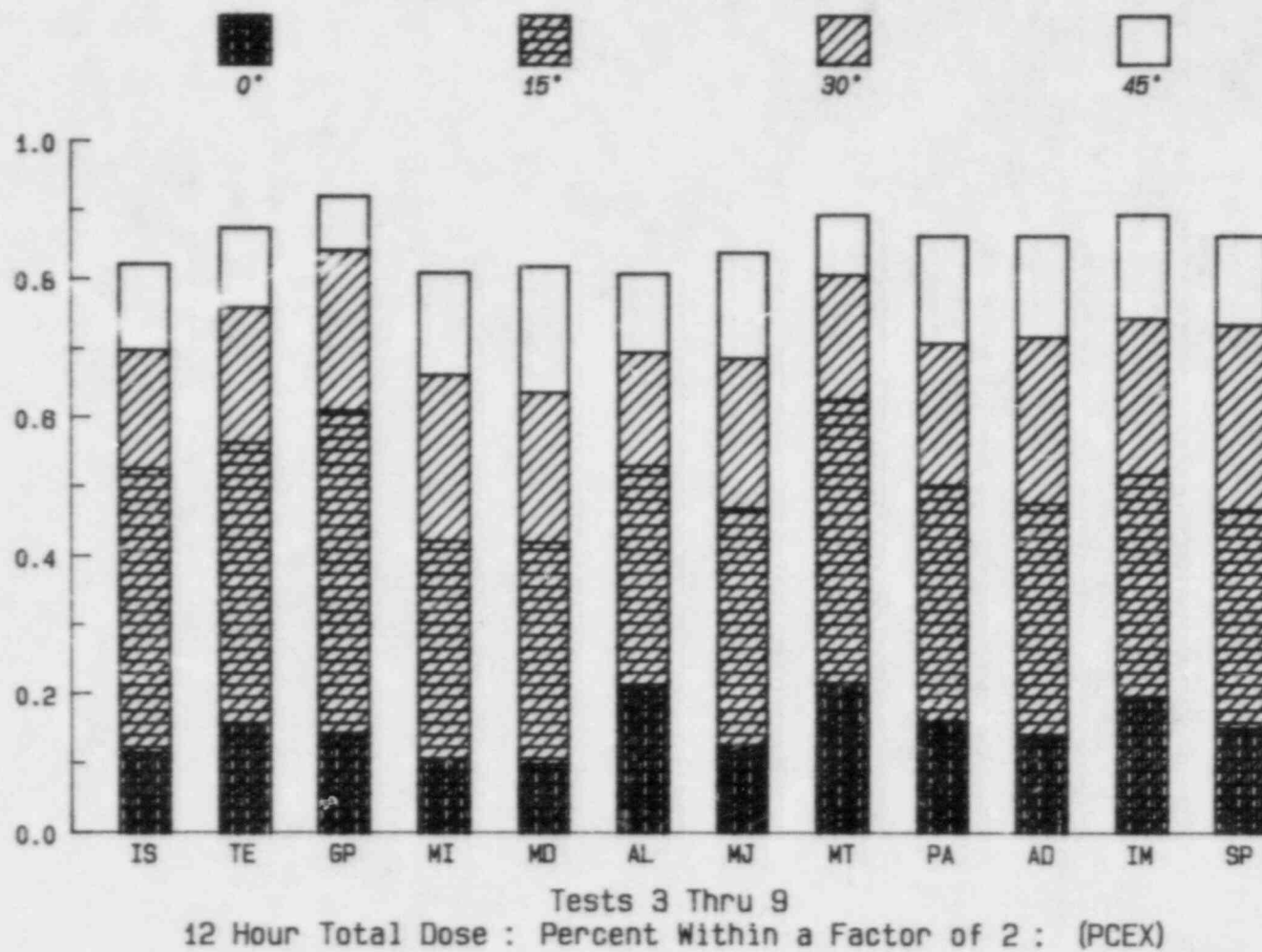


Figure 4.2

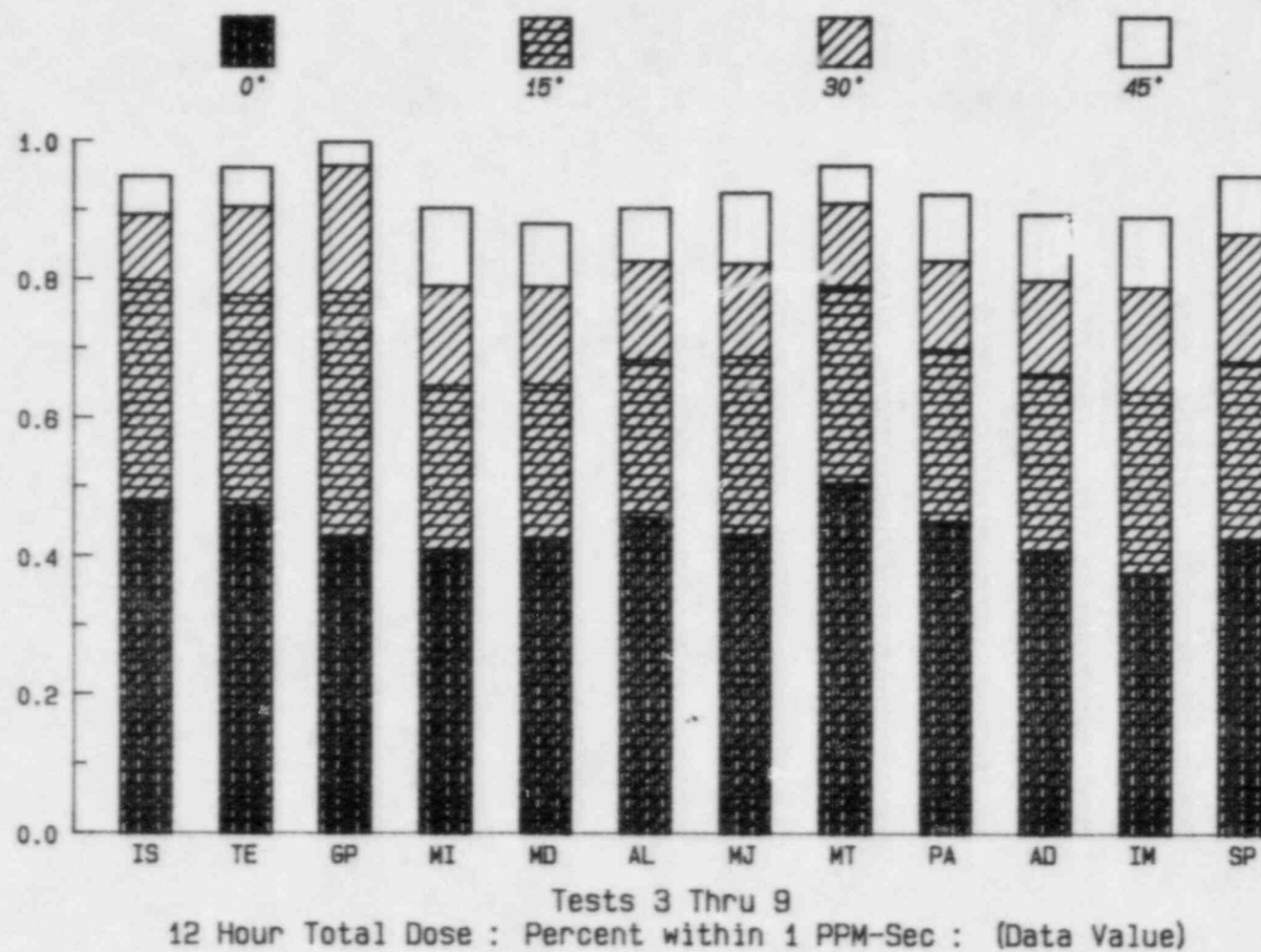


Figure 4.3

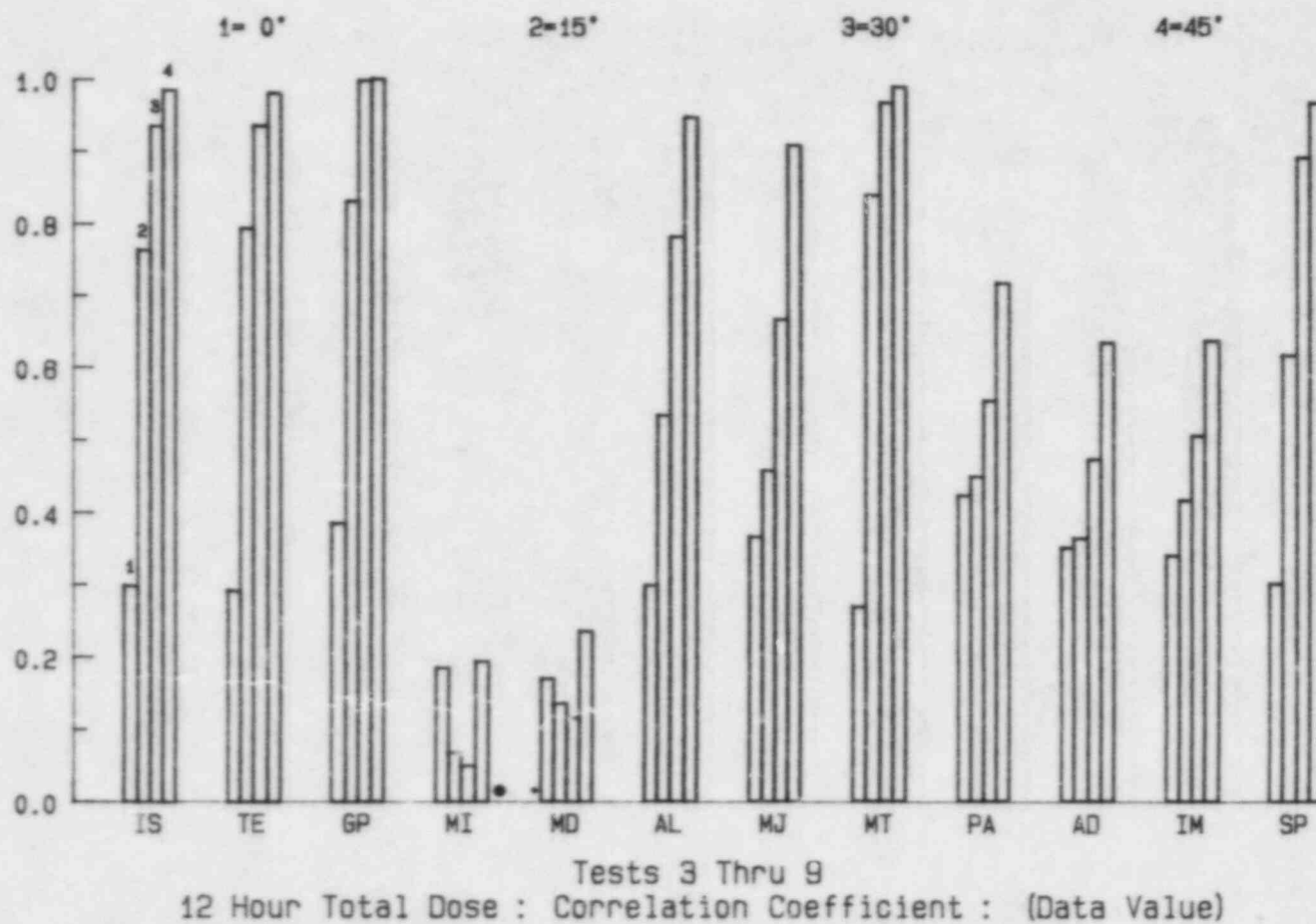


Figure 4.4



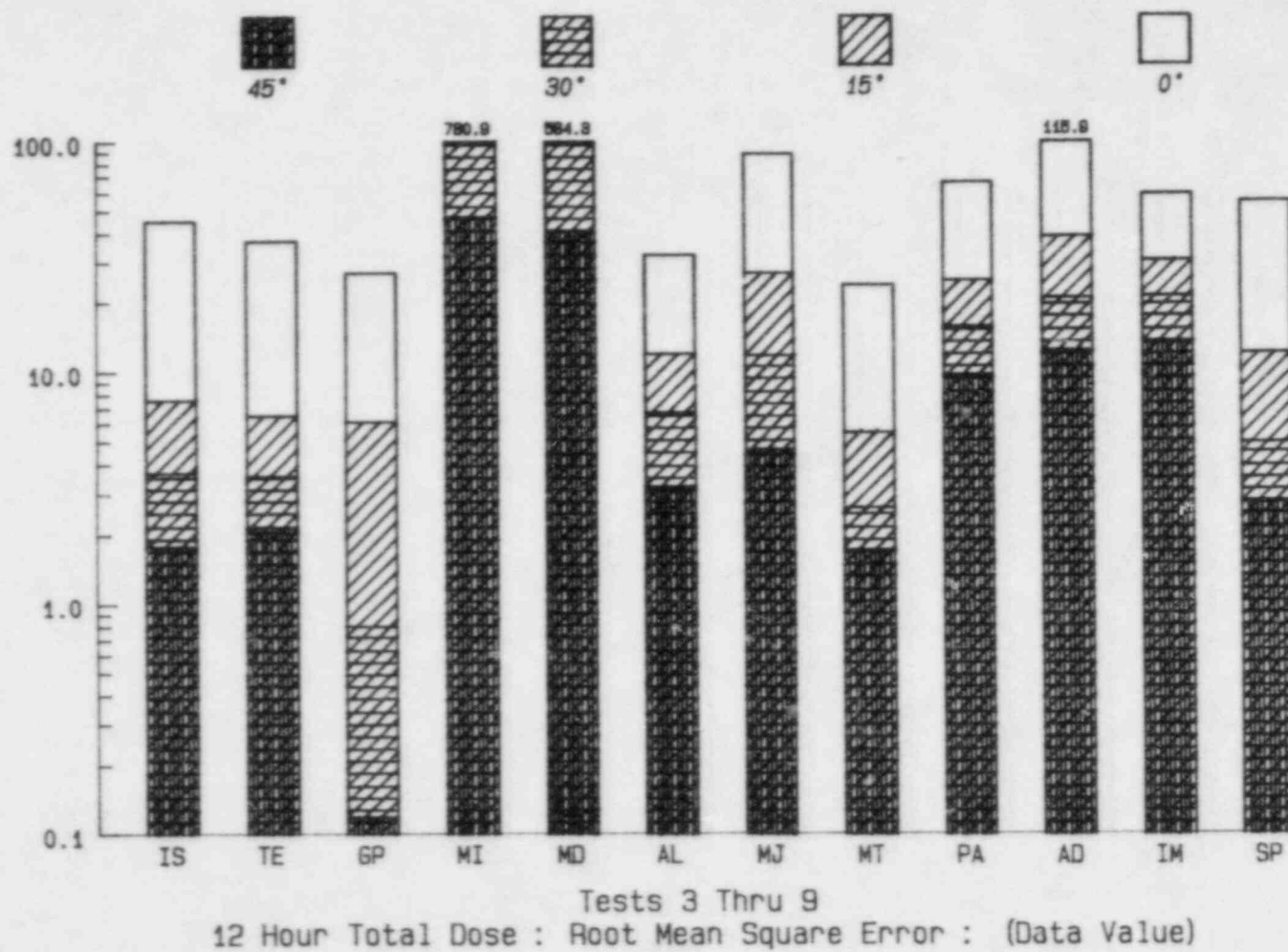


Figure 4.5



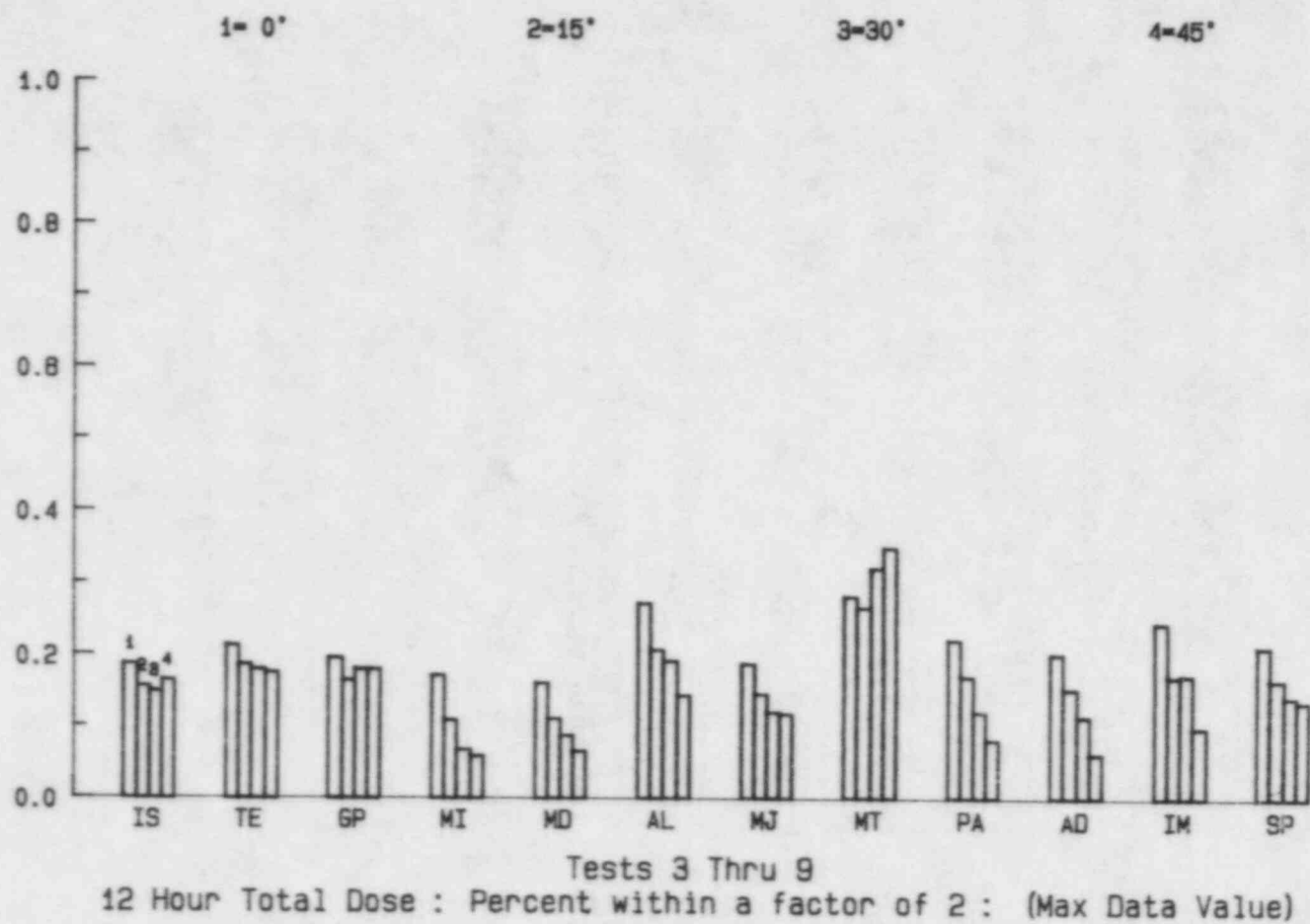
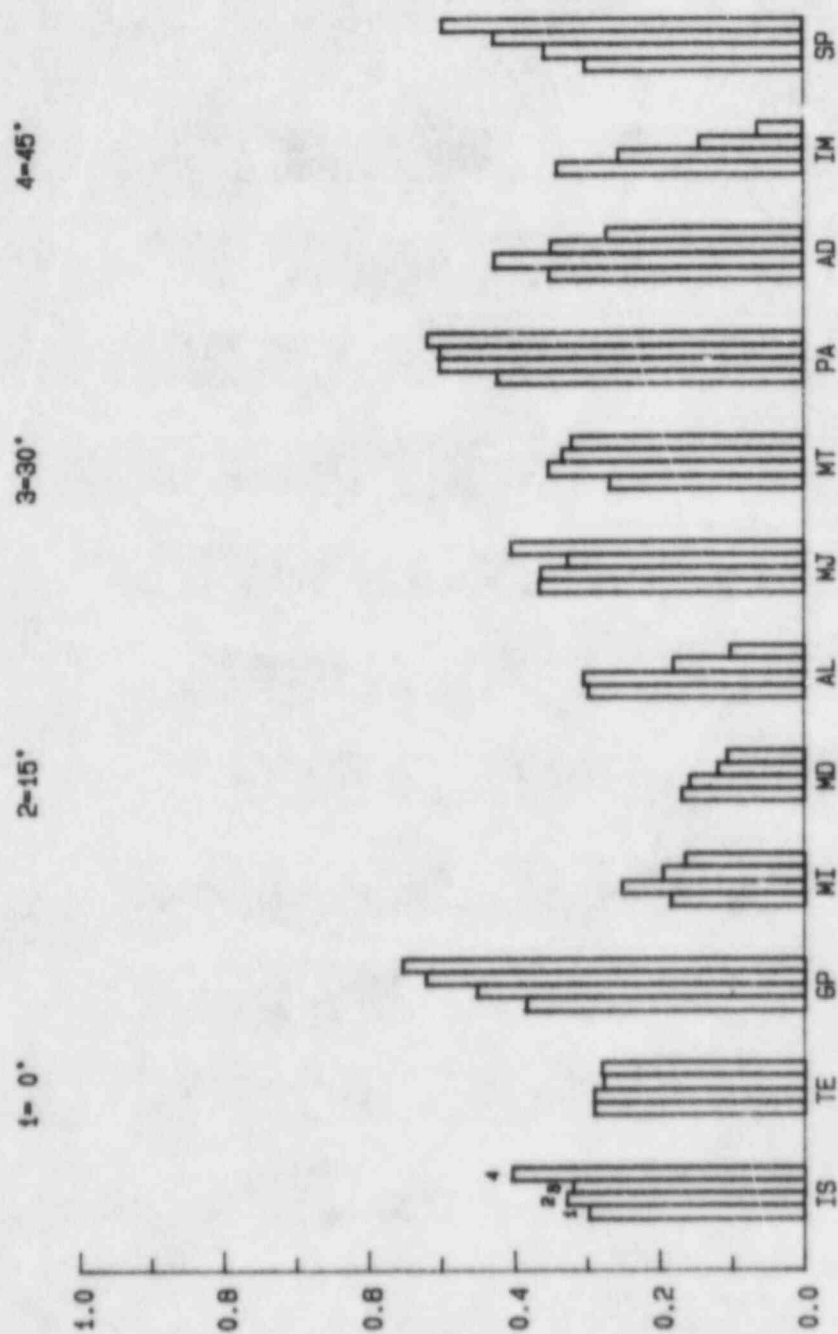
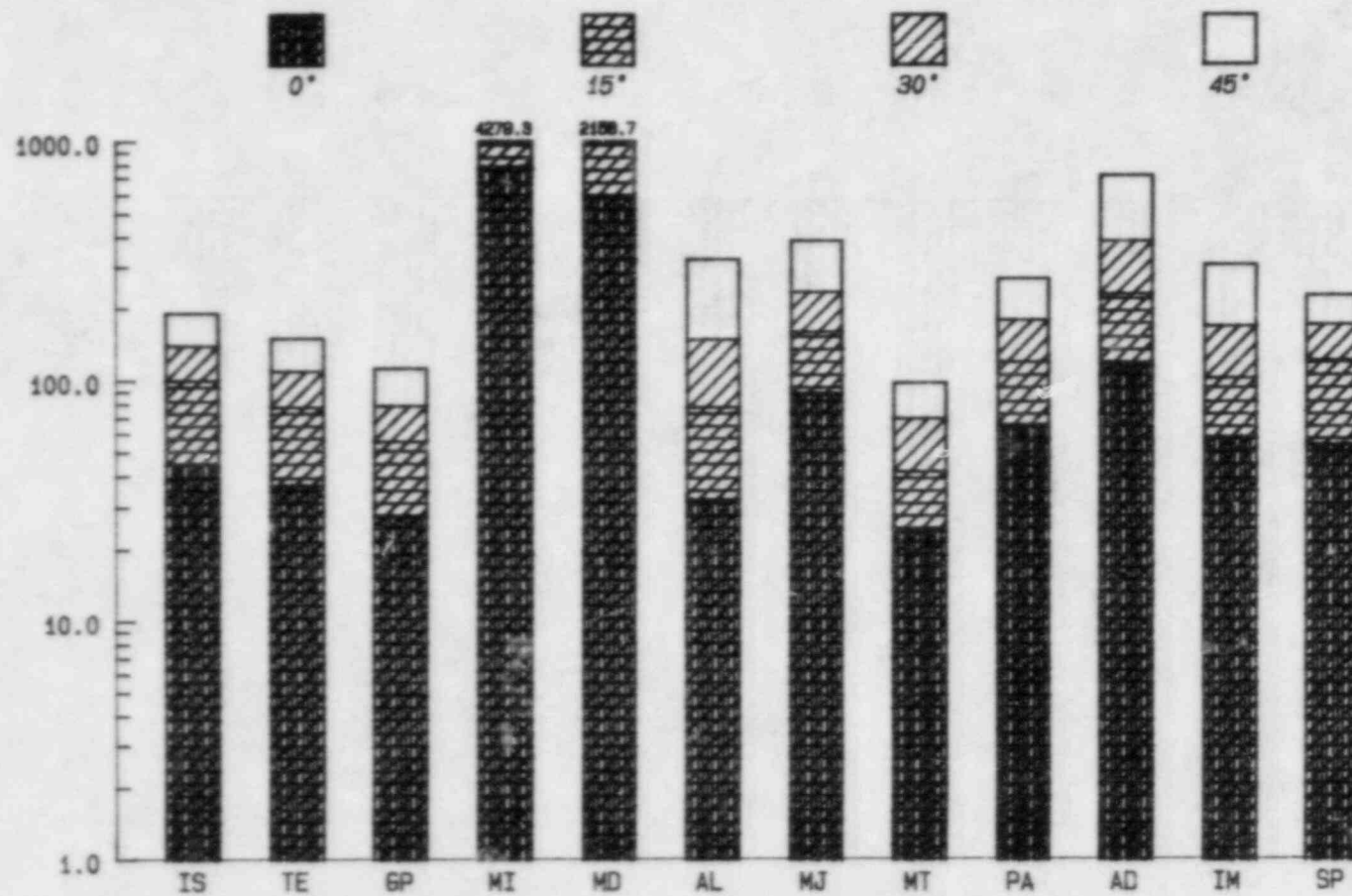


Figure 4.6



Tests 3 Thru 9  
12 Hour Total Dose : Correlation Coefficient : (Max Data Value)

Figure 4.7



Tests 3 Thru 9  
 12 Hour Total Dose : Root Mean Square Error : (Max Data Value)

Figure 4.8

penalizes the model more for over predictions in the larger area comparisons. The relative performance is often degraded by allowing the wider area comparison under this condition of only comparing the maximum values. The relative rankings of the individual models is not significantly changed from that of the earlier comparisons.

We can make several conclusions from the test. First, within this limited range of approximately 10 km, and for time averages as long as 12 hours, the Gaussian plume models perform as well or better than any of the other models. Second, among the Gaussian plume models, the new GP model demonstrates a definite edge over the two standard models. This is probably because the measured  $\sigma_g$  generally yielded a more diffuse plume than indicated for the stability class algorithms. However, it may also have been partly the result of the choice of winds more nearly identified with the source emissions. Third, Mesodif and MESOI suffer from an overprediction of dosage close to the source probably due to their simulation of the emissions as a surface release.

#### 4.2 Hourly Dose on the Fine Mesh

Figures 4.9 to 4.16 may be expected to show considerably less agreement between models and surface data when hour-by-hour comparisons are made rather than the 12 hour totals of the last section. This is not evident in the percent within a factor of two shown in Figure 4.9 which shows in excess of 40% as compared to the 20% of Figure 4.1. However, Figure 4.10 shows that a large fraction of these points are at or below the noise level. When these are eliminated and Figure 4.10 is compared with Figure 4.2 then the hourly dose shows somewhat fewer points agreeing within the factor of two particularly at the larger angles of comparisons. The percent within 0.1 ppm-sec shown in Figure 4.11 is higher than the comparable percent within 1 ppm-sec shown in Figure 4.3 due to the larger number of samplers recording data within an order of magnitude of the background value in the case of the hourly data. The fortuituous nature of the apparent better performance of many of the hourly comparisons is demonstrated in Figure 4.12 where for zero degrees

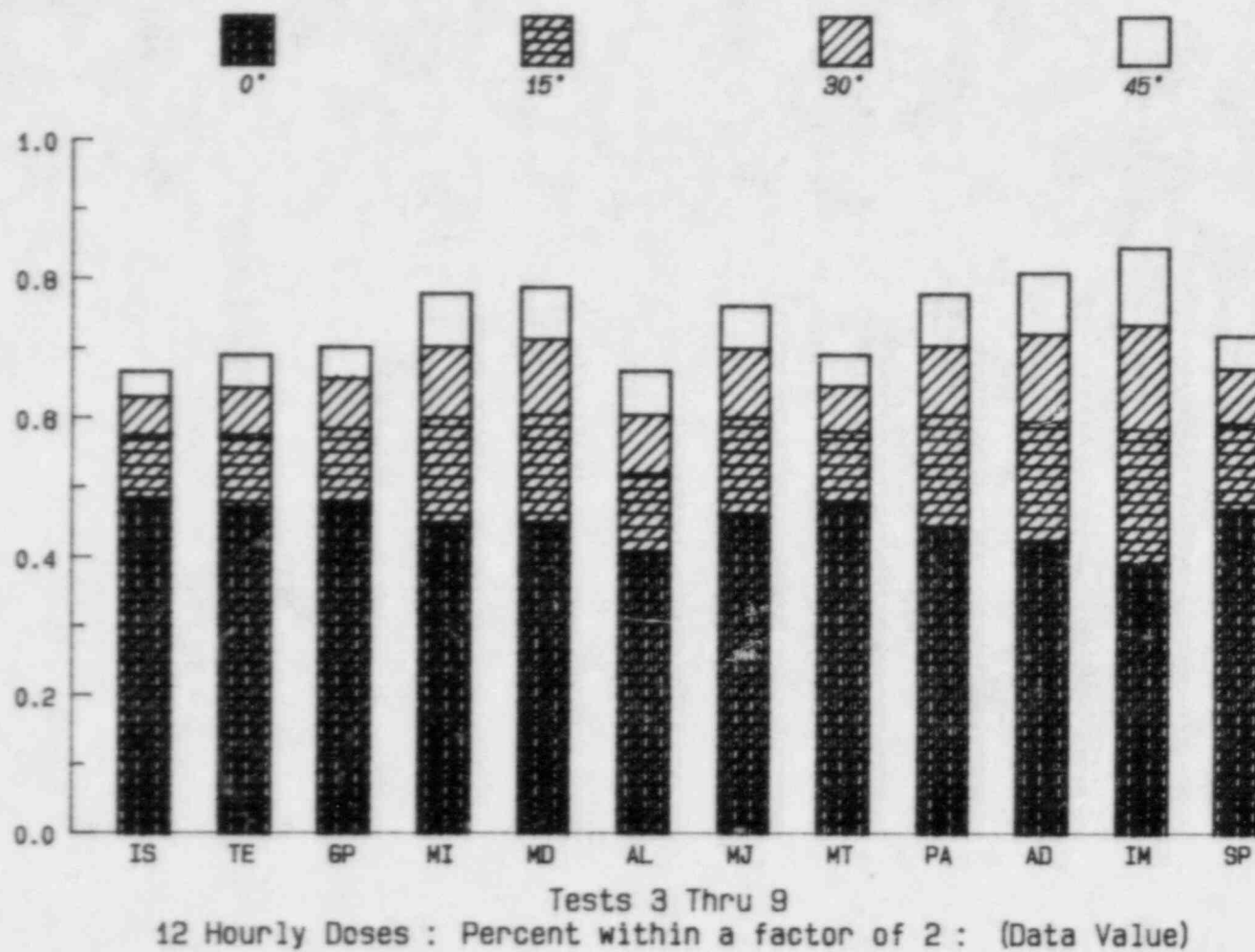


Figure 4.9

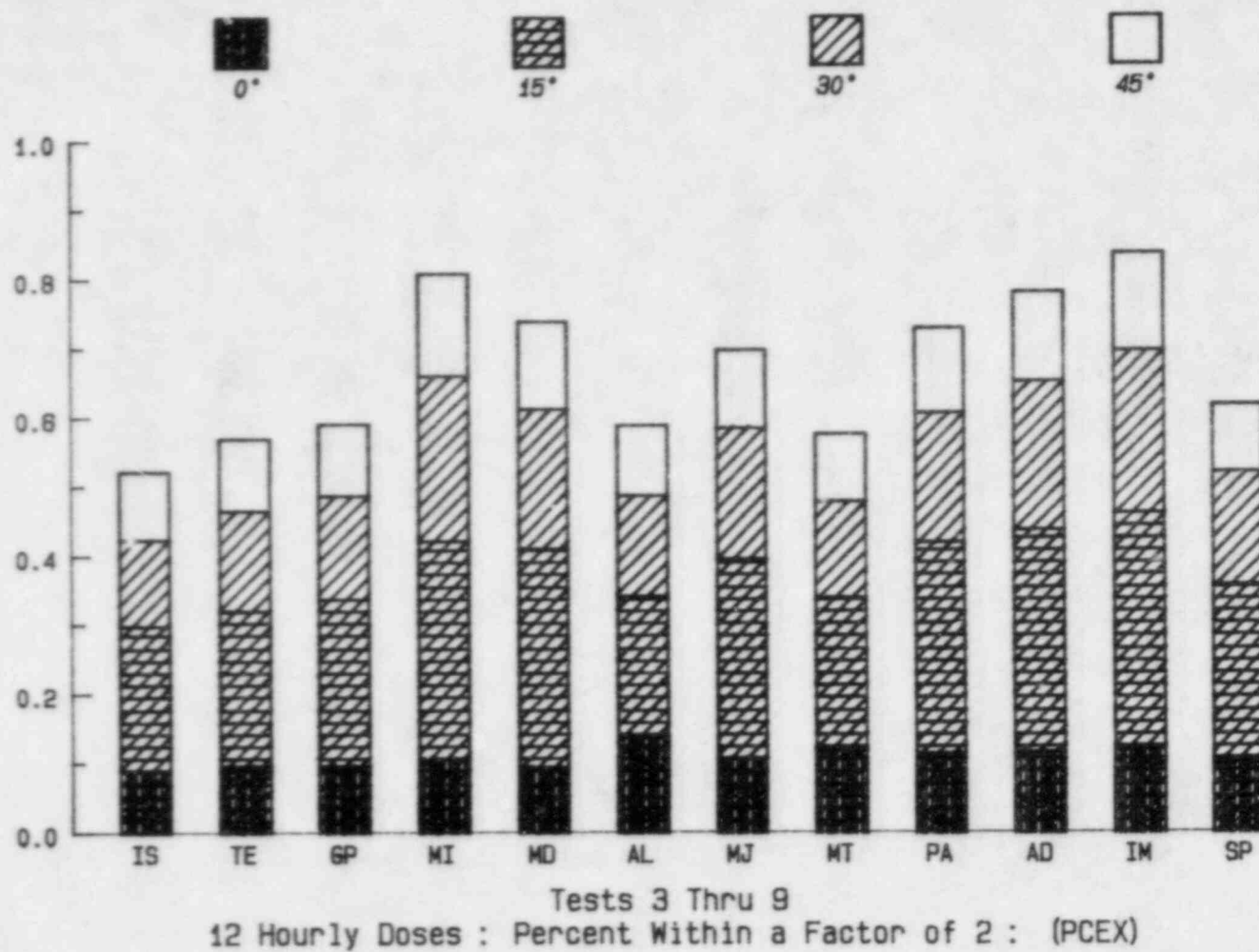
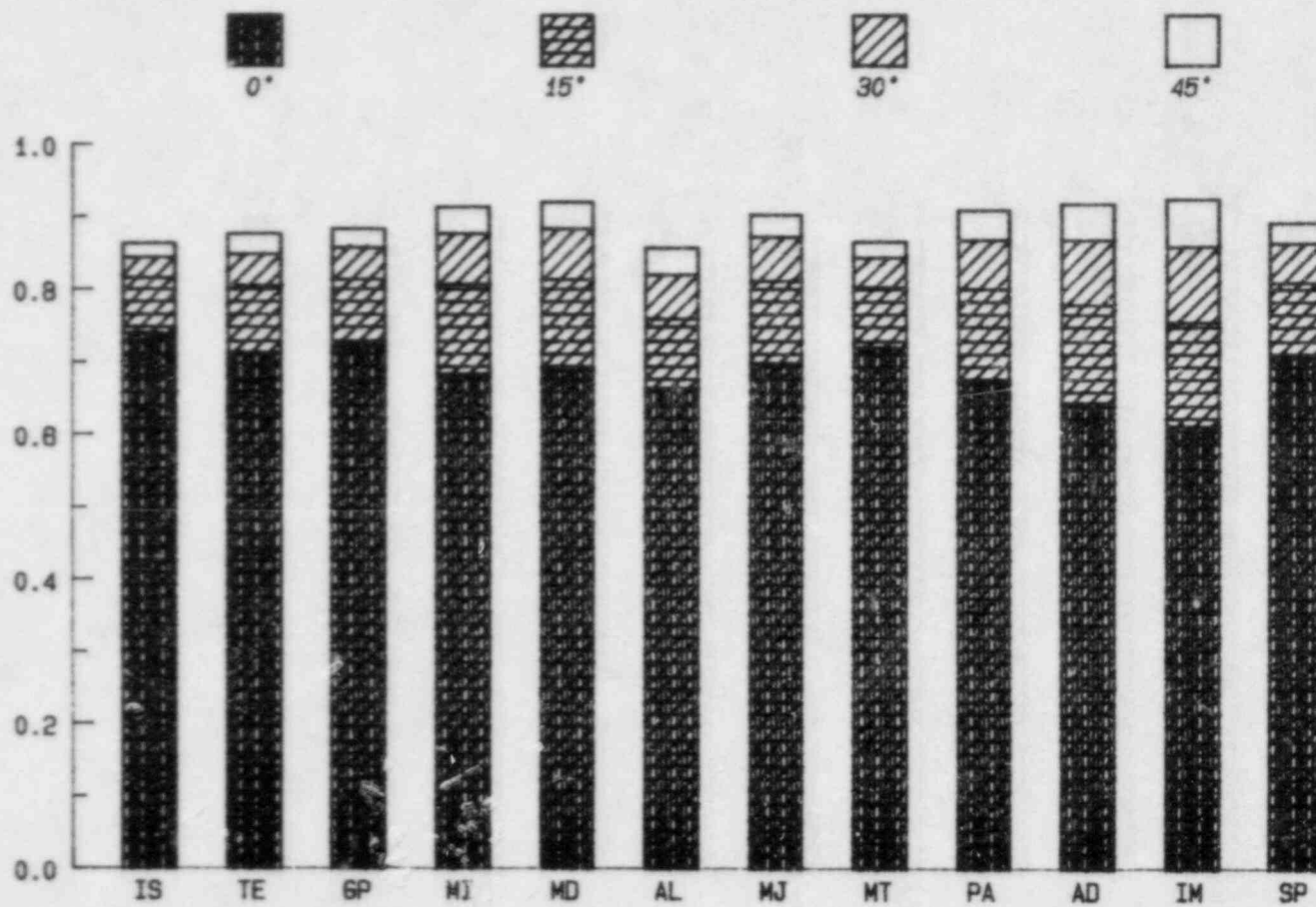


Figure 4.10



Tests 3 Thru 9  
12 Hourly Doses : Percent within 0.1 PPM-Sec : (Data Value)

Figure 4.11



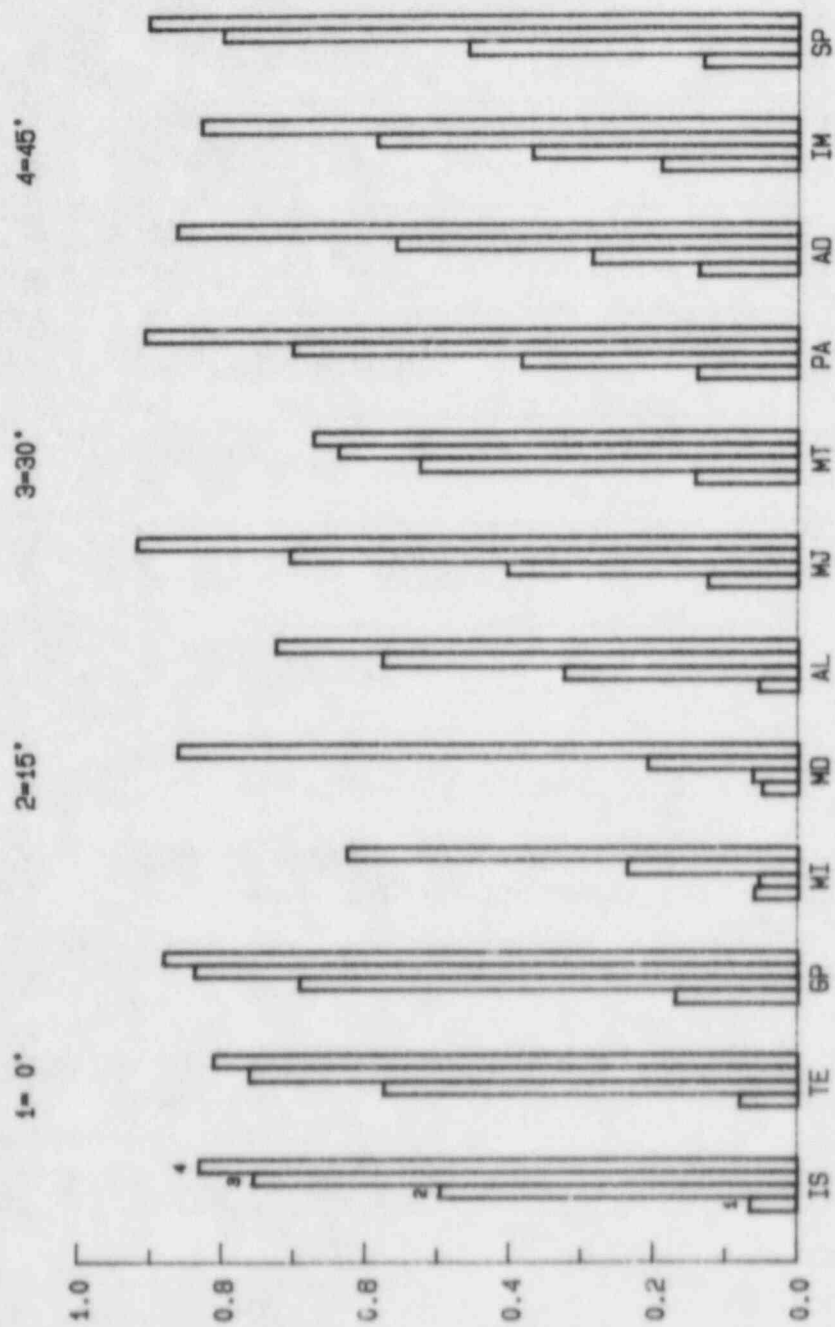


Figure 4.12

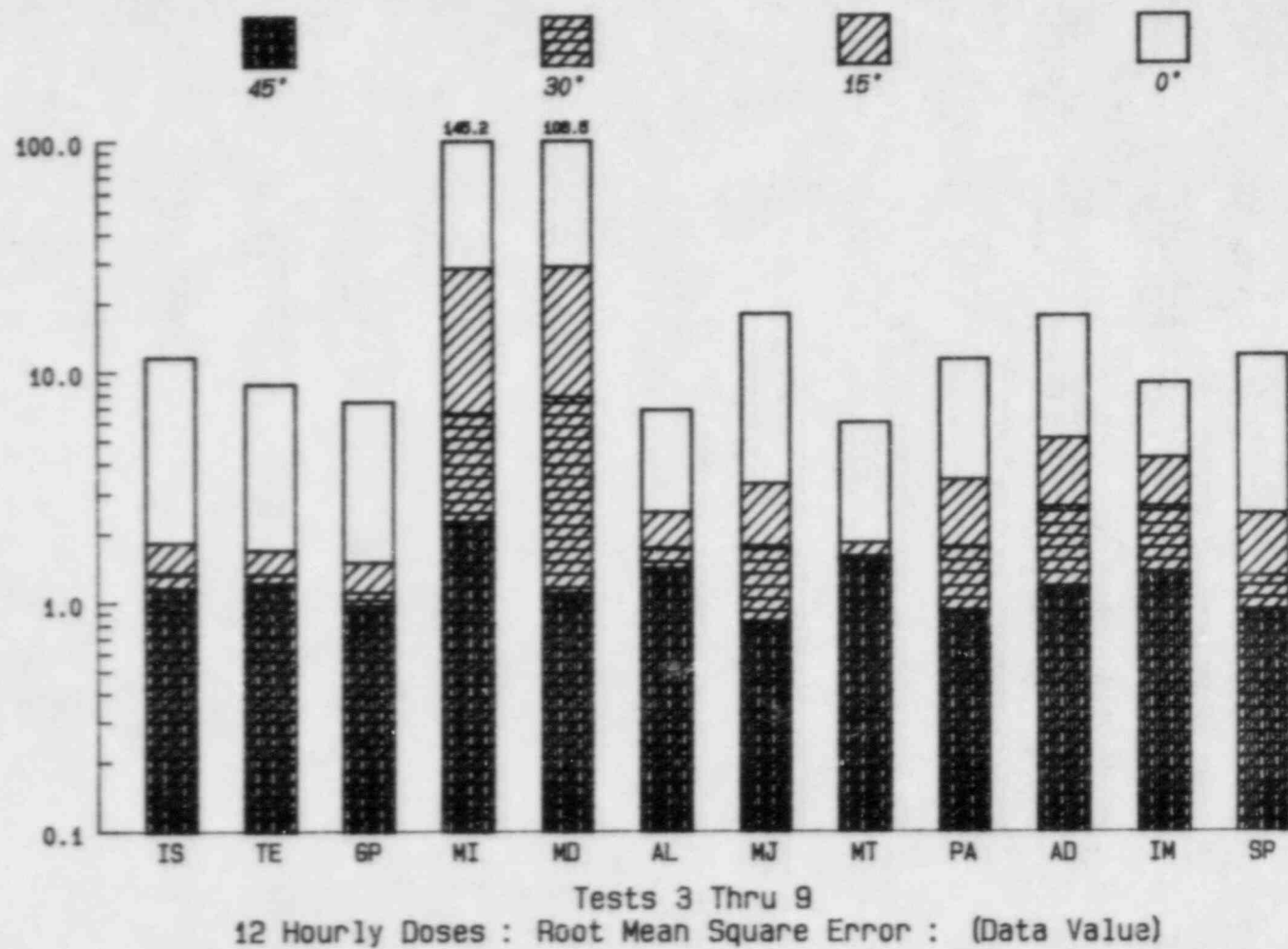
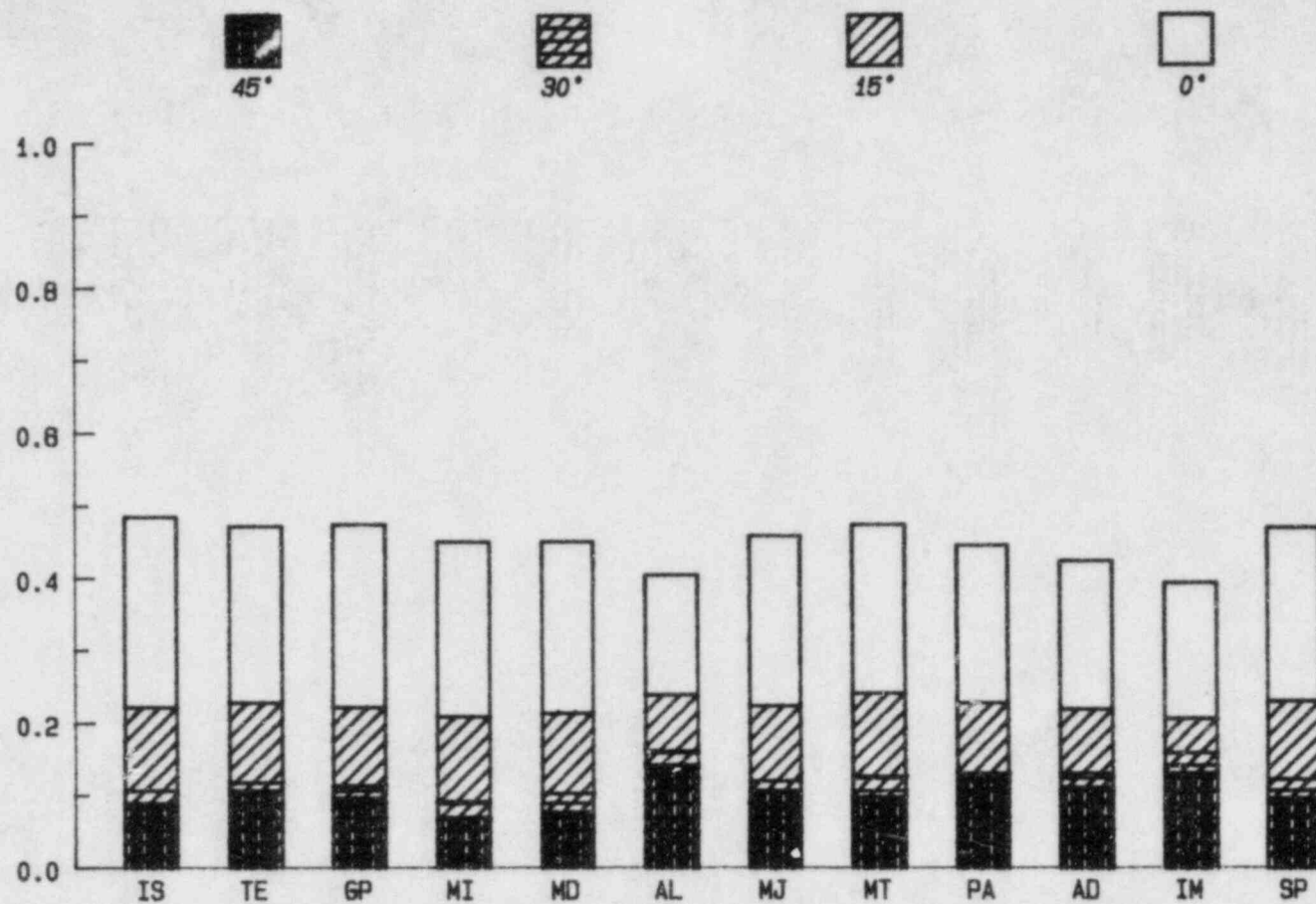


Figure 4.13



Tests 3 Thru 9  
12 Hourly Doses : Percent within a factor of 2 : (Max Data Value)

Figure 4.14

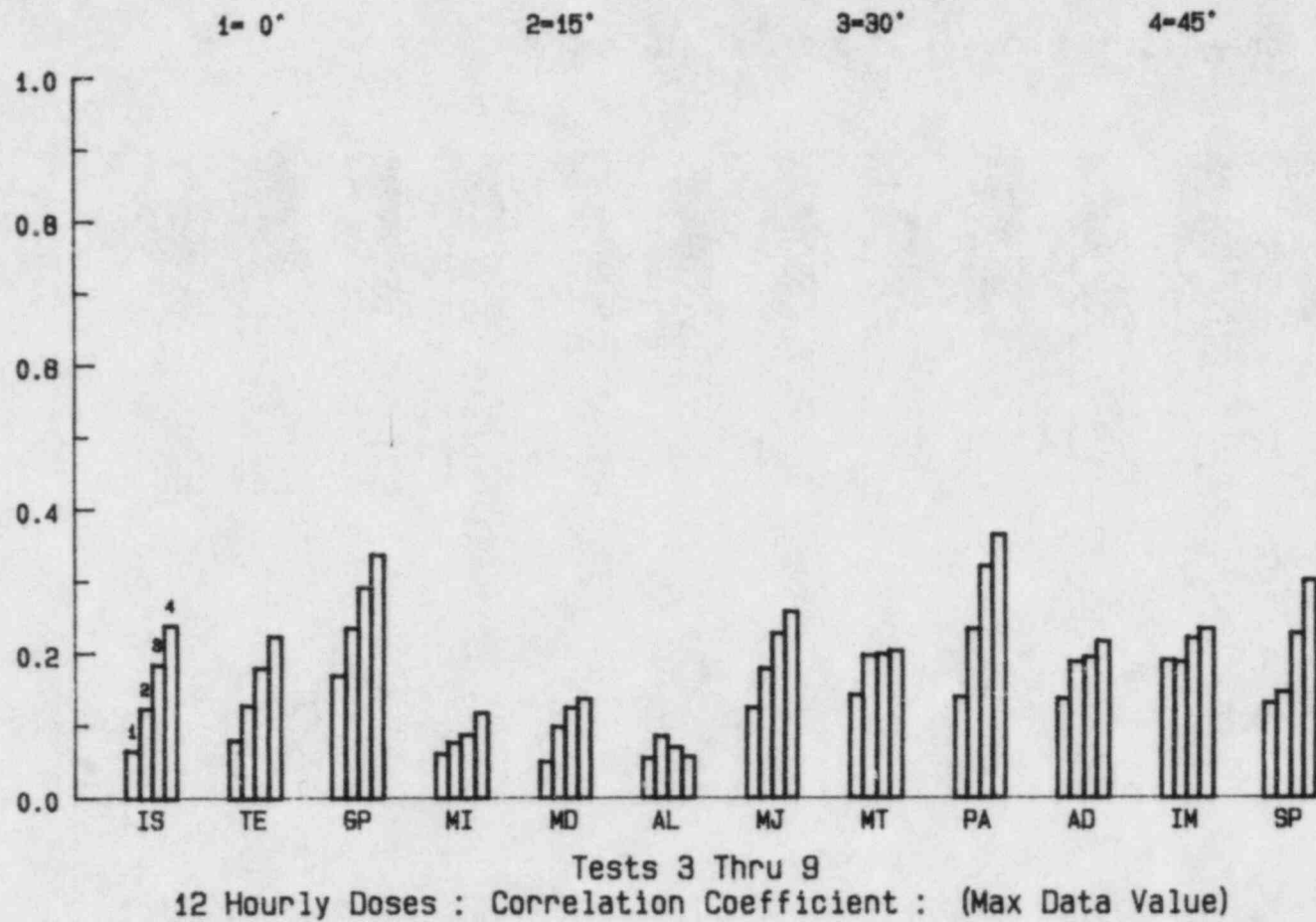
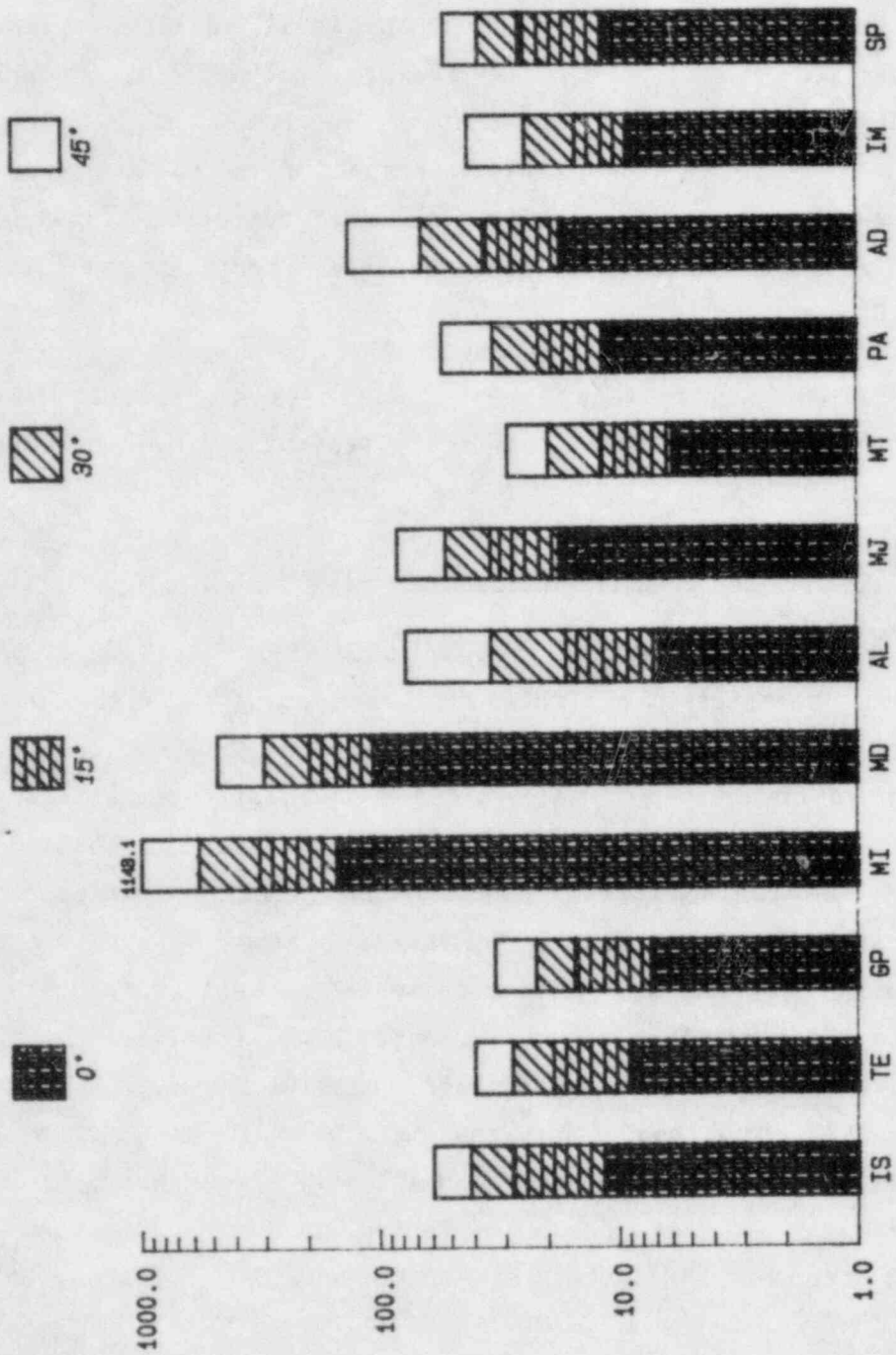


Figure 4.15



Tests 3 Thru 9  
12 Hourly Doses : Root Mean Square Error : (Max Data Value)

Figure 4.16

we see the correlation coefficient averages about 0.1, showing that on the basis of a point-by-point comparison there is almost no correlation between model results and data. When the models are given the benefit of shifts in position the correlation improves but still generally remains below the values for Figure 4.4. The average root-mean square error given in Figure 4.13 is also less than that in Figure 4.5 but not enough to preclude an increase in the relative error. Even the comparisons using only the maximum values in each test areas continues that trend of anomalously better performance on all the measures except the correlation coefficient in Figure 4.15.

The measures which show the biggest intermodel difference is the root mean square error which again show the effect of the overprediction of Mesodif and MESOI.

#### 4.3 Total Integrated Dose on the Coarse Mesh

Numerous problems were encountered in obtaining reliable samples from the total integrated bag samples (Dickson et.al. 1983). After detailed comparisons between the 12 hour total and the total dose samples in their region of overlap it was decided that total dose results for tests three thru six were much less reliable than that for the last three tests. Thus the comparisons used here for intermodel comparisons are confined to these last three tests. The actual patterns given by the data and calculated by the models are presented for all seven cases in Appendices A and B for qualitative comparisons. But, we believe that it is more appropriate to limit the detailed quantitative comparisons to those few cases where more confidence can be placed in the data. The quantitative comparisons were made based on all seven tests and it is, at least, reassuring that the models performed on average better in comparison with the more reliable data shown here than with the total data set.



The model expected to show the best performance over this extended range is MESOT (MT), since it has the advantage of using the input of the actual observed tetron tracks to determine the puff trajectories. This does not show up in the comparisons. There is a slight advantage indicated in Figure 4.17 and Figure 4.23, but it is surprising that it doesn't show a bigger advantage over the other puff models. We conclude that the precise knowledge of a few tetron tracks still does not provide sufficiently accurate trajectories of the ensemble of puffs released during the test.

The poorer performance of Mesodif and MESOI seen on the fine mesh has largely disappeared in these comparisons at the extended range. The most apparent remnant of this overprediction near the source is the larger r.m.s. errors in the max value comparisons of Figure 4.23. Although Mesodif shares the erroneous use of a surface release its use of six minute wind data apparently allows it to diffuse these high values faster and Mesodif shows no ill effect on this extended range.

The one curve where the more sophisticated models show a decided edge over the Gaussian plume models is Figure 4.22 for the correlation coefficient for the comparisons of the max values. This advantage is not apparent at the point-by-point comparisons of zero degrees but is apparent for the areas defined by  $15^{\circ}$  or more. The transport and diffusion models do not show an advantage over the puff models for any of the test measures.

#### 4.4 Lidar Plume Cross Sections

As part of our attempt to determine the reasons for the less-than-desirable agreement between model results and observations demonstrated in the last sections, we compared plume diffusion with data taken with the SRI Alpha-1 lidar system (Johnson et.al 1983). Table 1 provides the estimates of plume spread for a few specific hours during the test series as supplied to us by Dr. Johnson. These are compared with the corresponding model determined o's in Figures 4.24 and 4.25.

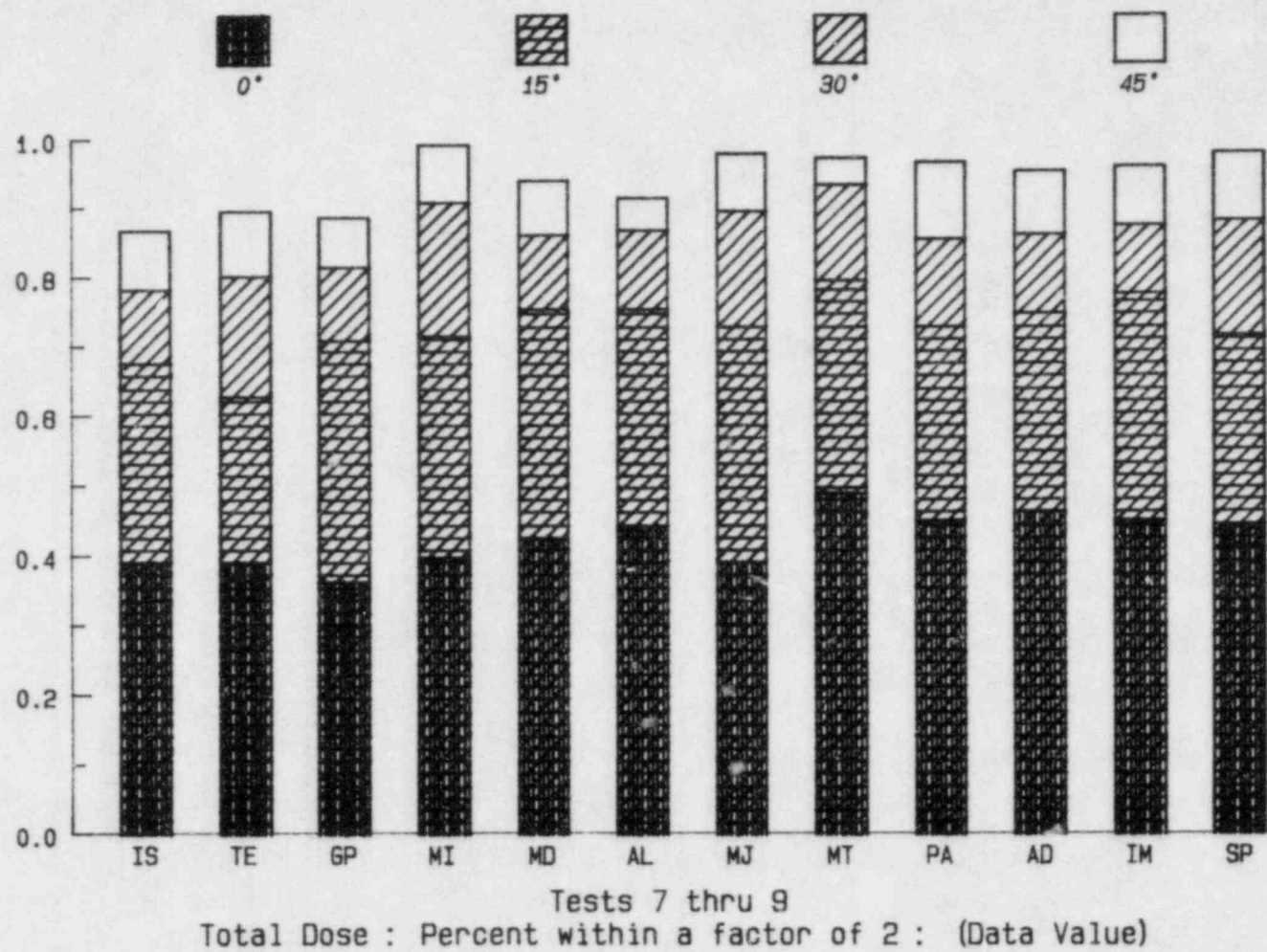


Figure 4.17

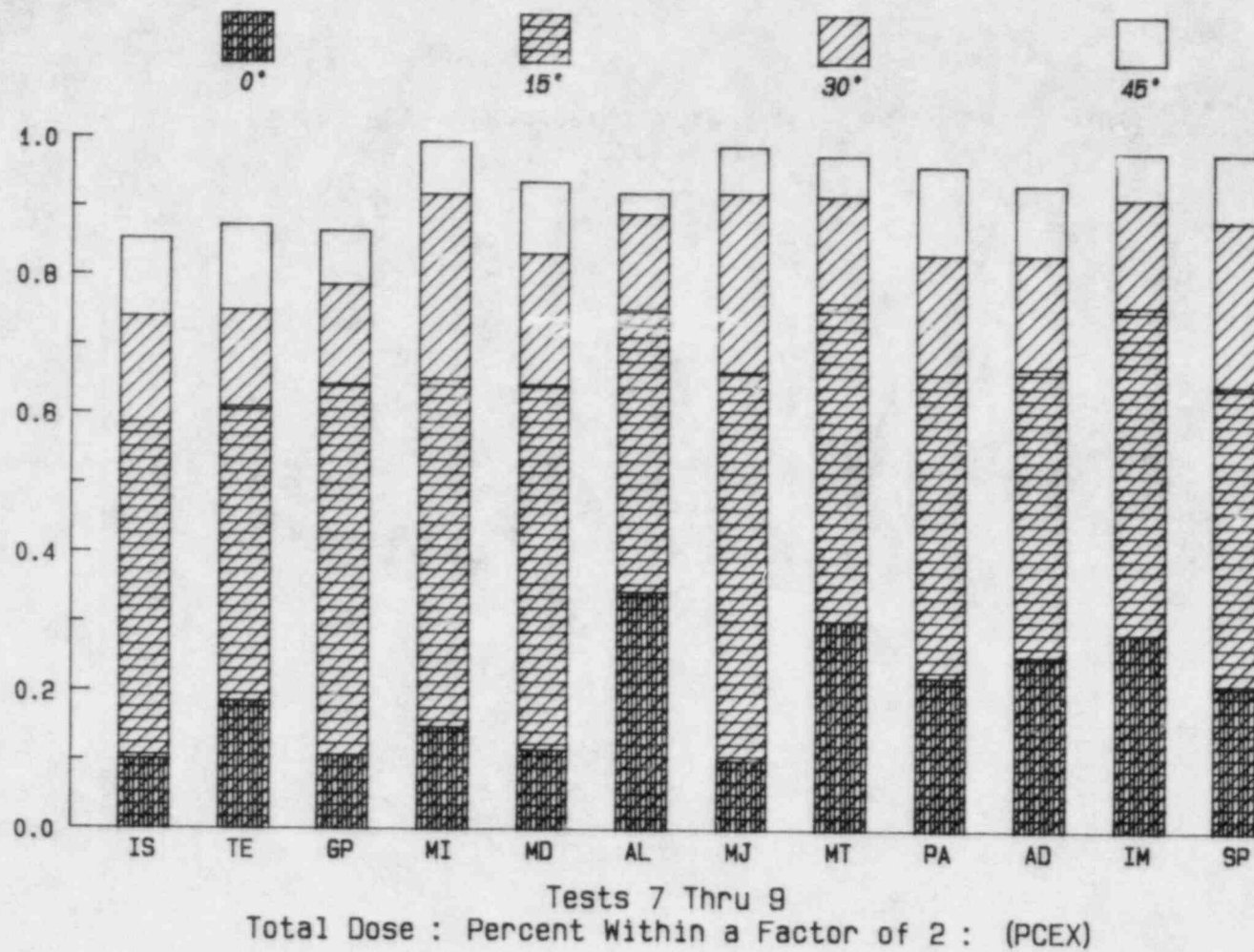
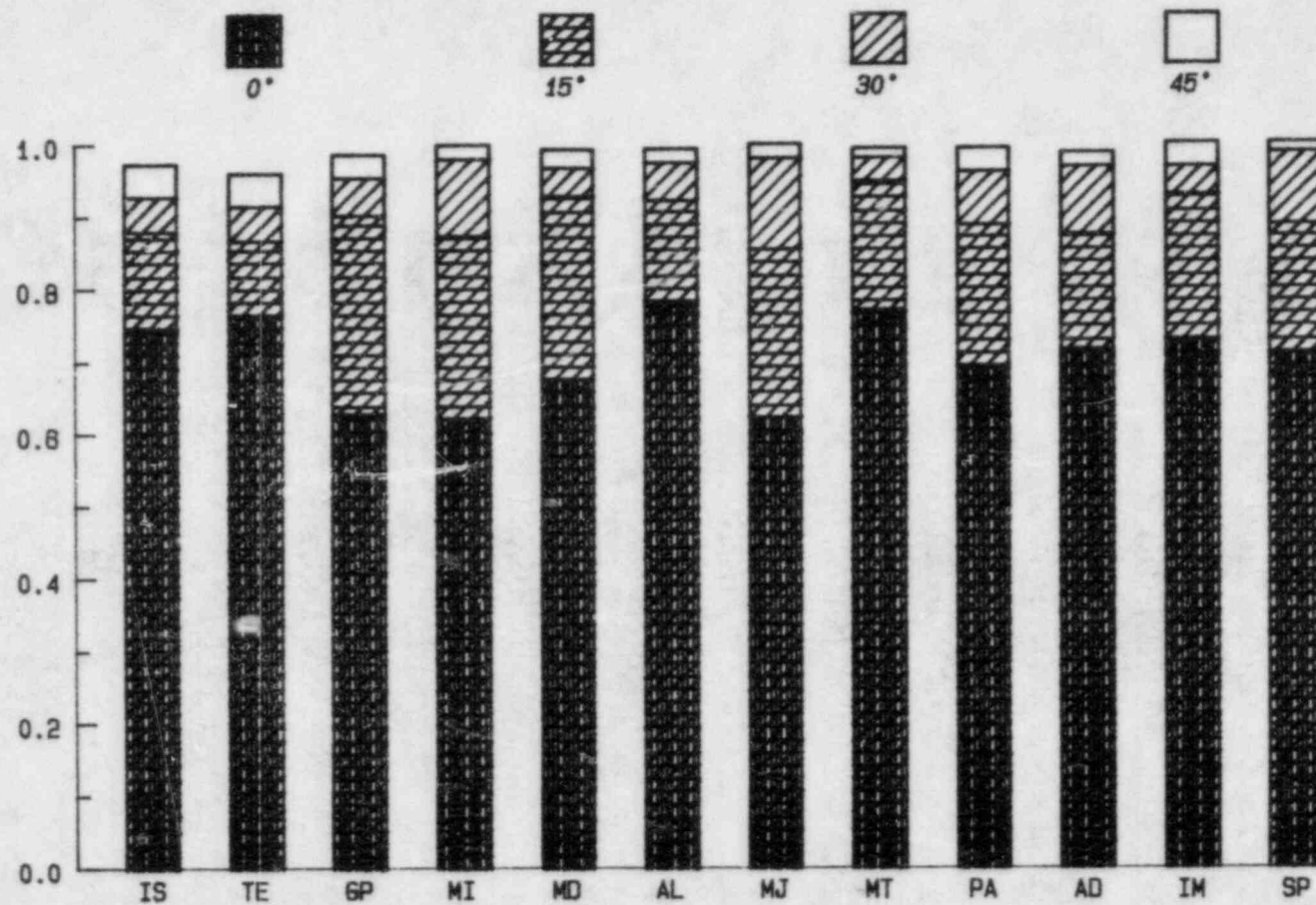


Figure 4.17b



Tests 7 thru 9  
 Total Dose : Percent within 1 PPM-Sec : (Data Value)

Figure 4.18

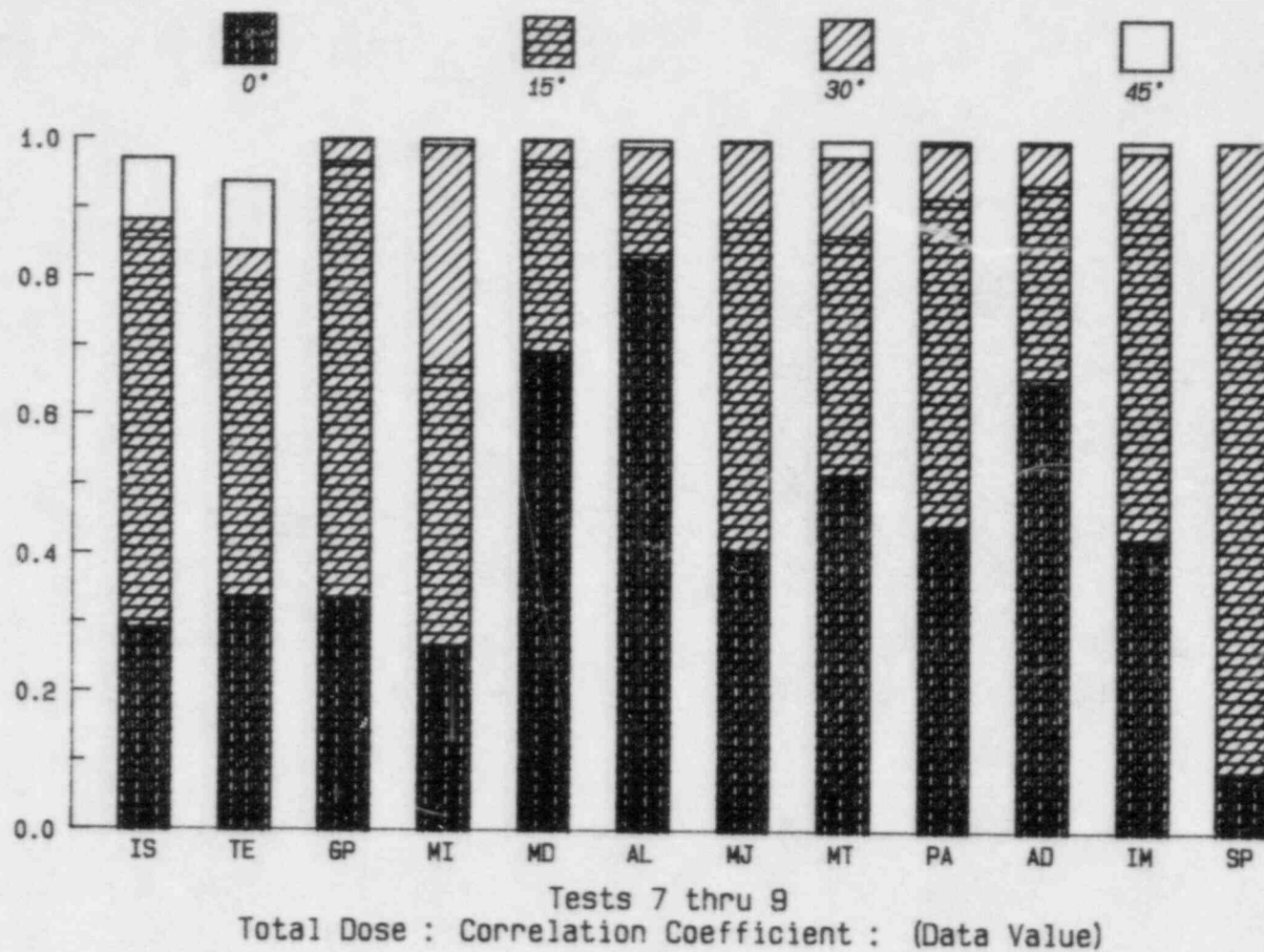


Figure 4.19



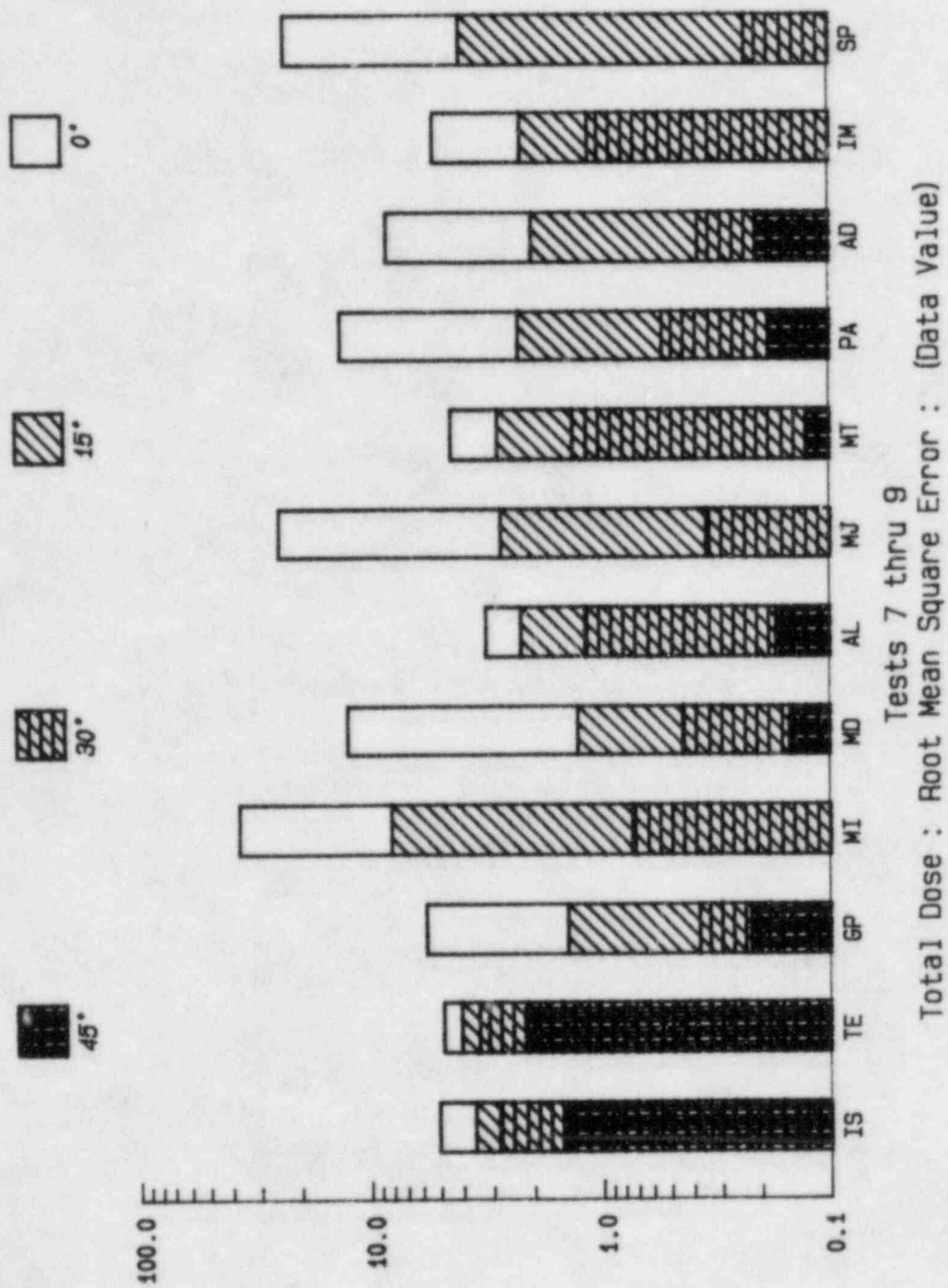


Figure 4.20



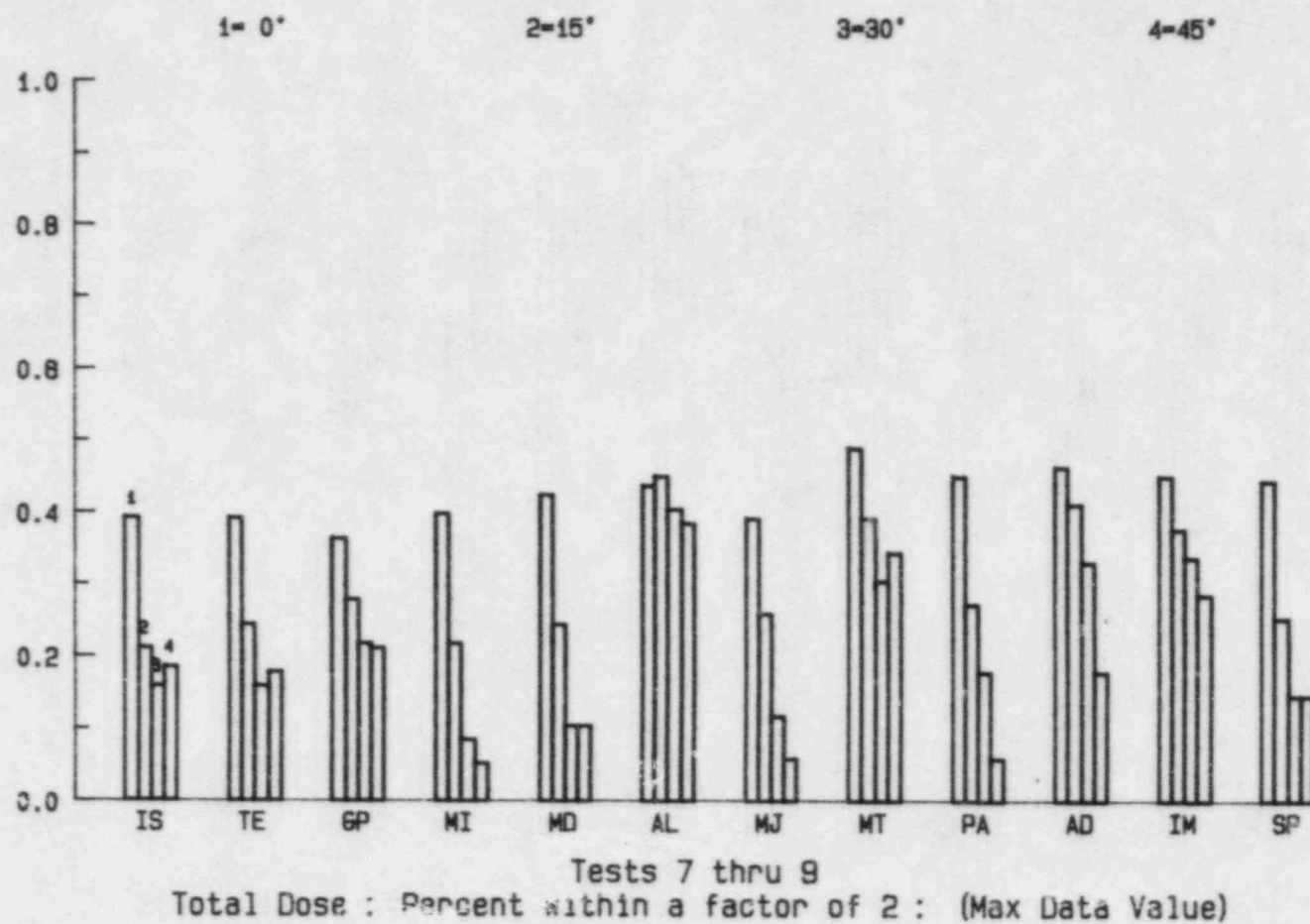


Figure 4.21

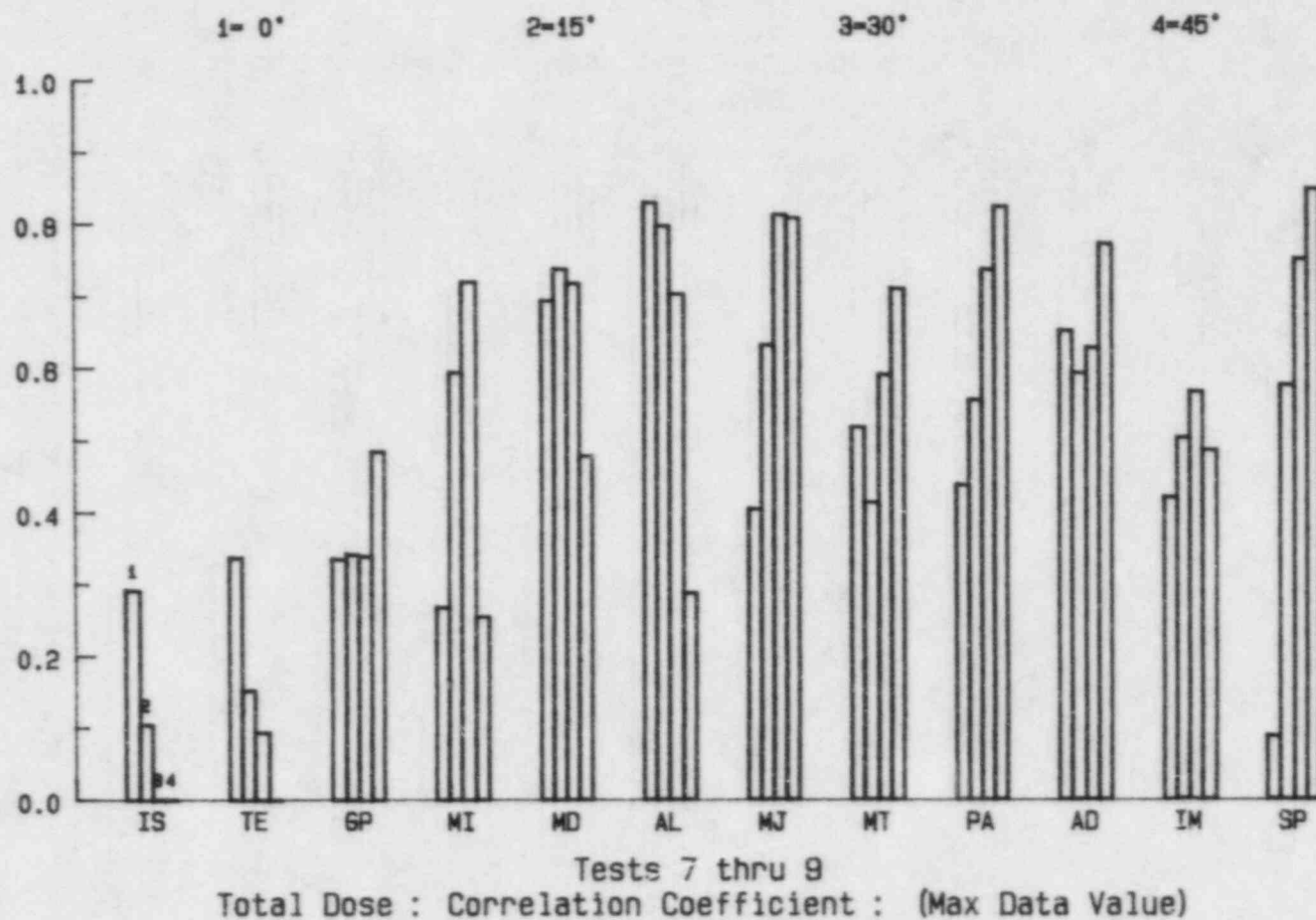


Figure 4.22

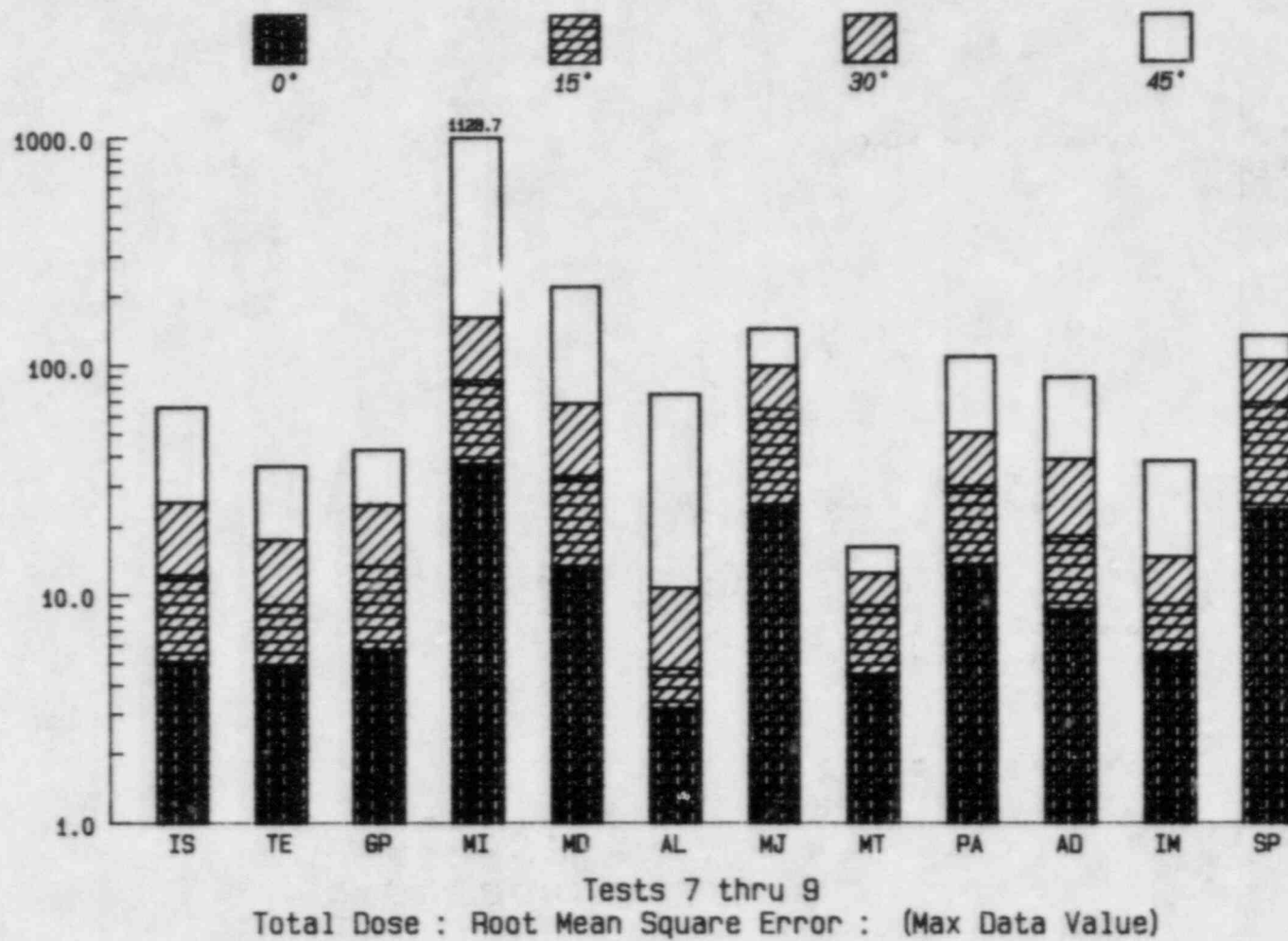


Figure 4.23

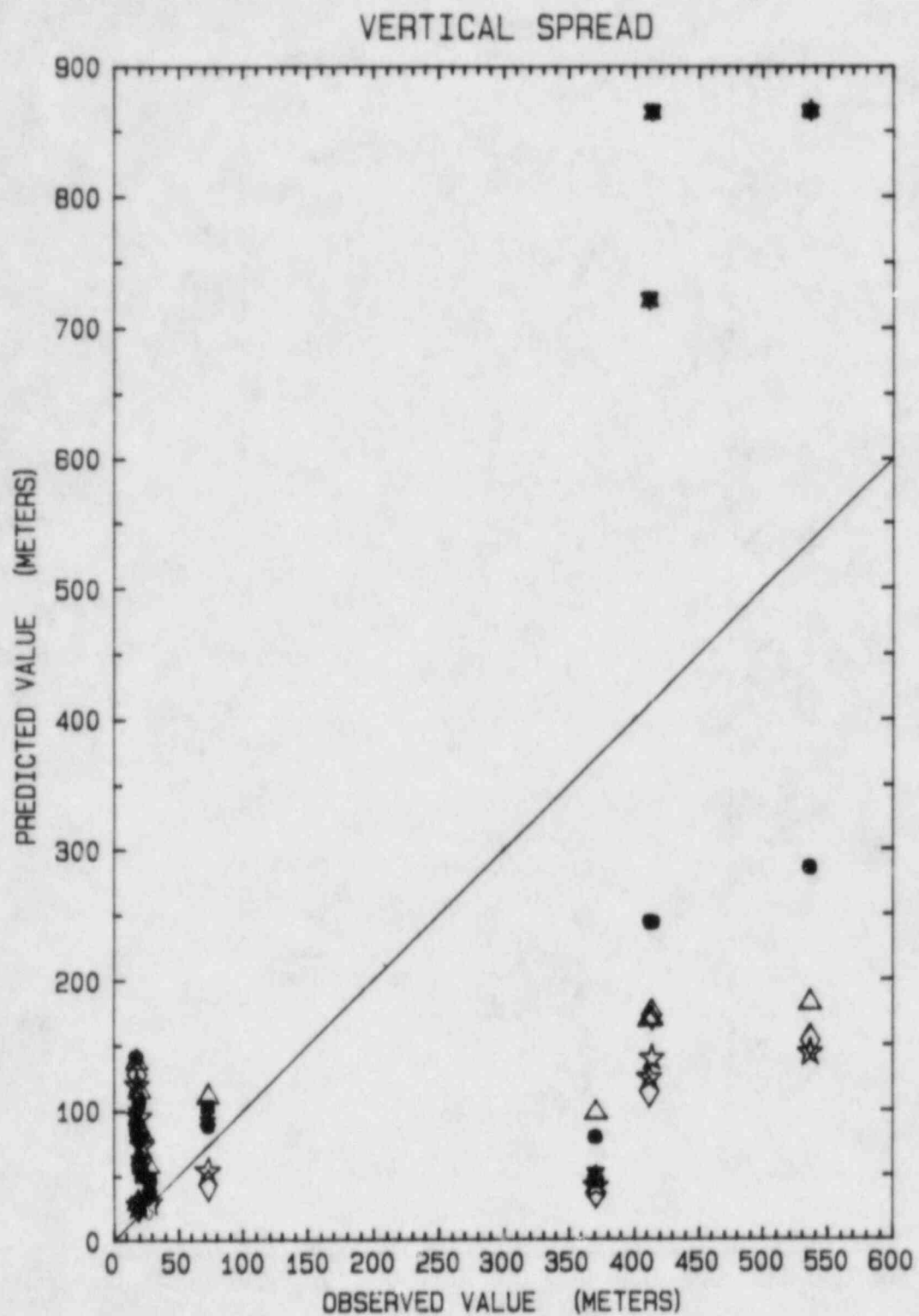
TABLE 1  
LIDAR OBSERVATIONS OF  $\sigma_y$  and  $\sigma_z$

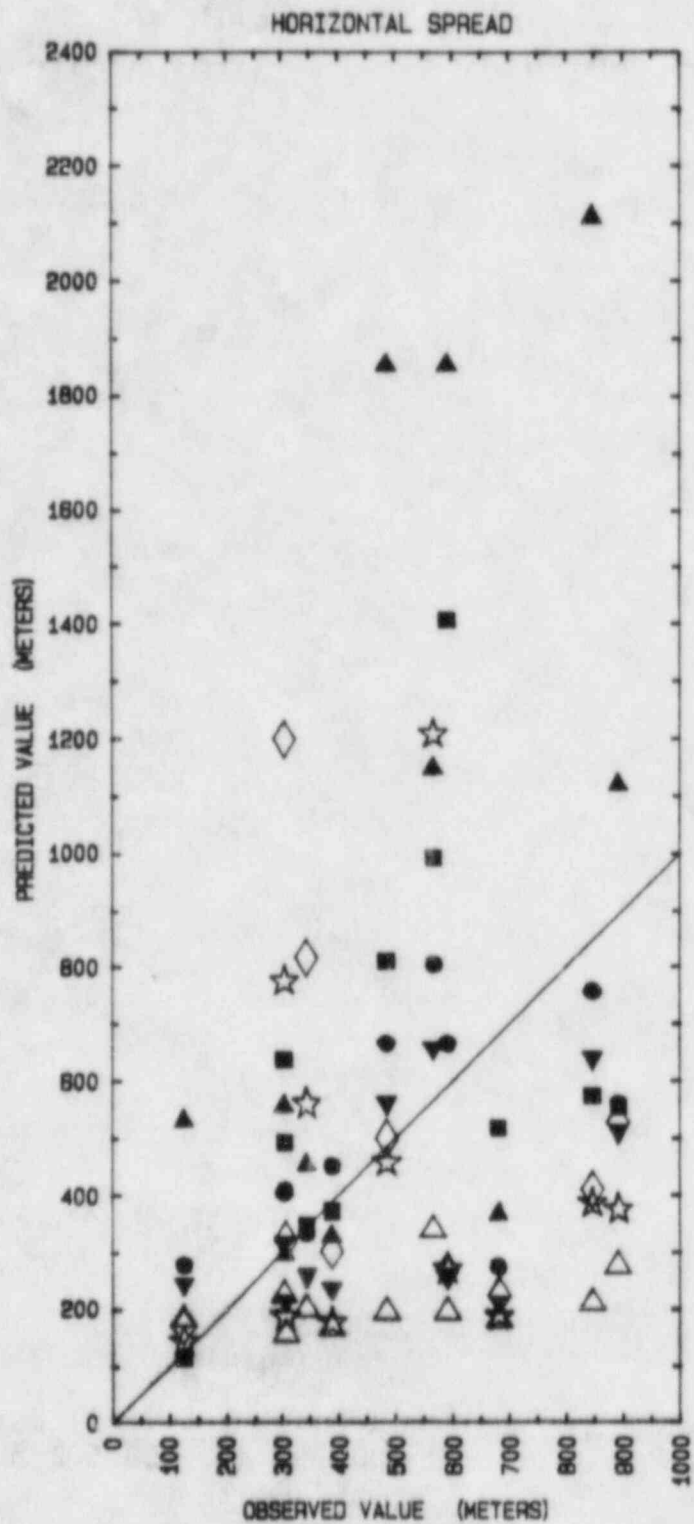
DAY	HOUR	RADIUS (M)	$\bar{U}$ (m/sec)	SIGMA $\theta^\circ$	INVERSION (m)	STABILITY CLASS	DATA		
							$\sigma_z$ (M)	$\sigma_y$ (M)	
1.	7-15	18-19	5900	5.6	11.	3000	C	752	892
2.	7-17	17-18	3500	7.8	13.	3000	D	371	682
3.	7-23	07-08	4400	2.7	11.	300	D	22	344
4.	7-23	12-13	3100	5.8	42.	2500	A	412	591
5.	7-25	23-00	5500	9.1	6.5	200	E	28	388
6.	7-26	00-01	4900	7.6	9.9	100	E	19	306
7.	7-27	14-15	3100	3.1	30.	3000	A	414	485
8.	7-27	15-16	3600	4.4	17.	3000	A	536	847
9.	7-27	20-21	2600	7.7	3.6	800	C	73	127
10.	7-29	07-08	12400	2.3	19.	500	D	18	566
11.	7-29	07-08	5500	2.3	19.	500	D	20	304

-----

Symbol Key for Figures 4.24 and 4.25

GP	-	Closed Square
ISC	-	Closed Inverted Triangle
TEM	-	Closed Triangle
MESODIF	-	Closed Circle
ADPIC	-	Open Star
ARL	-	Open Diamond
IMPACT	-	Open Triangle





MODEL PREDICTED HORIZONTAL SPREAD,  
 $\sigma_z$ , VERSUS LIDAR OBSERVED SPREAD.  
 SEE TABLE 1 FOR TIMES AND MODEL  
 SYMBOLS.

Figure 4.25



The comparison indicates that the model values are scattered within a factor of 3 above and below the indicated value. The best performance on this limited test is made by Mesodif and the descendant models which share its diffusion algorithms. This is perhaps attributable to the fact that these algorithms were derived from data obtained at this same site.

As seen from the surface data comparisons, any possible advantage gained by Mesodif and MESOI by their diffusion algorithms is lost by their use of a surface release. Thus if Figures 4.24 and 4.25 are a true reflection of the relative accuracy of the diffusive algorithms throughout the tests then MESOJ and MESOT should show more advantage in their performance on Figures 4.1 to 4.23 than is in fact evidenced.

## V. Real time tests of the ARAC System

The ARAC system was tested in real time on two of the cases, five and seven which form the basis of this report. In consultation with ARAC personnel, arrangements were made for the transfer of meteorological data from the INEL site to Lawrence Livermore National Laboratory as quickly as was possible under the experimental conditions. A report of LLNL's experiences during this exercise is given by Rosen (1982).

The MESONET wind system is accessible by telephone for interrogation, and the ARAC computer was linked into the MESONET computer to continuously monitor the surface winds during the test.

Estimates of mixed layer depth and stability category were passed to ARAC by telephone every hour.

Wind profiles from the RABAL site next to the source were sent by telecopier to ARAC approximately once per hour. These profiles were generally 30-40 minutes old since the data had to be processed before sending.

Temperature profiles from the radio sonde were telecopied every 3 hours, and one sounding was made 3 hours prior to the start of the release, so that a sounding was available with the initial notification of the release.

Finally, ARAC requested 24 hours notice of the release time, in order to arrange personnel scheduling efficiently. It is difficult to make a realistic assessment of response time under emergency conditions, since the system was ready and waiting for the release. However, the time taken to produce the first predictions of surface dose using the MATHEW/ADPIC codes was about 1 hour in both tests. This compares with a time of 3-4 minutes for a Gaussian plume model, and about 15 minutes for MESODIF (these timings obviously depend on the speed of the computer to some extent).

The general method of operation of the ARAC system was to update the prediction each hour using a 2-hour persistence forecast. Thus, ARAC predictions were generally about 1 hour ahead of real time, since the calculations took about an hour to set up and run. The profiles used for the runs were also slightly out of date, since it took 30-40 minutes to transfer

the data to ARAC. The persistence forecast was replaced with measured data when it was available, and the forecast then moved on in time. The results included in the comparisons here are the final ARAC calculations, i.e., using the measured data without any forecast.

The ARAC calculations were made on the large domain, i.e., with a 2.5 km grid length in the horizontal. However, to facilitate comparison with the observations and other model results, the calculated doses are plotted in the small domain where appropriate.

Figure 5.1 shows the ARAC prediction for test five. The pattern for the third hour shows some extension toward the West, and some toward the South. The values to the West are significantly lower than the observations in Figure A15, and the highest predicted values are up to five times the highest observation. As in the other models, the lack of horizontal spread produces overestimates of the surface dose. The two total dose results are also shown in the figure. These should be compared with the observations in Figure A18.

The prediction for test seven is shown in Figure 5.2. The hourly dose for hour two shows reasonable agreement with the observations in Figure A27, but the magnitudes are too high. The general shape of the fields is in line with the other models, and the statistical measures are also similar.

The ARAC results are different from our own MATHEW/ADPIC results for these same two cases for several reasons. ARAC used a slightly different grid system, so that the source does not lie exactly on a grid node, and they also used the real-time data which was both limited in extent and delayed in time. There was also one code modification which was made at ARAP with a view to improving the prediction close to the source; surface concentrations for sub-grid particles were calculated using the sub-grid Gaussian shape assumption, rather than averaging over a 2.5 km wide grid-box.

Figures 5.3-5.14 show the data comparison test results for the ARAC real-time prediction. We also show the Gaussian plume model results from TEM and ISC, and the puff model MESOJ. These last three models could have been run in real time since they only use the surface network winds which were directly available to ARAC. A cursory examination of the figures reveals that

the ARAC results yield performance measures which are very similar to the other models, and do not show any advantage over the Gaussian plume results.

July 1981 INEL Field Experiment : Test 5  
Real Time Model Predictions : ARAC System

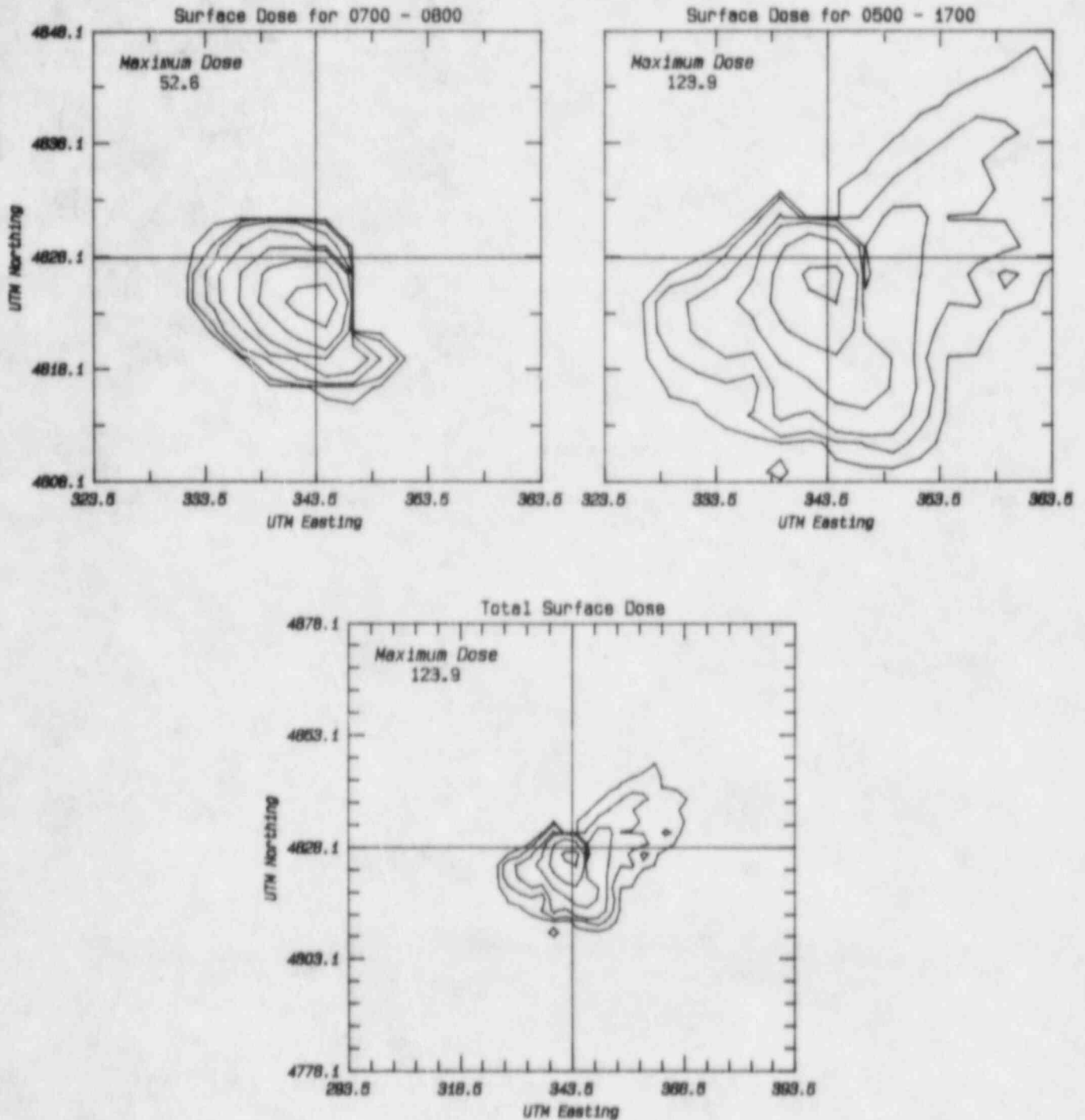


Figure 5.1

July 1981 INEL Field Experiment : Test 7  
Real Time Model Predictions : ARAC System

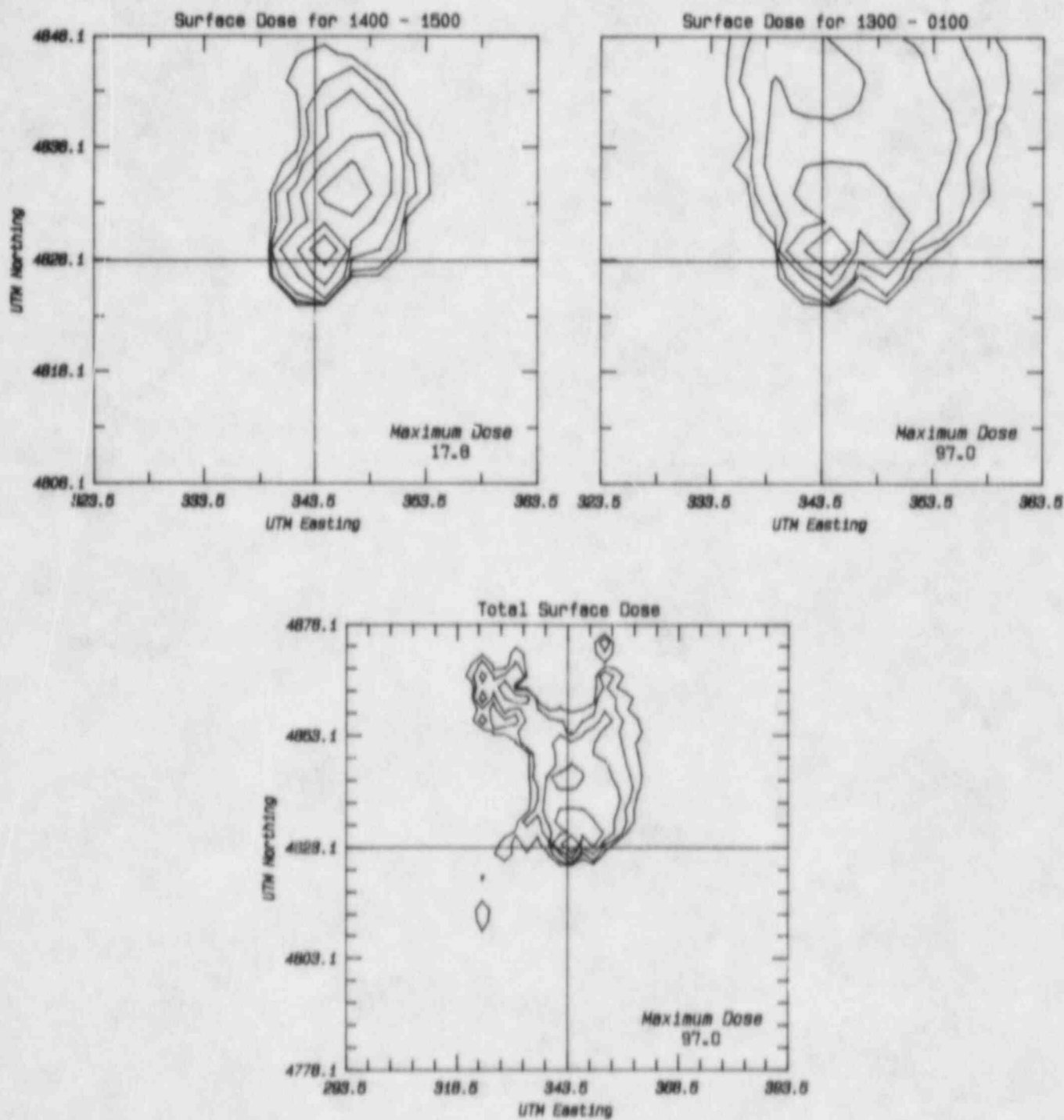
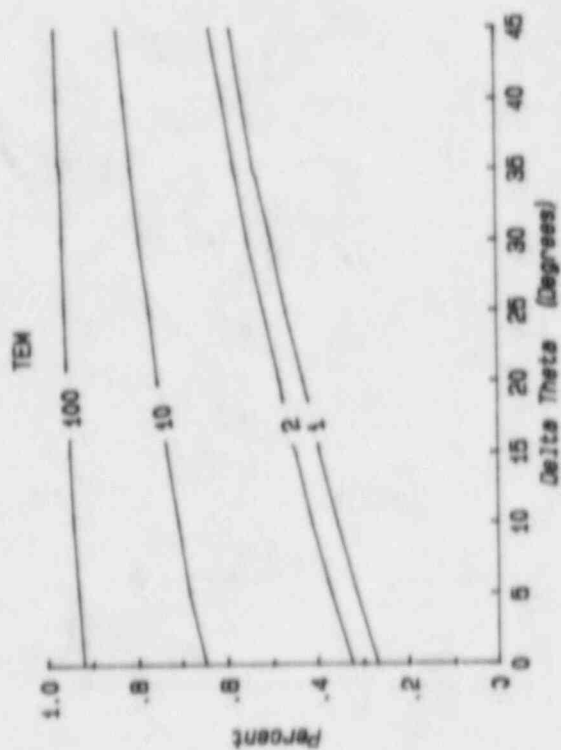
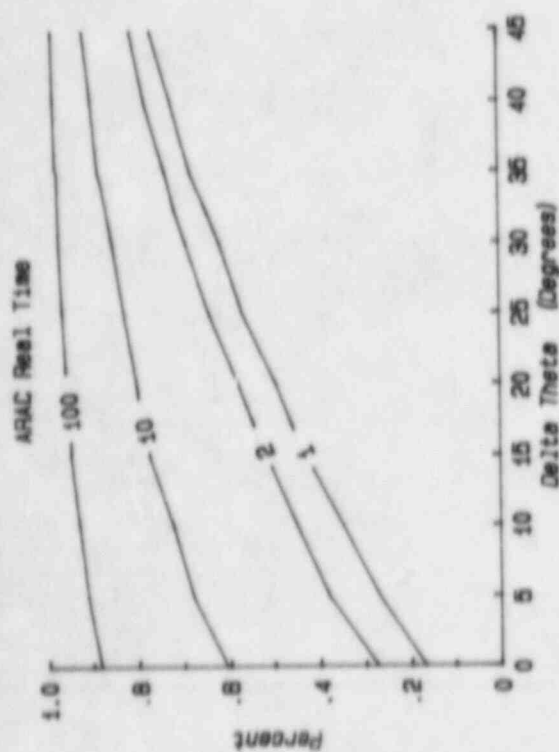
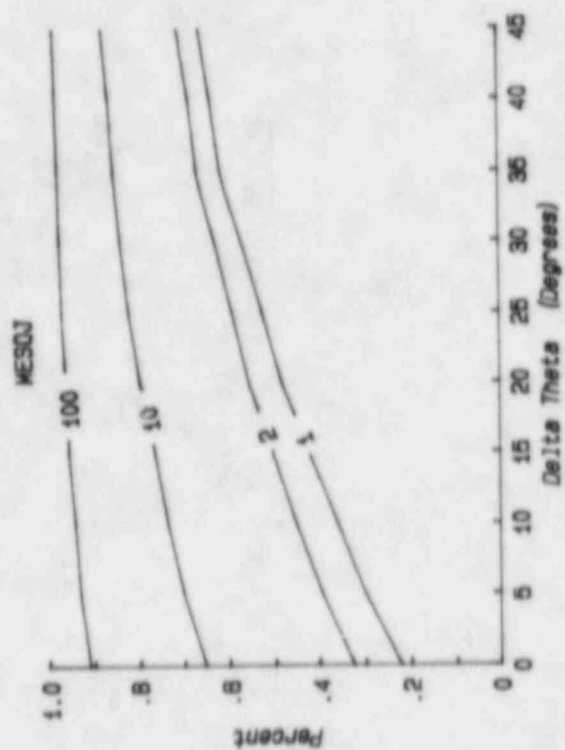
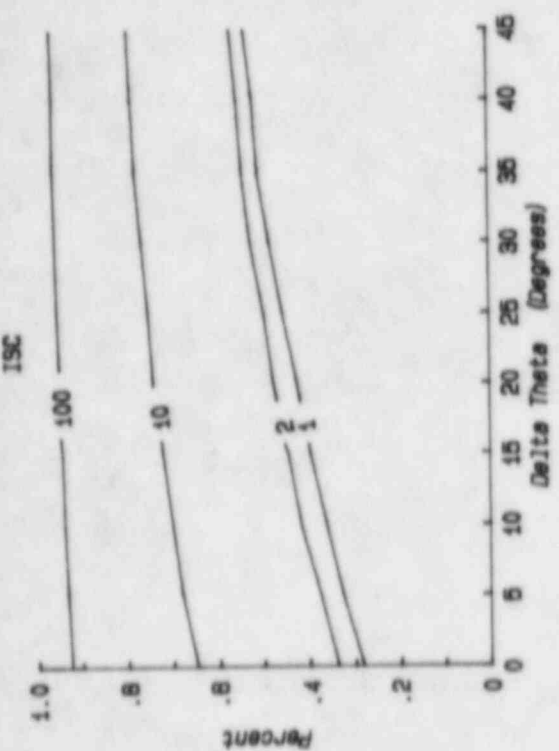


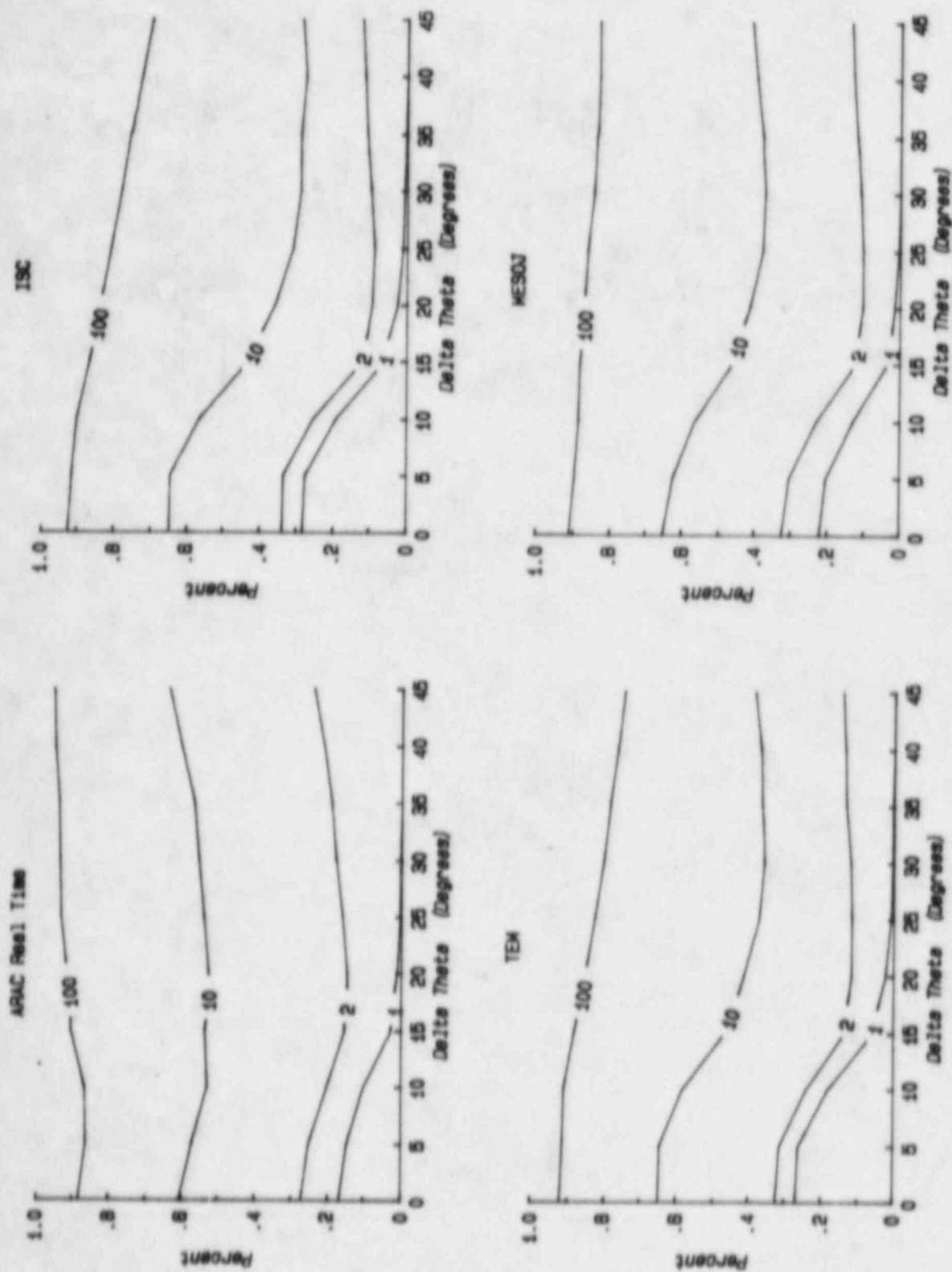
Figure 5.2





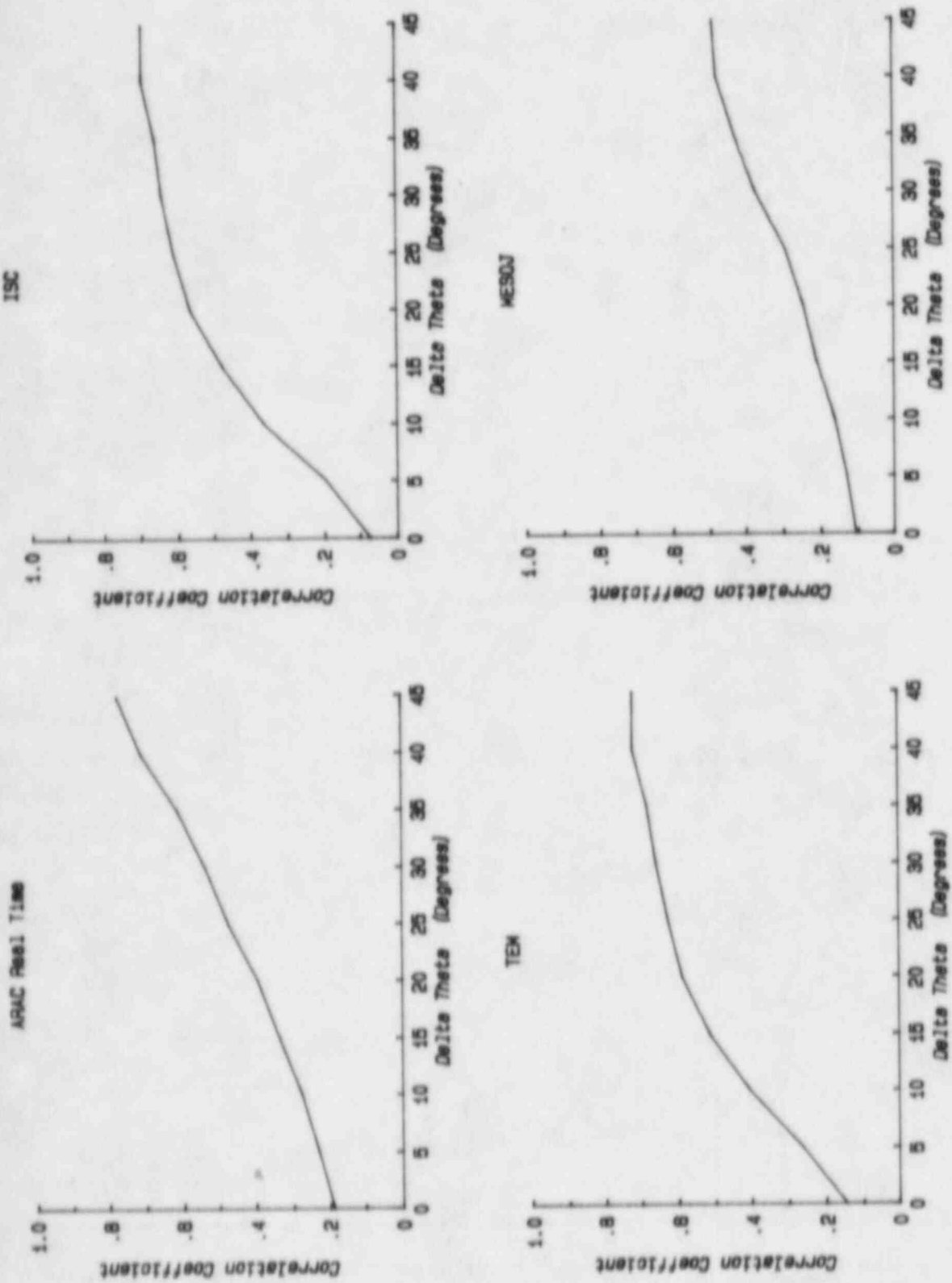
Tests 5 and 7  
12 Hourly Doses : Percent within a factor : (Data Value)

Figure 5.3



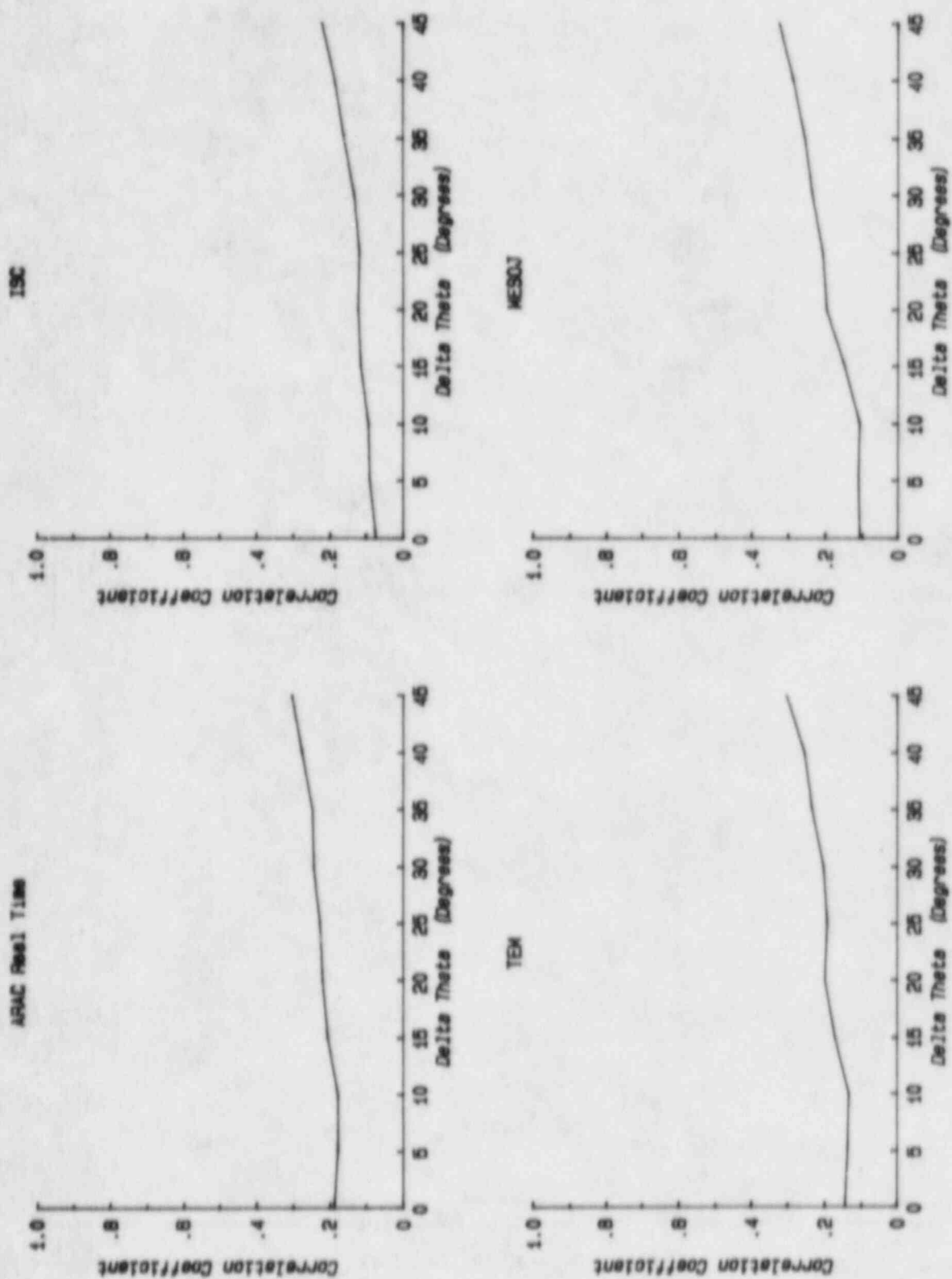
Tests 5 and 7  
12 Hourly Doses : Percent within a factor : (Max Data Value)

Figure 5.4

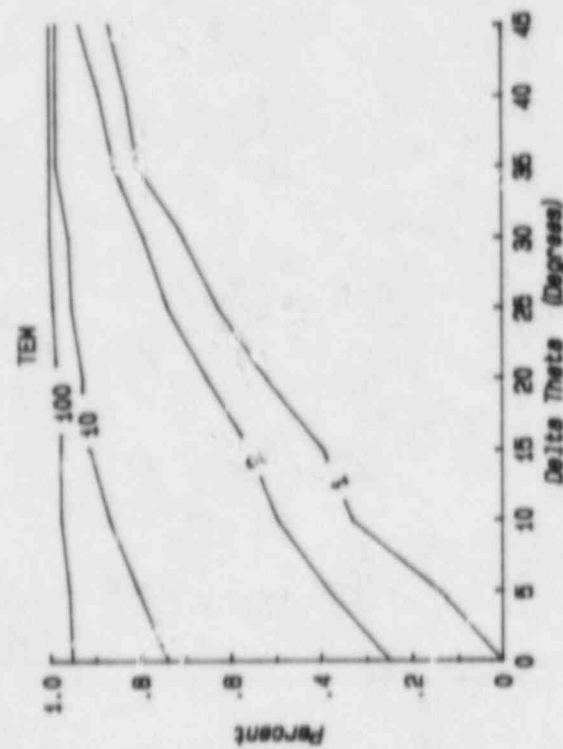
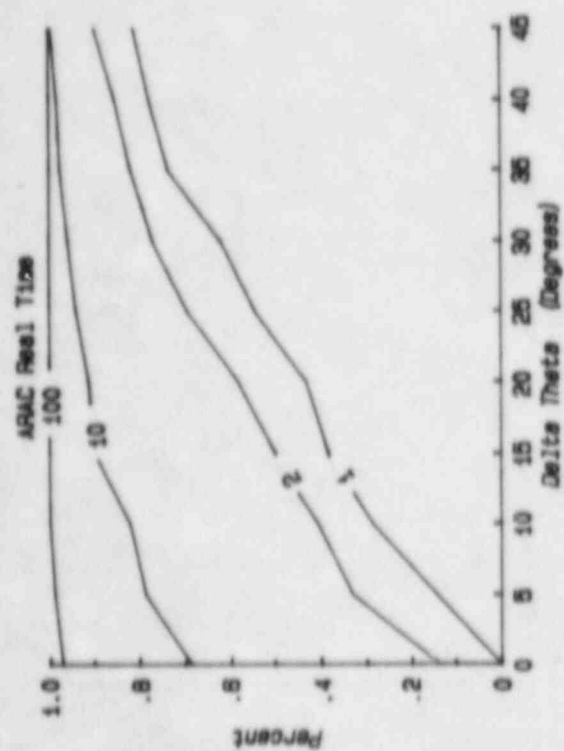
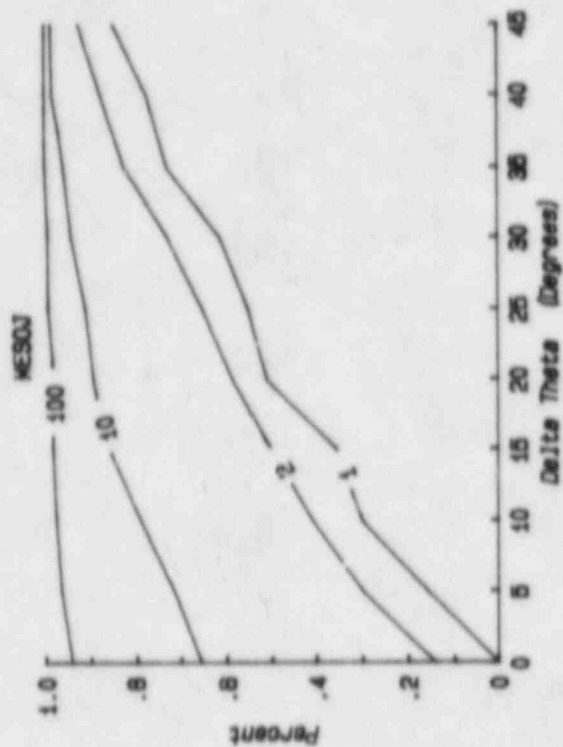
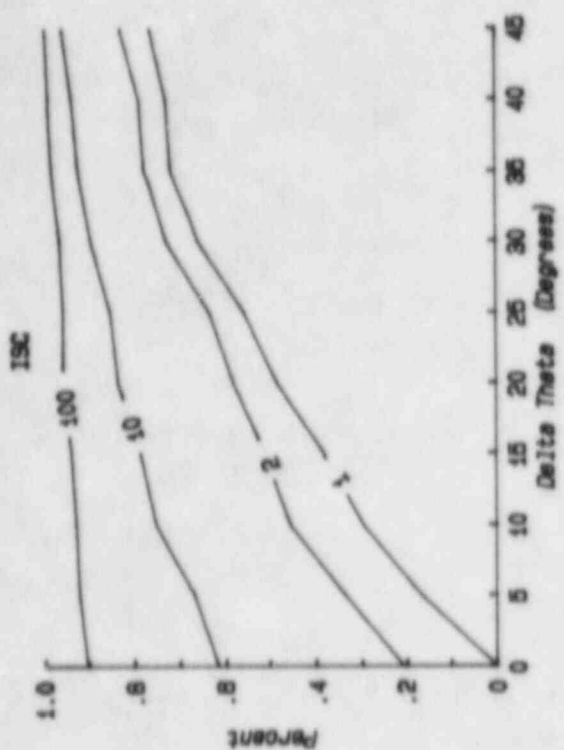


Tests 5 and 7  
12 Hourly Doses : Correlation Coefficient : (Data Value)

Figure 5.5

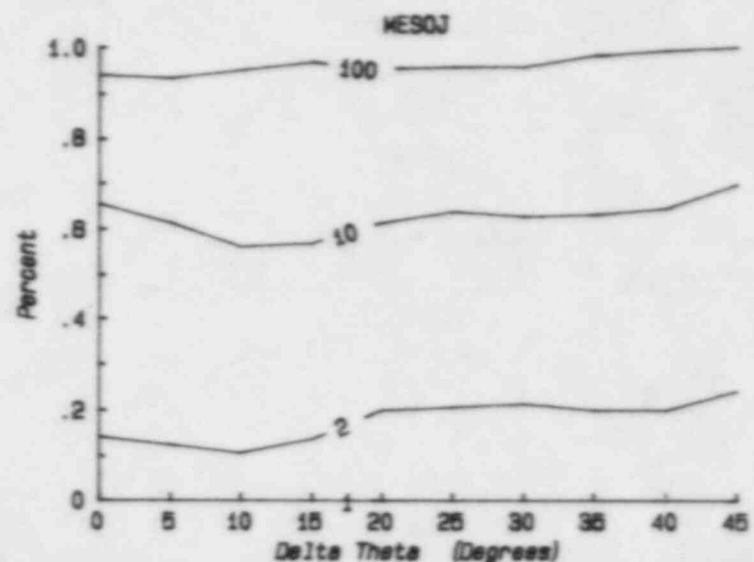
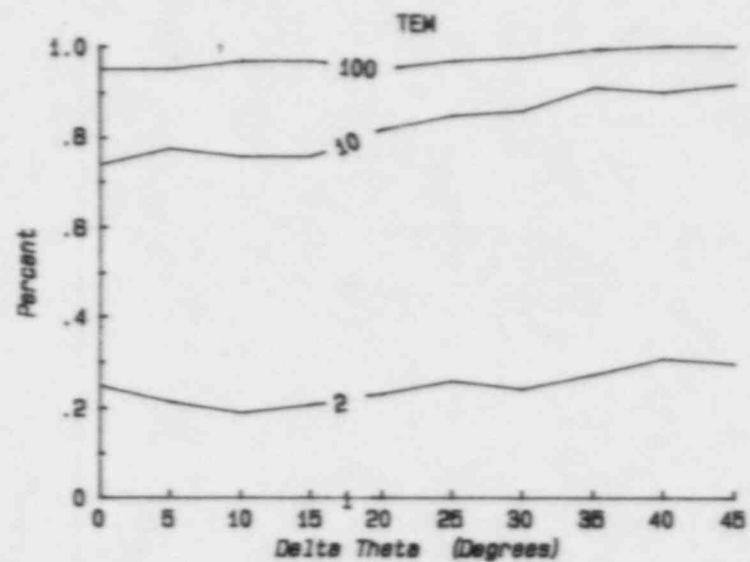
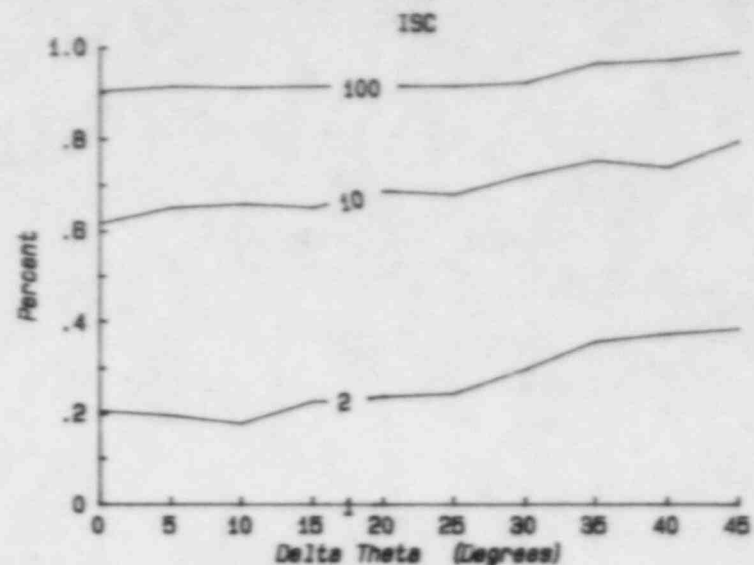
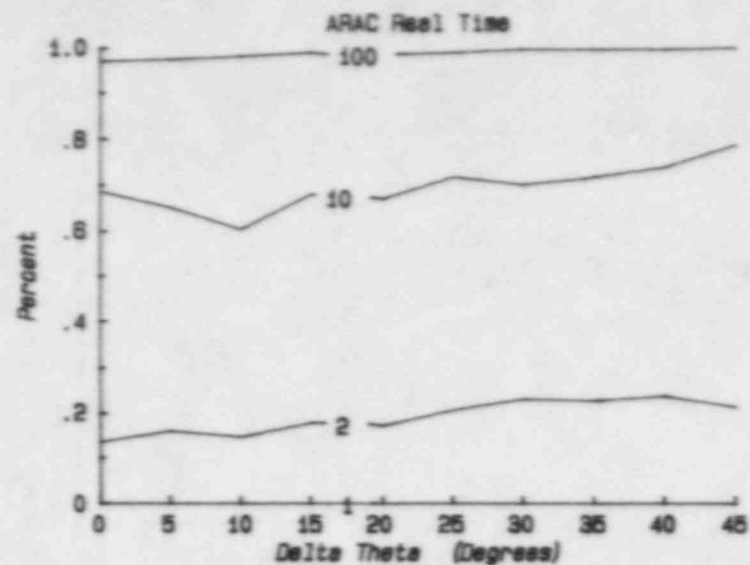


Tests 5 and 7  
12 Hourly Doses : Correlation Coefficient : (Max Data Value)



Tests 5 and 7  
12 Hour Total Dose : Percent within a factor : (Data Value)

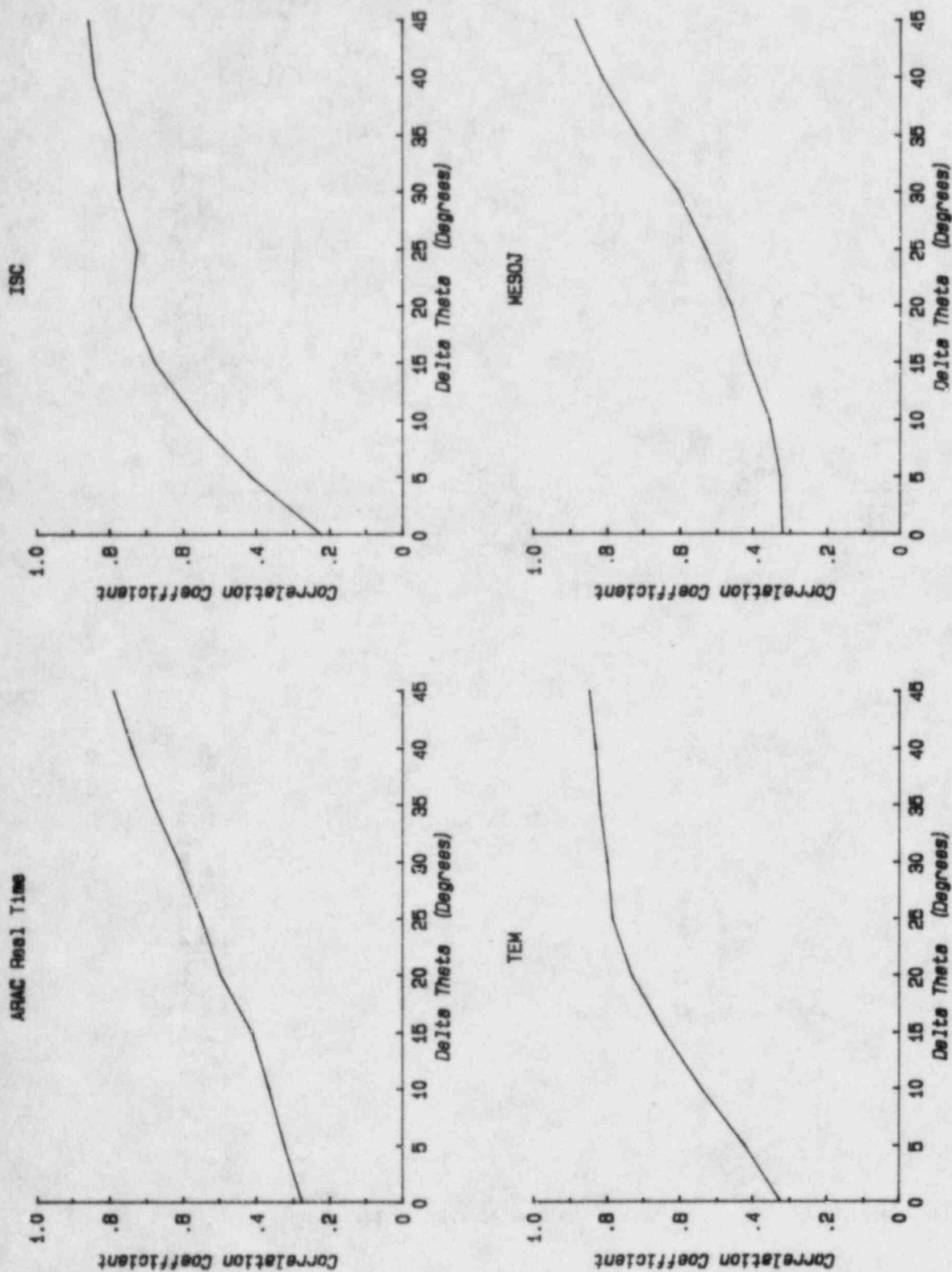
Figure 5.7



Tests 5 and 7  
12 Hour Total Dose : Percent within a factor : (Max Data Value)

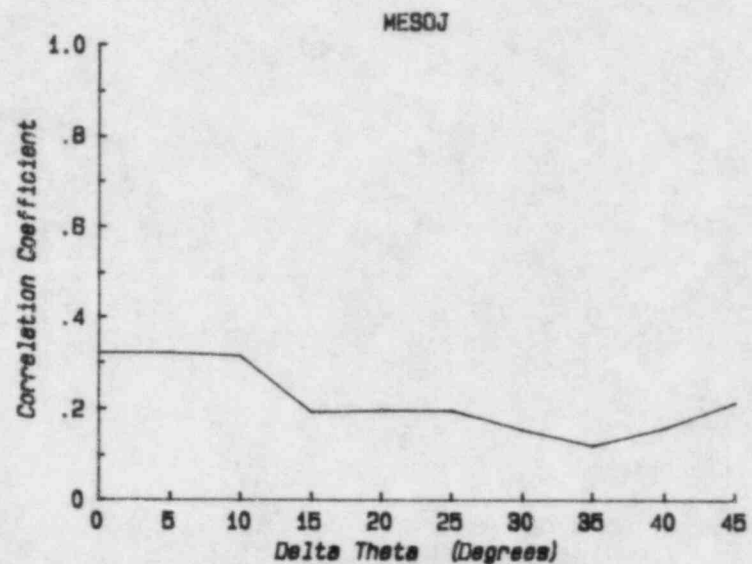
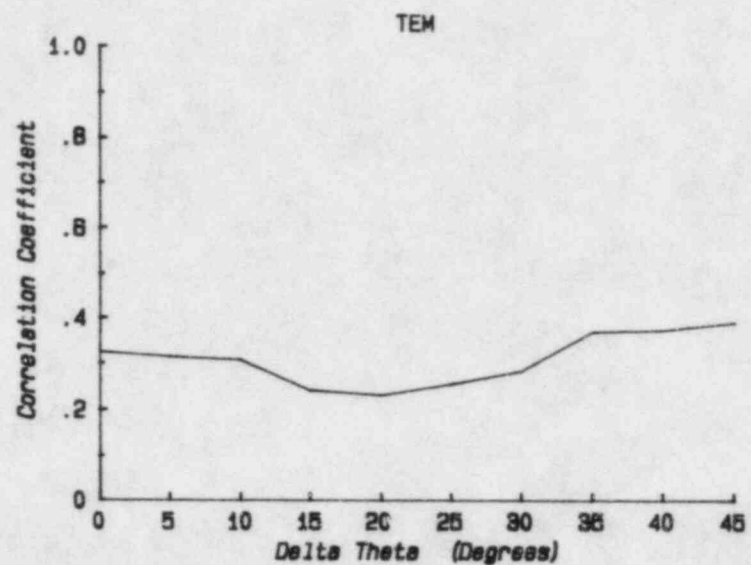
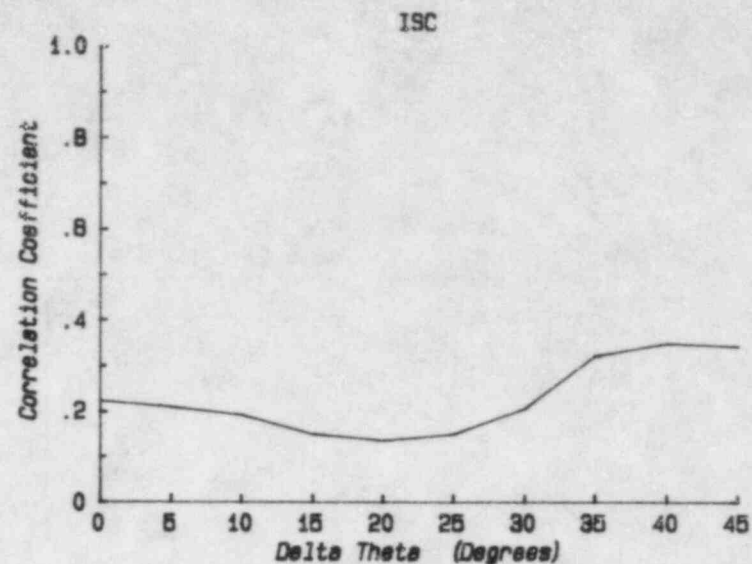
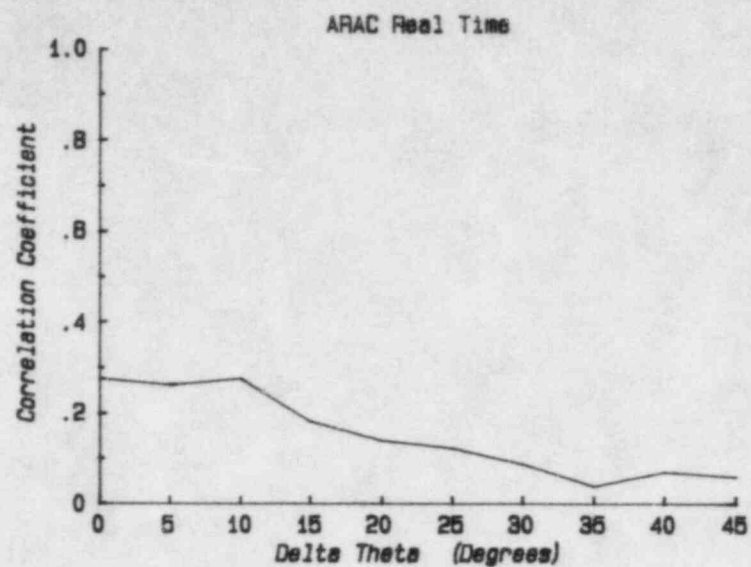
Figure 5.8





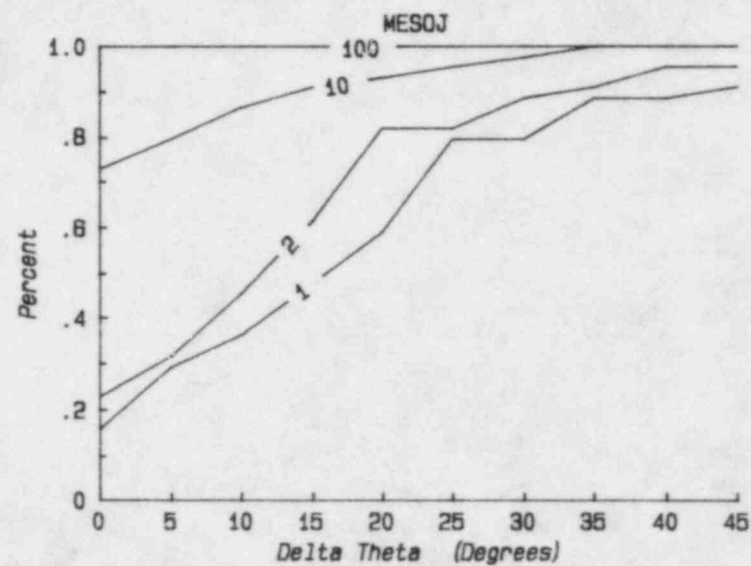
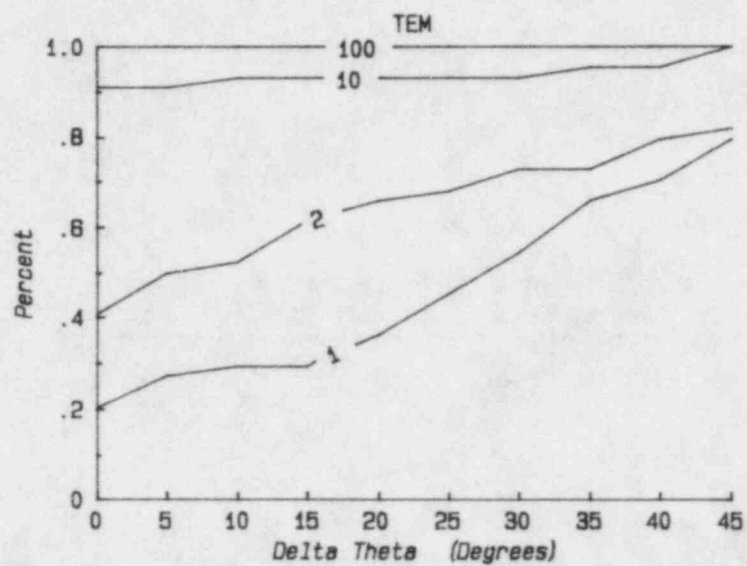
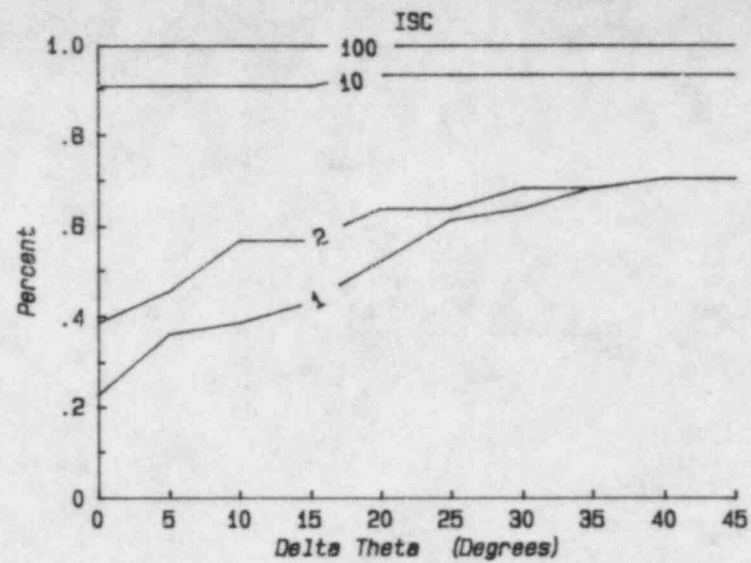
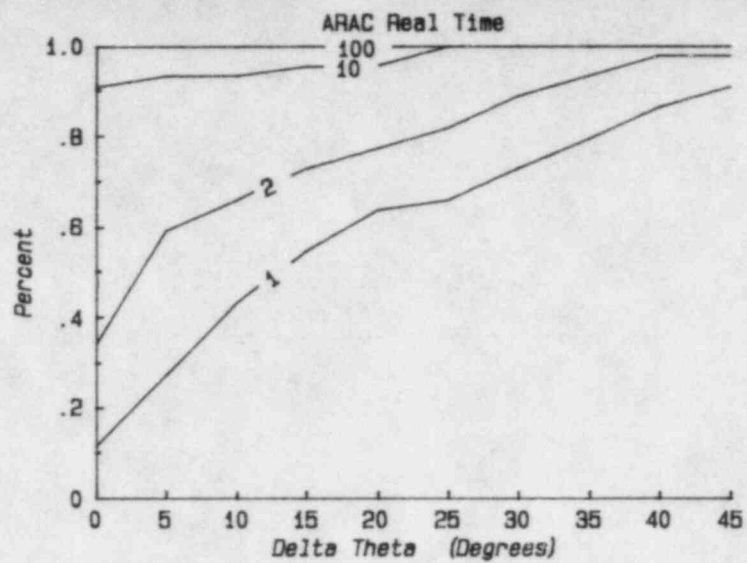
Tests 5 and 7  
12 Hour Total Dose : Correlation Coefficient : (Data Value)

Figure 5.9



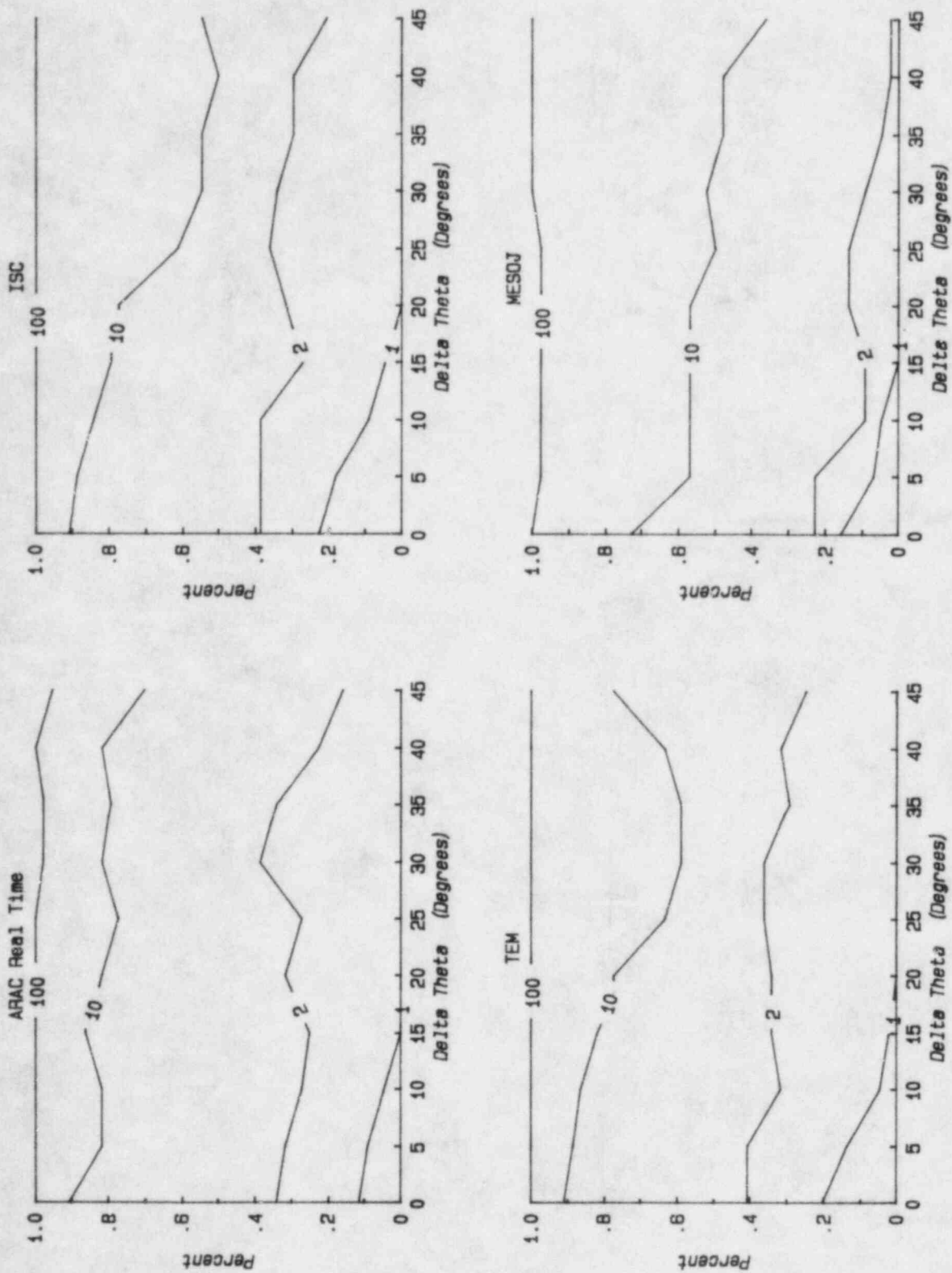
Tests 5 and 7  
12 Hour Total Dose : Correlation Coefficient : (Max Data Value)

Figure 5.10

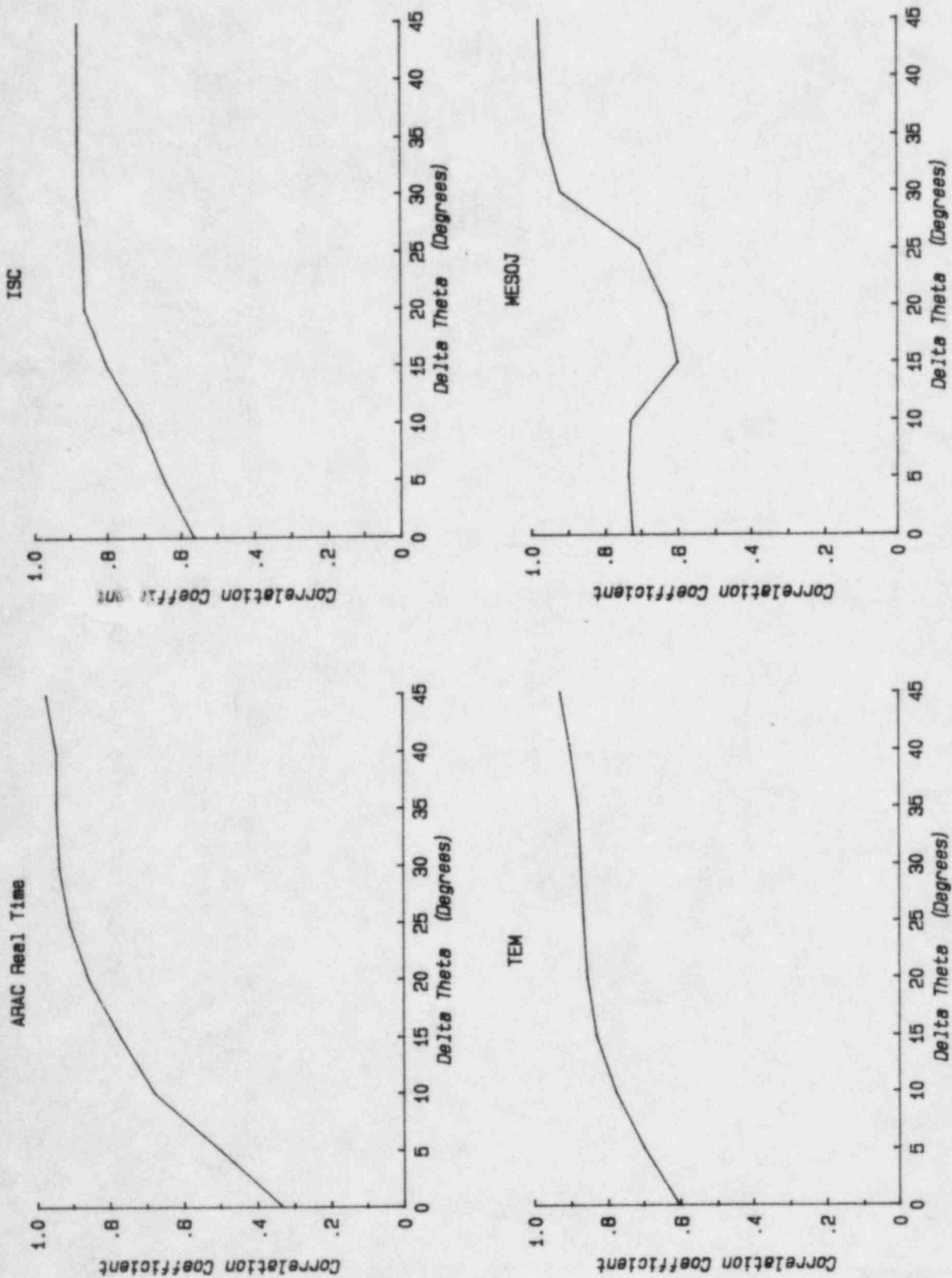


Test 7  
Total Dose : Percent within a factor : (Data Value)

Figure 5.11

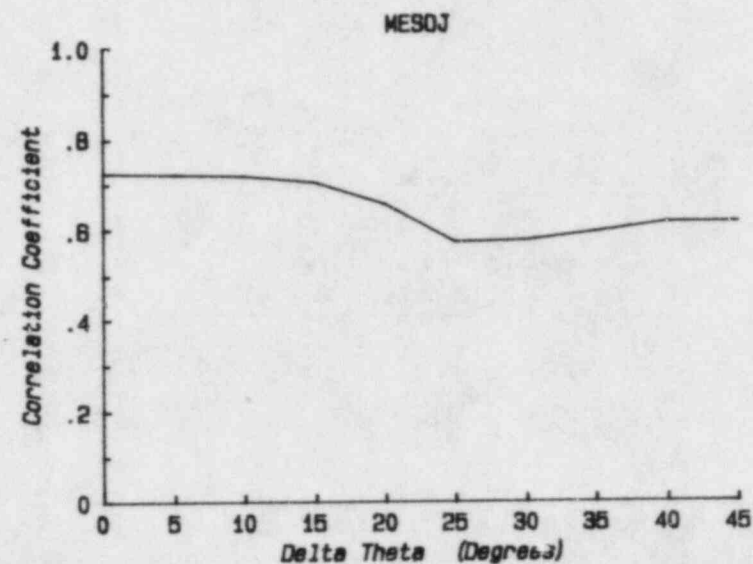
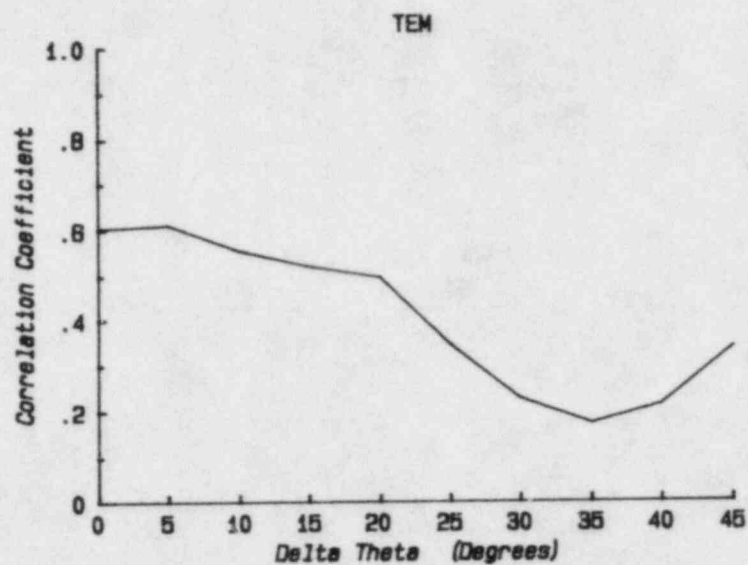
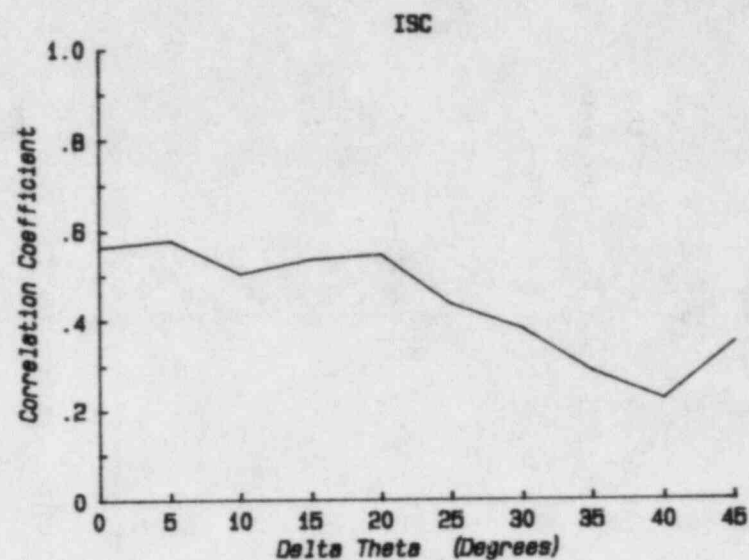
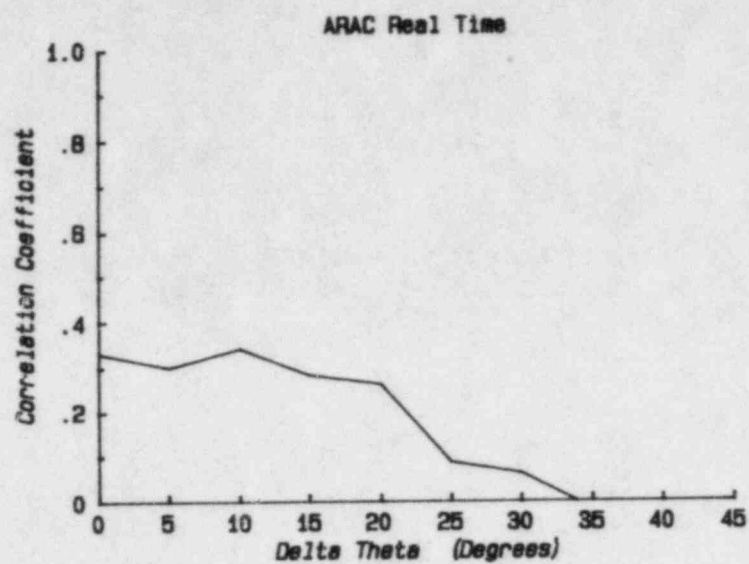


Test 7  
Total Dose : Percent within a factor : (Max Data Value)



Test 7  
Total Dose : Correlation Coefficient : (Data Value)

Figure 5.13



Test 7  
Total Dose : Correlation Coefficient : (Max Data Value)

Figure 5.14



## VI. Concluding Remarks

Within the limited range appropriate for class A models this data shows the Gaussian plume models to perform as well as either the puff models or the transport and diffusion models. Among these steady state plume models the new GP model shows a slight improvement over the standard ISC and TEM models. This is most noticeable in Figures 4.5 and 4.7, and 4.15.

The puff and transport and diffusion class models do show a slight edge in performance in comparison with the total dose over the extended range appropriate for B models. This advantage is demonstrated in Figure 4.22. It is surprising that this expected result does not show up stronger in the other performance measures. This may be a result of the unfortunate necessity to disregard the total dose comparisons on cases three thru six because of data difficulties. Of the three remaining cases, both seven and nine are cases where the winds remain relatively steady during the period required to flush the emissions from the domain. On such cases the Gaussian plume models can perform as well as the unsteady models even at the extended range. The transport and diffusion class models show no performance advantage over the simpler puff models.

Absolute measures of model accuracy are more difficult to quote because they are highly dependent on the particular comparison mode. If it is assumed that higher data values may occur at stations between the actual sampler sites then the best results for the hourly samples show approximately 40% calculated within a factor of two when a  $15^\circ$  uncertainty in plume position is permitted and data values at the noise level are omitted. This is increased to 60% calculated within a factor of two when a  $15^\circ$  position uncertainty is permitted for the 12 hour integrated dose. In comparisons on the extended range the best models show approximately 70% for the same performance measure. If it is assumed that the data has correctly captured the maximum surface values calculated within a factor of two within the area defined by a  $15^\circ$  uncertainty is reduced to 25%, 35%, and 45% for the hourly, 12 hour, and total dose respectively.

Disagreements between model calculations and data shown here may be divided into four classes: 1) those due to model structure; 2) those due to a poor selection of model input quantities; 3) those due to data errors; 4) those due to an inherent unpredictability of individual turbulent eddies. Only errors of the first type are distinguished by the intermodel comparisons of Chapter 4. The strong similarity of the performance of quite different model patterns suggests that many of the disagreements must fall in one of the last two classes. The discussion in Section 3 of Lewellen, et. al. (1983) suggests that at least half the test periods were conducted under conditions which would lead to high plume variability, i.e. a small source dispersed within a deep turbulent layer. The patchiness of the observed patterns tends to confirm this. Further analysis will be required to determine the extent to which this variability can explain the differences between model results and data.

The results of this limited comparison between model calculations and field observations are consistent with the results of the scientific critique of available models which supported puff models as the most viable candidates for both class A and class B models. The best puffs model scored as high as any of the more sophisticated models in either the class A or class B test. Since they can be run sufficiently fast to qualify as a class A model, it appears to satisfy both requirements.

Five puff models were considered in this test. The tests suggest that standard puff models such as MESODIF and MESOI can be improved as demonstrated by our MESOJ code. By allowing for an elevated release, MESOI can be improved slightly. These models also appear to need to allow for more influence of wind shear. The simplest way of accomplishing this is to increase horizontal dispersion to simulate the increased spreading due to wind shear. This is believed to be the reason the ARL-Puff model performed slightly better than MESOJ. We expected the best puff model performance to be obtained by allowing the puffs to be rearranged as wind shear acts on the plume. However, the SPLITPUFF model gave disappointing results. The reason for this is not clear at the present writing.

## REFERENCES

- Dickson, C. R., G. E. Start and J. H. Cate (1981); "1981 Idaho Field Experiment," (April 1981 Draft report to Nuclear Regulatory Commission).
- Lewellen, W. S., R. I. Sykes and D. Oliver (1981); "The Evaluation of MATHEW/ADPIC as a Real-Time Dispersion Model," Aeronautical Research Associates of Princeton, Inc., Final Report No. 442. NUREG/CR-2199.
- Lewellen, W. S., R. I. Sykes, S. F. Parker, A. K. Varma, R. W. McCullough, H. T. S. Philander, G. Sandri and D. A. Oliver (1983); ARAP Report No. 472, "A Scientific Critique of Available Dispersion Models", Prepared for Union Carbide Corporation, Nuclear Division, Contract #19X-70507V,
- Rosen, L. C. (1982); "ARAC Testing for Potential Nuclear Regulatory Commersion Meteorological Staff Use," NUREG/CR-2779.
- Uthe, E. E., Nielsen, N. B. (1980); "Airborne Lidar plume and haze Analyzer (ALPHA-1)", Bull. Am. Met. Soc., 61, pp. 1035-1043.

## Appendix A

### Review of Data Used for the Model Tests

Details of the data used in the model tests are given in this appendix. More details of the field test program are available in a report by Dickson, Start, et.al. (1983). A brief narrative of each of the tests is provided with the data. We begin with test 3 because no data from the first 2 tests were used for the model comparisons in this report. The SF<sub>6</sub> release rate is given in lbs/hr for each test.

Test 3: 2300:7/18 - 0700:7/19: 200 lbs/hr.

This first test was a nocturnal release, commencing one hour before midnight. The period of the actual release was characterized by light winds and a stable temperature gradient. The hourly average surface winds (Figure A.1) at 0100-0200 MDT show a general flow from the Northwest of  $1-2\text{ms}^{-1}$ ; this flow has reversed by 0400-0500 but the speed is roughly the same. Topographic contours at an interval of 200m are also shown on the figures. Around 0800, the stable layer is eroded by the solar heating and a convective layer begins to develop; the layer grows to a depth of 2-3 km by noon. The surface winds remain out of the southwest throughout the morning, but increase in speed up to about  $5\text{ms}^{-1}$  by noon; this development is evident in the winds at 0900-1000.

The tetron trajectories are shown in Figure A.1; the earliest tetron travels southwest initially, then reverses direction later. All the other tetrons, released after 0300, move towards the northeast.

Vertical winds profiles at four times are shown in Figure A.2. The early times, 2330 and 0200, both show northeasterly winds below 1000m, and a strong jet flow at 500m; this speed is considerably reduced in the stable layer near the surface. The flow above 1000m is from the west and is controlled by the synoptic gradients. By 0500, the direction profile is unchanged but the jet

# July 1981 INEL Field Experiment : Test 3

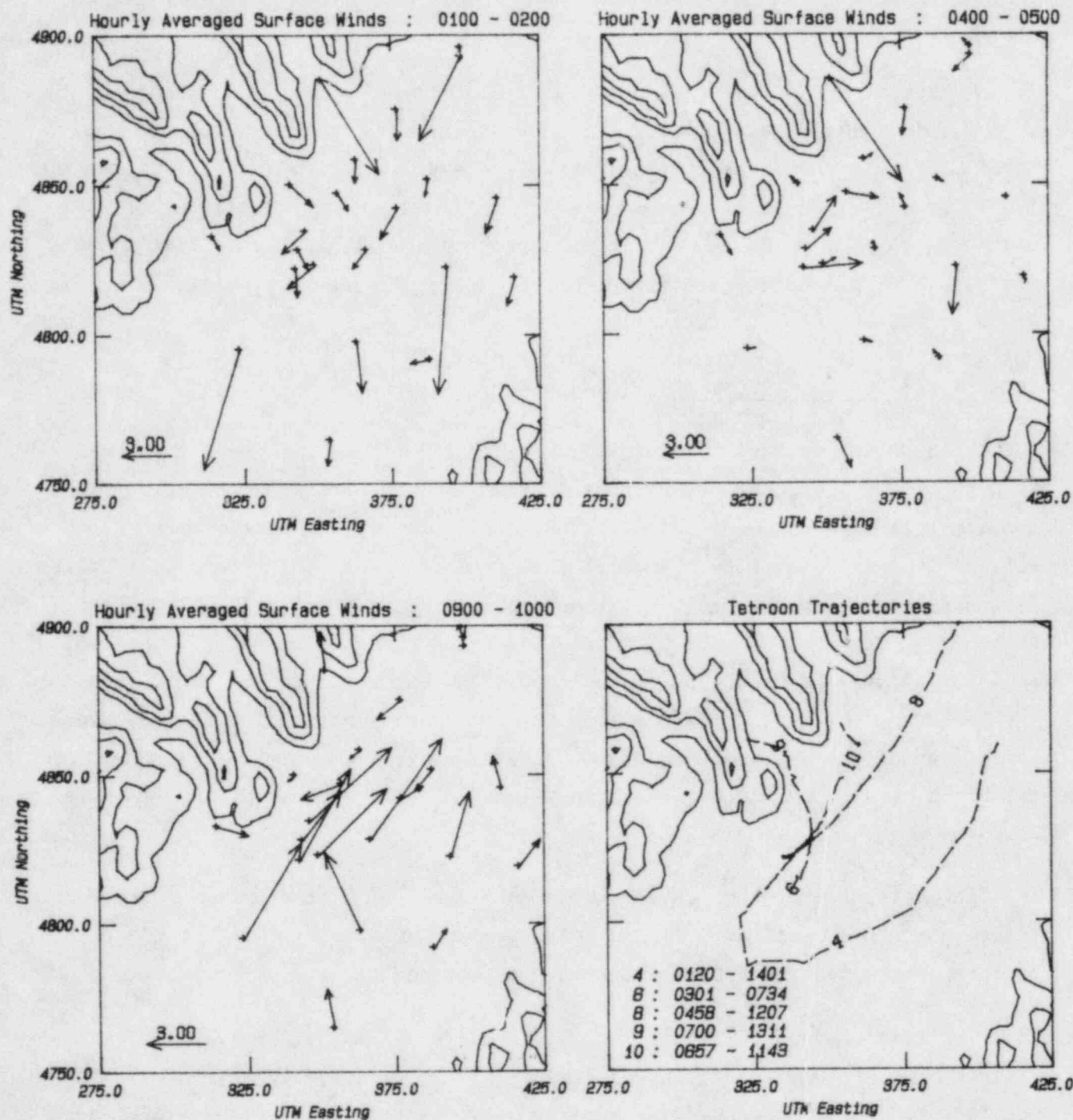


Figure A1



# July 1981 INEL Field Experiment : Test 3

Vertical wind profiles at the tracer release site

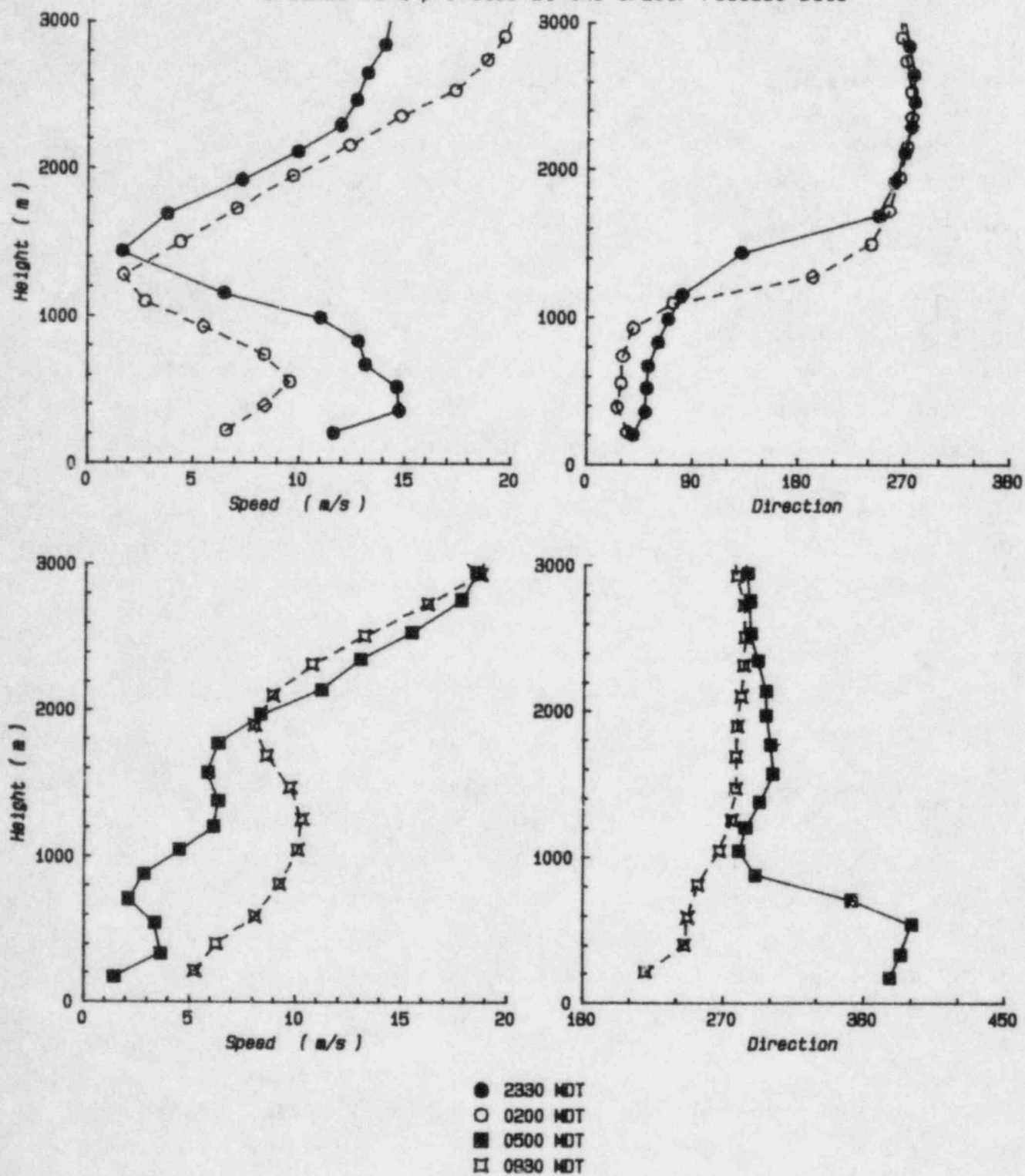


Figure A2



has subsided below 1000, and the surface winds actually show a direction reversal by this time. The final profile at 0930 illustrates the increasing flow from the southwest in the developing convective layer.

The hourly averaged surface concentration patterns shown in Figures A.3-5 are extremely erratic. The doses are generally small, consistent with an elevated release into a stable layer; however the complete lack of directionality in the fields is somewhat unsettling. In the early hours, the winds are certainly light and variable, but later there is a consistent southwesterly wind. There seems to be some indication that the tracer moves initially toward the southwest, in accord with the early tetraon, at least in the dose patterns for 0100-0300, but following this period there are significant doses in virtually every quadrant in each hour.

The integrated dose over the 12 hours is shown in Figure A.6. The maximum occurs in the southwest, but there is also a region of relatively high dose toward the northwest. The dose pattern from the large bags also is shown in Figure A.6 and indicates Maxima in the south and the northeast.

Test 4: 2300:7/20 - 0700:7/21: 320 lbs/hr.

This test was made exactly two days after test 3, and the meteorological conditions were similar. The flow was stable near the surface until about 0700, but the surface winds in Figure A.7 show a much stronger westerly component in the early hours. This flow extends too far across the plain to be attributable to drainage flow from the western valleys, and must be controlled by larger scale forces. The southwesterly flow is again established throughout most of the area by 1000.

The tetraon trajectories show a stronger and more persistent flow to the south and east in the early hours, and again the flow reversal is evident. At 2300, the tetraon moves away to the southeast, while those released at 0100 and 0300 move southward for about 50 km before turning toward the northeast.

# July 1981 INEL Field Experiment : Test 3

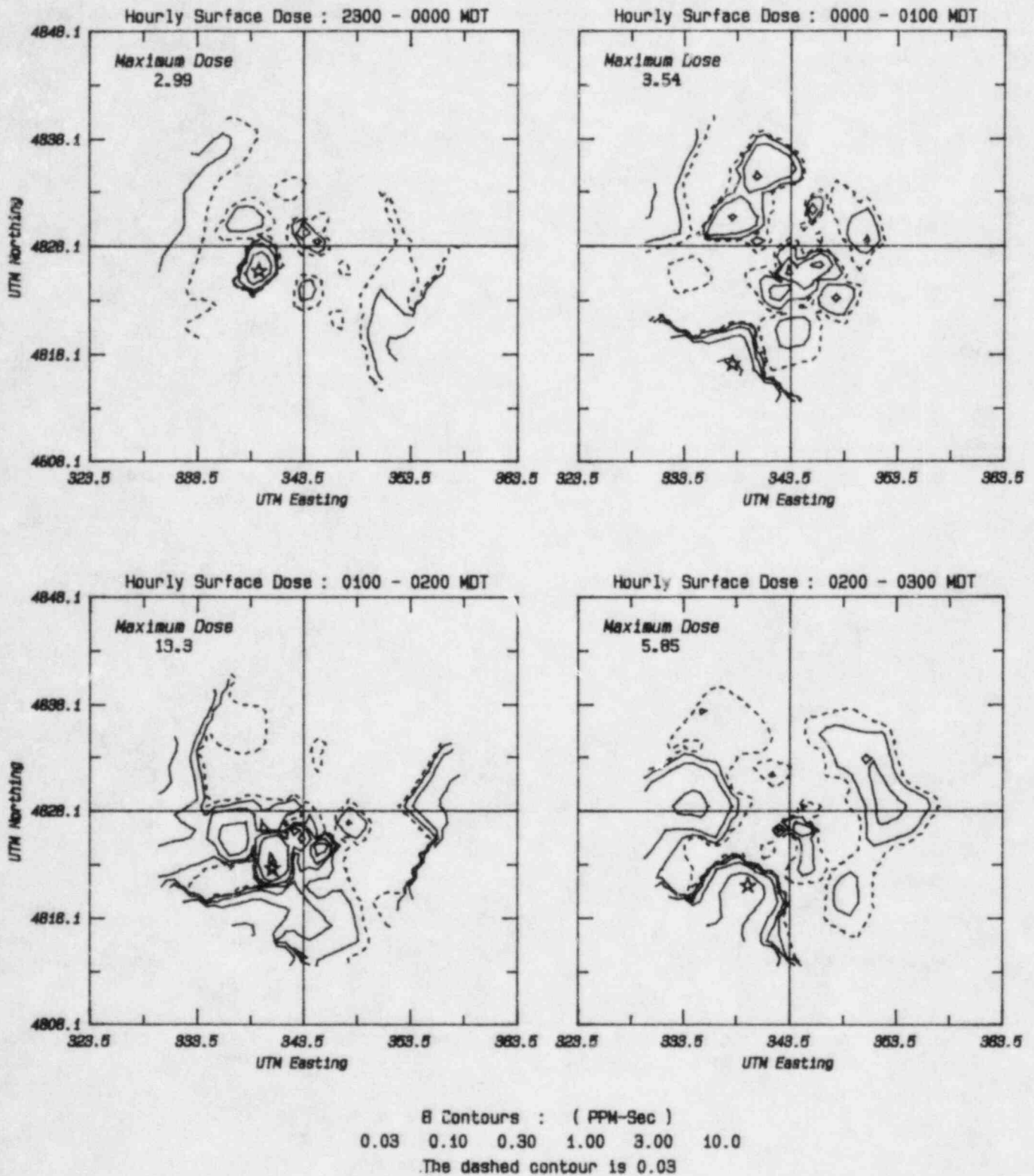


Figure A3

# July 1981 INEL Field Experiment : Test 3

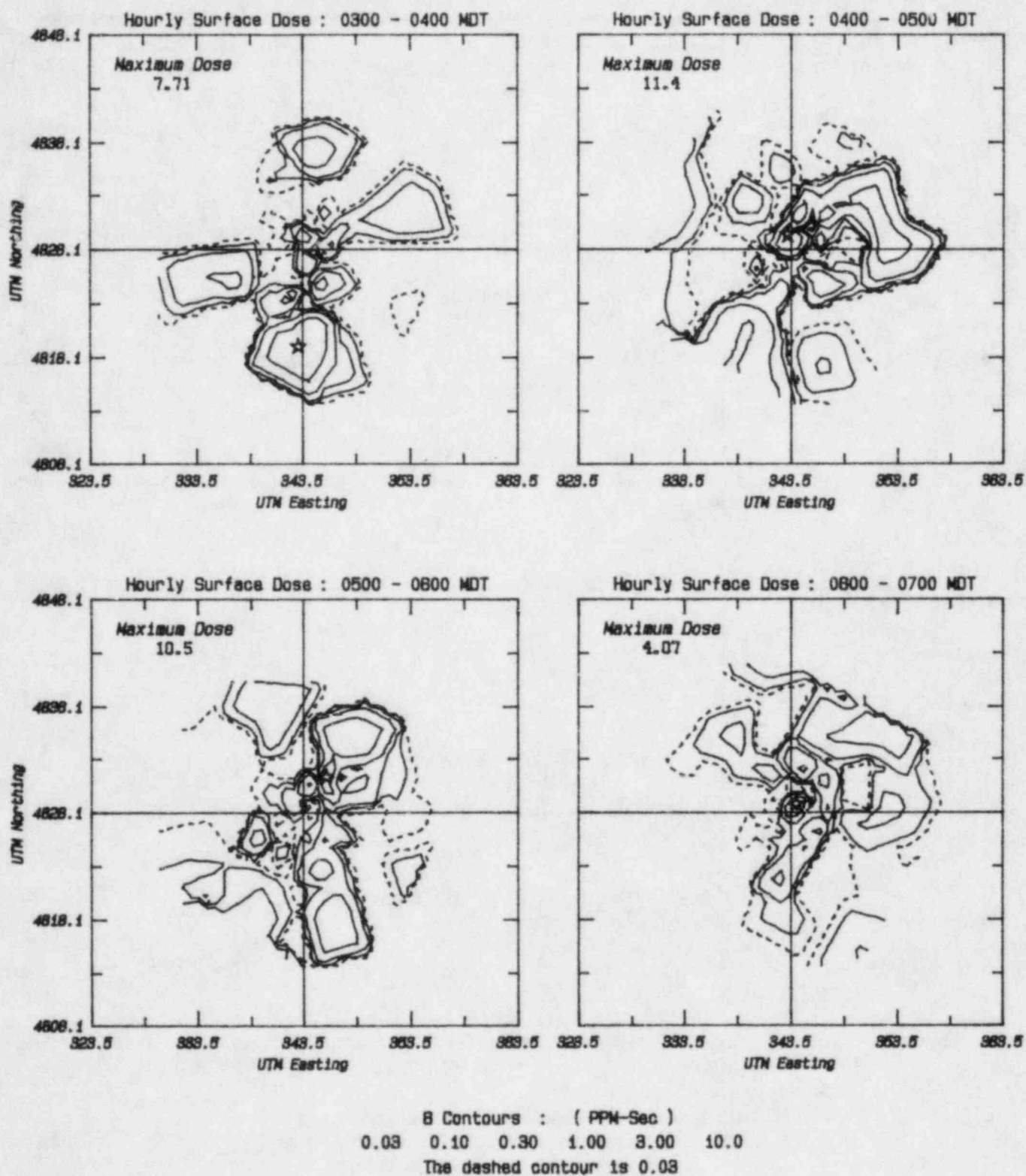


Figure A4

# July 1981 INEL Field Experiment : Test 3

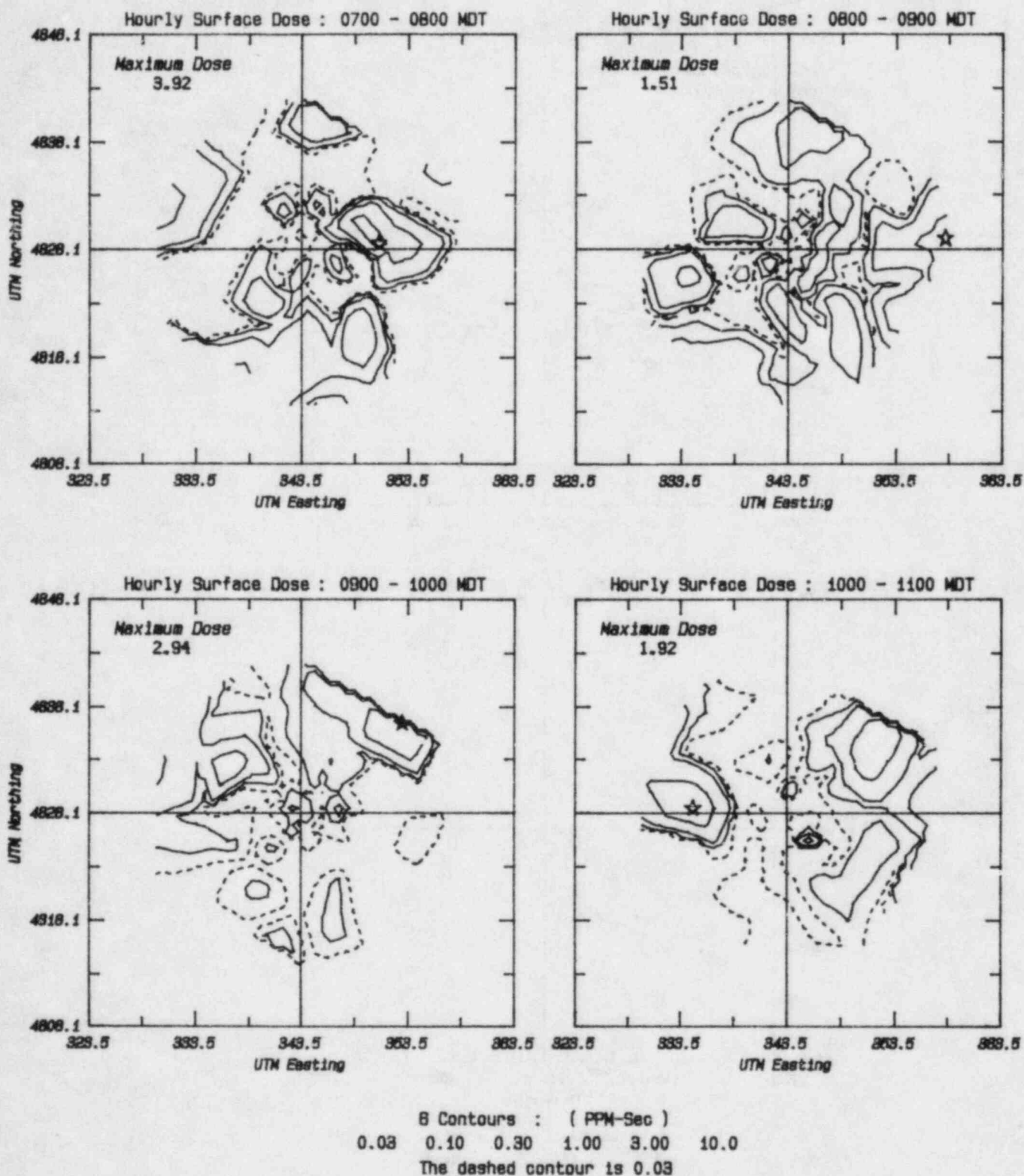


Figure A5

# July 1981 INEL Field Experiment : Test 3

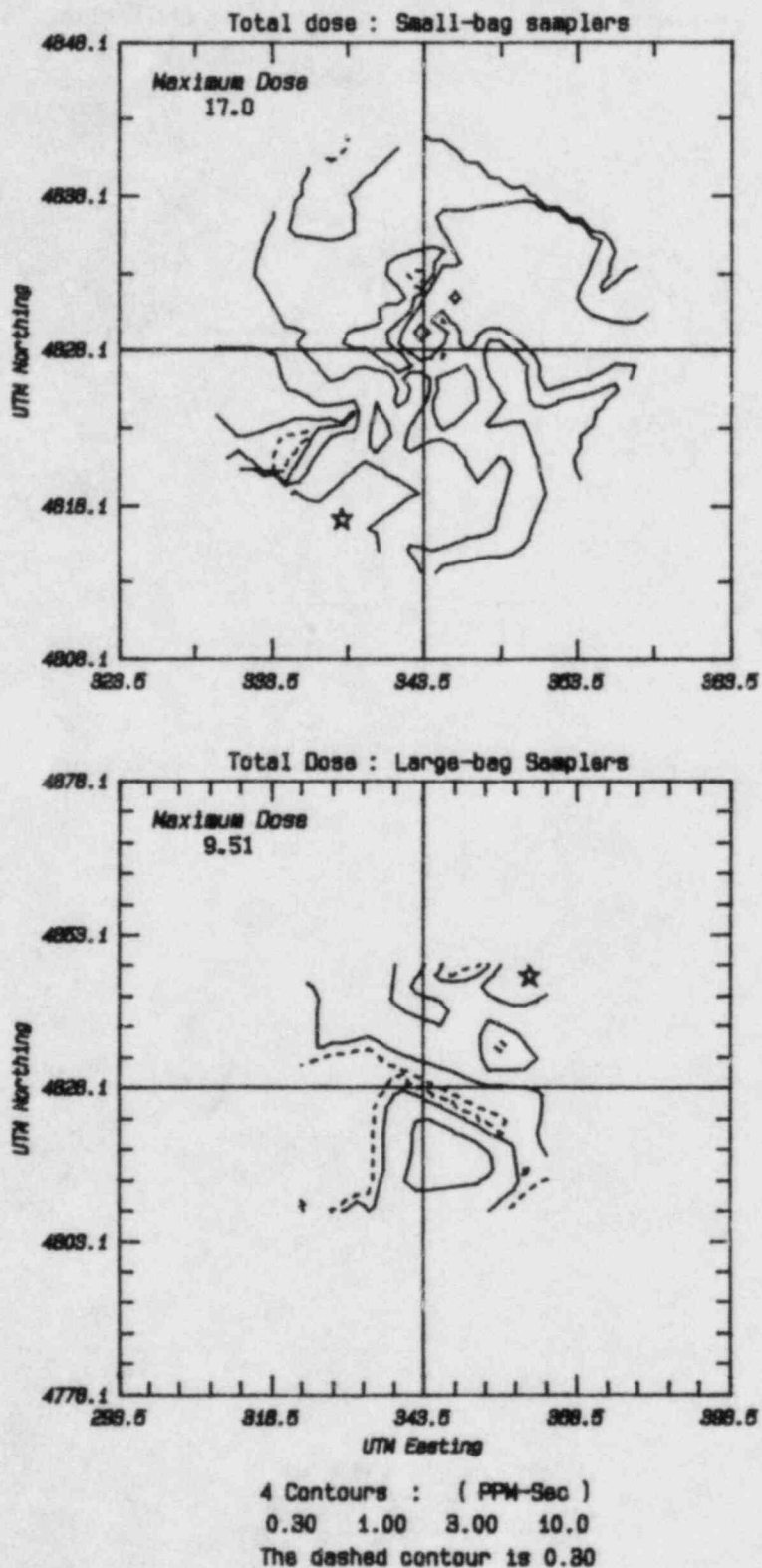


Figure A6



# July 1981 INEL Field Experiment : Test 4

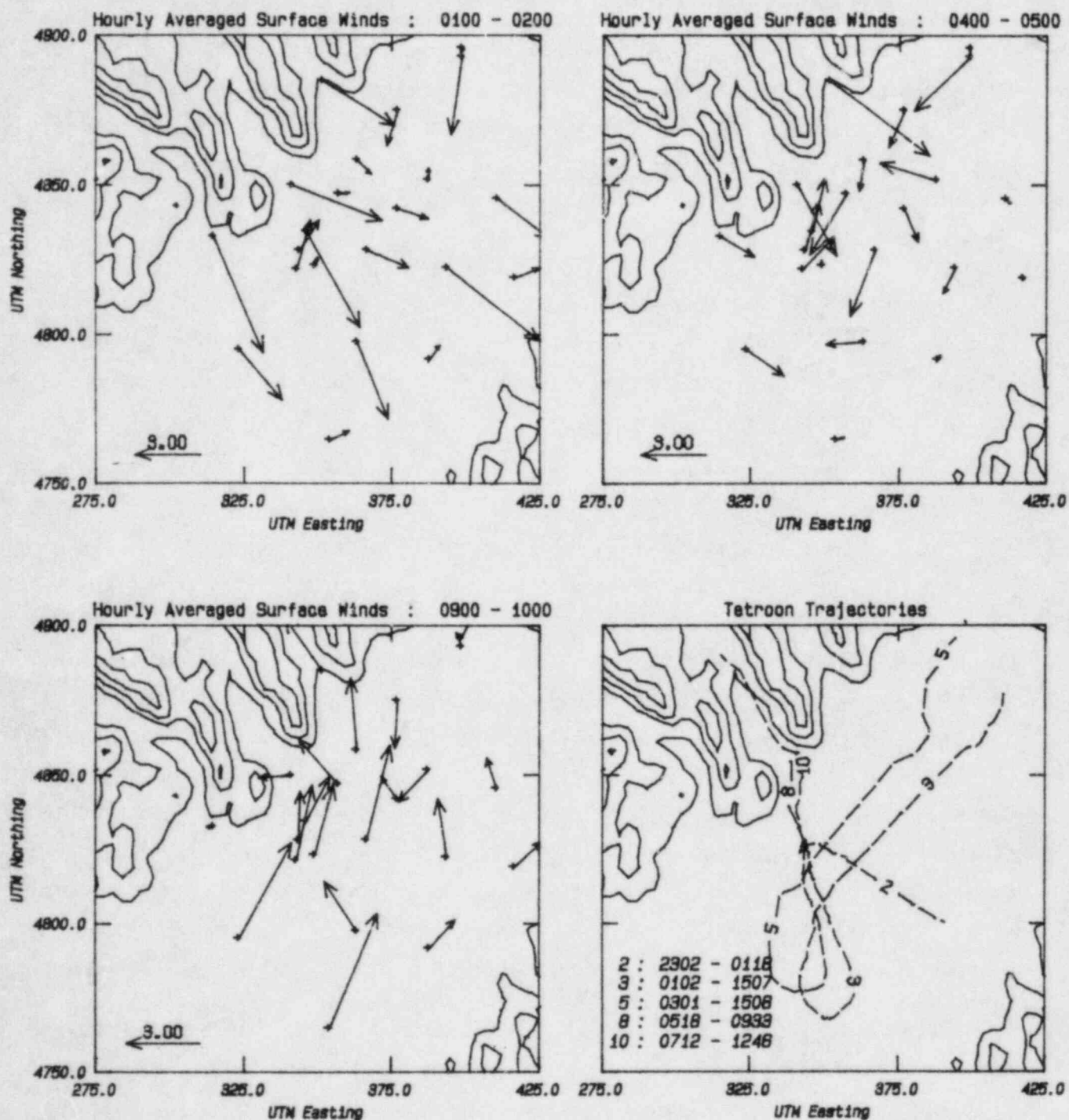


Figure A7



The wind profiles in Figure A.8 show northwesterly winds in the early hours, swinging round through north or northeast at 0600 to southerly in the layer by 1000.

The hourly surface  $SF_6$  dose patterns (Figures A.9-11) show more consistency than in test 3. The doses are higher, due presumably to the 50% increase in release rate, but there is also a clear movement of the tracer towards the east in the first five hours, swinging northeast later. After the end of the release at 0700, the tracer is swept out of the area and the doses are extremely small.

The total integrated dose for 12 hours, Figure A.12, show a clear plume extending eastward, and some significant doses toward the north. However, the large bag samples over the larger area show maximum doses in the southwest in contradiction to the small bags.

Test 5: 0500-1300 MDT-7/23/81:380 lbs/hr.

Test 5 was a morning release, beginning after dawn but before an unstable mixed layer had developed. The winds are very light and variable in the region of the source at 0600-0700 (Figure A.13), with a general flow from the North. There appears to be surface drainage flow out of the deep valleys in the Northwest of the domain at this time. Three hours later, Figure A.13 indicates continuing light northerly winds around the source, but now the wind is being drawn into the valleys in response to the surface heating. By 1300-1400 the winds are about  $10 \text{ ms}^{-1}$  from the Southwest over most of the plain. The light nocturnal drainage wind pattern is replaced by the strong southwesterly flow at about 1100, and this flow continues throughout the afternoon; the latter winds are driven both by the synoptic pressure gradient, and by the large scale heating of the Snake River valley.

Figure A.13 also shows tetroon trajectories for the test; only six of the total of ten tetroons are shown since they illustrate the significant features of the flow. The early tetroons were set to fly fairly low since the mixing layer was shallow and the source height was 46 m. They generally

July 1981 INEL Field Experiment : Test 4  
Vertical wind profiles at the tracer release site

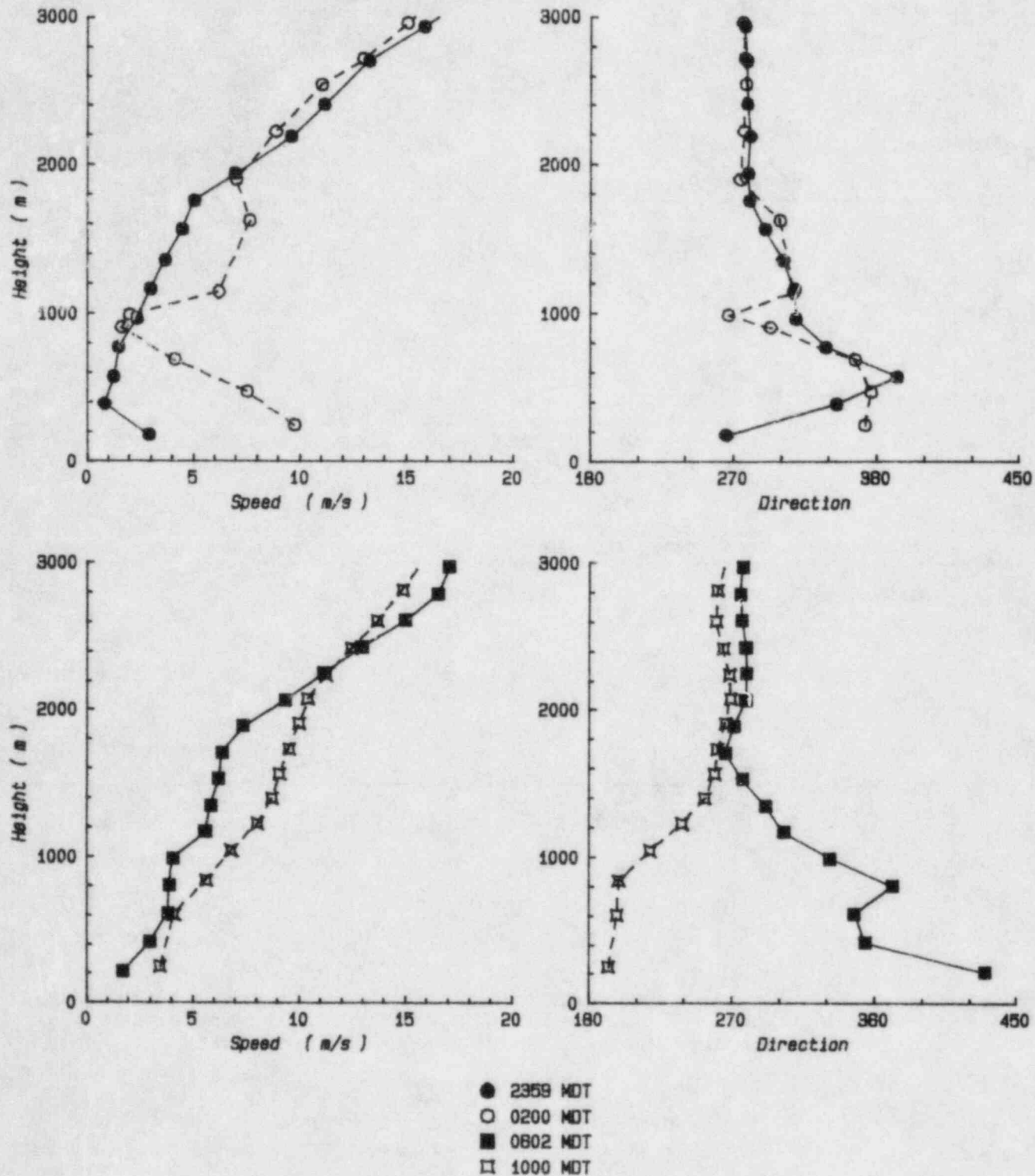


Figure A8

# July 1981 INEL Field Experiment : Test 4

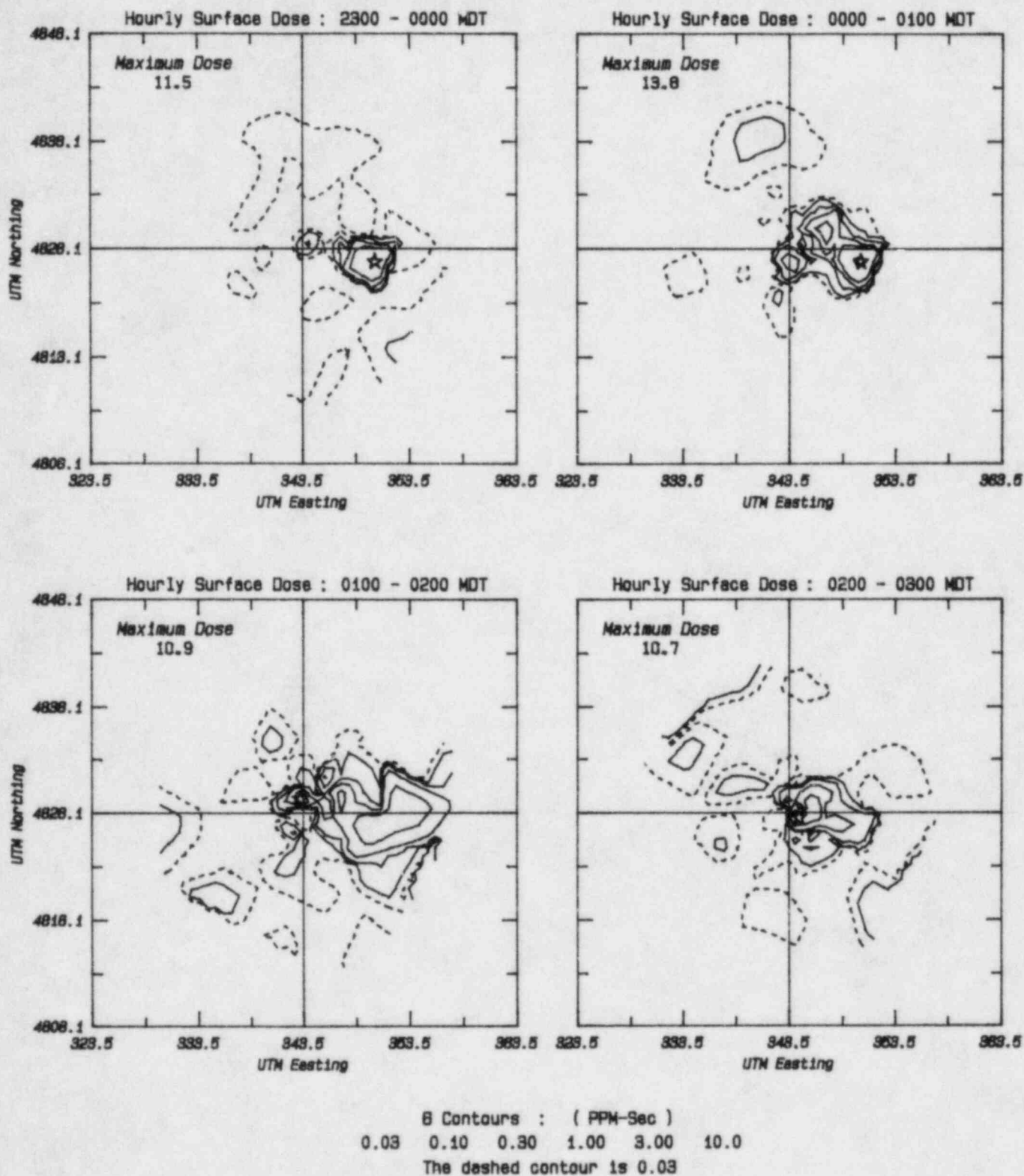


Figure A9

# July 1981 INEL Field Experiment : Test 4

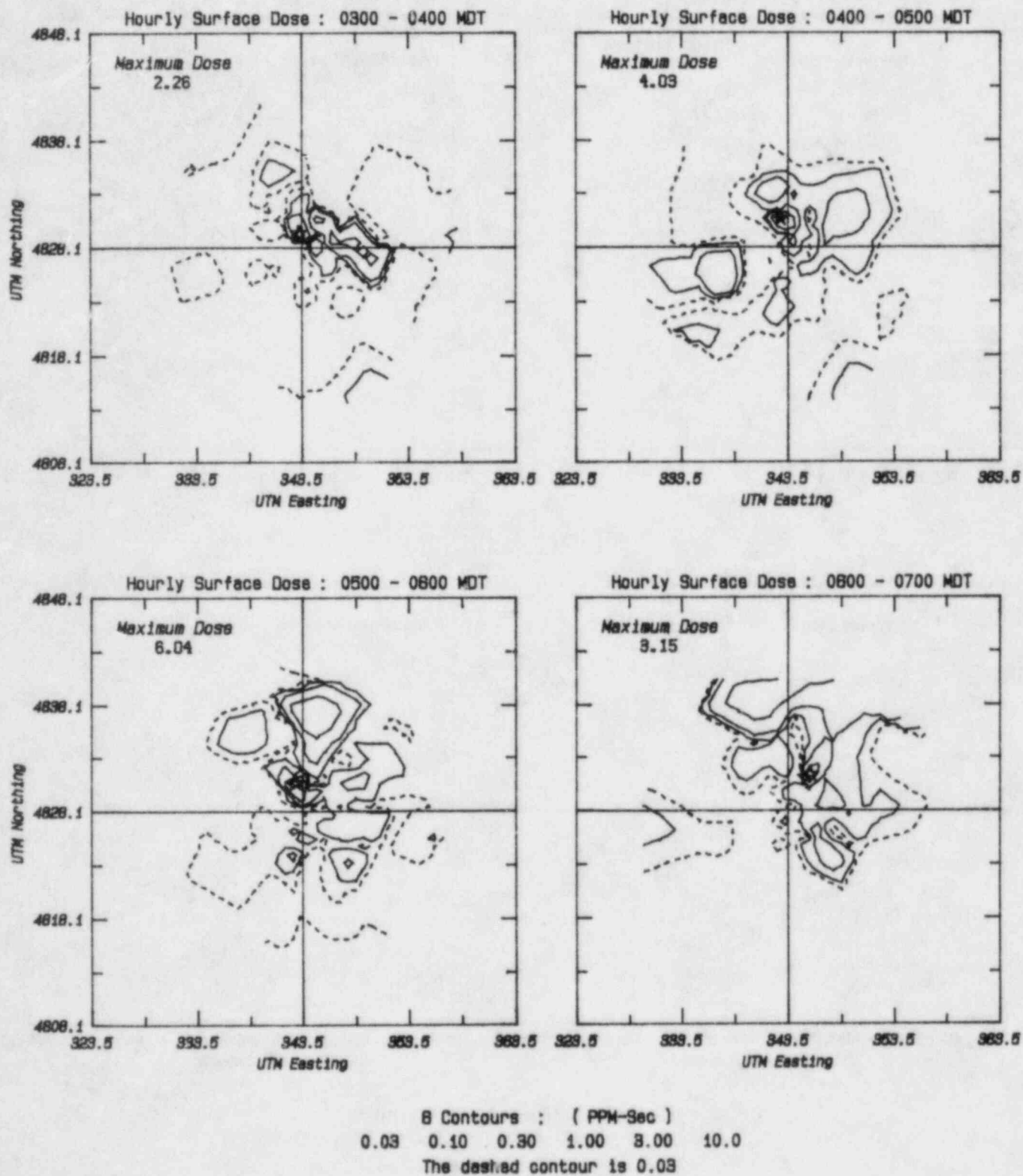


Figure A10

# July 1981 INEL Field Experiment : Test 4

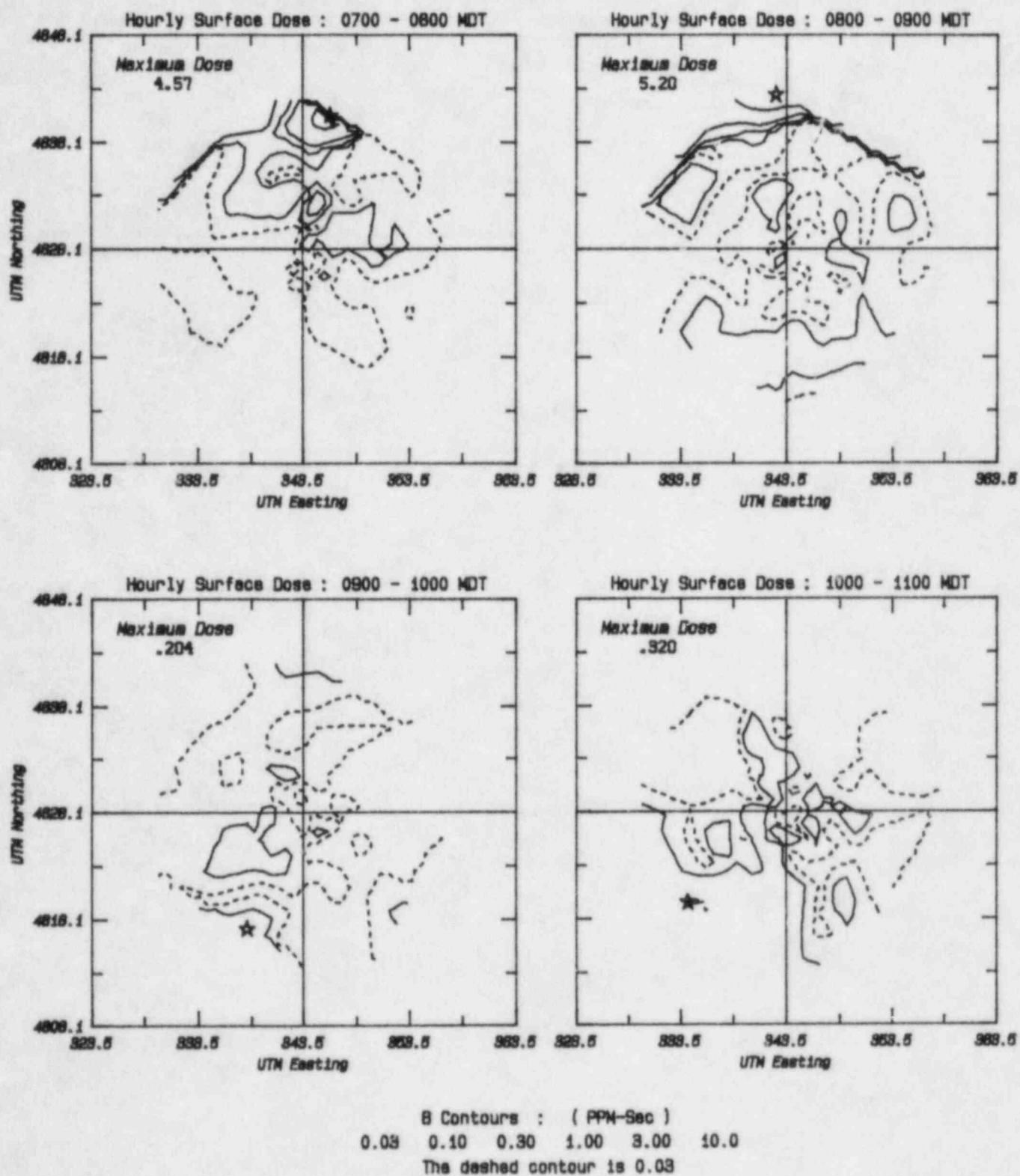


Figure A11



# July 1981 INEL Field Experiment : Test 4

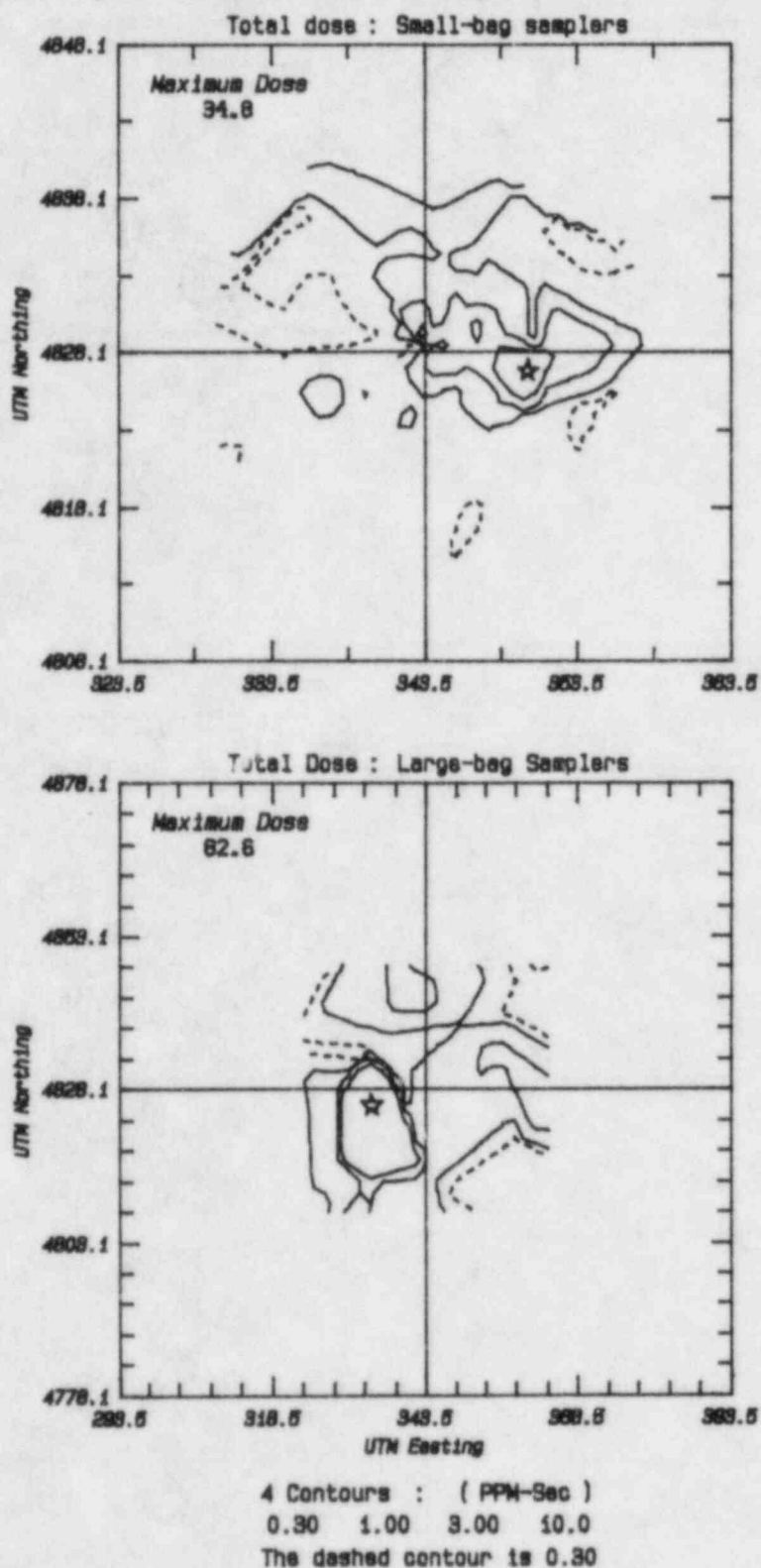


Figure A12

# July 1981 INEL Field Experiment : Test 5

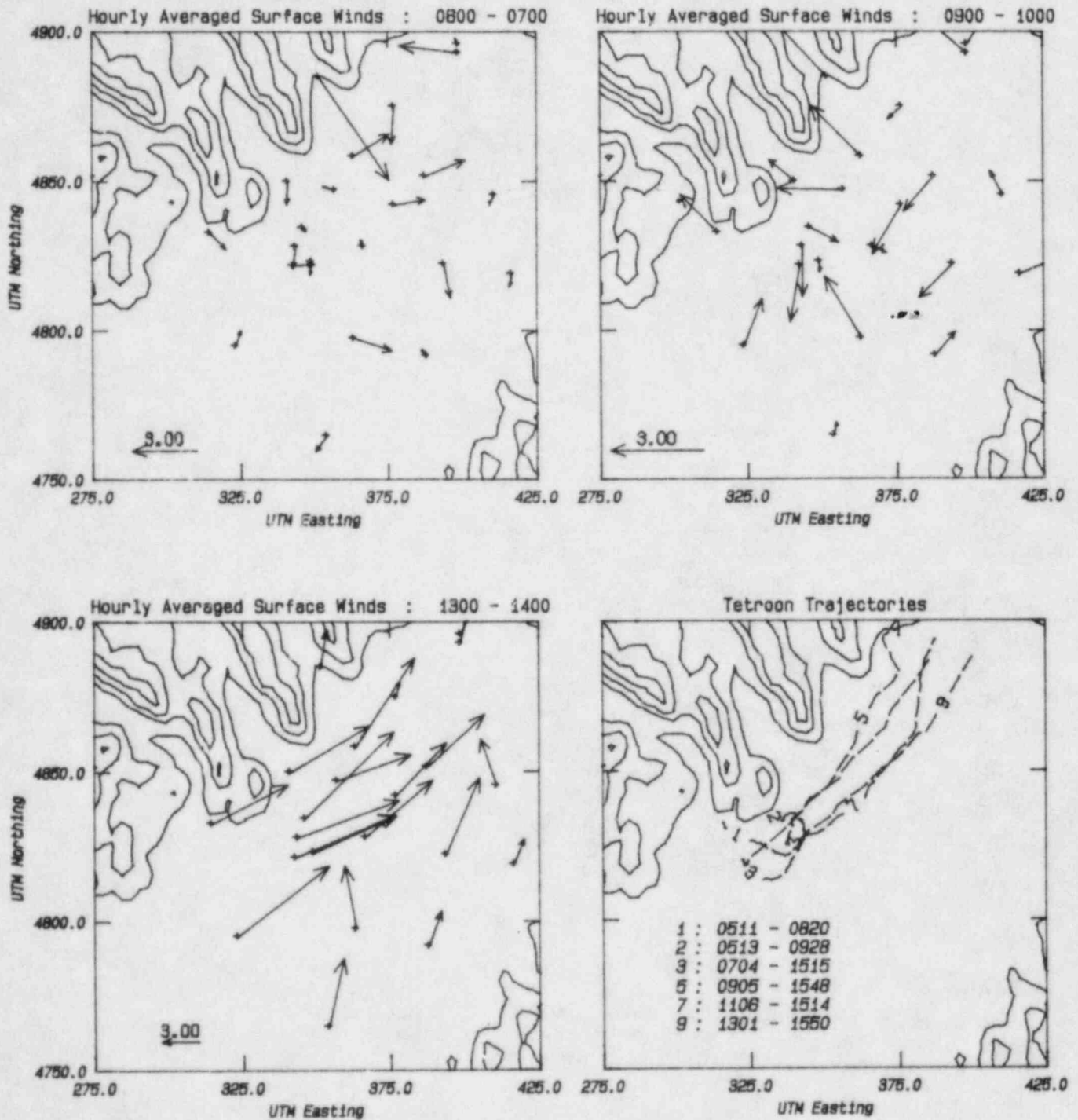


Figure A13



drifted toward the West with the first two tetroons apparently impacting on the topography. The variability of the wind at the source point is evidenced by the wide range of initial directions, even for tetroons released at almost the same time. Tetroon number 3 moves to the Southeast, and is the first to be caught in the southwesterly flow which is established around 1100. After this time, all the tetroons move rapidly to the Northeast and out of the domain. The last tetroon leaves the domain after covering the 70 km to the boundary in 2-1/2 hours, i.e., at an average speed of  $8 \text{ ms}^{-1}$ .

Some impression of the vertical wind structure can be obtained from Figure A.14 which shows profiles of speed and direction at four different times at the tracer release point. The two early profiles show fairly light winds below 1000 m, with a direction shift from almost northeasterly at 150 m through the North back to westerly at 1000 m. At the two later times, the winds are very uniform over the 2000 m profile with a direction from the Southwest, and speed increasing from  $5 \text{ ms}^{-1}$  at 1200 to  $10 \text{ ms}^{-1}$  at 1400.

These profiles are also consistent with our assumed stability and mixing depth development, which begins with a stable layer (stability F) with depth 200 m. The morning transition begins at 0700 when the layer becomes neutral up to 300 m, then surface heating produces a deepening layer which reaches 2000 m with stability B at 1100, and 3000 m with stability A at 1300. The stability falls back to C in the afternoon as the heating is reduced, in view of the relatively high wind speeds.

The measurements of tracer concentration on the surface are shown in Figures A.15-17. The hourly averages are clearly very patchy, even on the small horizontal scale covered by the small-bag samplers. The early hours show the largest surface impact to be west of the source; this is consistent with the early tetroon trajectories, but does not correlate with any of the Mesonet wind measurements. For later hours, the flow was from the Southwest, and the surface concentrations are lower because of the greater mixing depth. The patterns are still very patchy, and show that material has been mostly swept out of the area by the twelfth hour

July 1981 INEL Field Experiment : Test 5  
Vertical wind profiles at the tracer release site

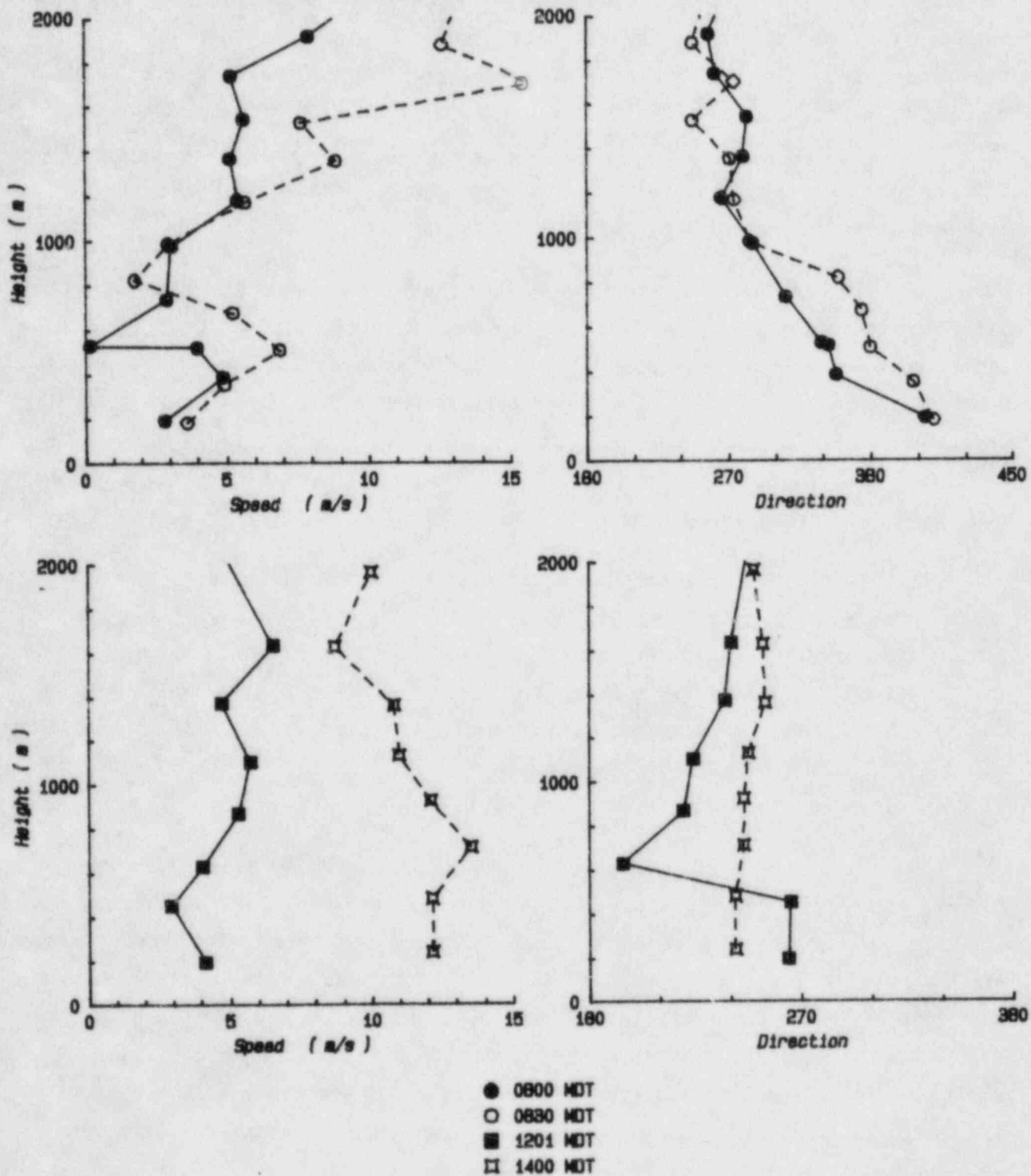


Figure A14

# July 1981 INEL Field Experiment : Test 5

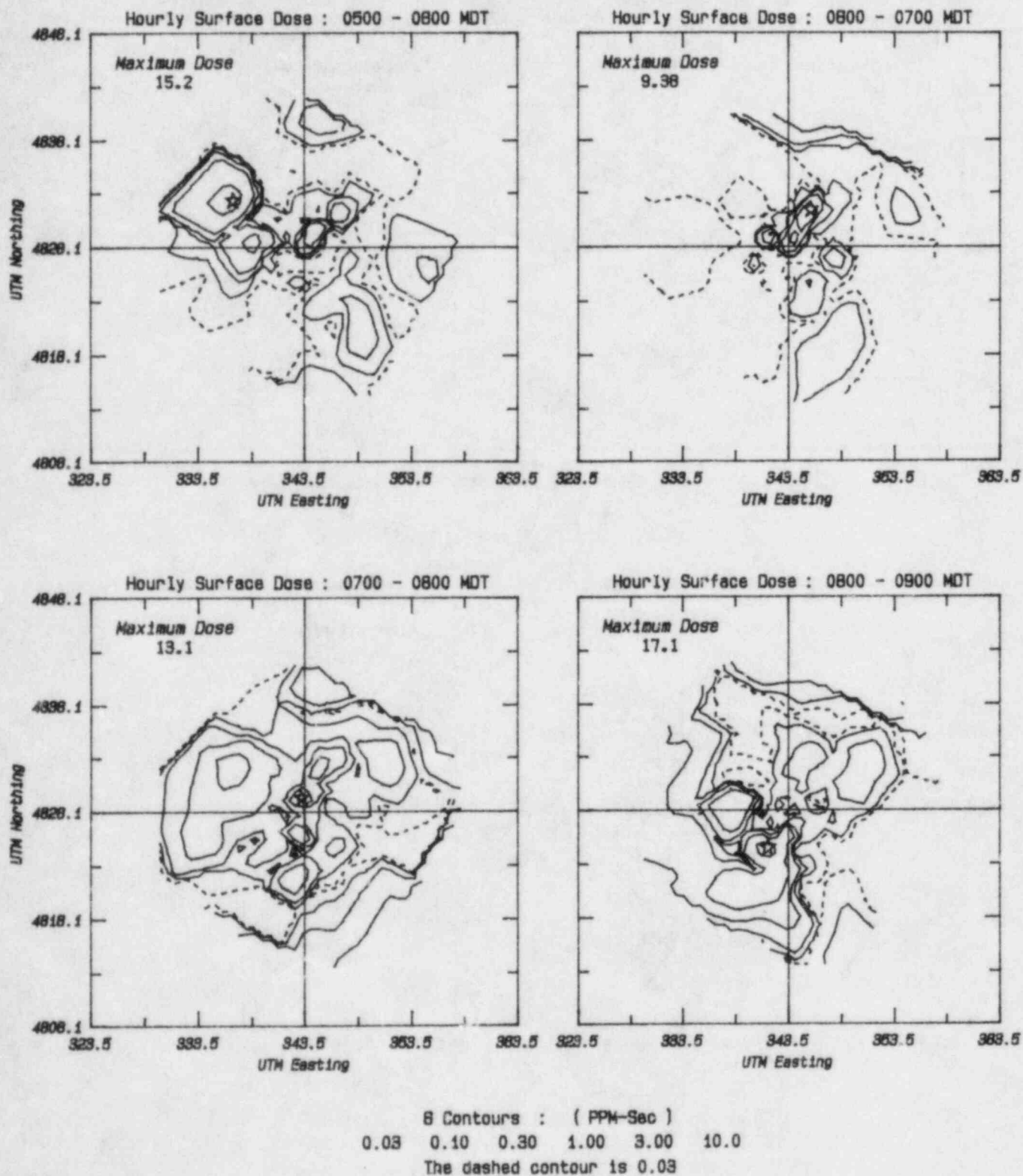


Figure A15

# July 1981 INEL Field Experiment : Test 5

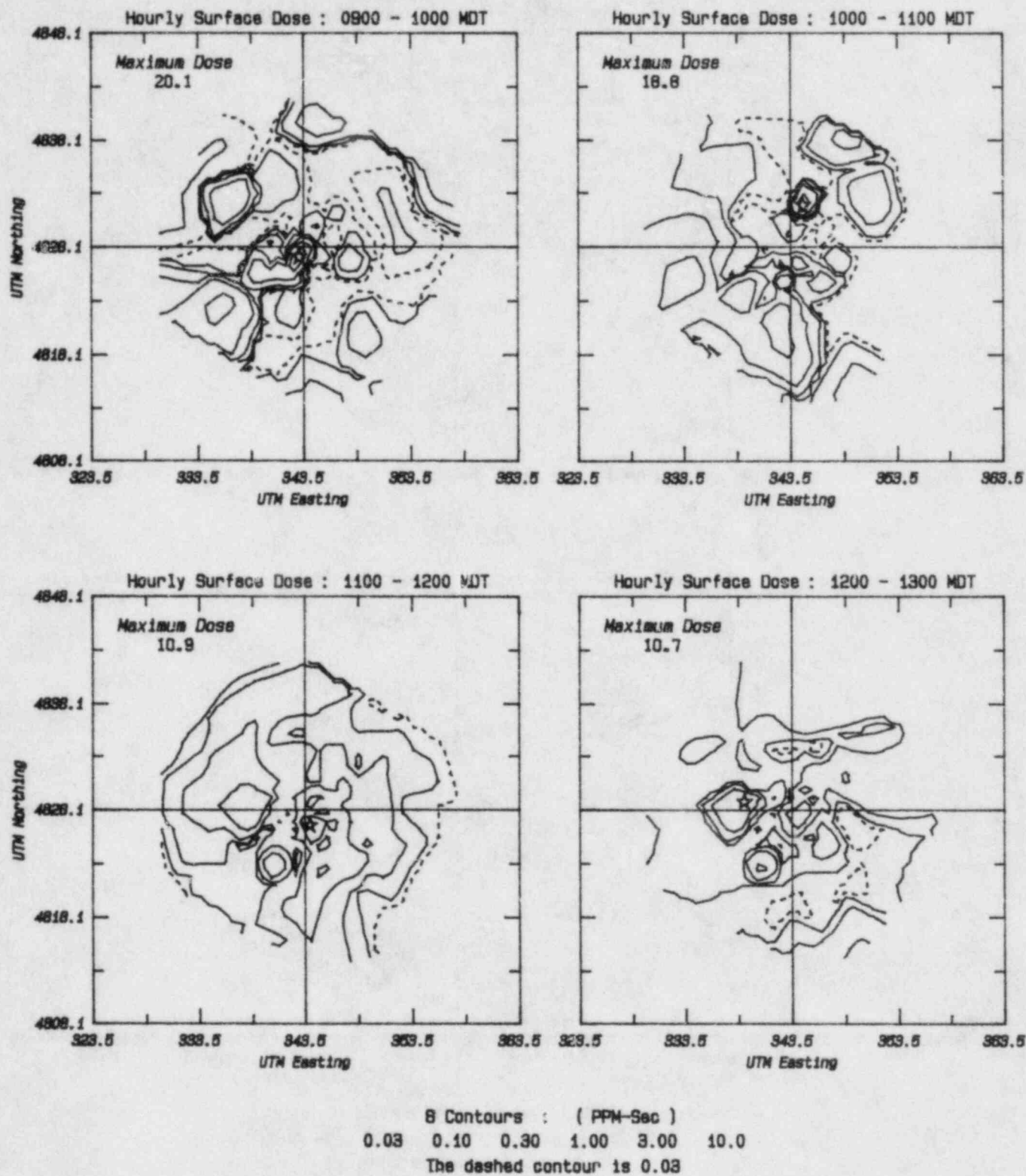


Figure A16

# July 1981 INEL Field Experiment : Test 5

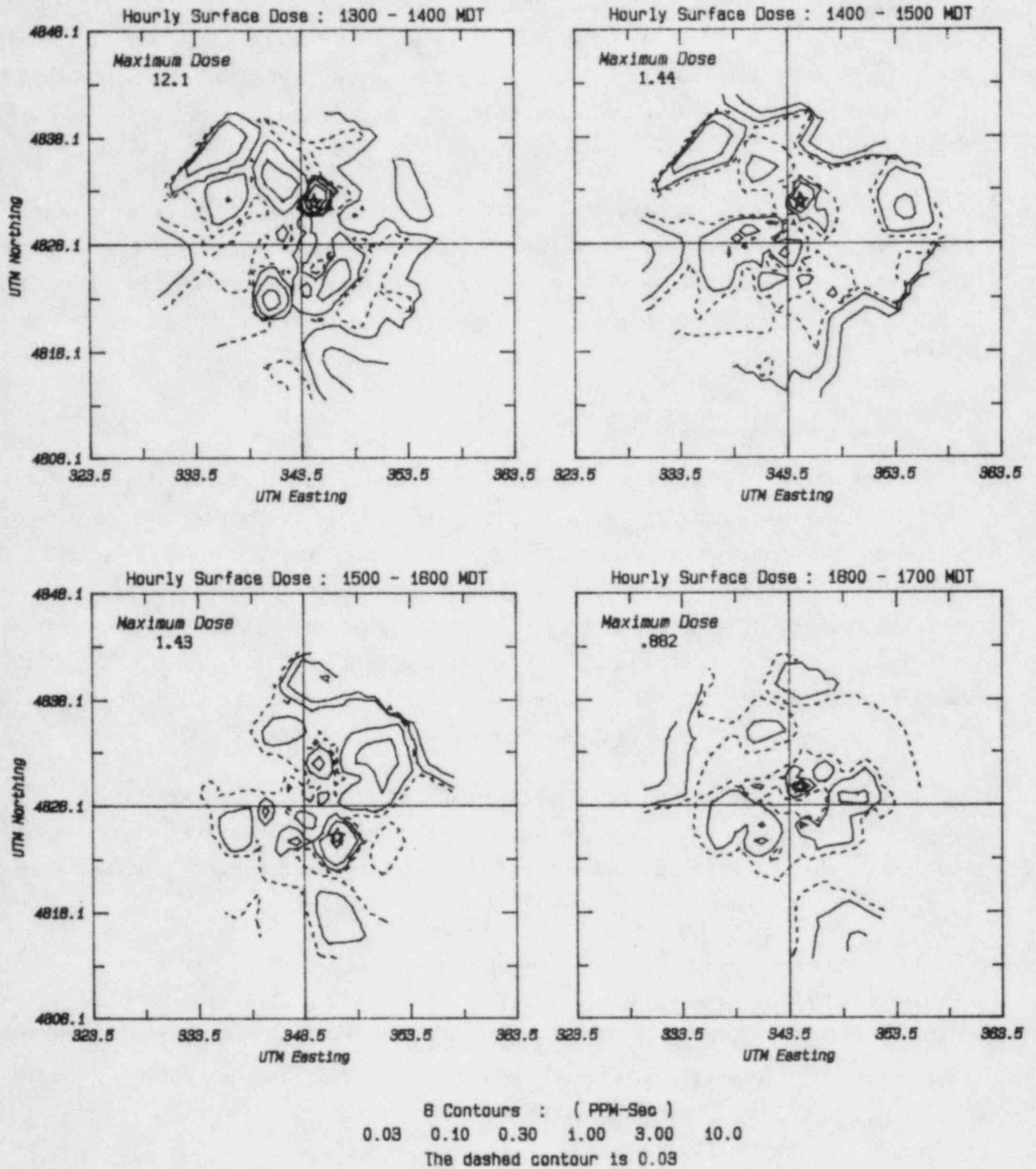


Figure A17



Figure A.18 shows the total integrated dose in the small-bag samplers over the first twelve hours. The pattern is much smoother than the individual hours, and indicates the highest doses are to the West of the source. There are significant surface measurements out to the Northeast, and in virtually every direction except far to the Southwest.

The doses from the large bags which are spread over a larger area are also shown in Figure A.18. These results are in general agreement with the small-bag samples in the very limited region of overlap; they also give a maximum dose to the Northwest of the source, and very small doses in the southeastern regions.

Test 6: 1700:7/25 - 0100:7/26:400 lbs/hr.

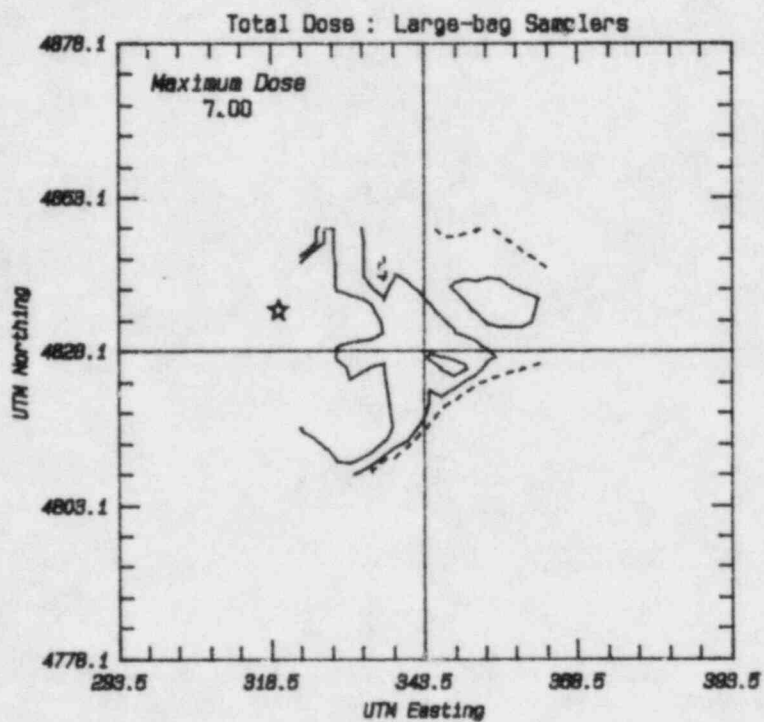
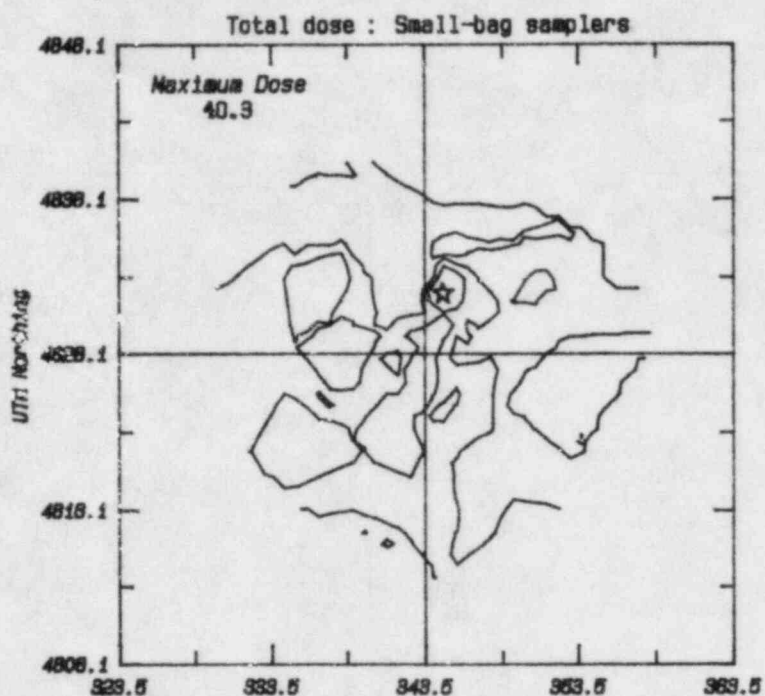
In contrast to the previous tests, the meteorological situation for test 6 was very simple. For the eight hours of the test release the surface winds decreased from about  $10\text{ms}^{-1}$  to  $5\text{ms}^{-1}$  but were constant in direction, being from the northeast. This direction was maintained throughout the night although the wind speeds continued to decrease. For most of the test, therefore, conditions were neutral, becoming slightly stable after 2300. The surface wind patterns in Figure A.19 demonstrate the consistency of the flow. The tetroon trajectories also show an unambiguous flow direction.

The vertical wind profiles in Figure A20 show that the northeasterly flow extends up to 1000m above the ground, with a reversal to westerly winds above 2000m. We therefore expect the entire plume to be transported southwest in this 1000m layer.

The surface doses from the  $\text{SF}_6$  samplers, Figures A.21-23 confirm our expectations from the meteorology. All 12 hours show a plume in the southwest quadrant, with doses dropping off after the end of the release. The 12 hour integrated dose consequently shows a strong plume in this direction, Figure A.24, and the large bag samples confirm it, although they also show some tracer in the northeast.



# July 1981 INEL Field Experiment : Test 5



4 Contours : ( PPM-Sec )  
 0.30 1.00 3.00 10.0  
 The dashed contour is 0.30

Figure A18

# July 1981 INEL Field Experiment : Test 6

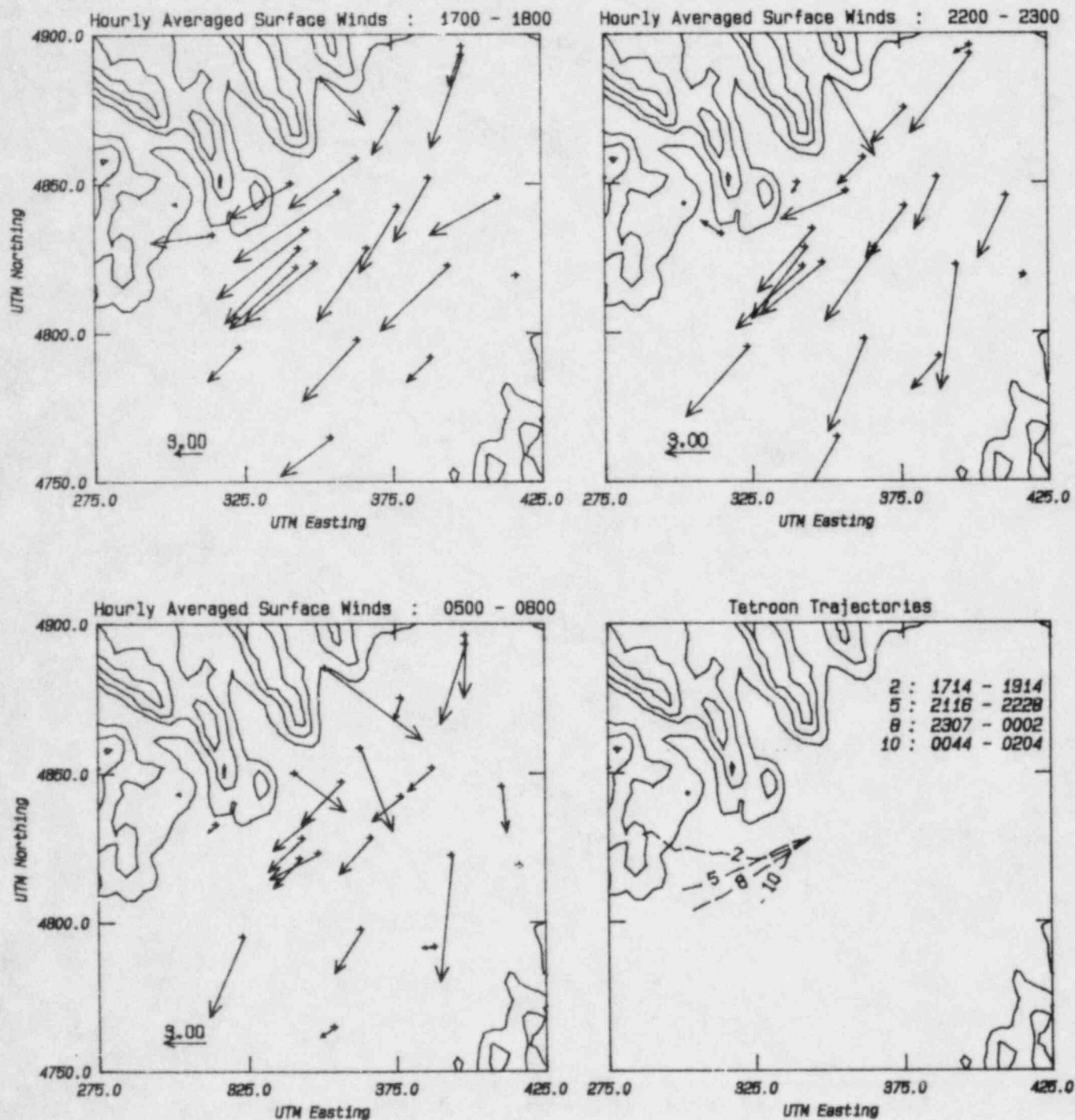


Figure A19

# July 1981 INEL Field Experiment : Test 6

Vertical wind profiles at the tracer release site

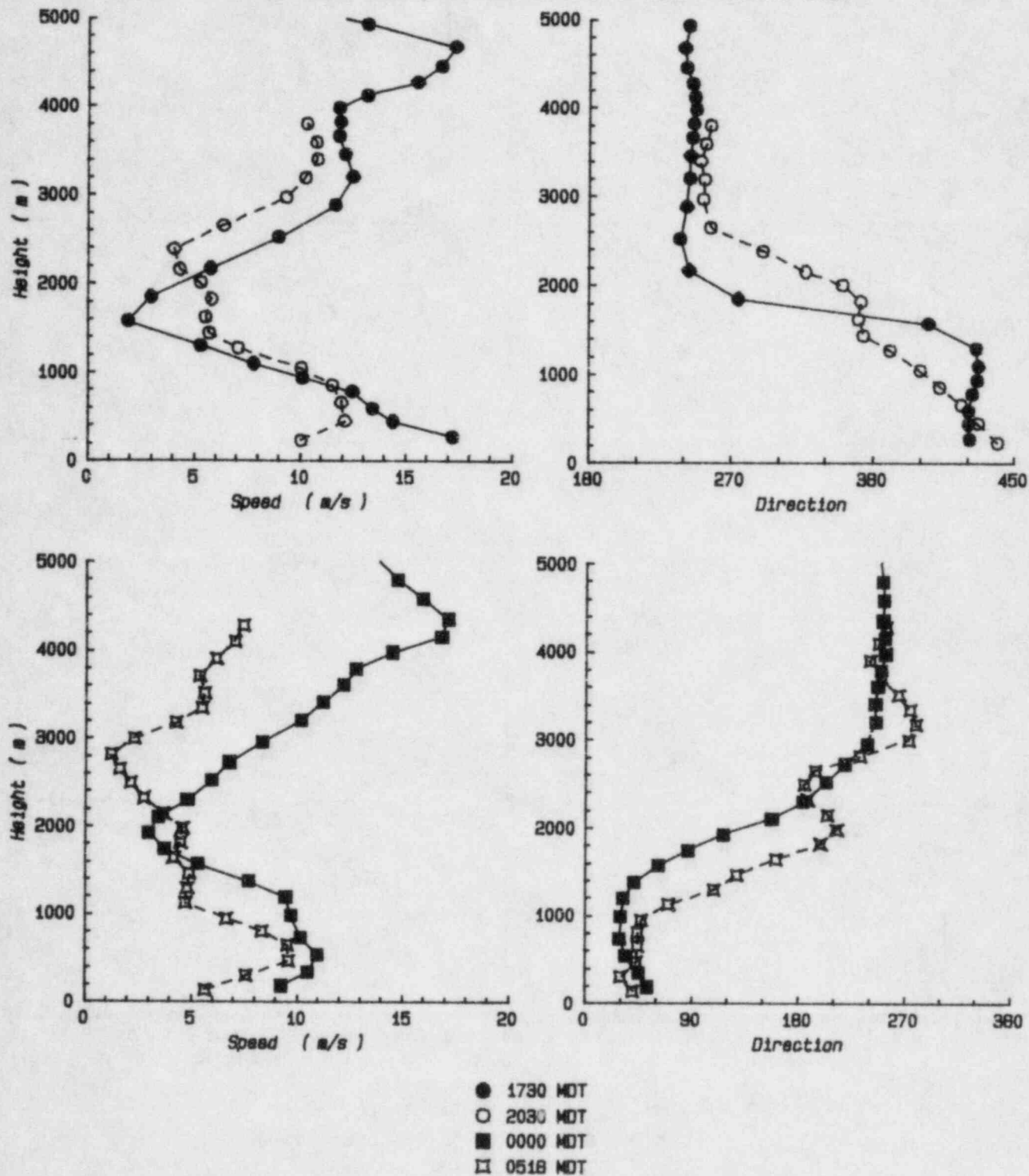


Figure A20

# July 1981 INEL Field Experiment : Test 6

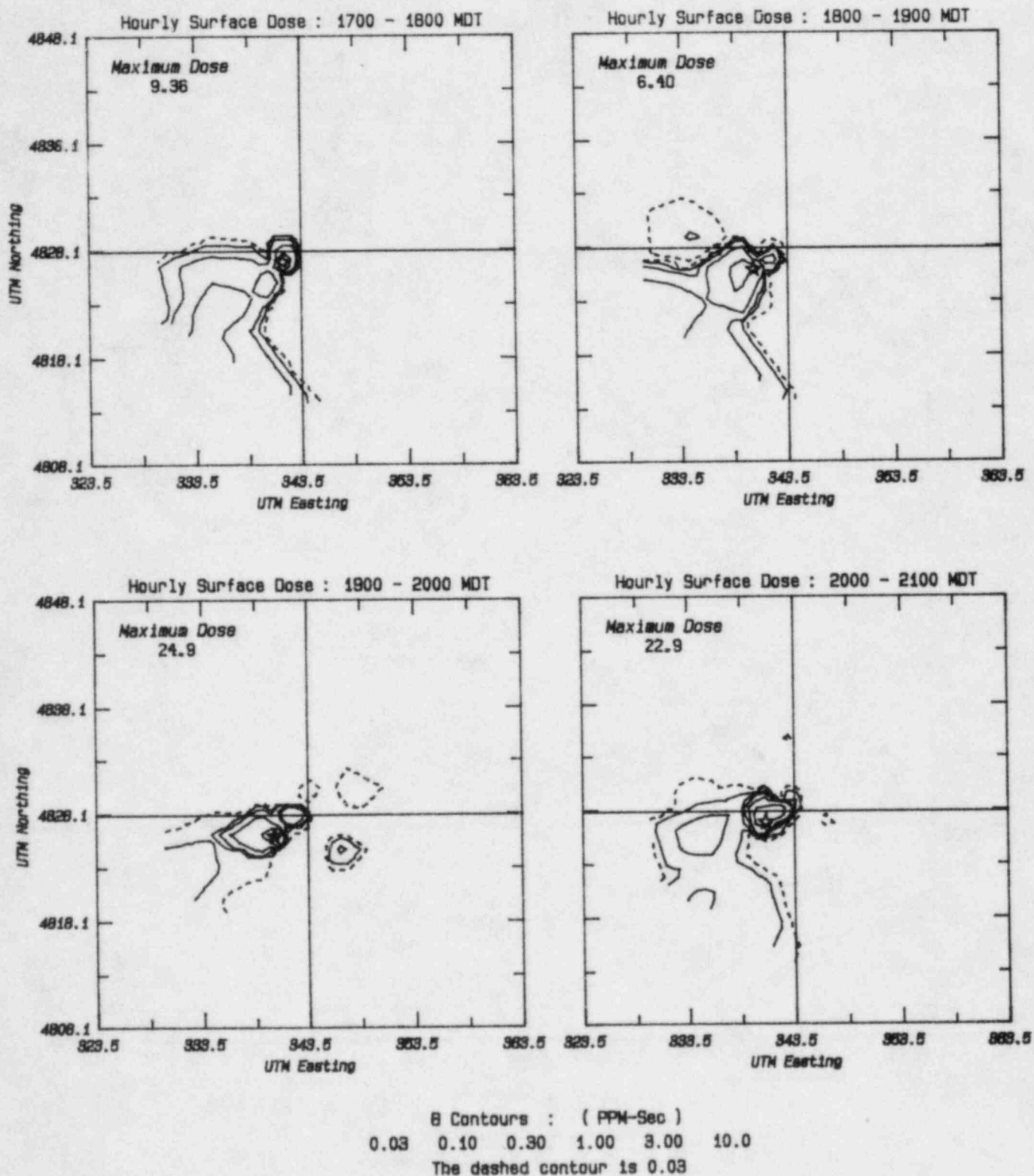


Figure A21

# July 1981 INEL Field Experiment : Test 6

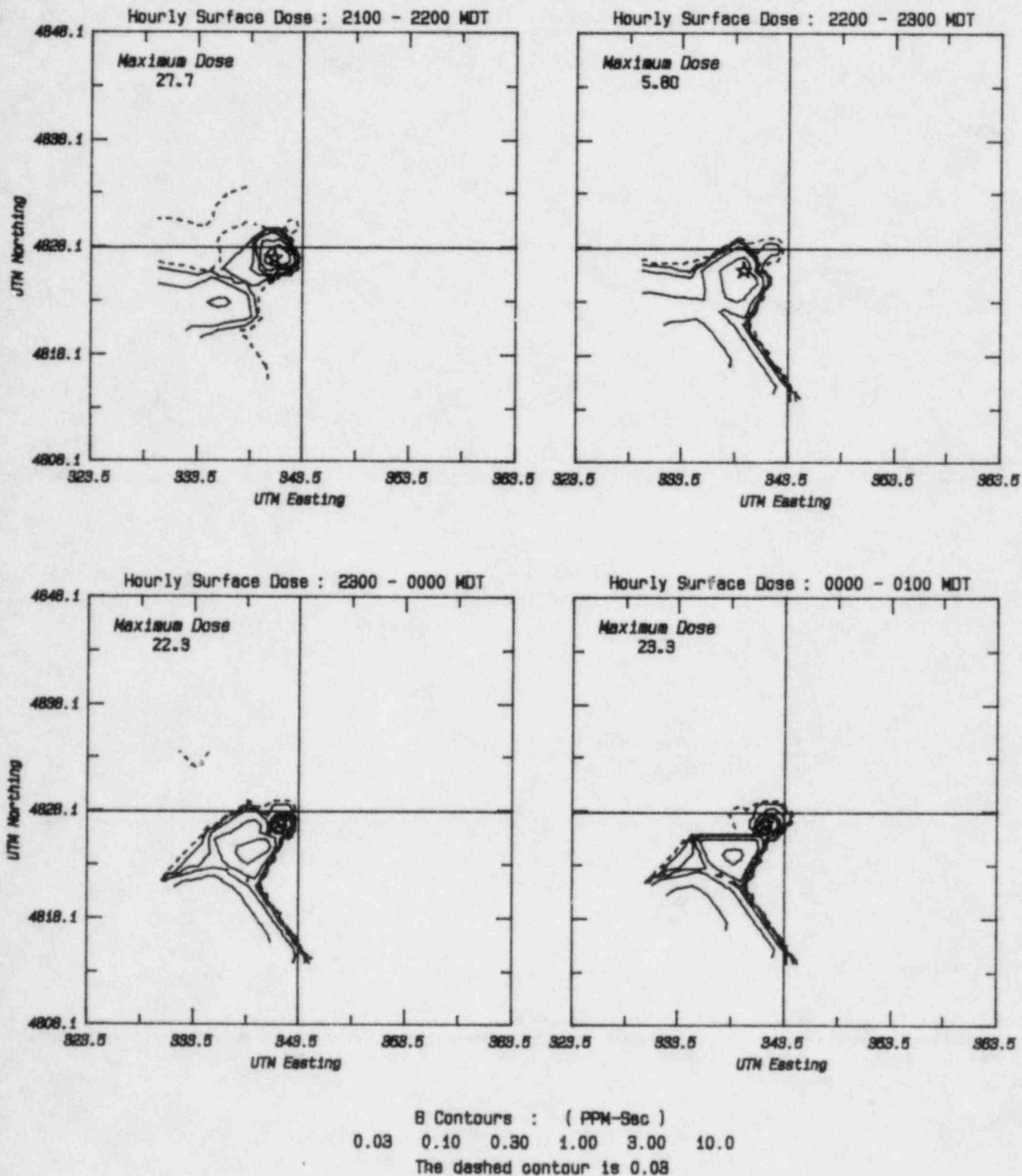


Figure A22



# July 1981 INEL Field Experiment : Test 6

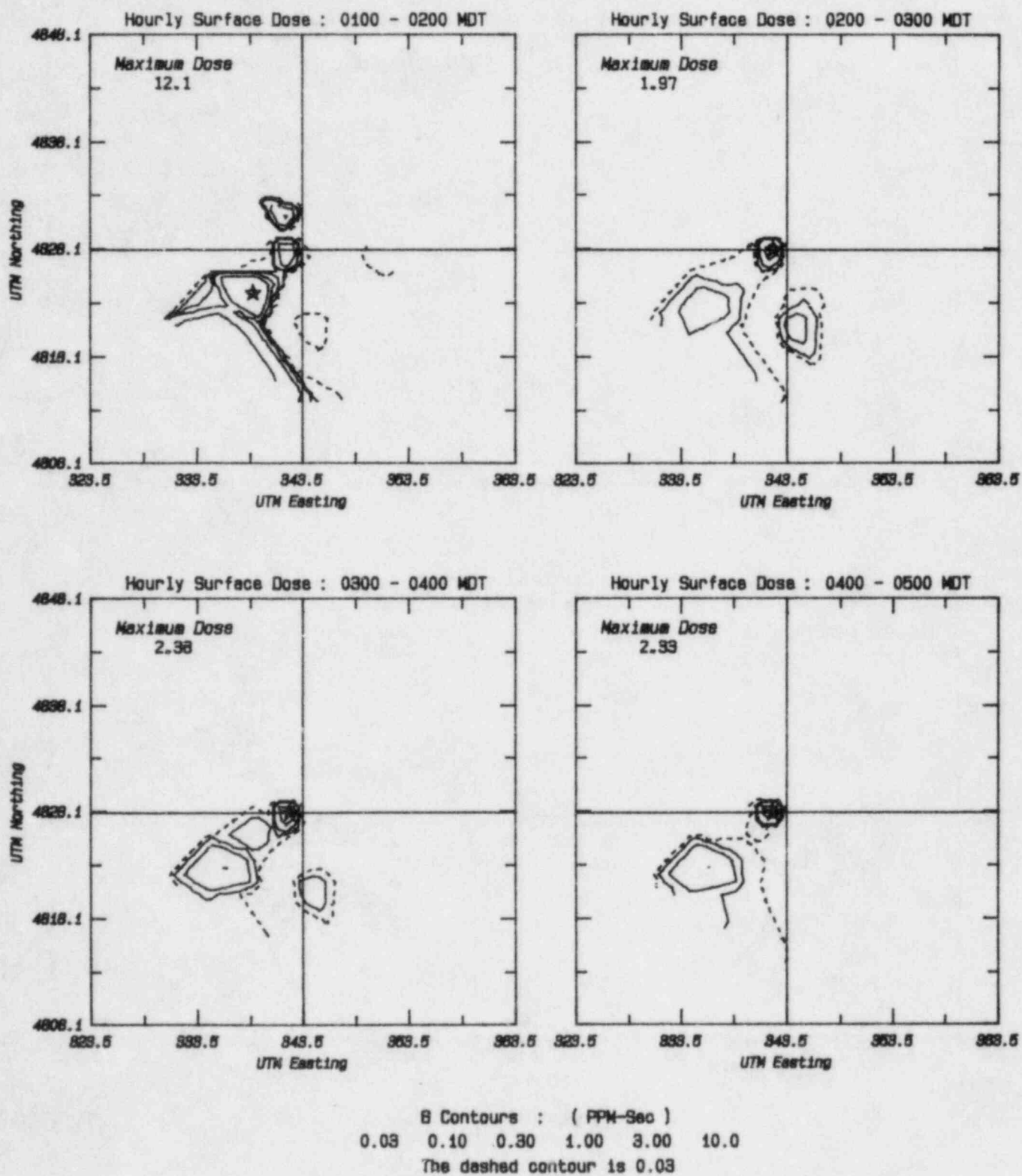


Figure A23



# July 1981 INEL Field Experiment : Test 6

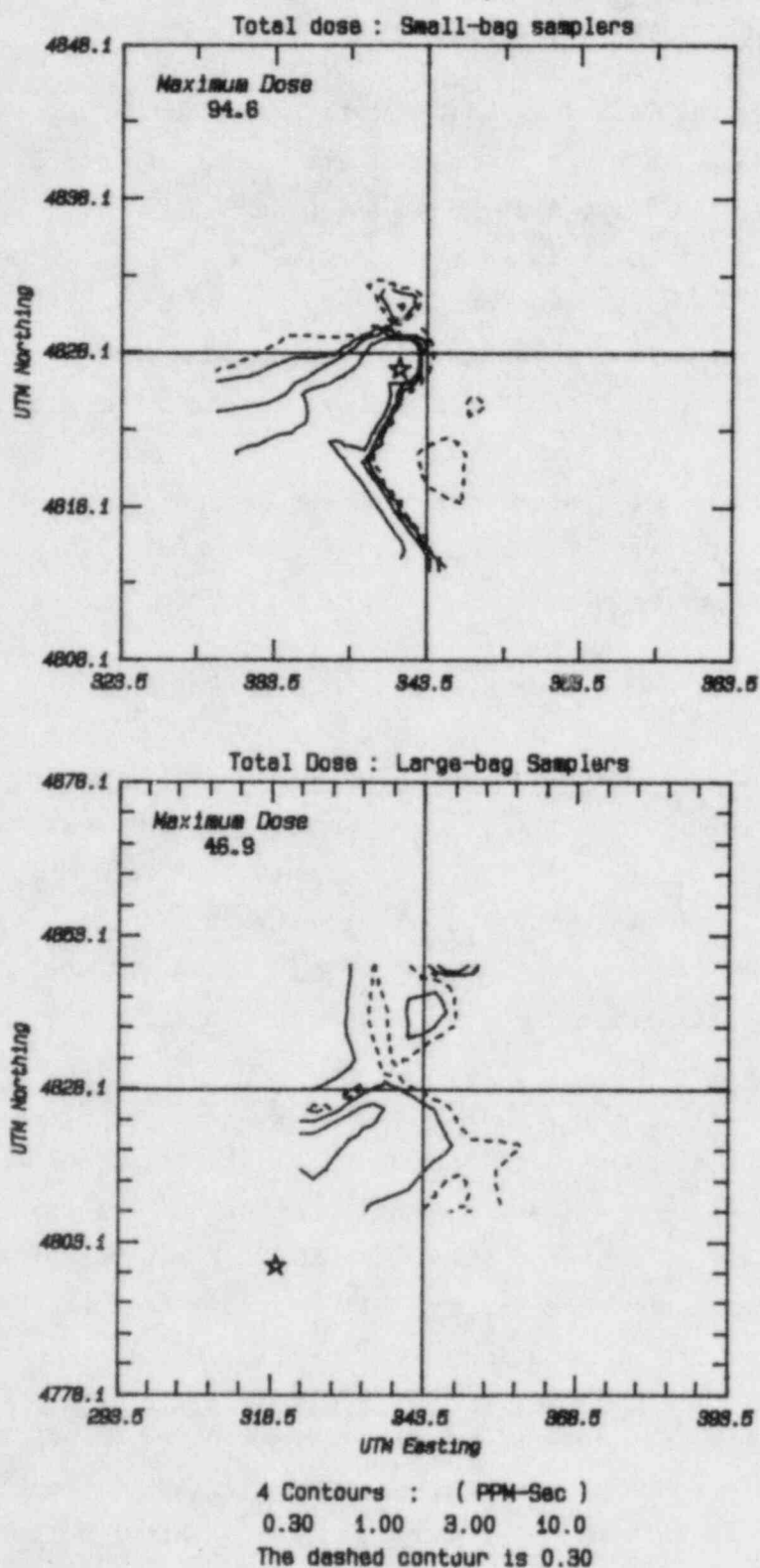


Figure A24

Test 7: 1300-2100 MDT. 7/27/81 400lbs/hr.

In many respects, Test 7 is complementary to Test 5 in that this case covers the afternoon flow and evening transition to nocturnal flow. Figure A.25 shows surface wind vectors at three times during the test. The winds at 1300 show a general southerly to southwesterly wind of about  $3 \text{ ms}^{-1}$  throughout the valley. This is the same general flow as in the afternoon period of Test 5, although somewhat reduced in speed. This surface flow pattern persists until the evening, when nocturnal cooling begins to dominate the winds. The wind vectors at 2200 show the flow beginning to change; in the upper or northern part of the valley, winds are reversed as the cold surface begins to drive a flow down the valley. At this time there is still southerly flow at the source, but the speed has been reduced. By 0200, the winds have been reversed throughout the domain, and the general flow is about  $2-3 \text{ ms}^{-1}$  from the North or Northeast.

The tetroon trajectories shown in Figure A.25 also help to describe the flow pattern throughout the test. The early tetroons, set to fly in the middle of the mixed layer around 1500 m, are swept out of the domain to the Northeast. Tetroon number 3, released at roughly 1700 MDT, also leaves the domain on the northern boundary around 2200, but later returns with the reversed flow which presumably builds upward from the surface as well as down the valley from the North. Later tetroons move up the valley to the North-Northwest of the release point and do not reverse direction. This is rather surprising, but apparently indicates that the downslope wind out of the narrow valley is either less well-established or is shallower. The latter seems likely, since the fetch for this flow is much shorter than the larger scale Snake River valley circulation. Thus it may be that the tetroons fly above the downslope wind and continue up the valley.

The vertical structure of the atmosphere is described by the mixing depth and stability, and by the vertical wind profiles. The mixing depth is taken to be 3000 m through the afternoon, collapsing after about 1800 down to 400 m around midnight, and then to 200 m after midnight. The stability is A from 1300 to 1600, going through neutral at 2000, to stability E at 2100.

# July 1981 INEL Field Experiment : Test 7

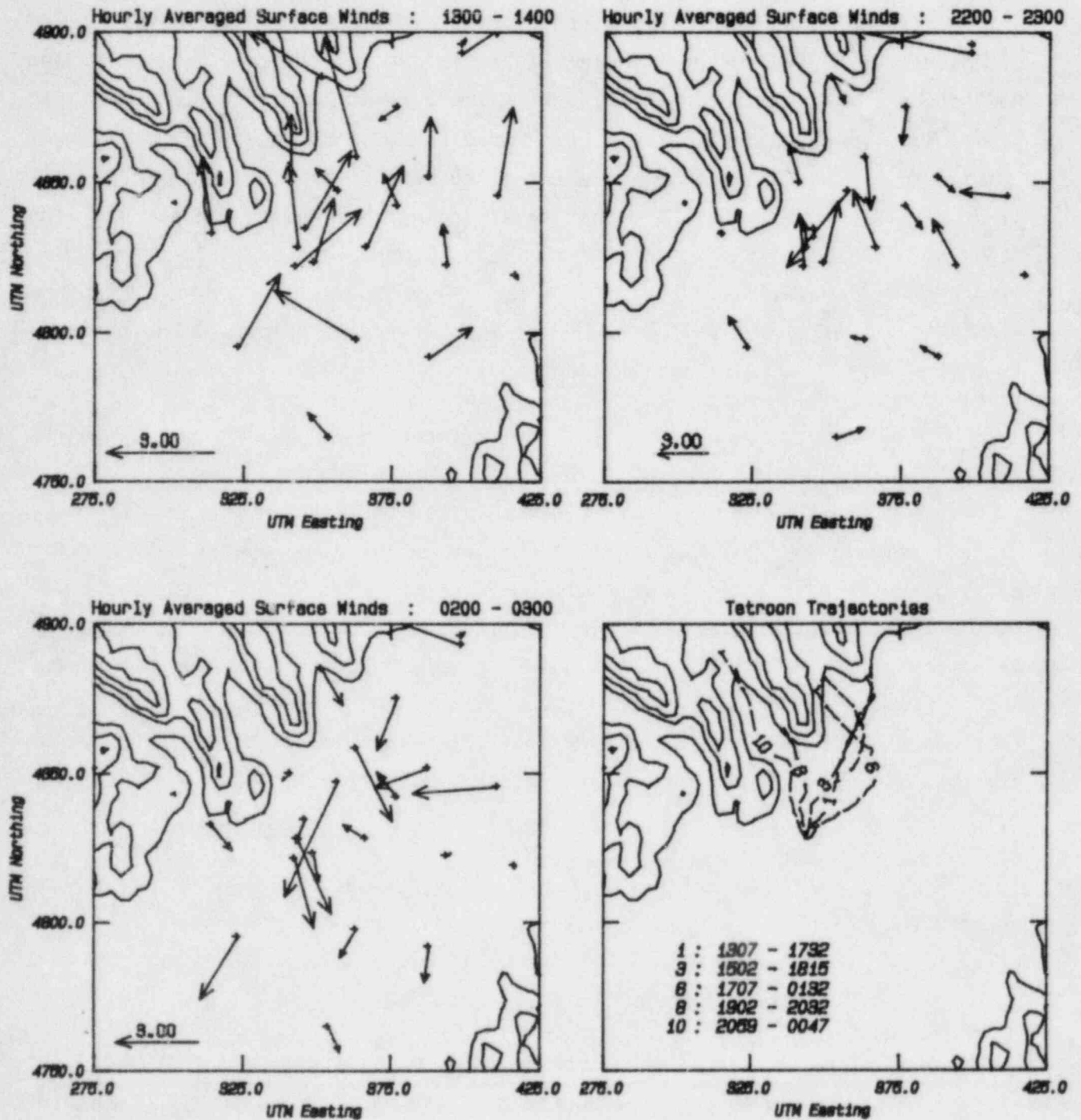


Figure A25

Vertical wind profiles are shown in Figure A.26. At 1300 a mixed layer of 2500 m is evident at the tracer release point, with a speed of about  $4 \text{ ms}^{-1}$ , and direction changing from southerly at the surface to westerly or northwesterly at the top of the mixed layer and above. By 1800 MDT, the speed has increased to  $6 \text{ ms}^{-1}$  and the direction is more uniform through the mixed layer, being southwesterly everywhere. At 2200 MDT, the speed is much higher,  $10 \text{ ms}^{-1}$  in the lowest 1000 m, while the direction is still south to southwest. At 0200, the wind below 400 m has reversed as indicated in the surface wind vectors. The wind changes from  $4 \text{ ms}^{-1}$  from the Northeast at 200 m through an almost stagnant layer at 400 m to  $8 \text{ ms}^{-1}$  from the Southwest at 600 m and above. At this time, we therefore have two streams flowing in opposite directions with a wind reversal at 400 m.

The deep mixing layer during the afternoon results in generally low surface concentrations throughout Test 7. As in Test 5, the hourly fields (shown in Figures A.27-29) are very patchy. For the first seven hours, there is a maximum concentration close to the source, within 3 km say, and regions of smaller doses spread throughout the region between  $270^\circ$  and  $120^\circ$  relative to the release point. After hour 7, the maximum close to the source begins to move outward, and disappears after hour 9 because the source is turned off after 8 hours. There are still regions of high concentration to the North of the source up to hour 12, indicating that the tracer is not being swept out of the domain. This is consistent with the wind measurements which show the wind reversing around this time.

The integrated dose for the first 12 hours, Figure A.30 shows a wide region of surface impact with a  $180^\circ$  spread about  $030^\circ$ . There is a maximum close to the source with a peak of nearly 25 ppm.-sec., and another peak of equal magnitude roughly 8 km to the North-Northwest.

On the larger domain, the large bag doses, Figure A.30, show that the tracer is brought back past the source and taken to the South over the longer averaging time. The measurements show little variation across the entire area, with values between 0.3 and 3 ppm.-sec. in almost every sampler. However, it should be noted that the background noise level in the data is

July 1981 INEL Field Experiment : Test 7  
Vertical wind profiles at the tracer release site

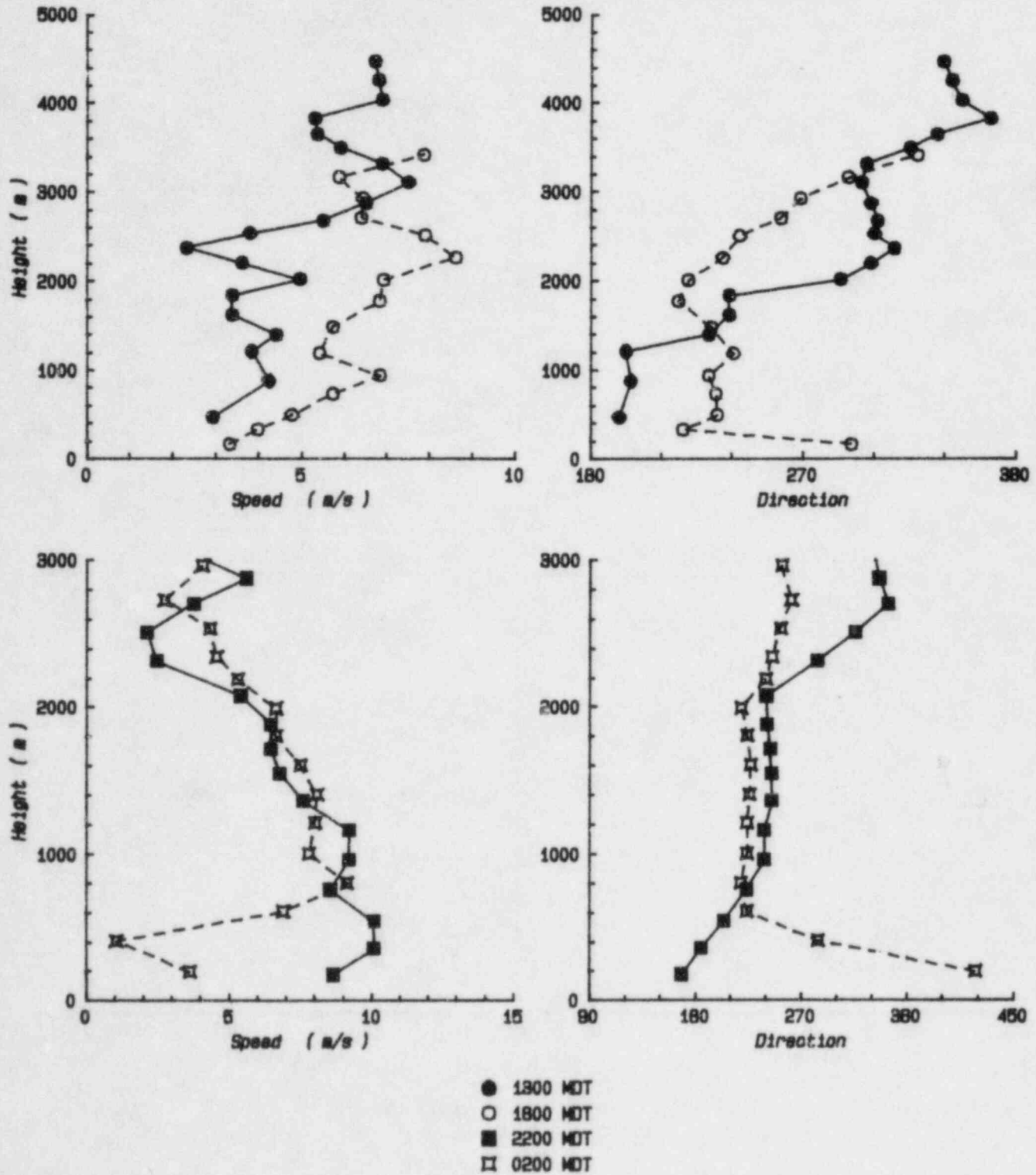


Figure A26



# July 1981 INEL Field Experiment : Test 7

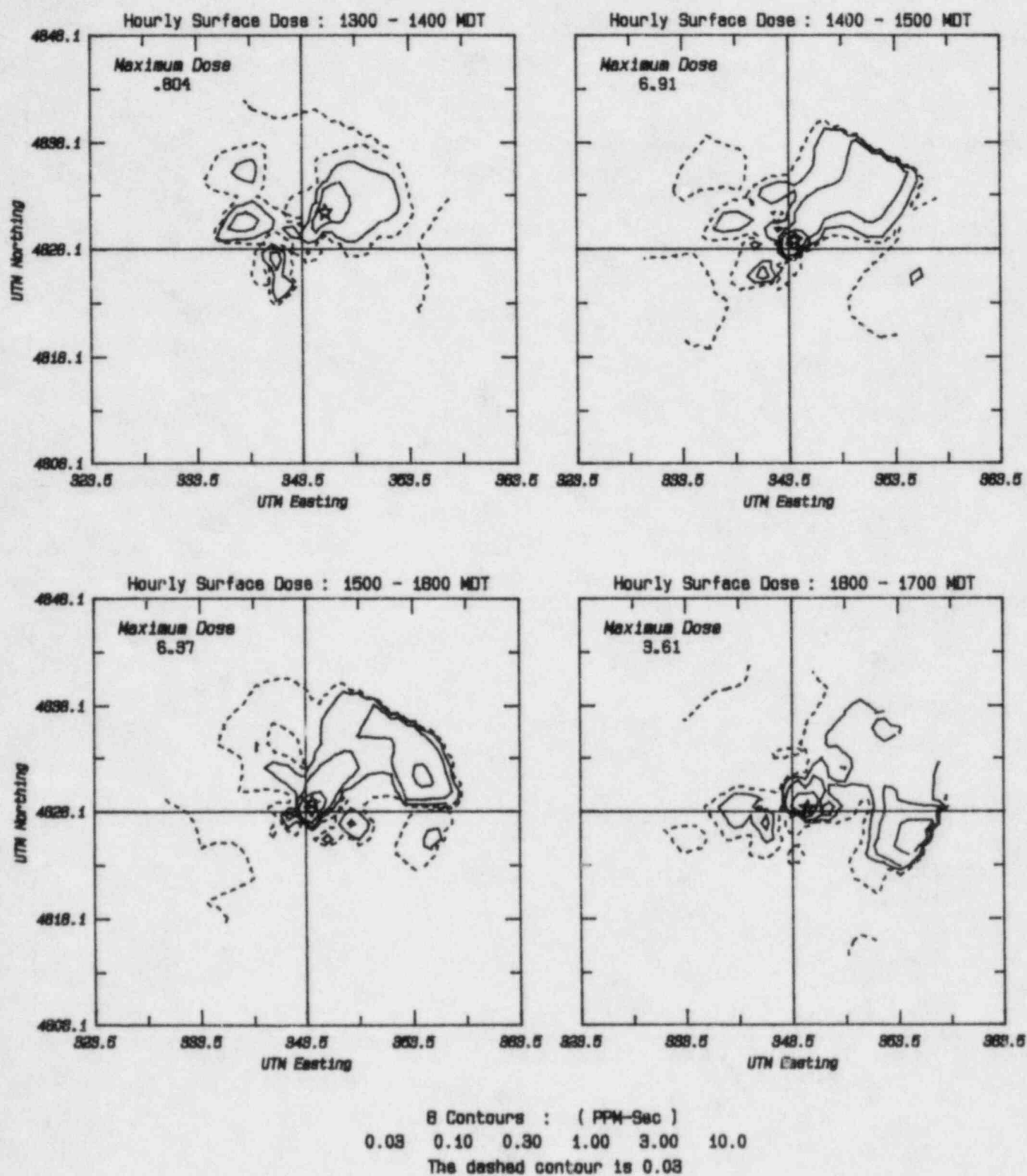


Figure A27



# July 1981 INEL Field Experiment : Test 7

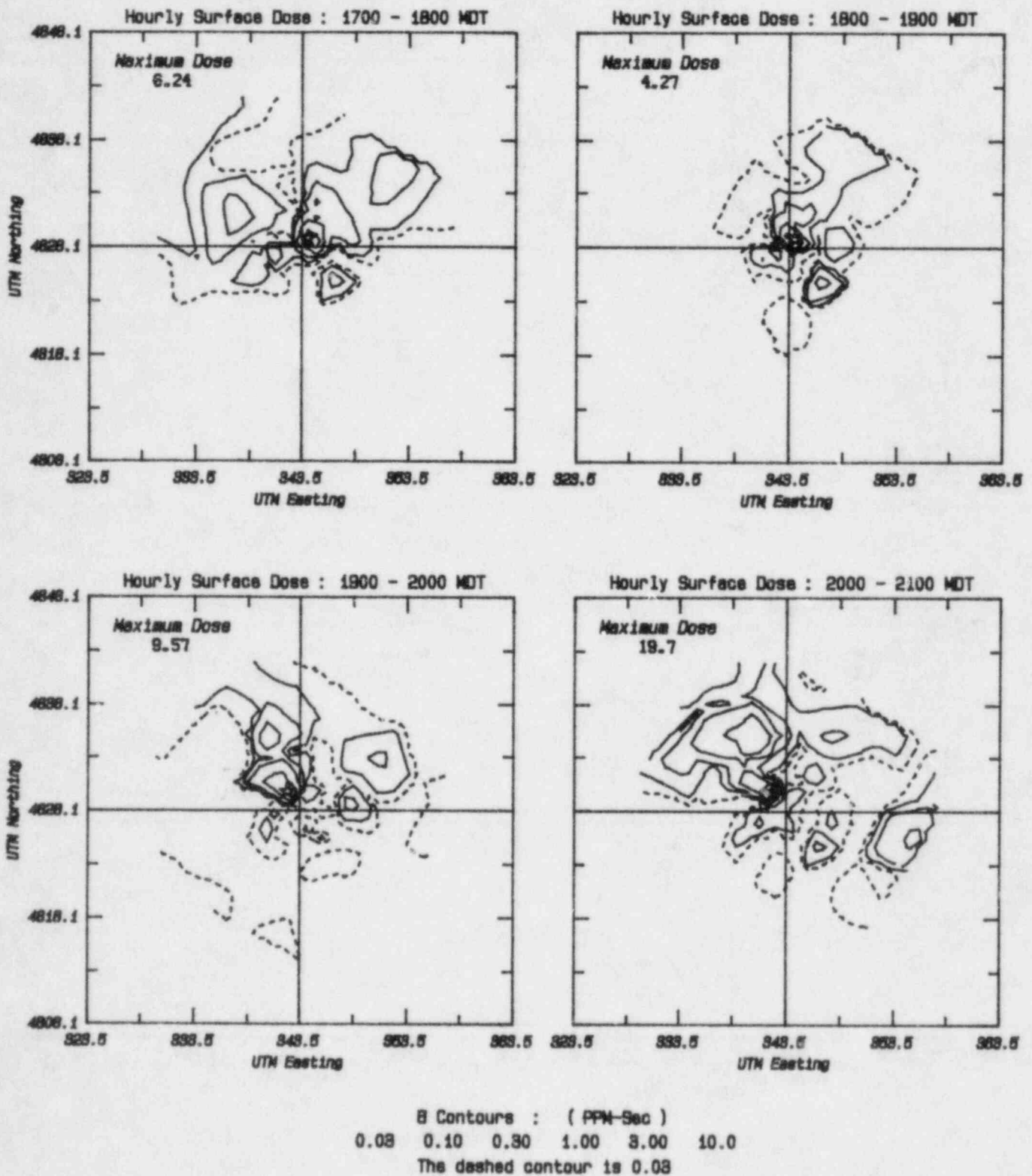


Figure A28

# July 1981 INEL Field Experiment : Test 7

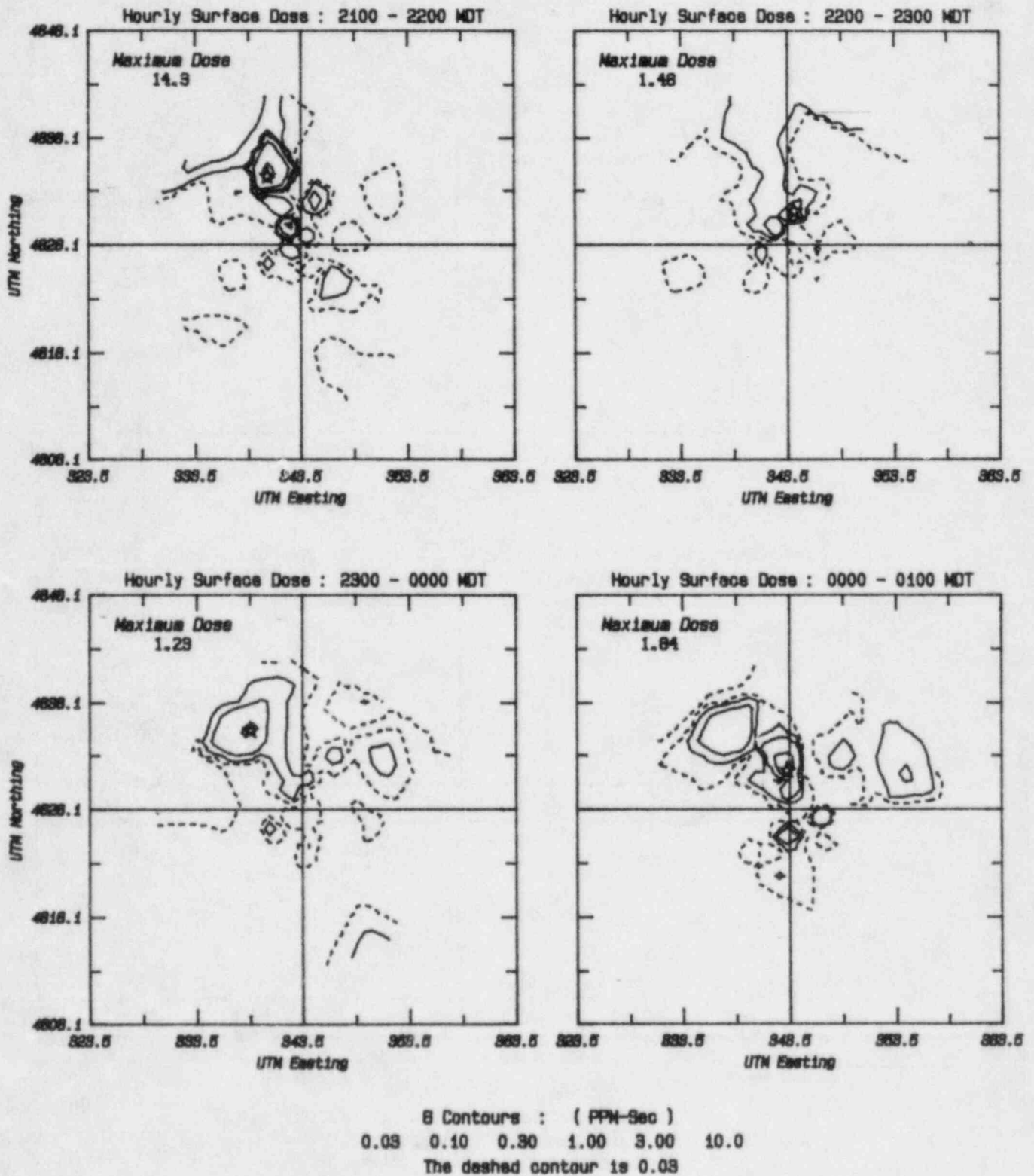
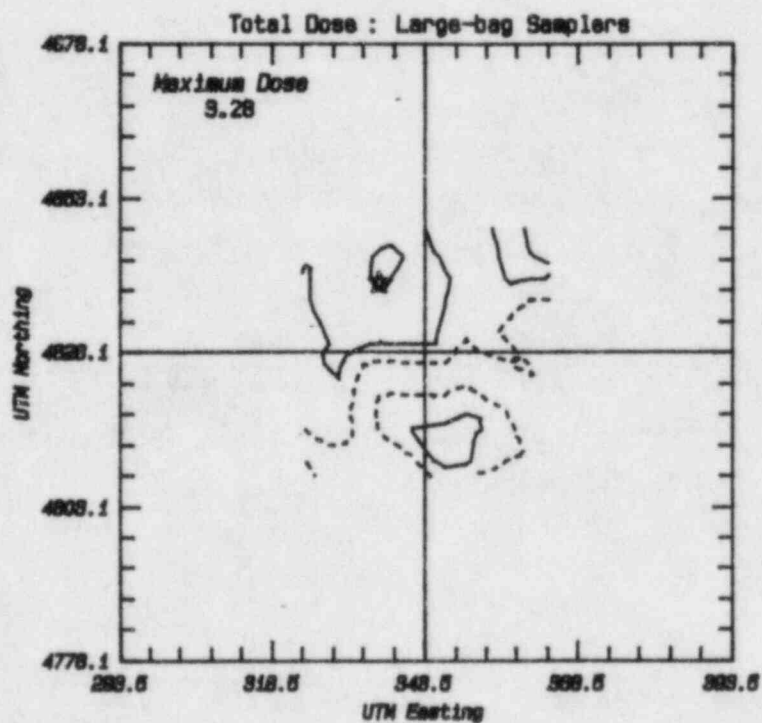
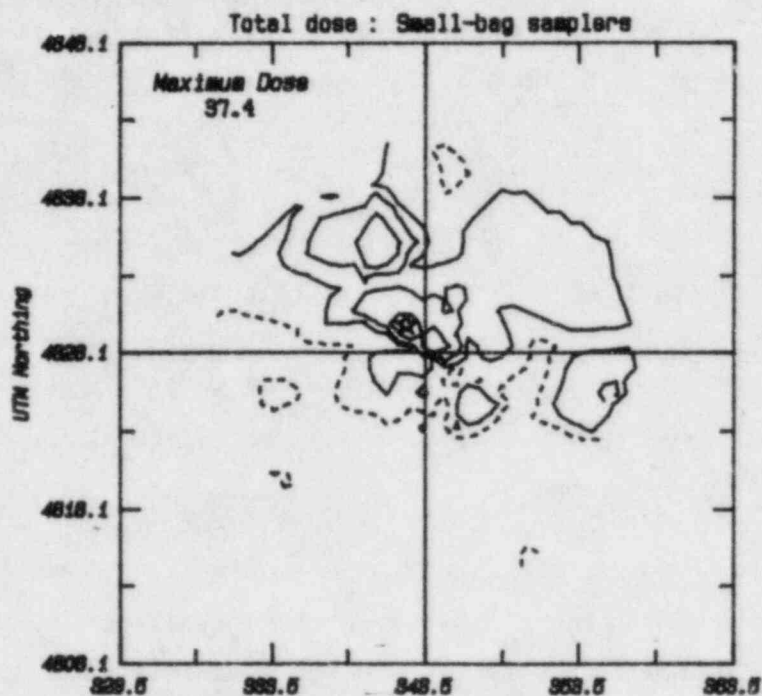


Figure A29

# July 1981 INEL Field Experiment : Test 7



4 Contours : ( PPM-sec )  
0.30 1.00 3.00 10.0  
The dashed contour is 0.30

Figure A30

roughly 0.2 ppm.-sec., so that there are actually very few measurements which are significantly higher than the noise.

Test 8: 0500 - 1300:7/29:400 lbs/hr.

Test 8 is similar to test 5 in its timing as an early morning release into a developing convective layer. The initial stable layer began to erode about two hours after the start of the release, and the boundary layer grew up to a depth of 2 km over a six hour period. The surface winds, Figure A.31, were very light and variable up to 1000, when a strong southwesterly flow set in and remained throughout the day.

The tetroons show a distinct flow to the southwest in the first half of the release, followed by strong flow to the northeast. This is confirmed by the wind profiles, Figure A.32 which show a northeasterly flow up to 400m at 0600 and 0930. This lower layer is destroyed by the convective mixing and later profiles show constant wind direction up to 2000m.

The surface  $SF_6$  hourly doses, Figures A.33-35, show somewhat indeterminate direction for the first three hours, followed by a southwest plume for three hours, and an eventual reversal toward the northwest. Shortly after the end of the release, all tracer material is removed from the sampler network.

The 12 hour dose, Figure A.36, shows highest values in a plume to the southwest with some extension in the opposite direction. This pattern is confirmed by the large bag sample data.

Test 9: 1700:7/30 - 0100:7/31:600 lbs/hr.

Test 9 was executed over the same time of day as test 6, and does bear some relation to that test, with the major difference that the wind is in the opposite direction. The surface winds at the start of the release are about  $10\text{ms}^{-1}$  from the southwest, as shown in Figure A.37. This direction persists throughout the release, although there is some reversal in the early morning of 7/31. The winds at 0500-0600 are light and variable, and the tetroons show

# July 1981 INEL Field Experiment : Test 8

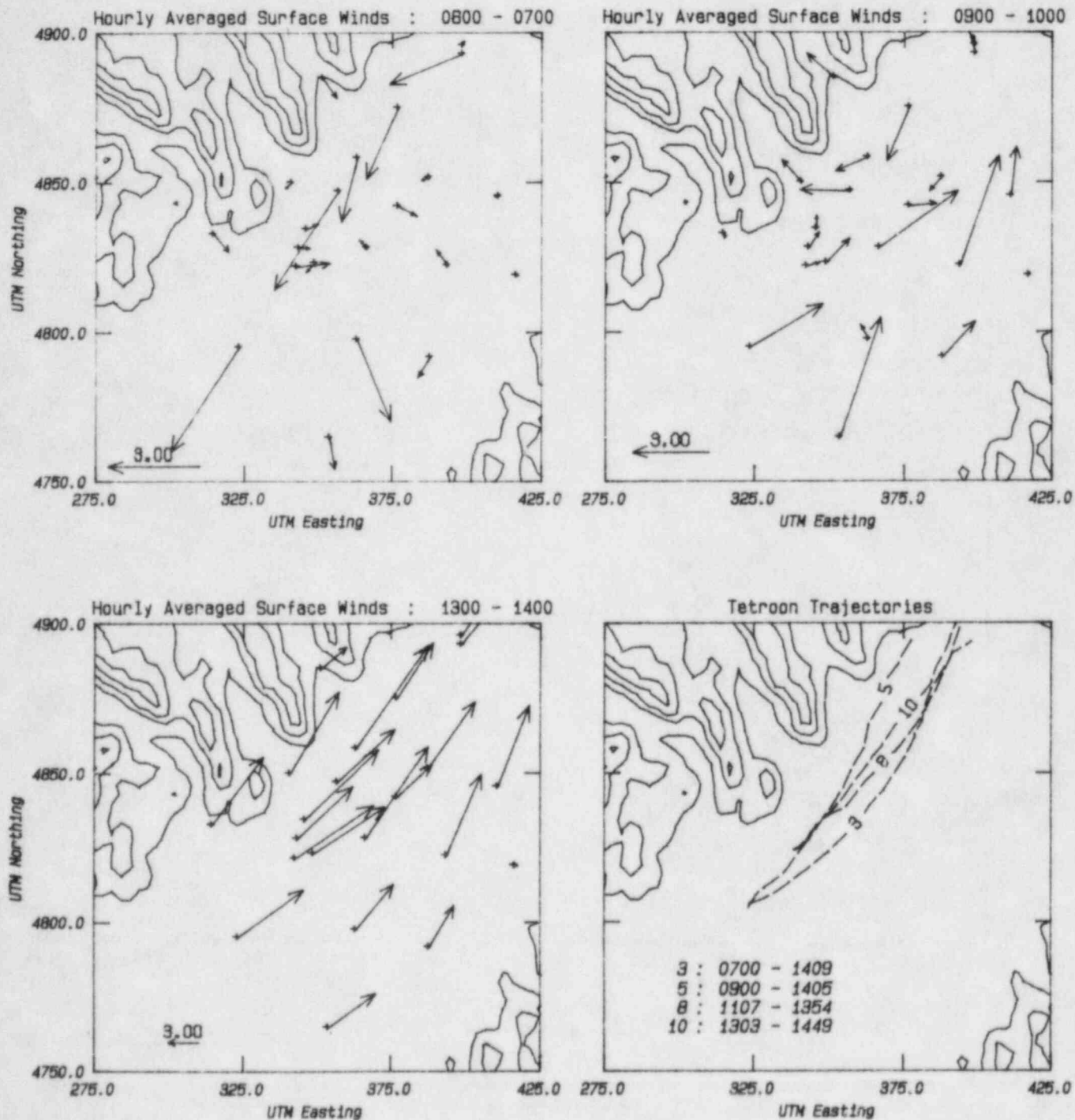


Figure A31



# July 1981 INEL Field Experiment : Test 8

Vertical wind profiles at the tracer release site

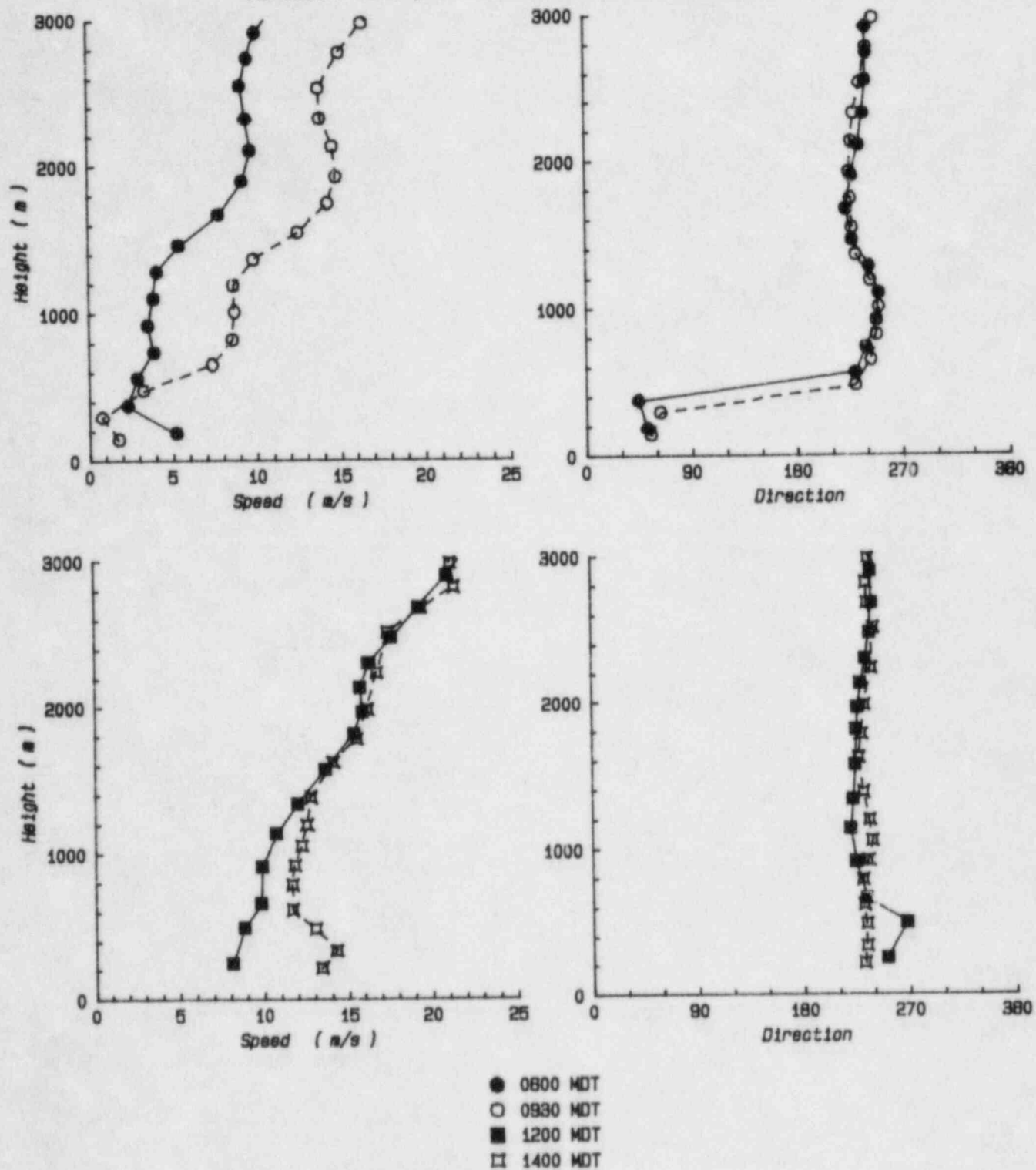


Figure A32



# July 1981 INEL Field Experiment : Test 8

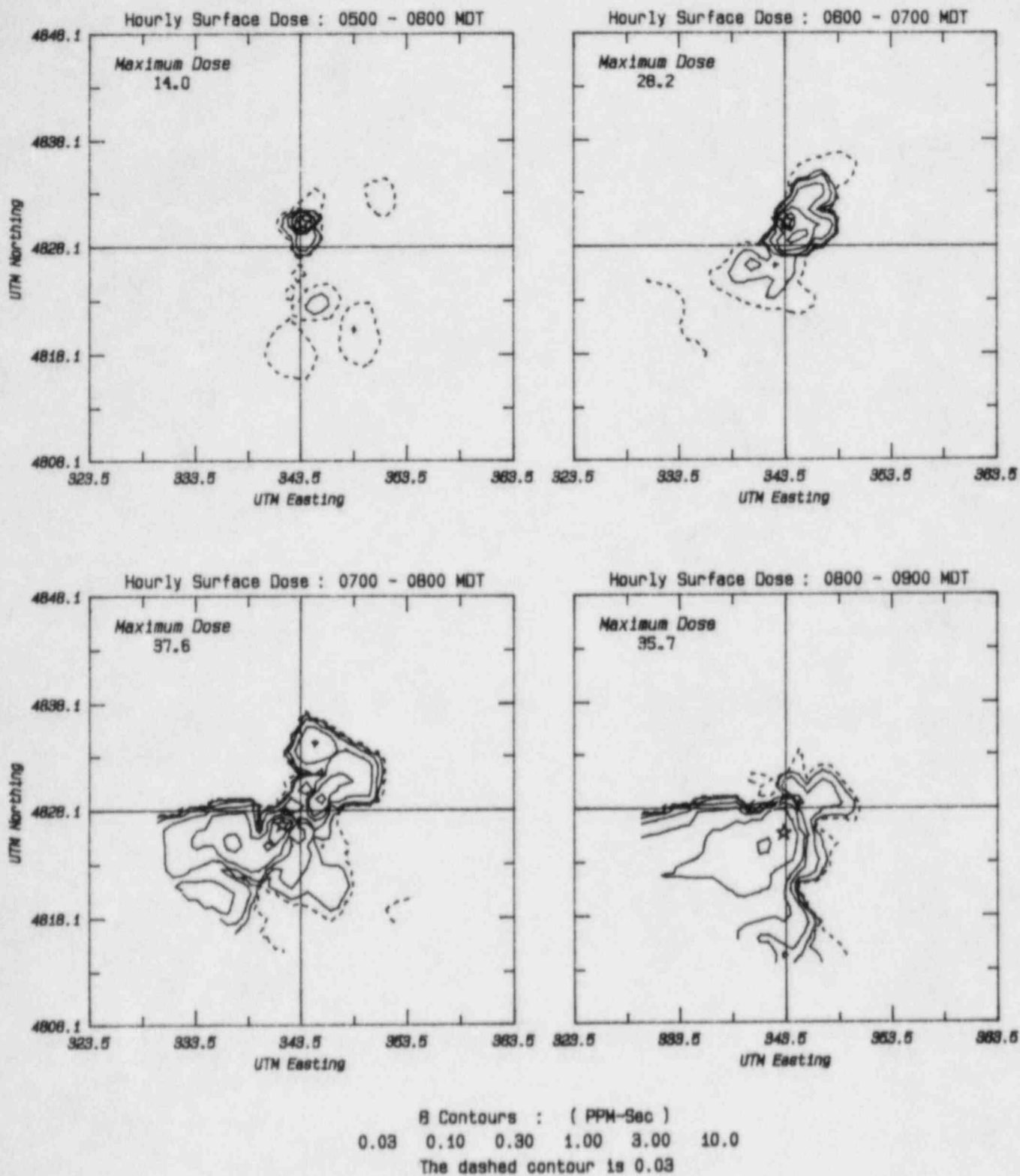


Figure A33

# July 1981 INEL Field Experiment : Test 8

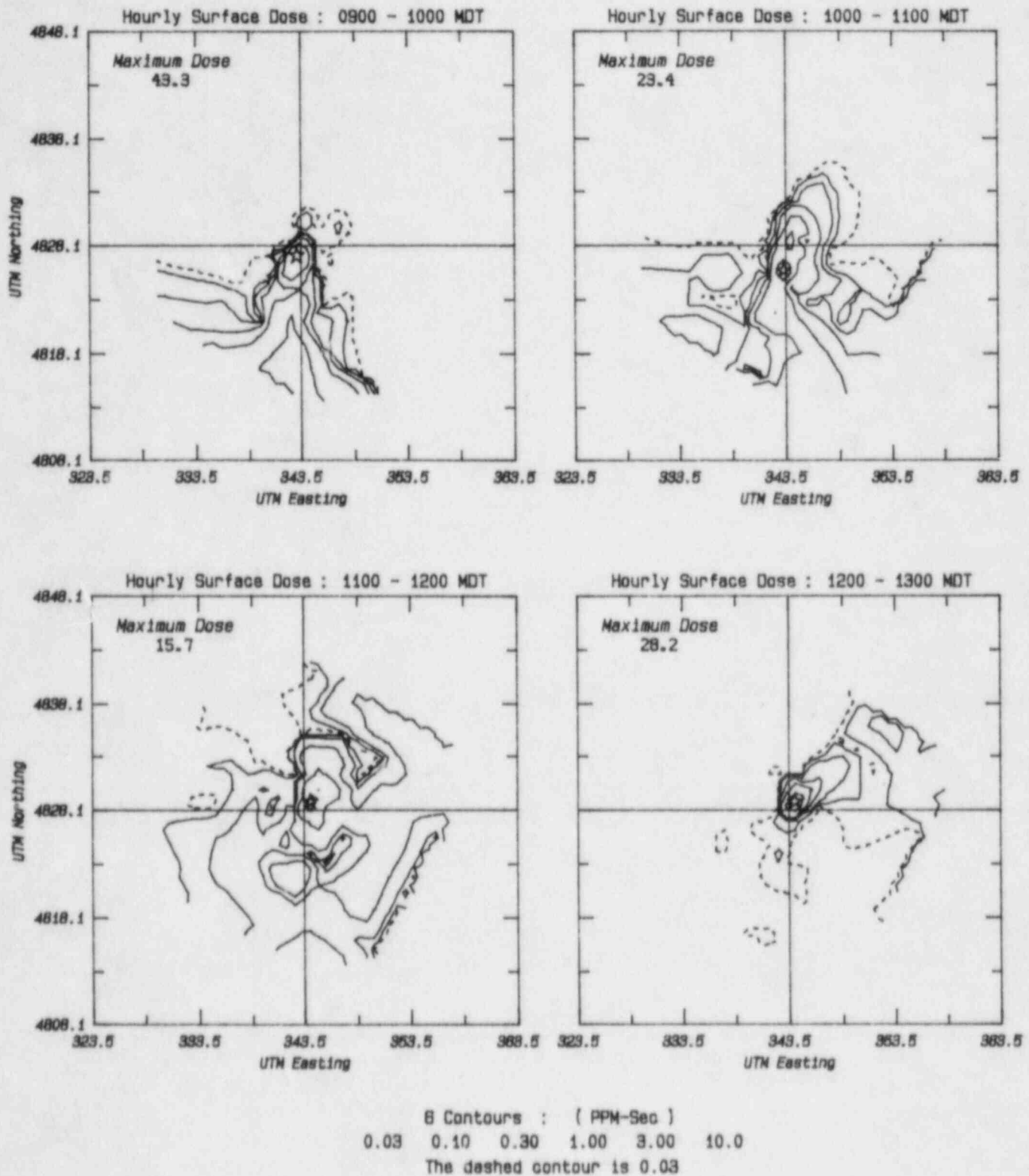


Figure A34

# July 1981 INEL Field Experiment : Test 8

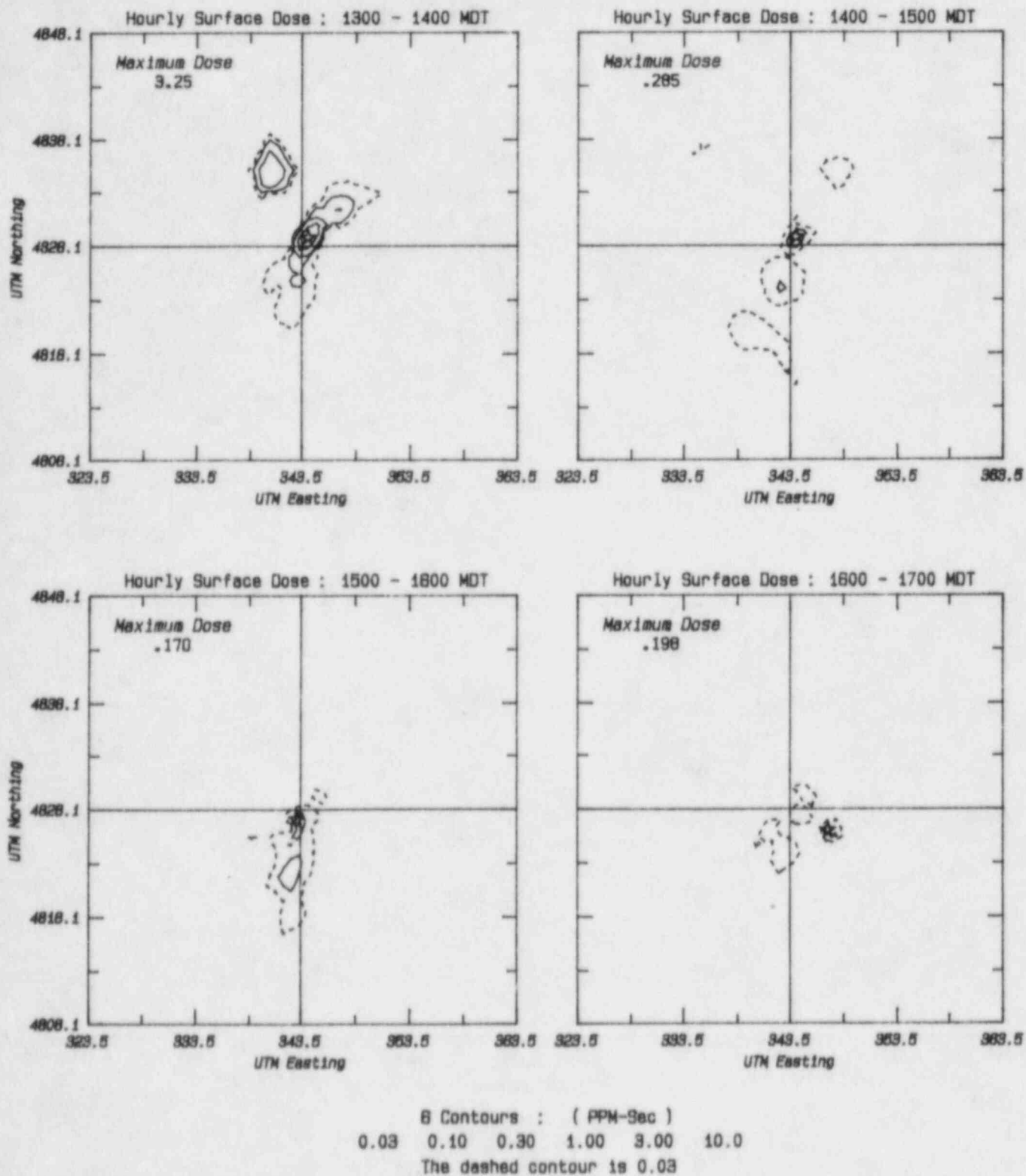
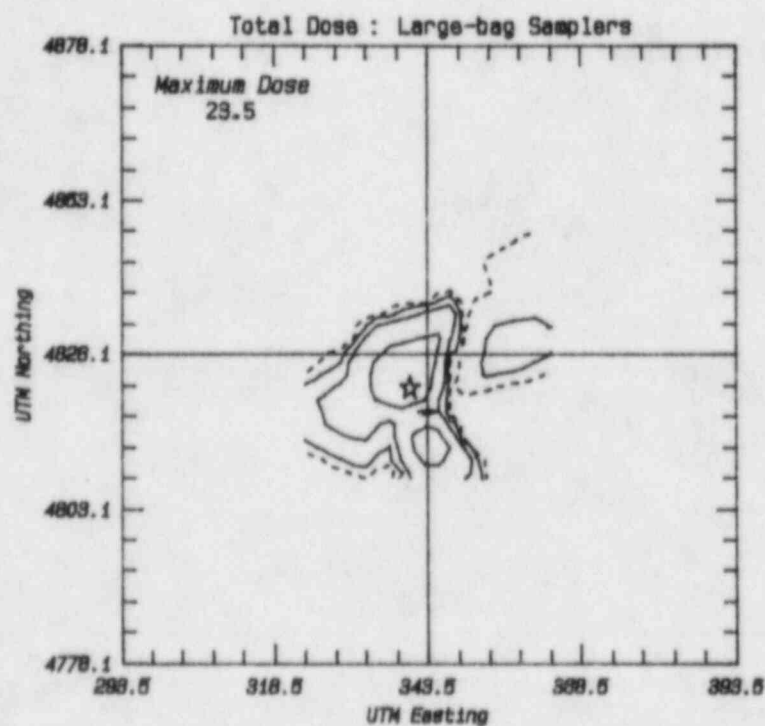
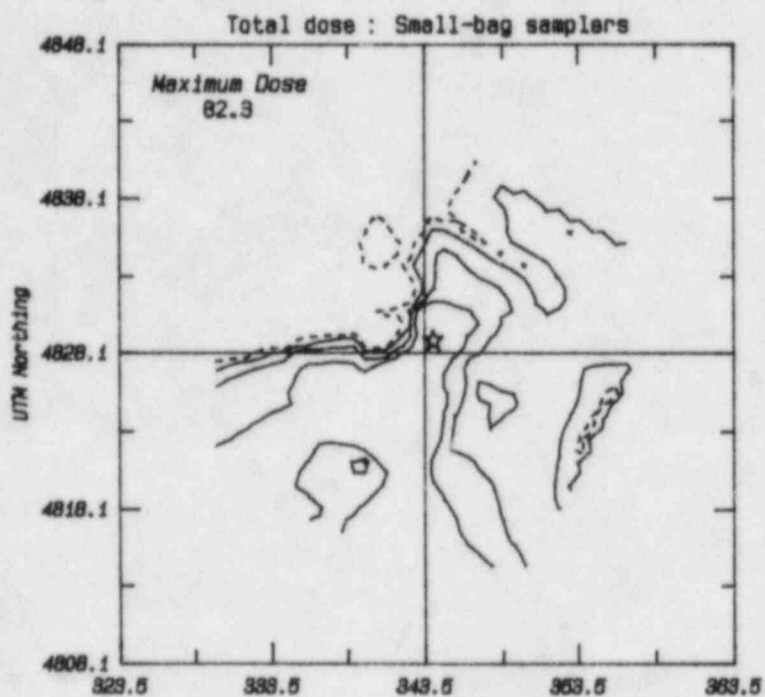


Figure A35

# July 1981 INEL Field Experiment : Test 8



4 Contours : ( PPM-Sec )  
0.30 1.00 3.00 10.0  
The dashed contour is 0.30

Figure A36

# July 1981 INEL Field Experiment : Test 9

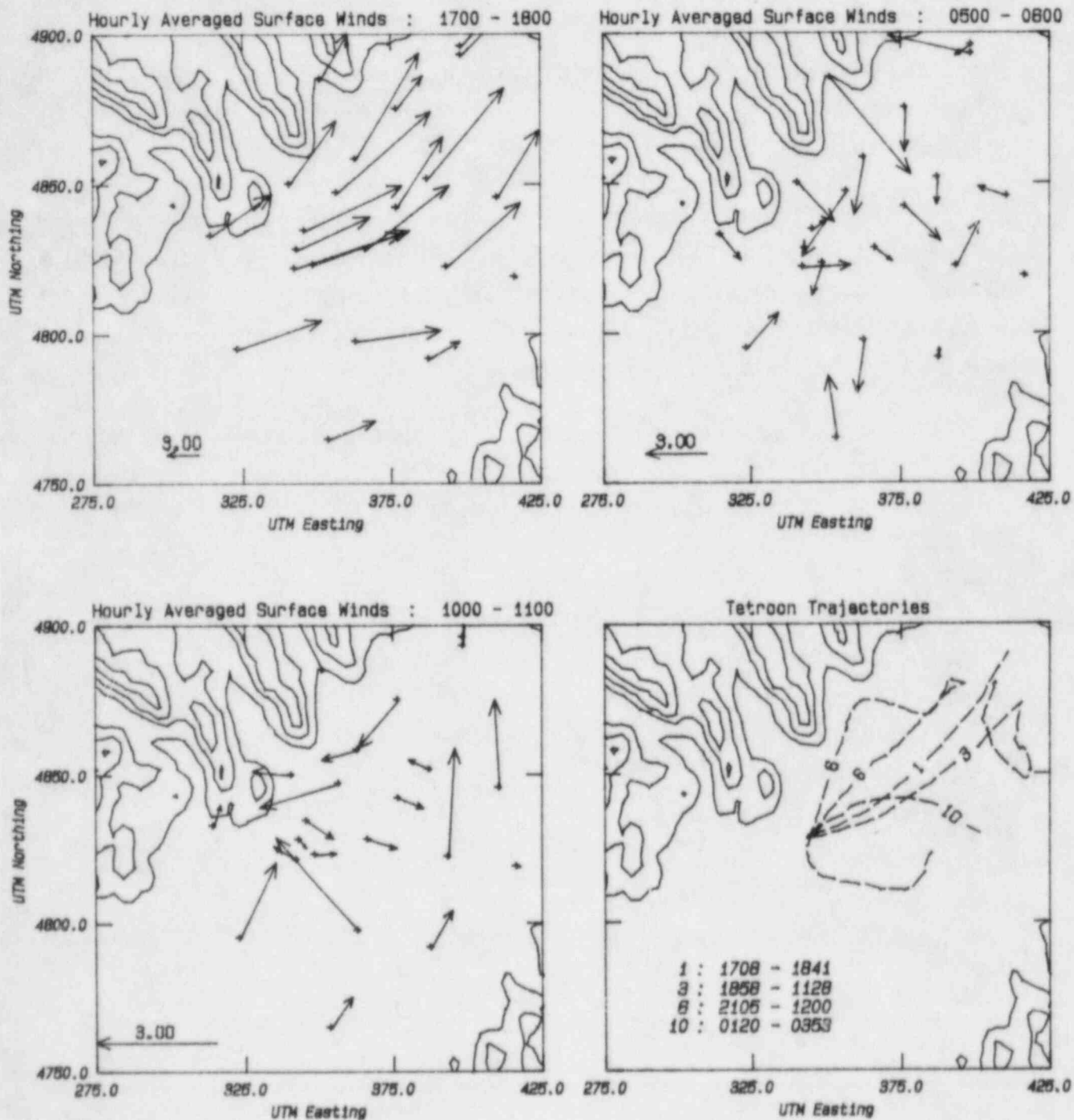


Figure A37

initial flow to the northeast followed by reversal later.

The vertical wind profiles, Figure A.38, illustrate the simple structure of the flow between 1830 and 0330. The direction is very steady around  $250^{\circ}$  at 1830 and a speed of  $13 \text{ ms}^{-1}$ ; at 0330 the direction is still southwest but the speed has dropped to  $3 \text{ ms}^{-1}$ . Later in the morning the flow reverses in the lowest 600m.

The hourly  $\text{SF}_6$  doses, Figure A.39-41, are generally consistent with the simple wind field. All 12 hours show a clear plume to the northeast, with dose values falling significantly after the end of the release. There are non-negligible doses away from the northeast quadrant in several of the hours, and these are difficult to explain in terms of the wind field.

The 12 hour dose pattern, Figure A.42, shows a distinct plume in the northeast quadrant, and this is also confirmed by the large bag measurements.



# July 1981 INEL Field Experiment : Test 9

Vertical wind profiles at the tracer release site

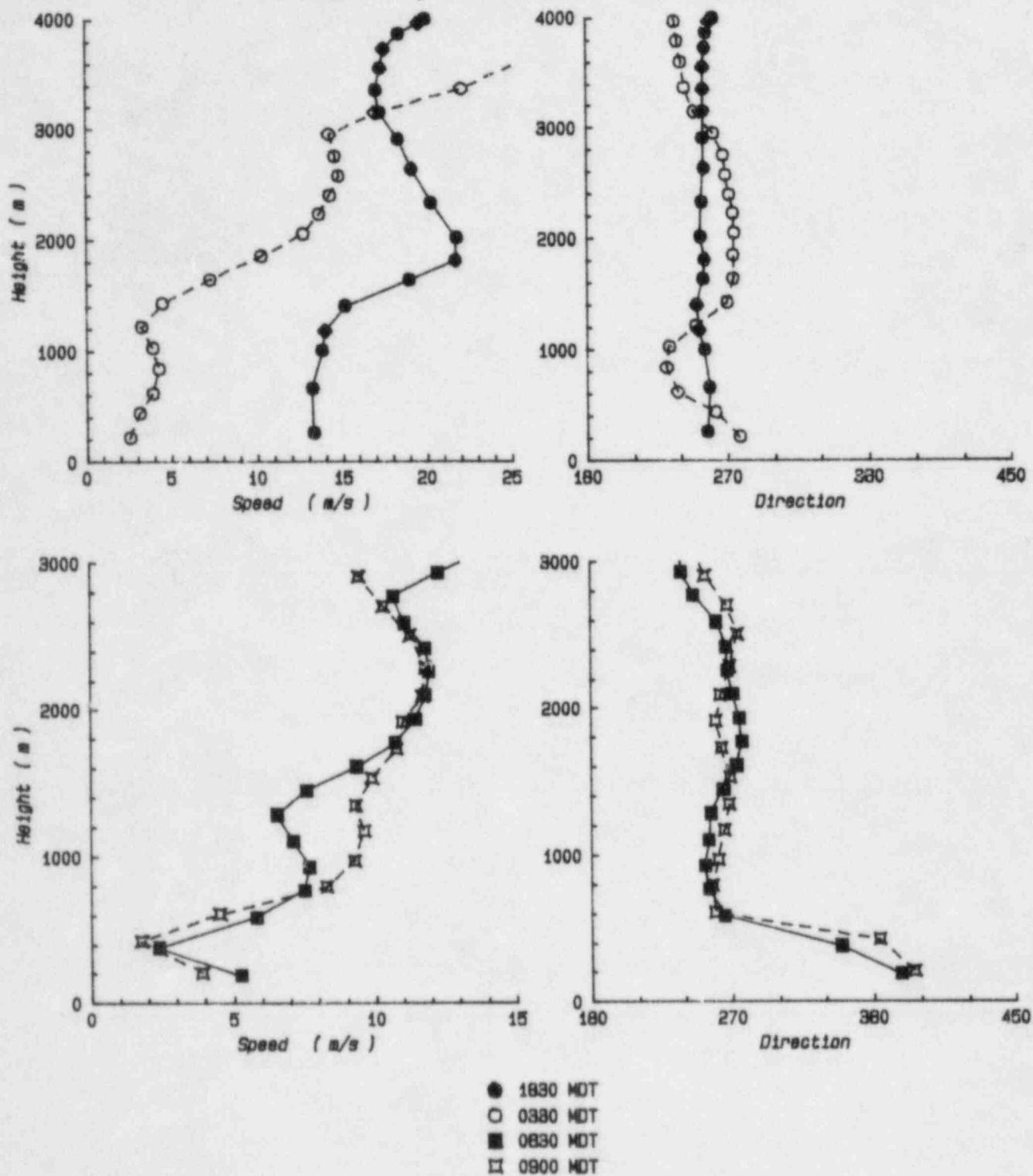


Figure A38

# July 1981 INEL Field Experiment : Test 9

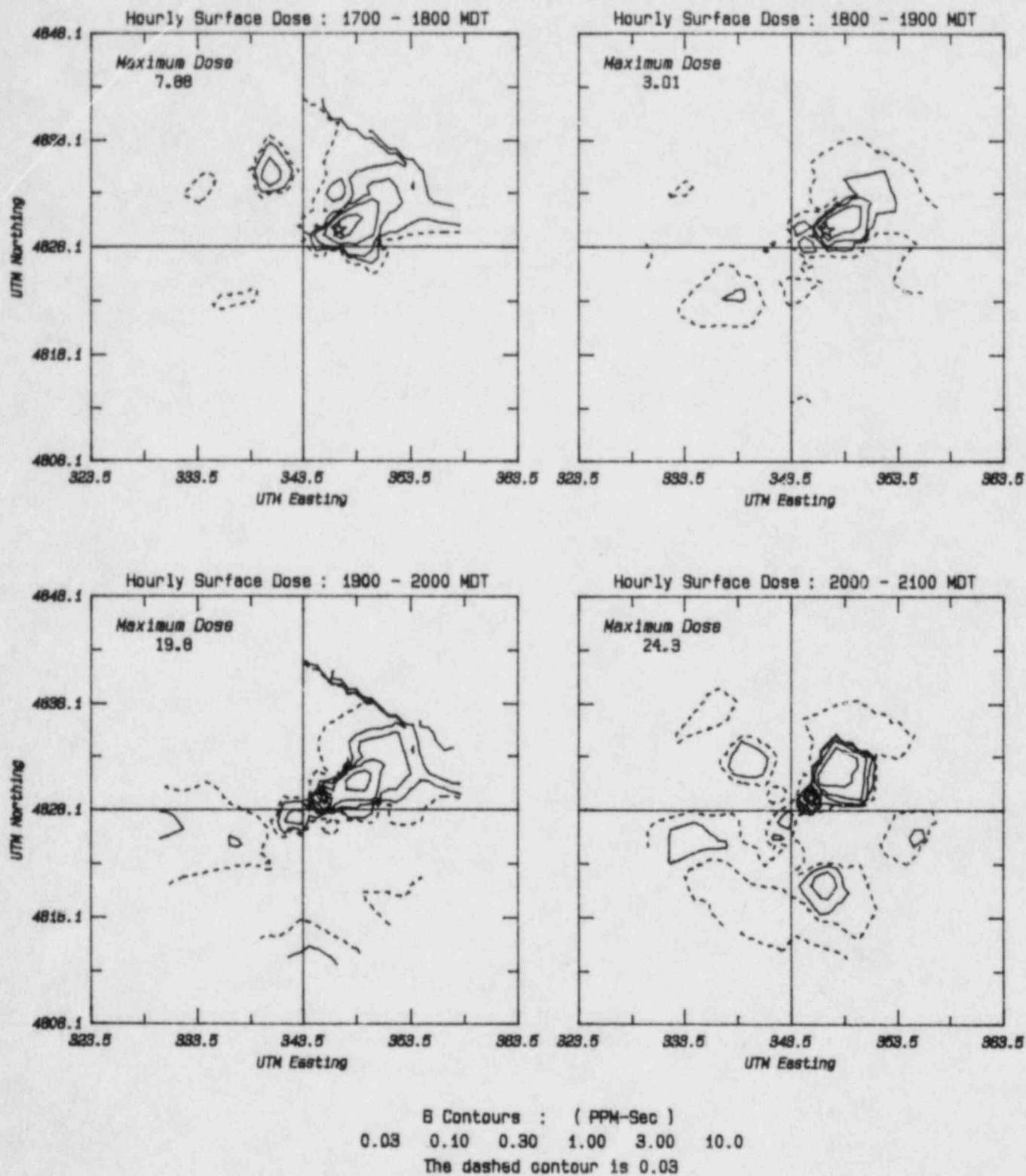


Figure A39

# July 1981 INEL Field Experiment : Test 9

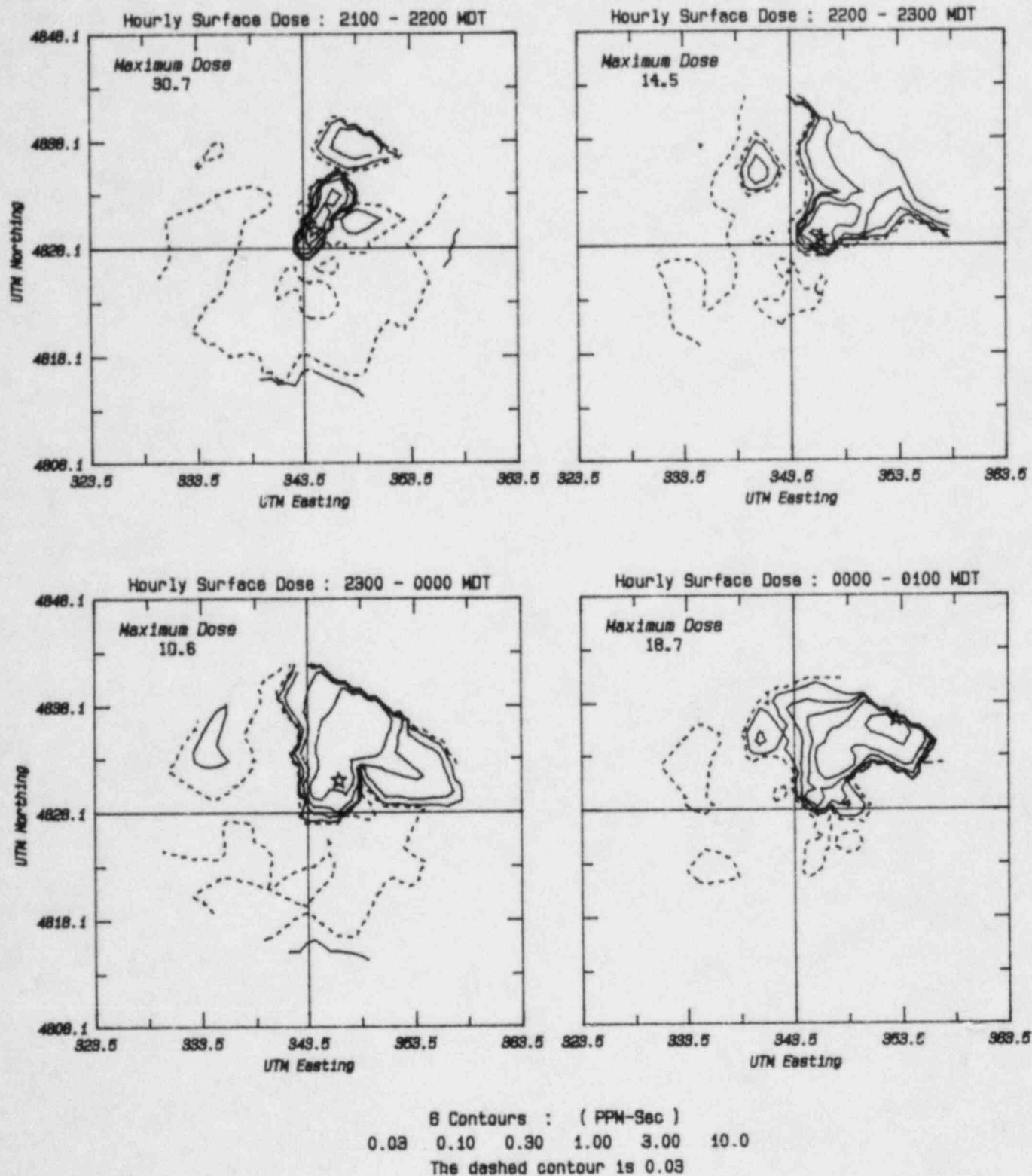


Figure A40

# July 1981 INEL Field Experiment : Test 9

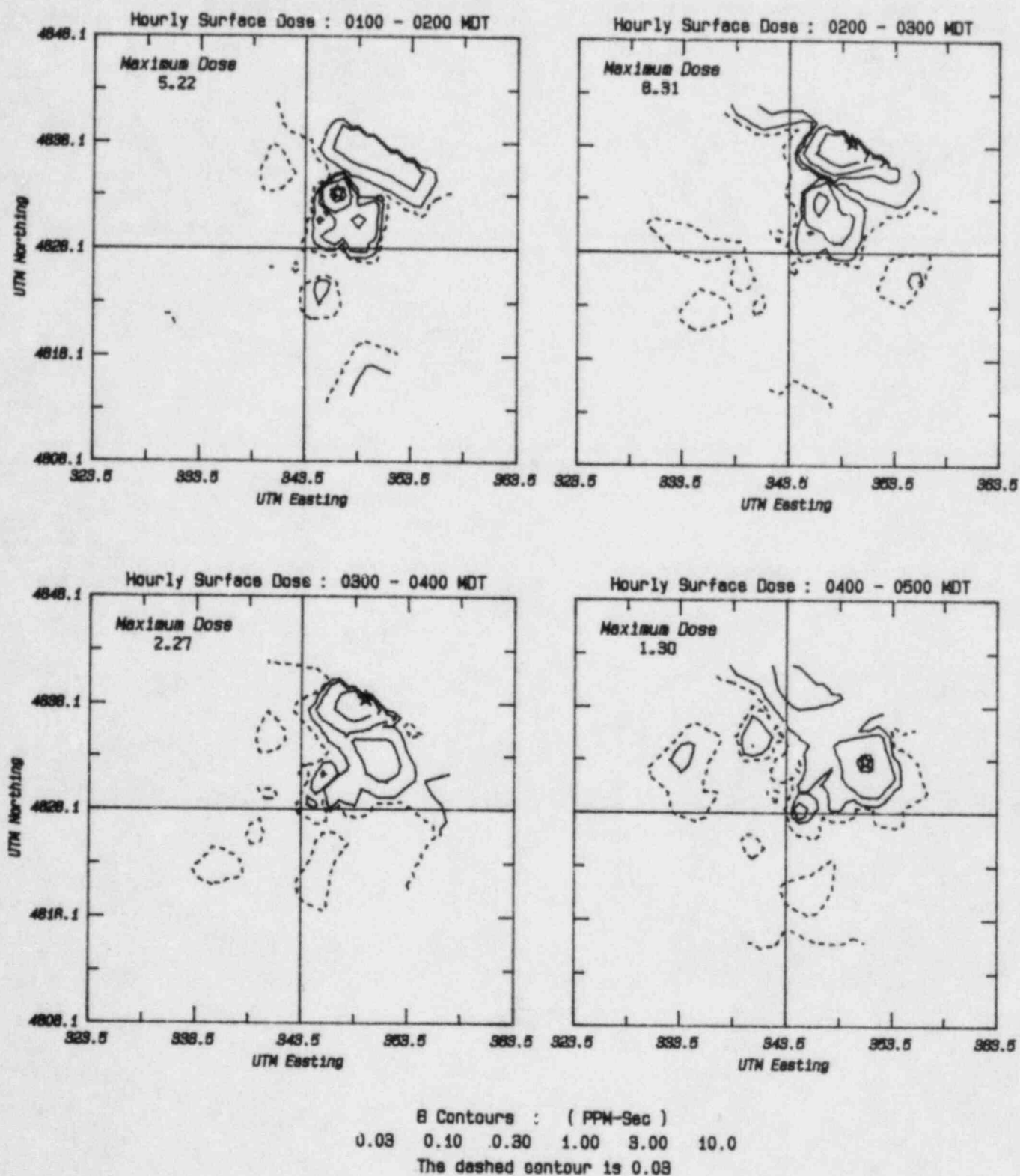
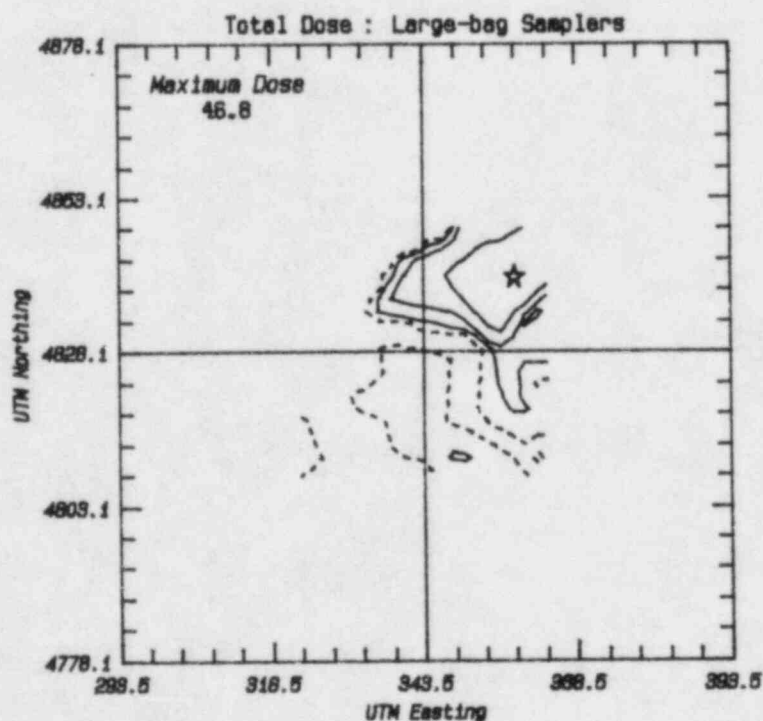
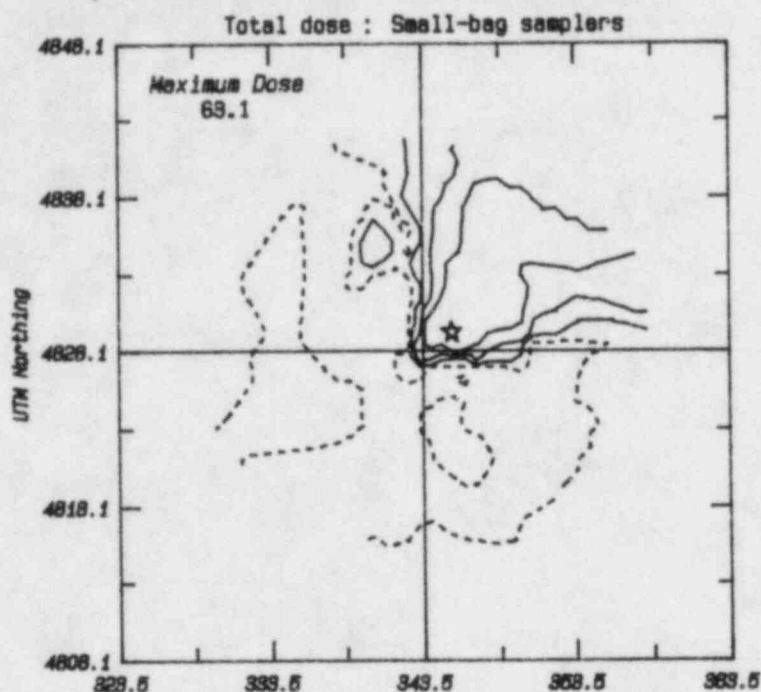


Figure A41

# July 1981 INEL Field Experiment : Test 9



4 Contours : ( PPM-960 )  
0.30 1.00 3.00 10.0  
The dashed contour is 0.30

Figure A42

## Appendix B

### Model Results for Integrated Dose

This appendix contains the results of model predictions for the 12 hour integrated dose on the fine mesh and the total 30 hour integrated dose on the course mesh for 12 models for each of seven tests. These may be compared directly with the same scale data plots provided in Appendix A.



July 1981 INEL Field Experiment : Test 3  
Model Predictions : Surface Dose for 2300 - 1100

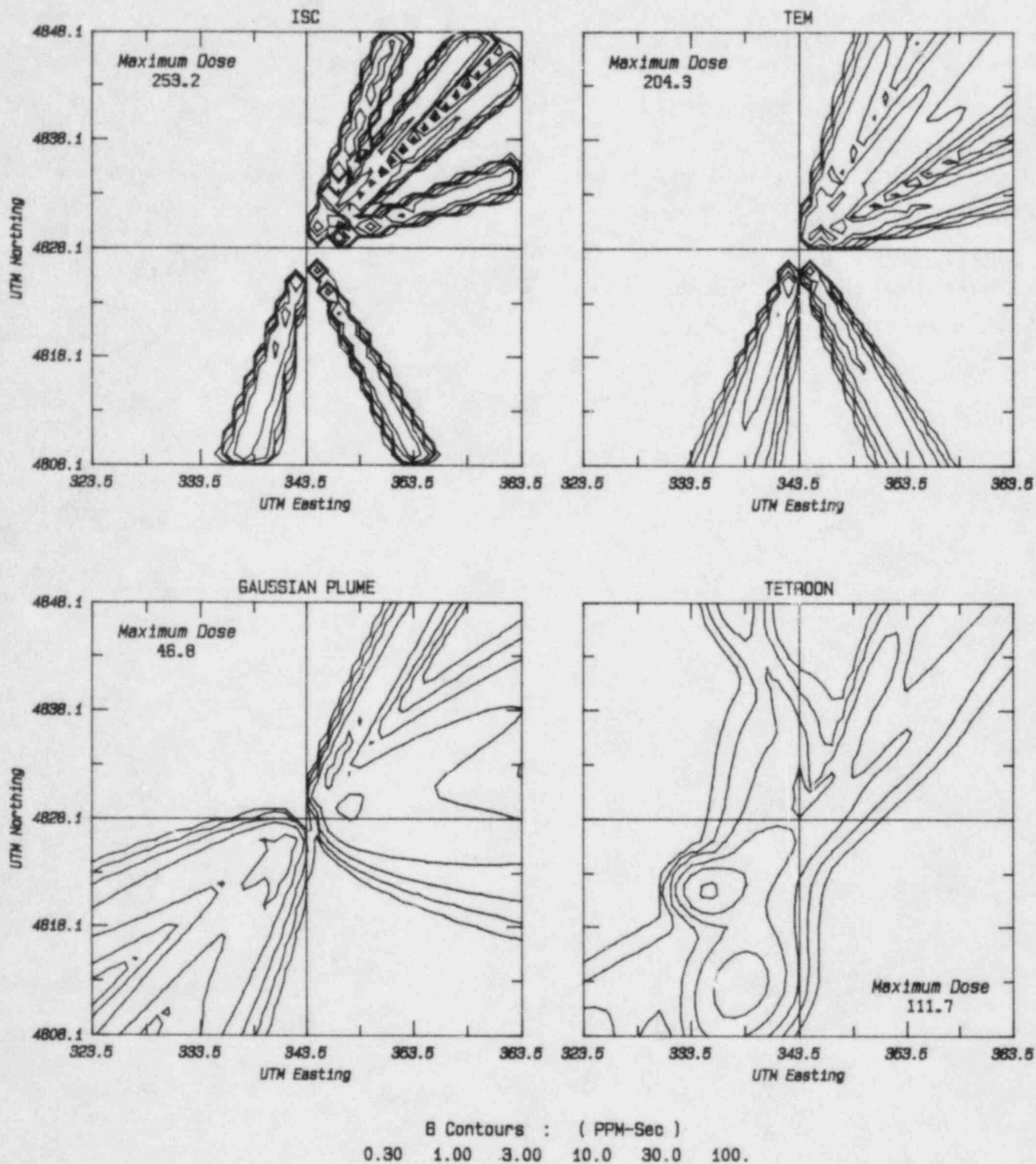


Figure B1

July 1981 INEL Field Experiment : Test 3  
 Model Predictions : Surface Dose for 2300 - 1100

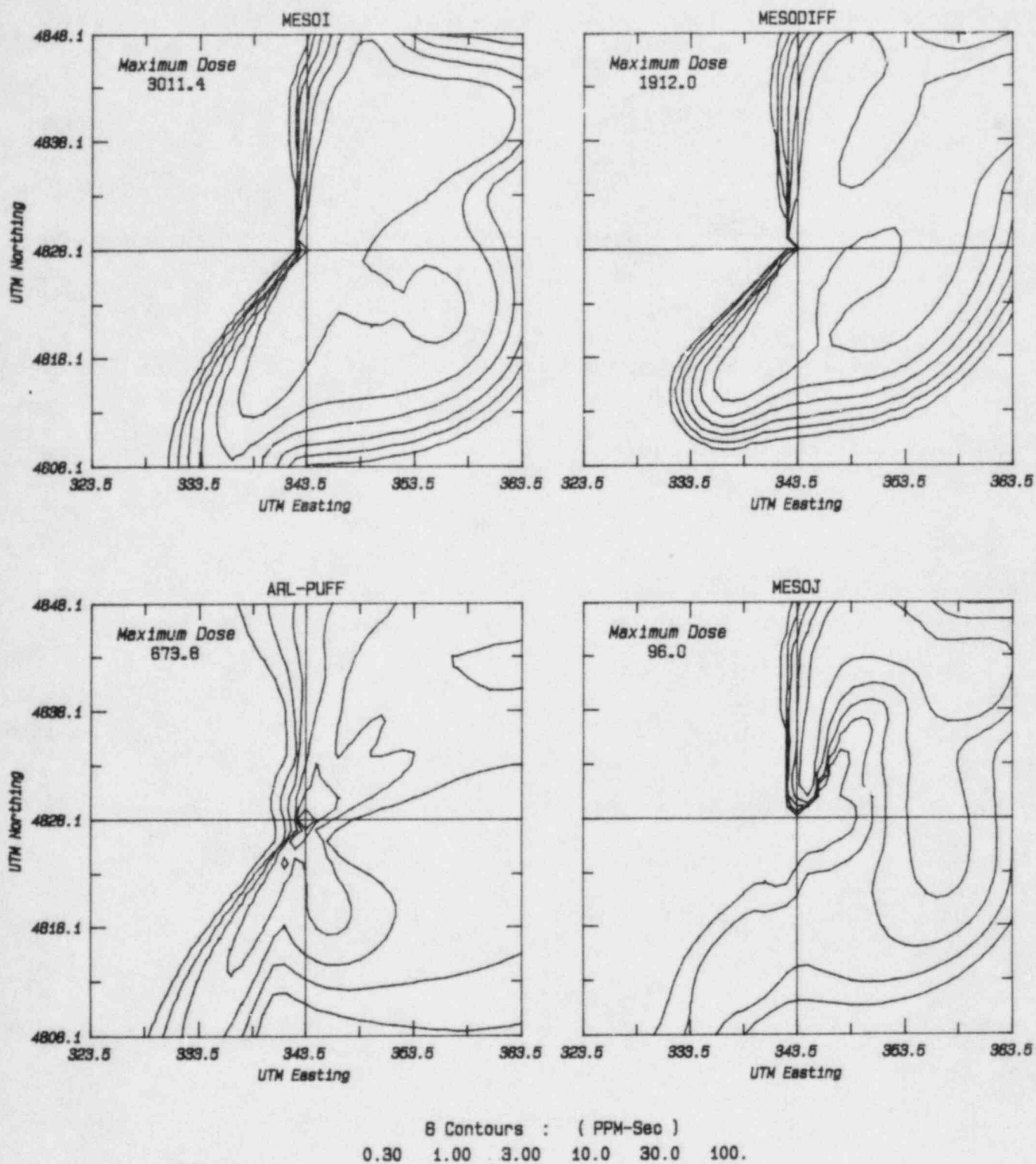


Figure B2

July 1981 INEL Field Experiment : Test 3  
 Model Predictions : Surface Dose for 2300 - 1100

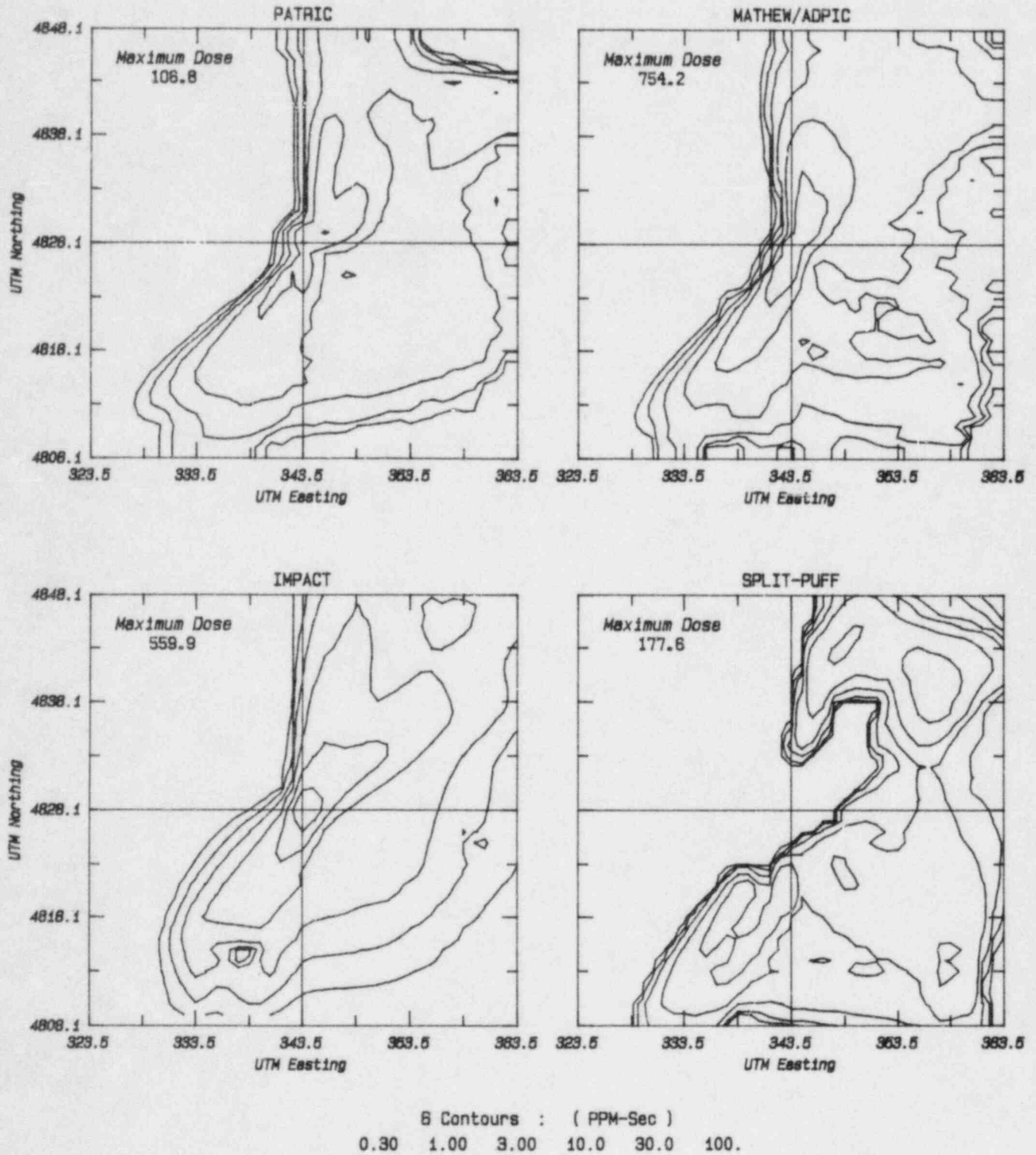


Figure B3

July 1981 INEL Field Experiment : Test 4  
 Model Predictions : Surface Dose for 2300 - 1100

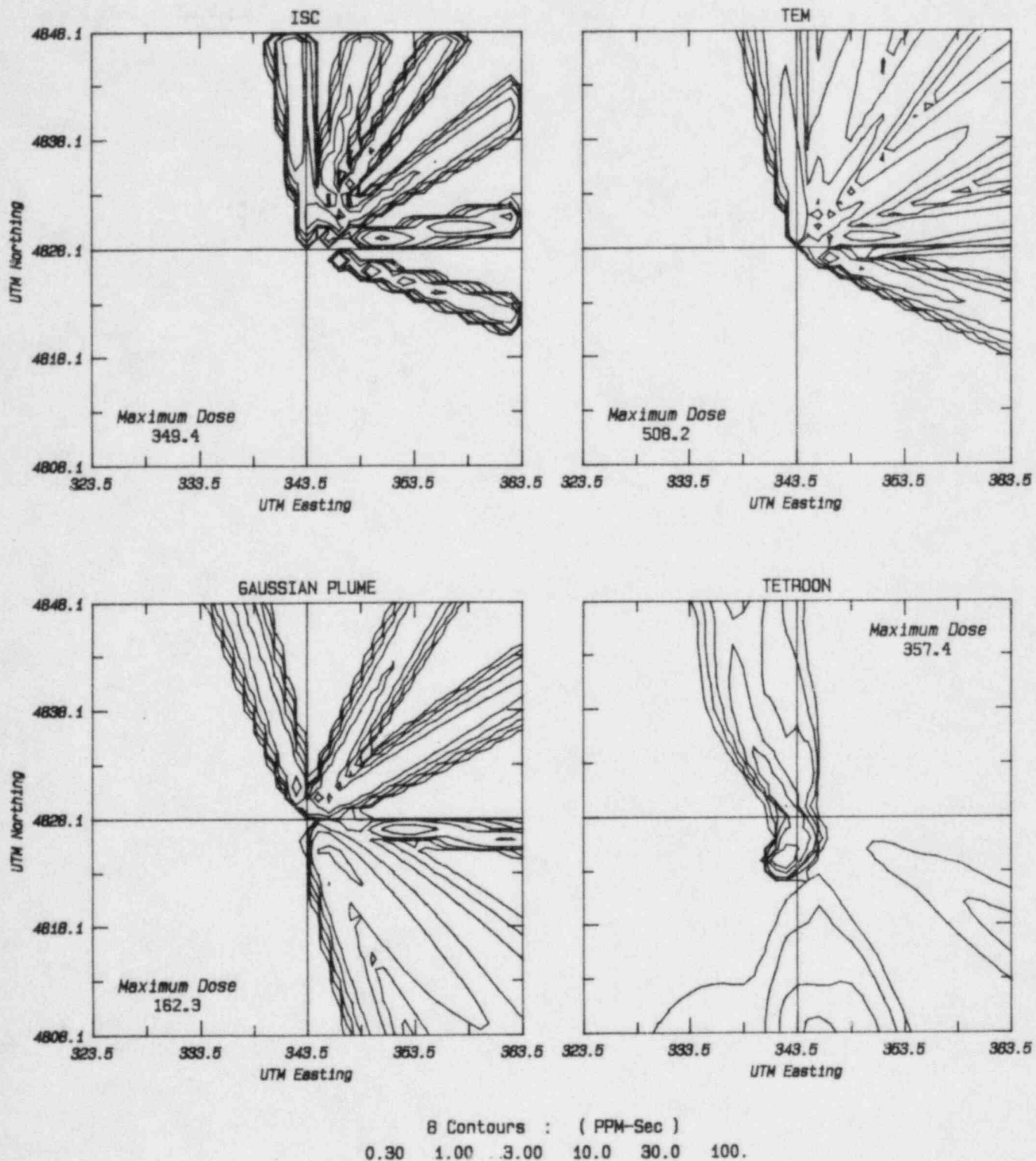


Figure B4

July 1981 INEL Field Experiment : Test 4  
Model Predictions : Surface Dose for 2300 - 1100

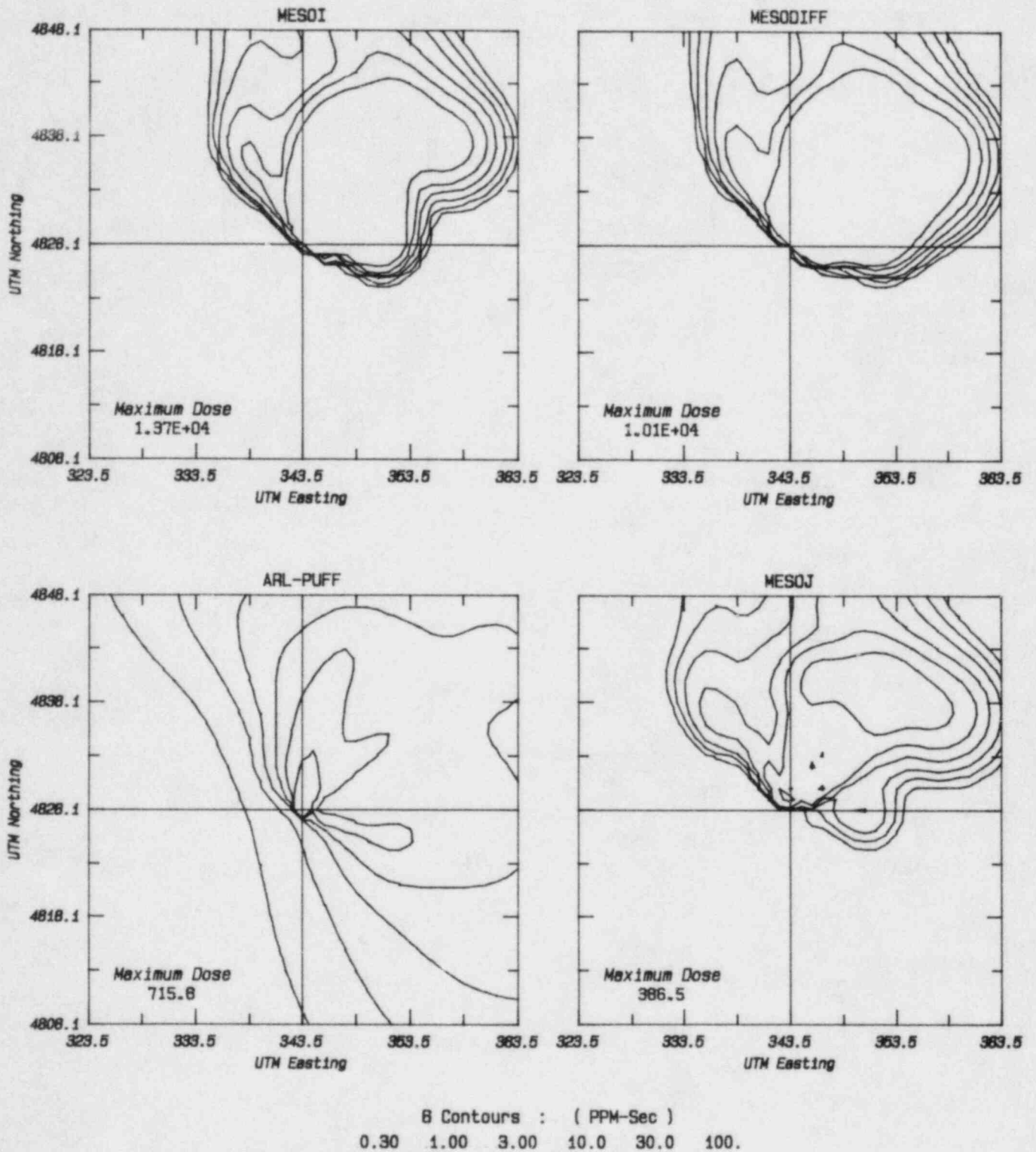
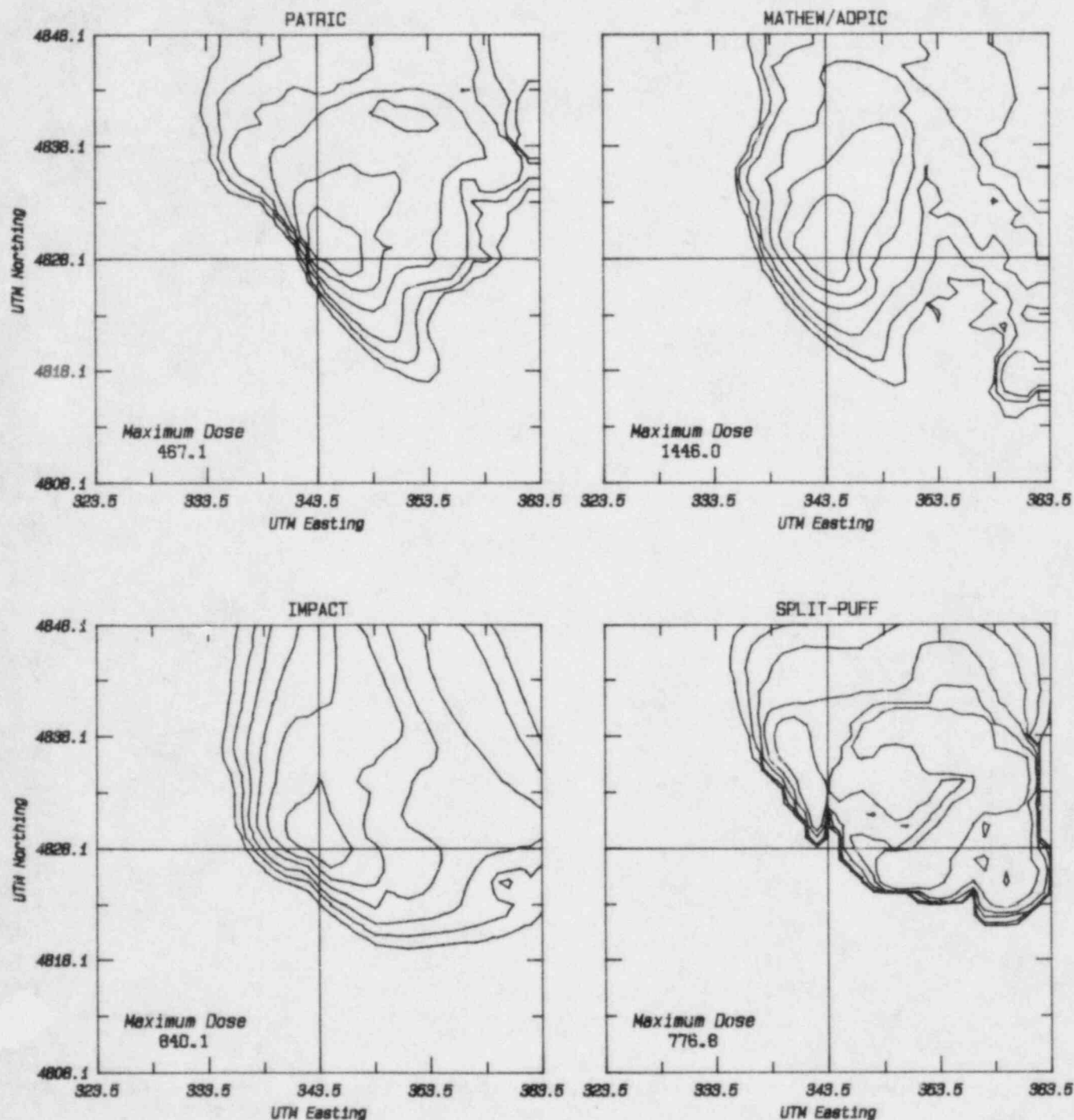


Figure B5



July 1981 INEL Field Experiment : Test 4  
Model Predictions : Surface Dose for 2300 - 1100

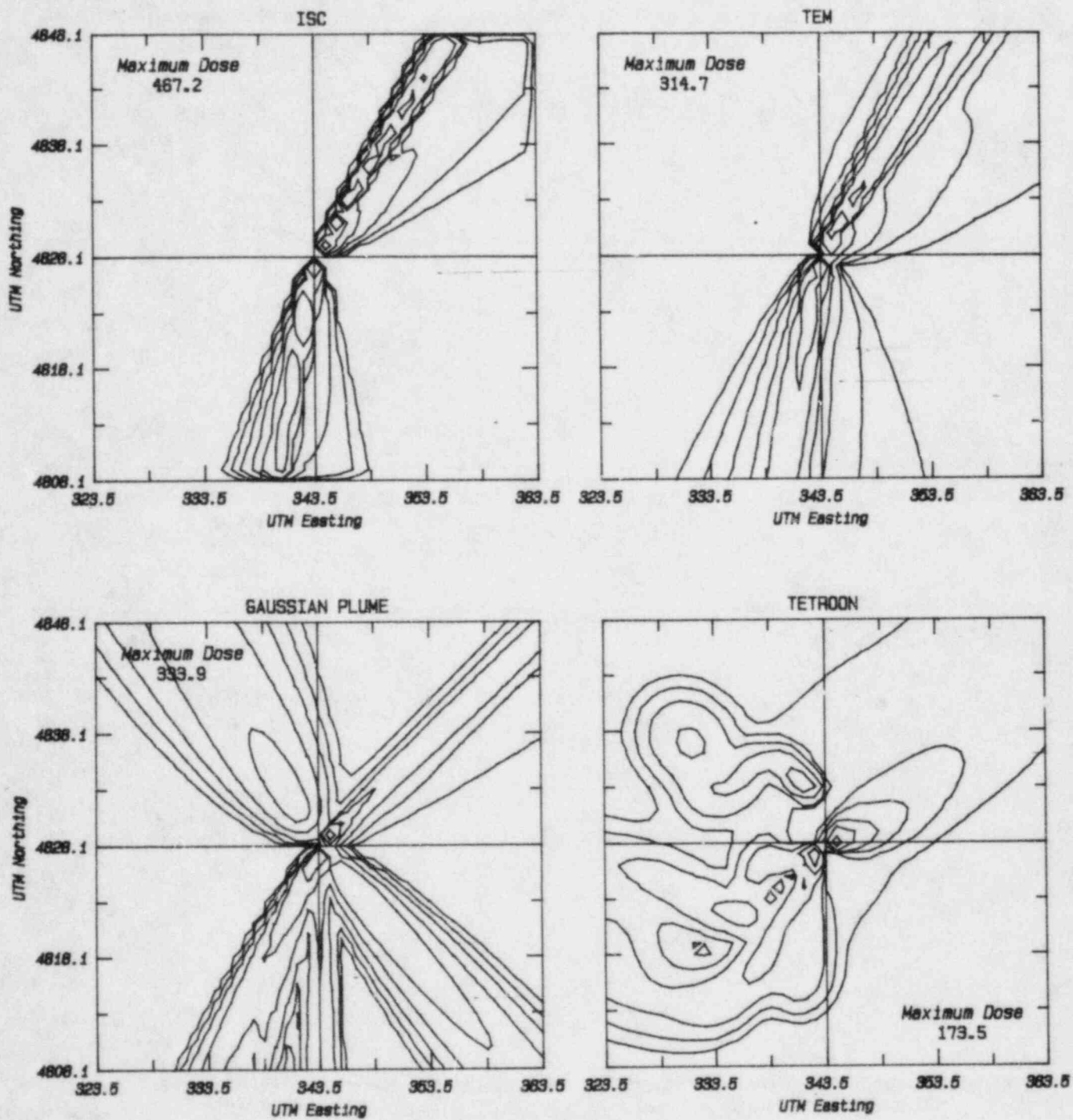


B Contours : ( PPM-Sec )  
0.30 1.00 3.00 10.0 30.0 100.

Figure B6



July 1981 INEL Field Experiment : Test 5  
 Model Predictions : Surface Dose for 0500 - 1700



B Contours : ( PPM-Sec )  
 0.30 1.00 3.00 10.0 30.0 100.

Figure B7

July 1981 INEL Field Experiment : Test 5  
 Model Predictions : Surface Dose for 0500 - 1700

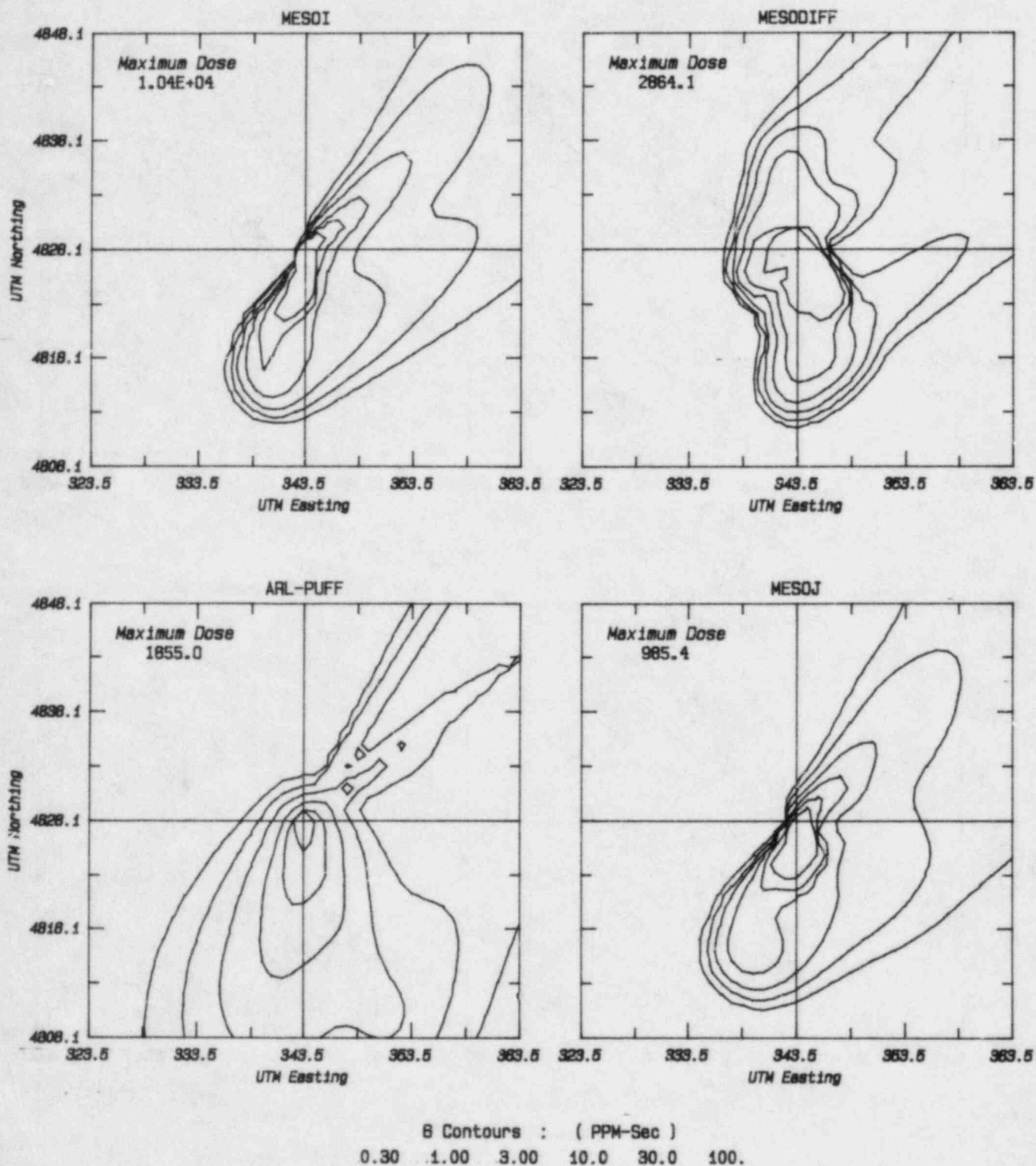


Figure B8

July 1981 INEL Field Experiment : Test 5  
Model Predictions : Surface Dose for 0500 - 1700

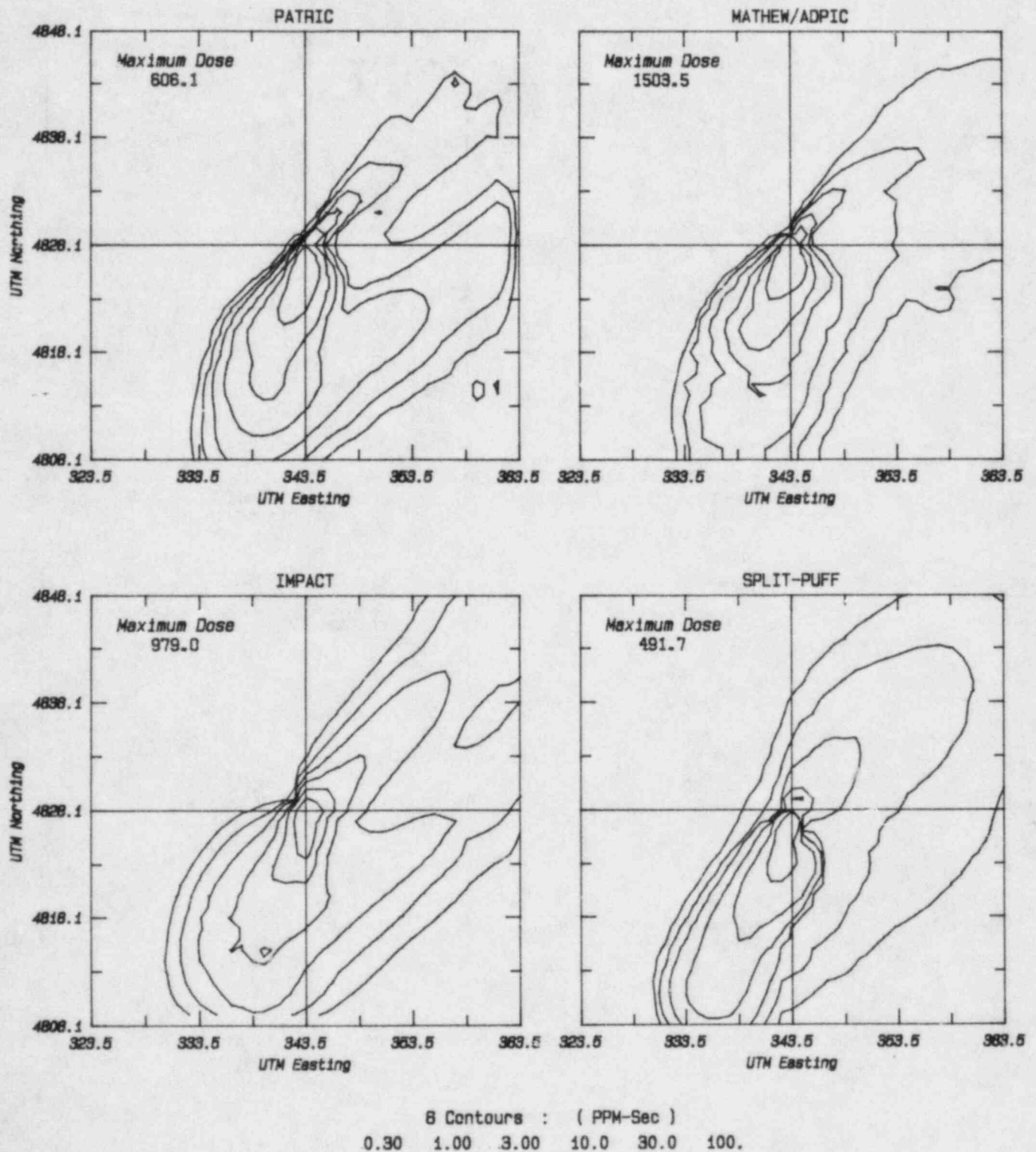


Figure B9

July 1981 INEL Field Experiment : Test 6  
 Model Predictions : Surface Dose for 1700 - 0500

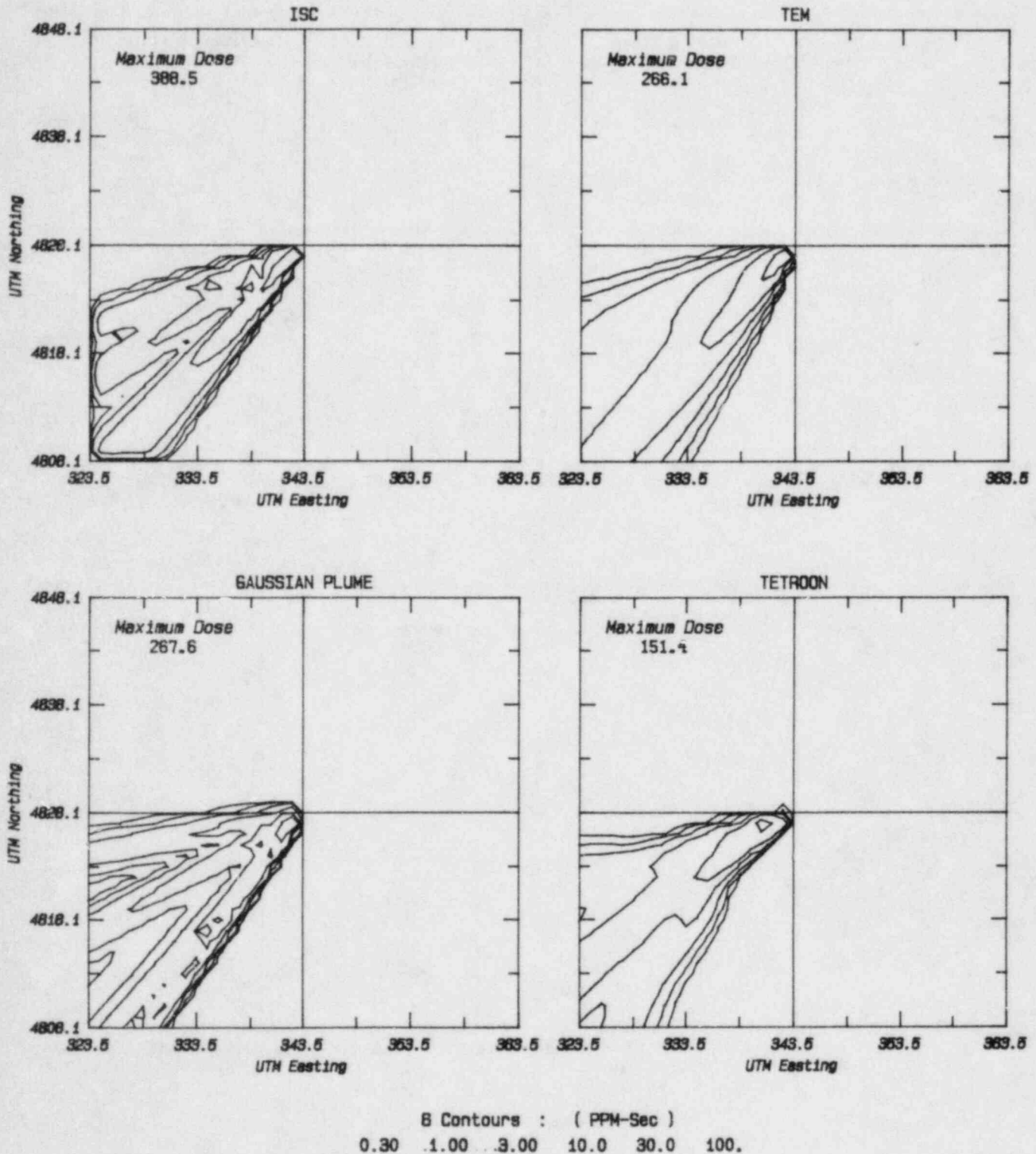


Figure B10

July 1981 INEL Field Experiment : Test 6  
 Model Predictions : Surface Dose for 1700 - 0500

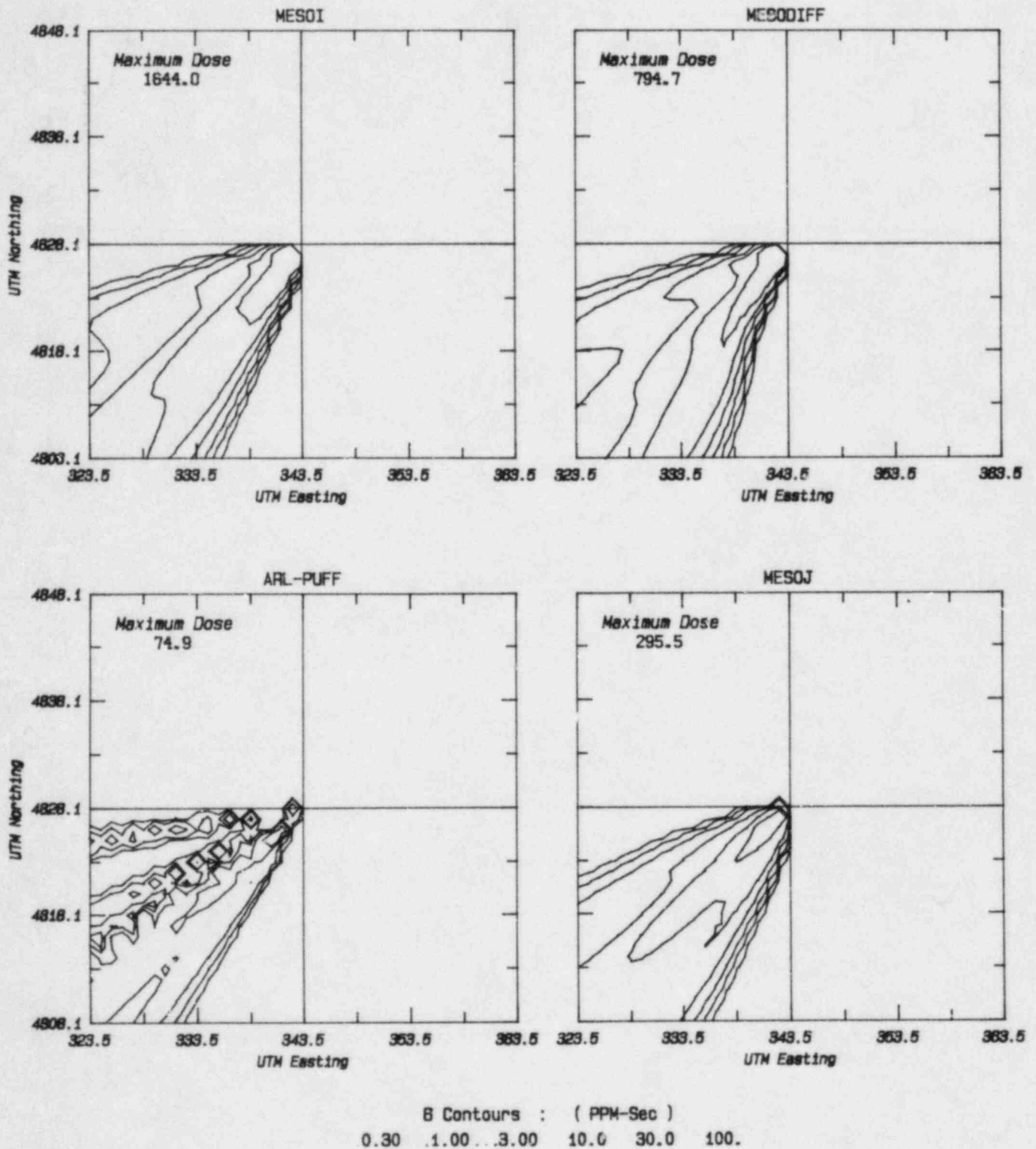


Figure B11



July 1981 INEL Field Experiment : Test 6  
Model Predictions : Surface Dose for 1700 - 0500

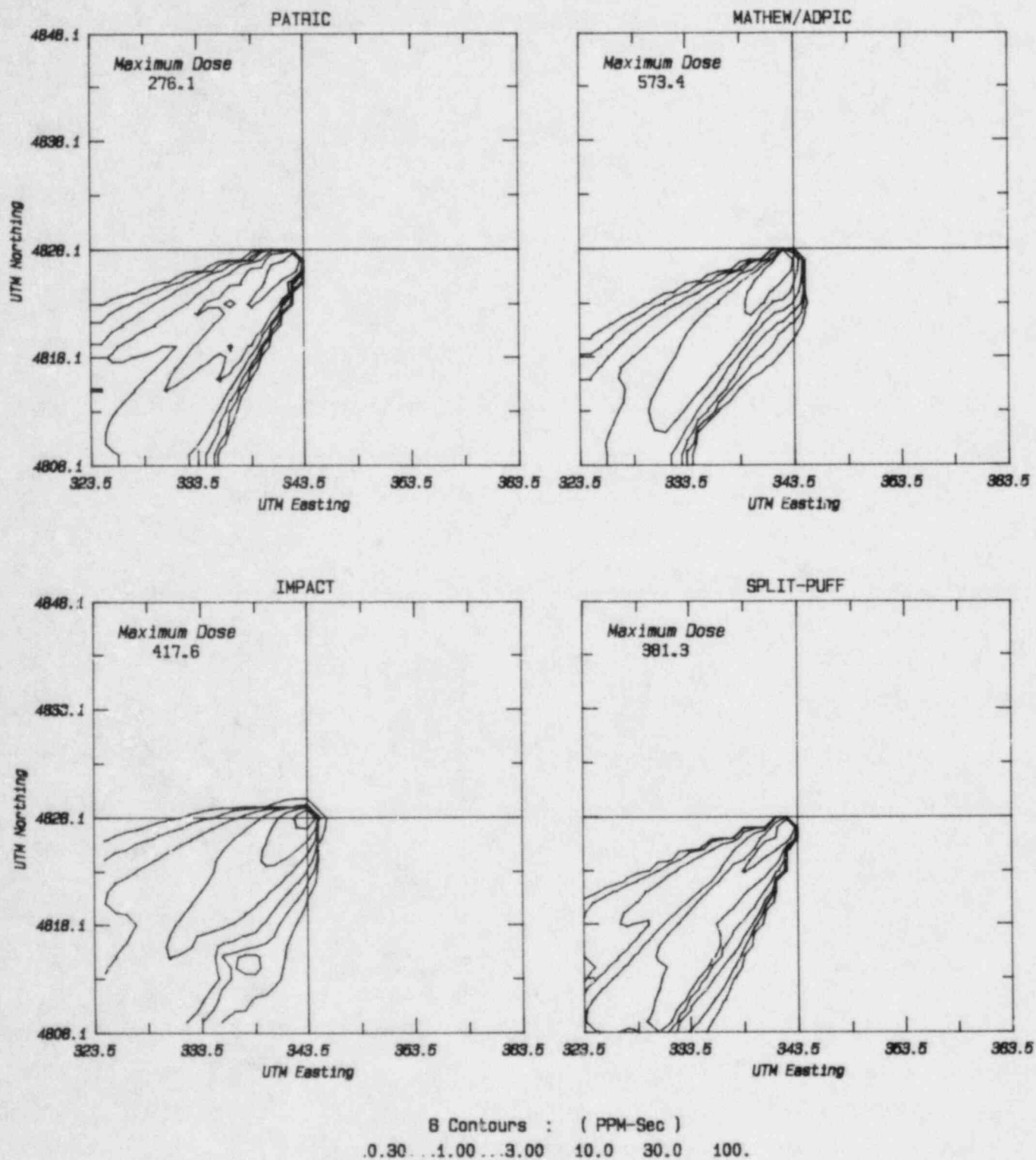


Figure B12



July 1981 INEL Field Experiment : Test 7  
 Model Predictions : Surface Dose for 1300 - 0100

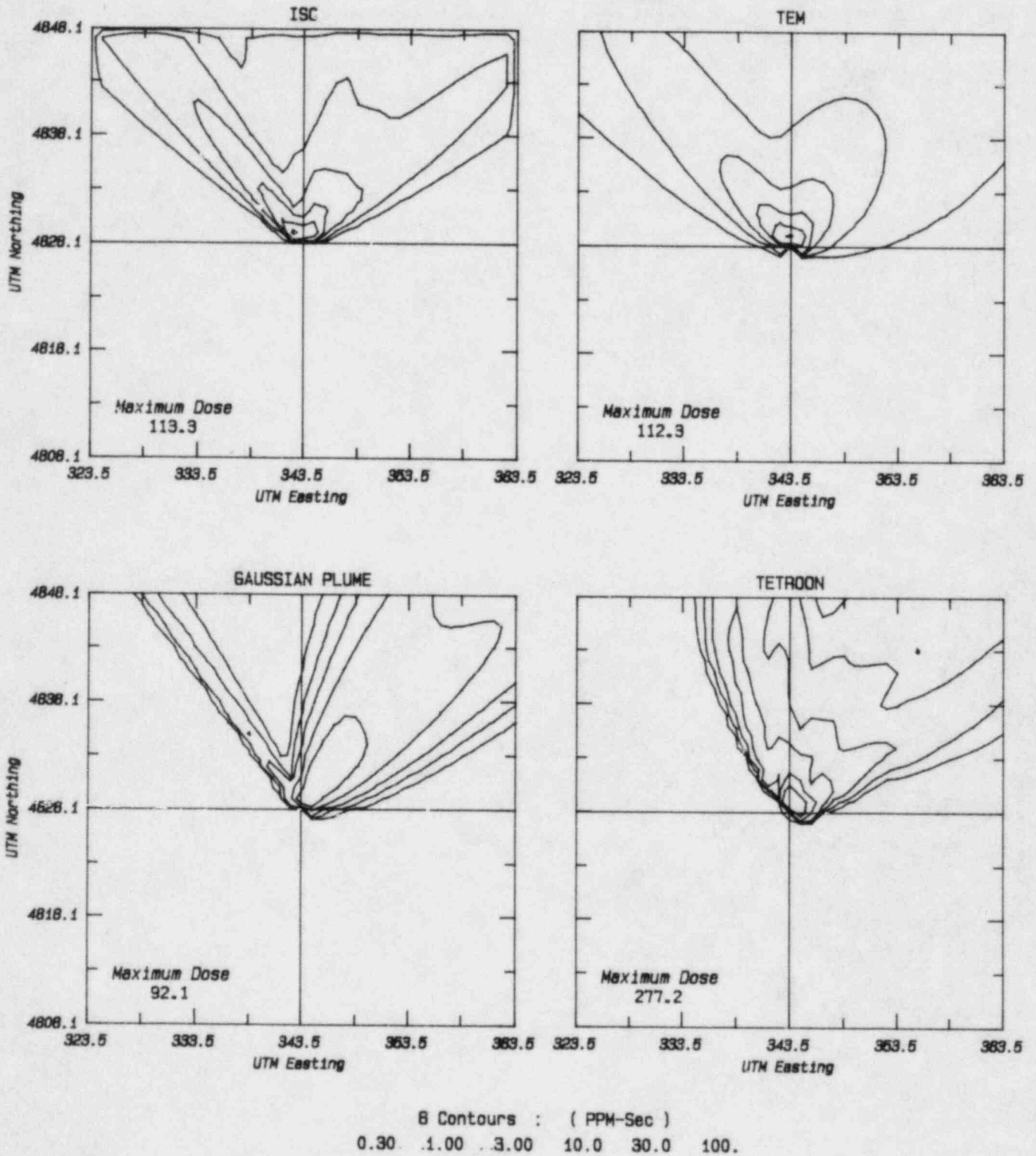
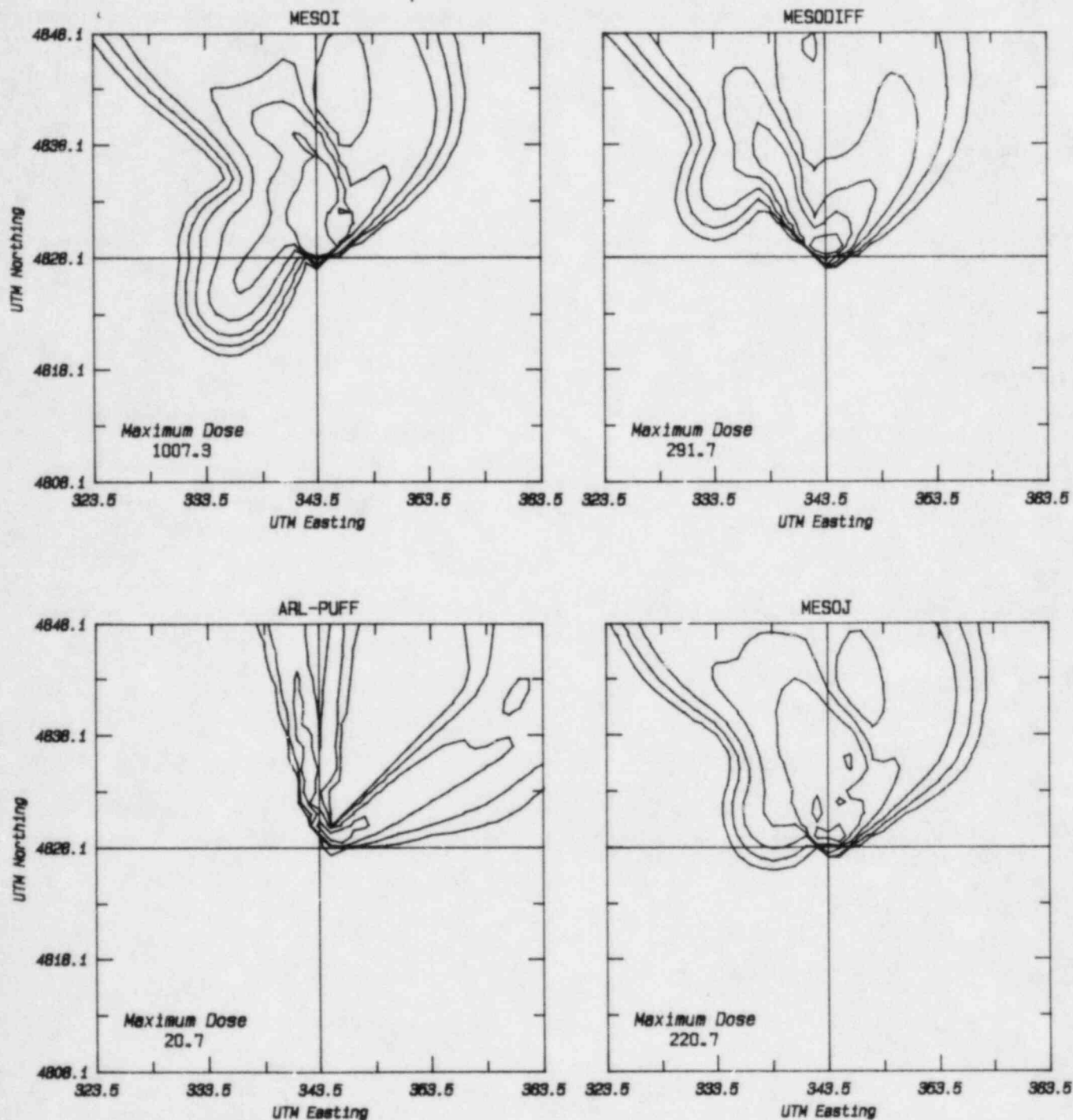


Figure B13

# July 1981 INEL Field Experiment : Test 7

Model Predictions : Surface Dose for 1300 - 0100



B Contours : ( PPM-Sec )  
0.30 1.00 3.00 10.0 30.0 100.

Figure B14

July 1981 INEL Field Experiment : Test 7  
 Model Predictions : Surface Dose for 1300 - 0100

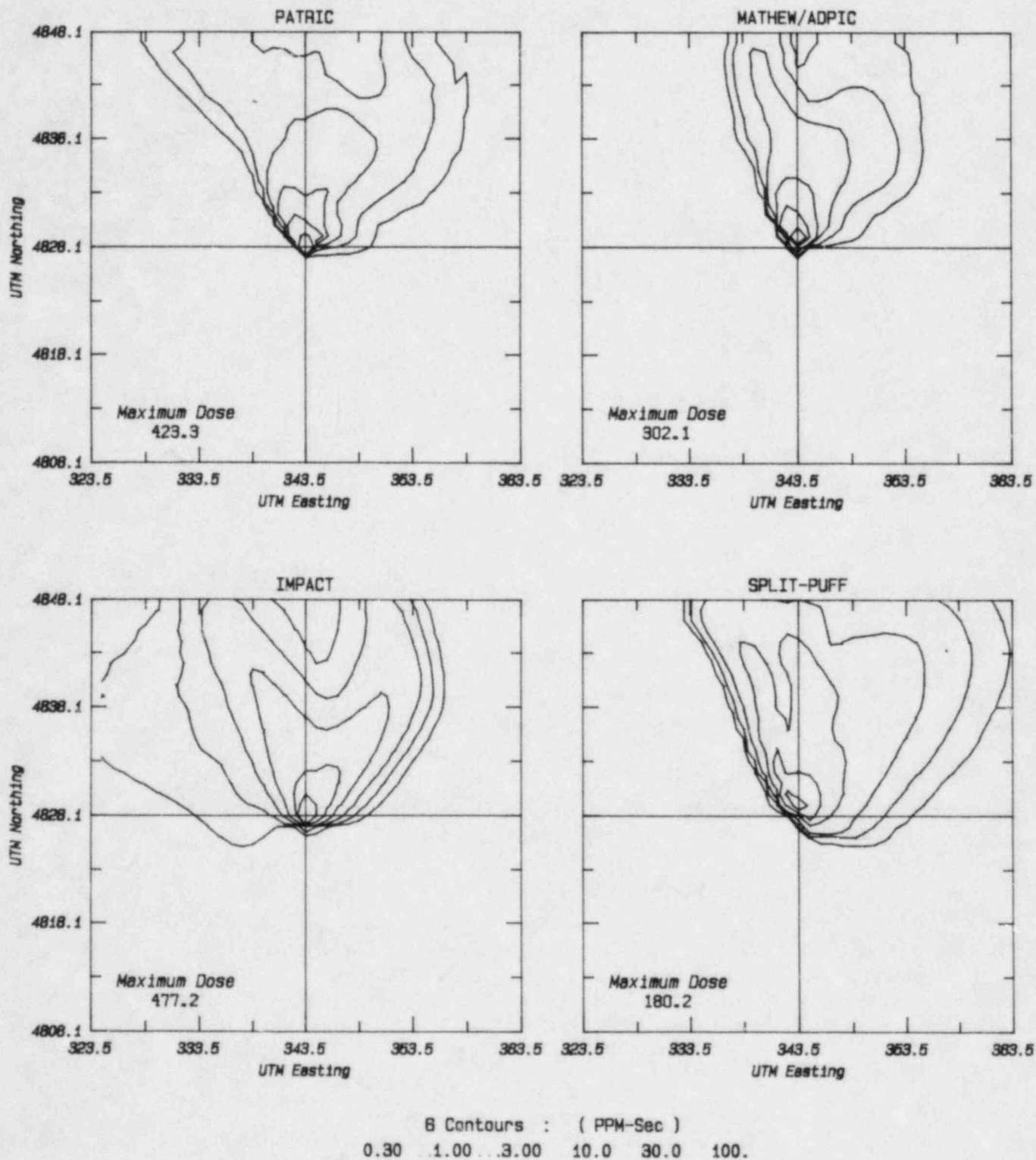


Figure B15

July 1981 INEL Field Experiment : Test 8  
 Model Predictions : Surface Dose for 0500 - 1700

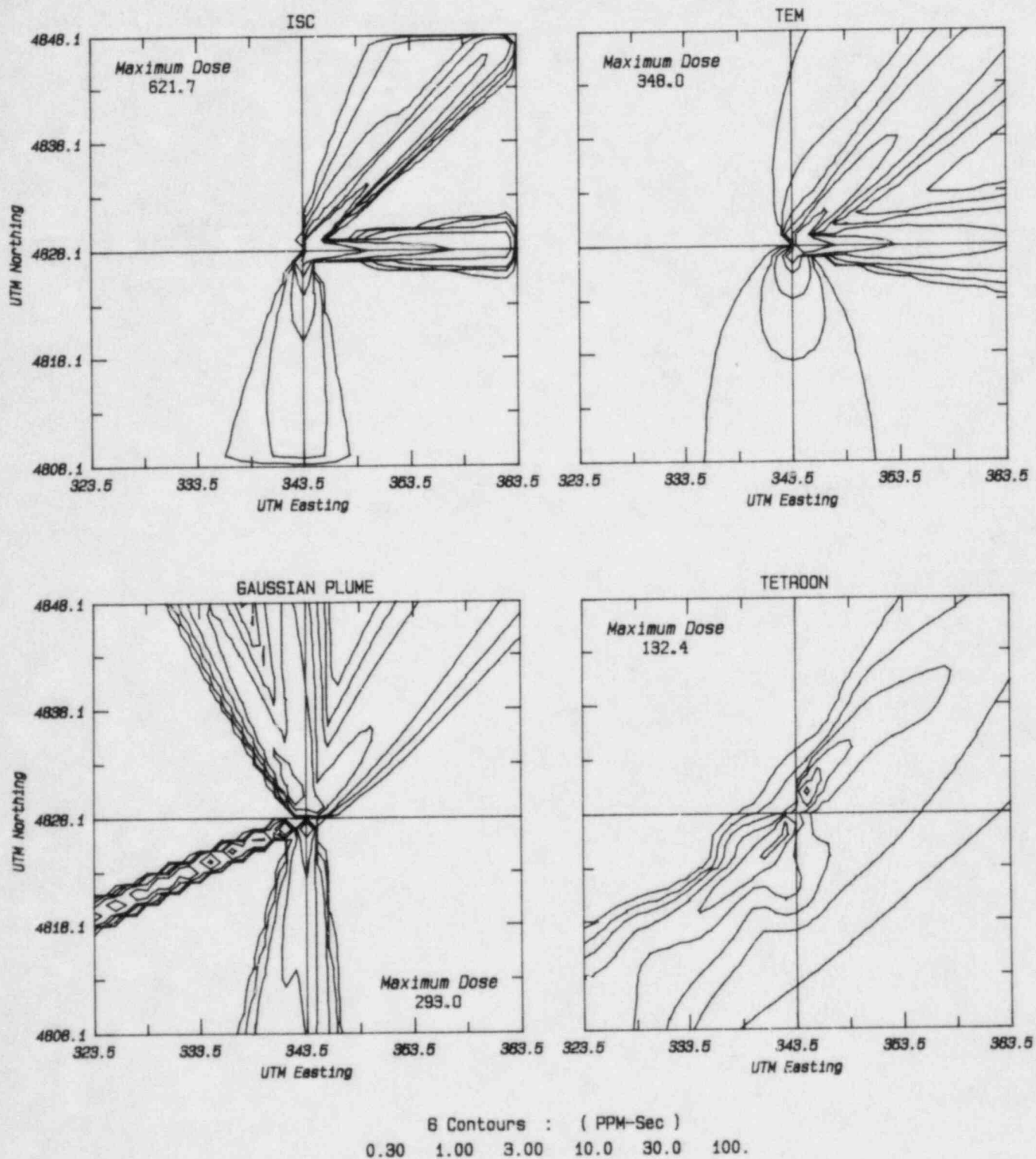


Figure B16

July 1981 INEL Field Experiment : Test 8  
 Model Predictions : Surface Dose for 0500 - 1700

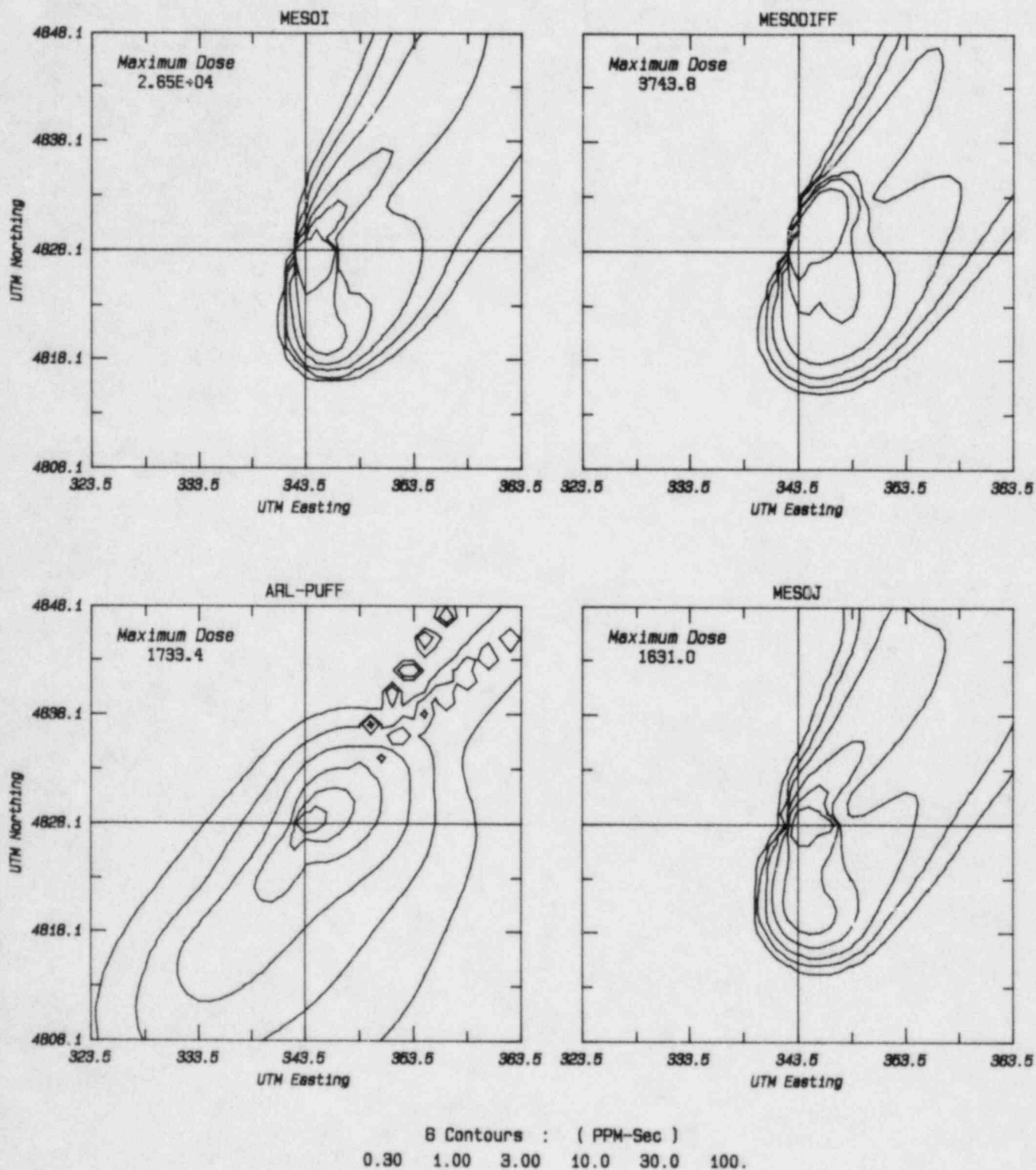


Figure B17



July 1981 INEL Field Experiment : Test 8  
 Model Predictions : Surface Dose for 0500 - 1700

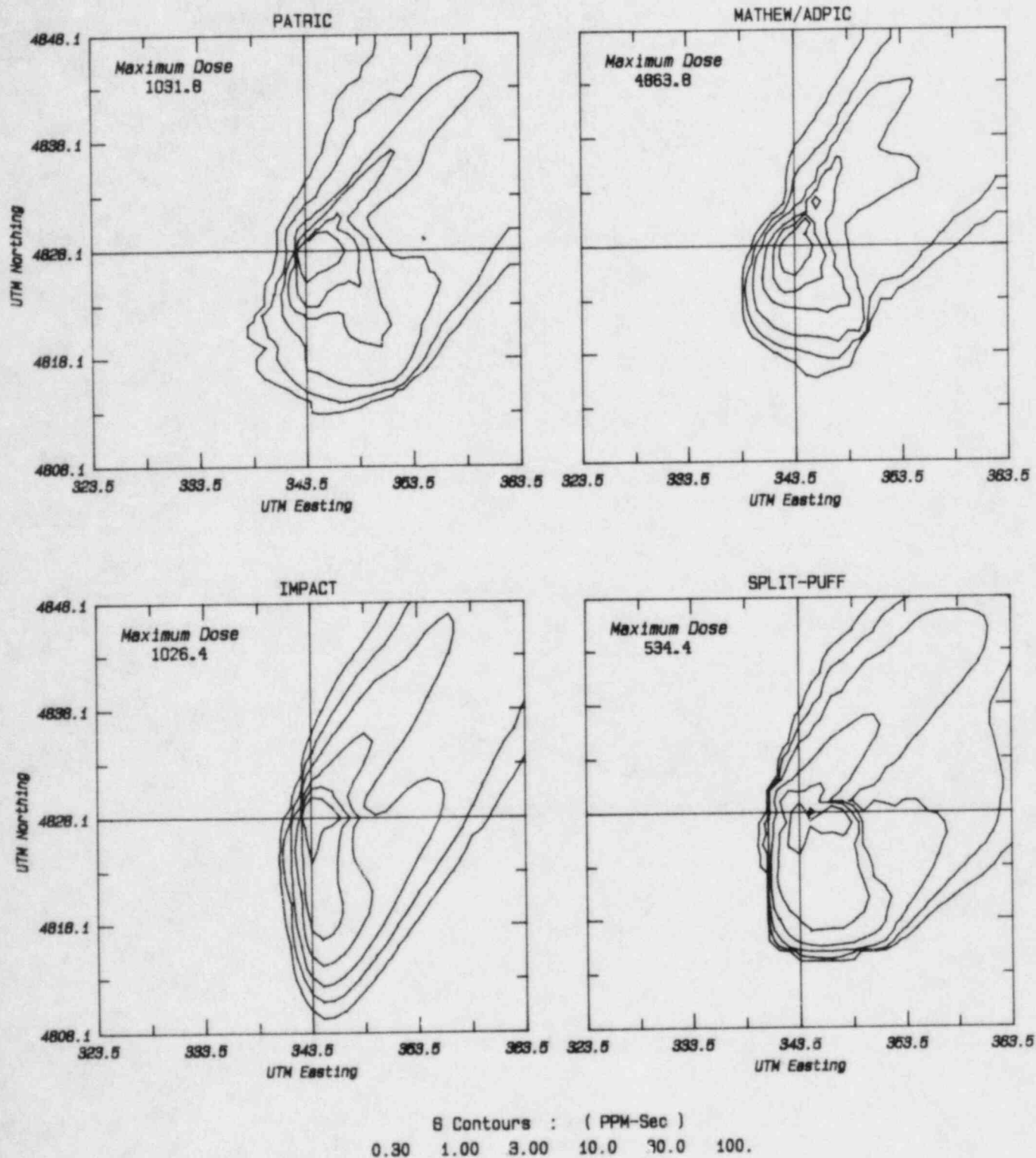


Figure B18



July 1981 INEL Field Experiment : Test 9  
 Model Predictions : Surface Dose for 1700 - 0500

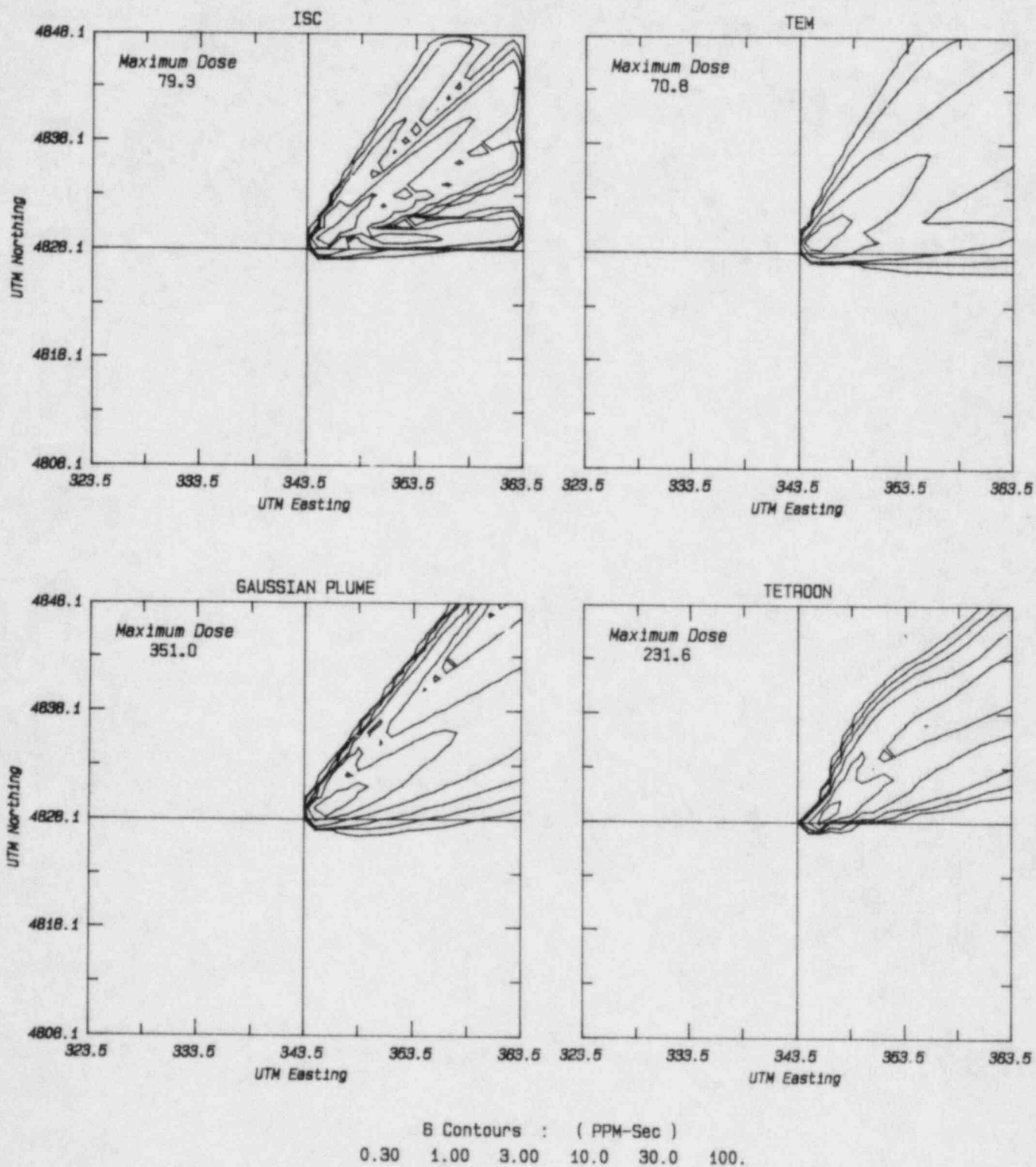


Figure B19

July 1981 INEL Field Experiment : Test 9  
 Model Predictions : Surface Dose for 1700 - 0500

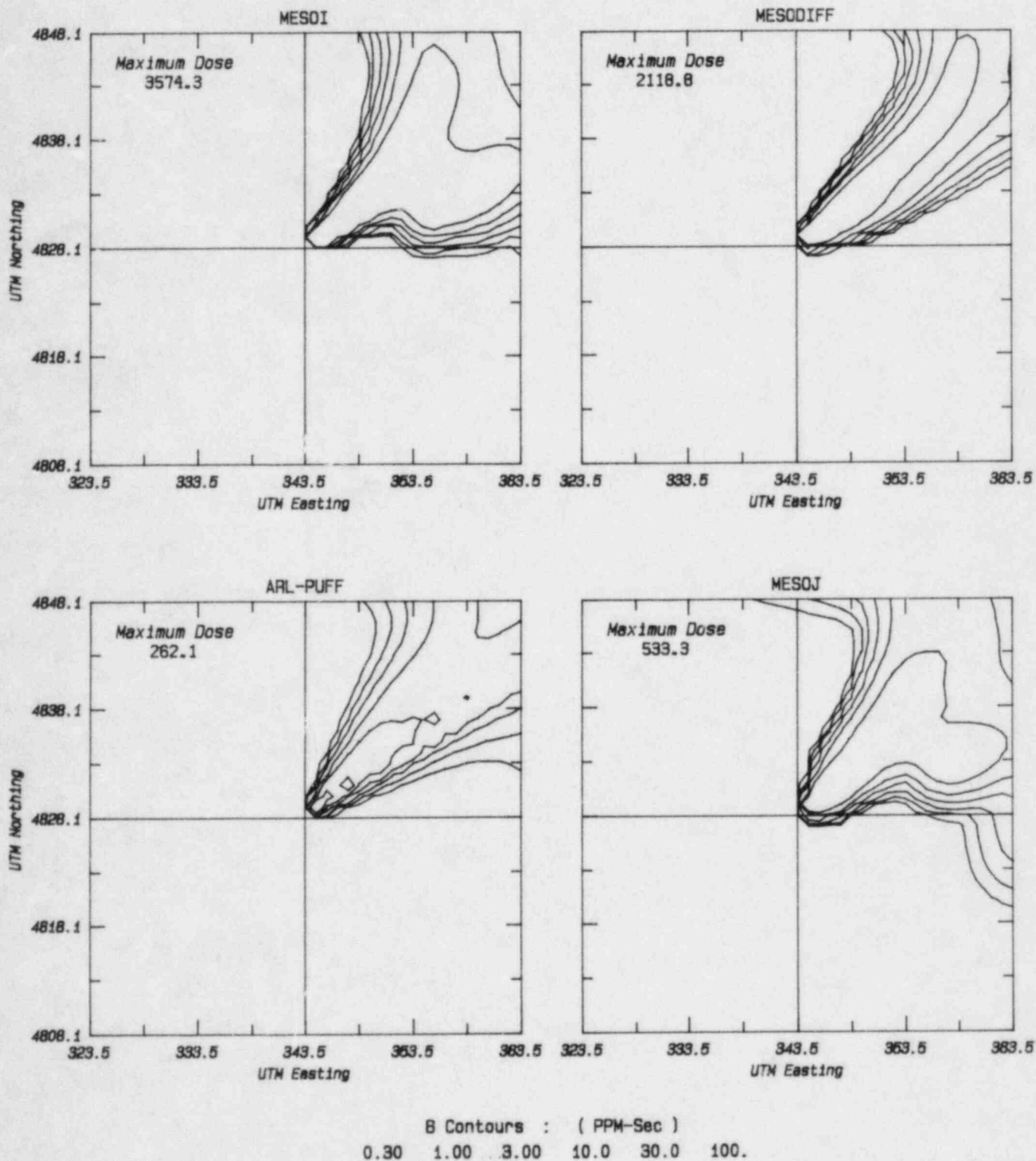


Figure B20

July 1981 INEL Field Experiment : Test 9  
 Model Predictions : Surface Dose for 1700 - 0500

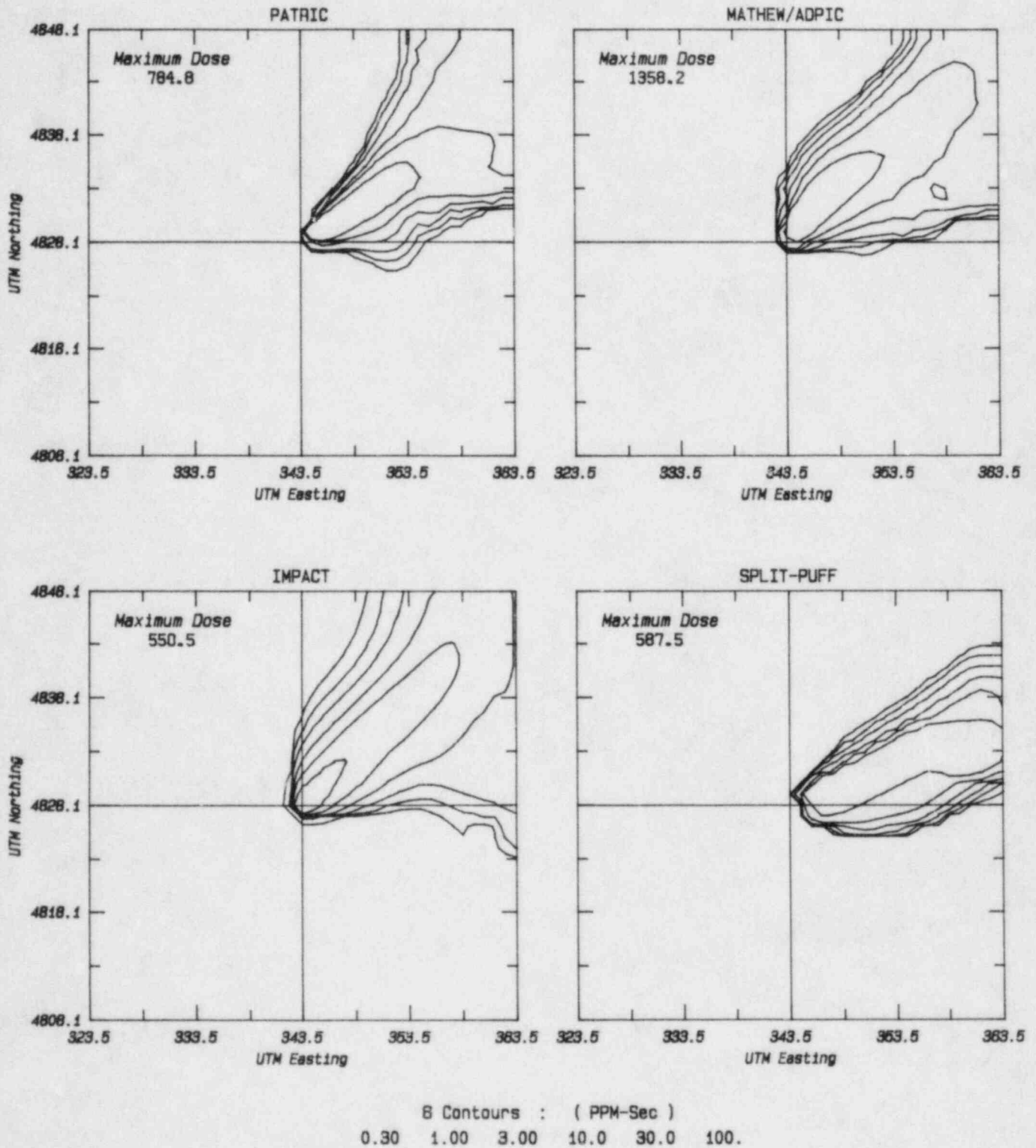
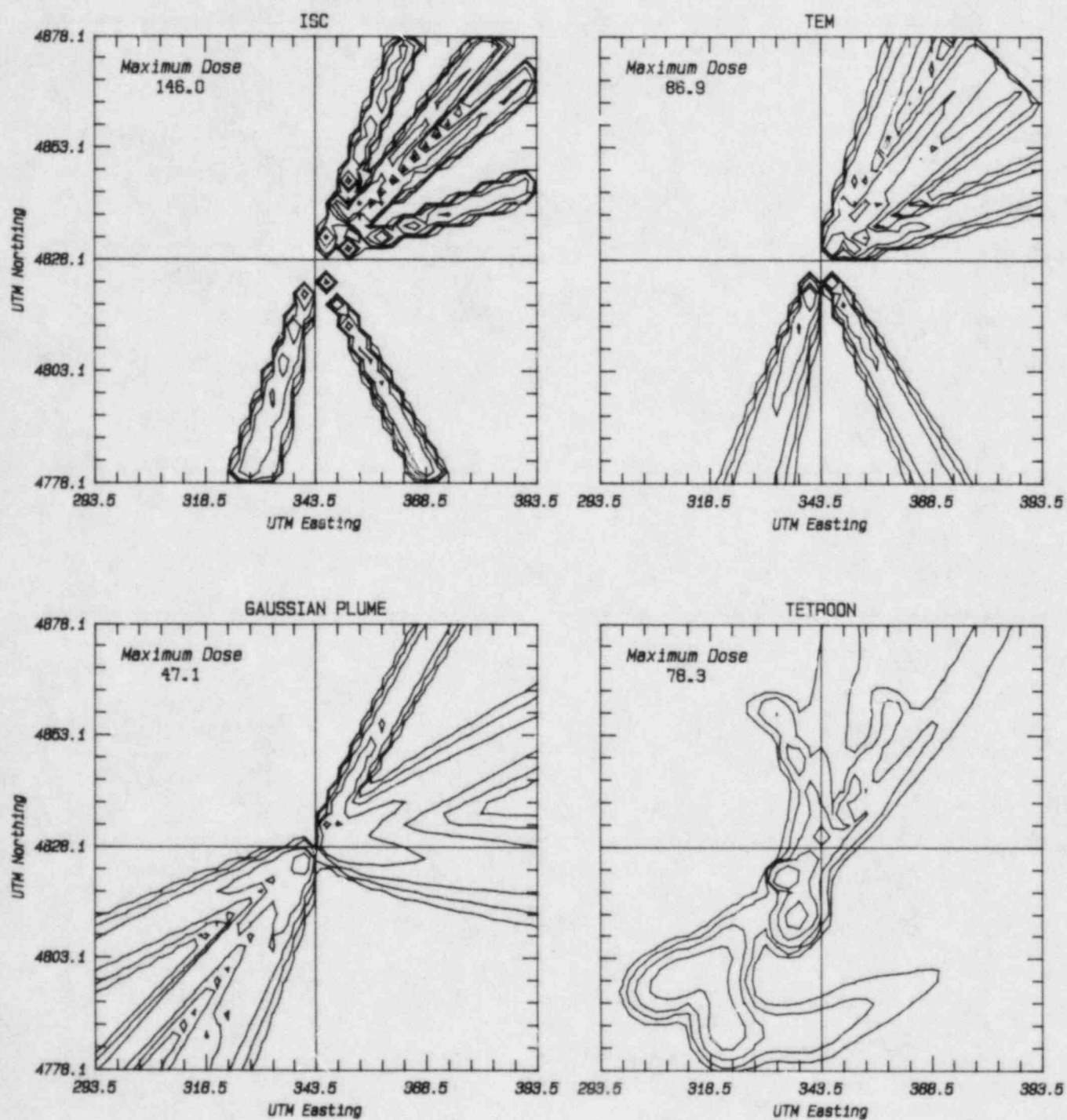


Figure B21

July 1981 INEL Field Experiment : Test 3  
Model Predictions : Total Surface Dose



B Contours : ( PPM-Sec )  
0.30 1.00 3.00 10.0 30.0 100.

Figure B22

July 1981 INEL Field Experiment : Test 3  
Model Predictions : Total Surface Dose

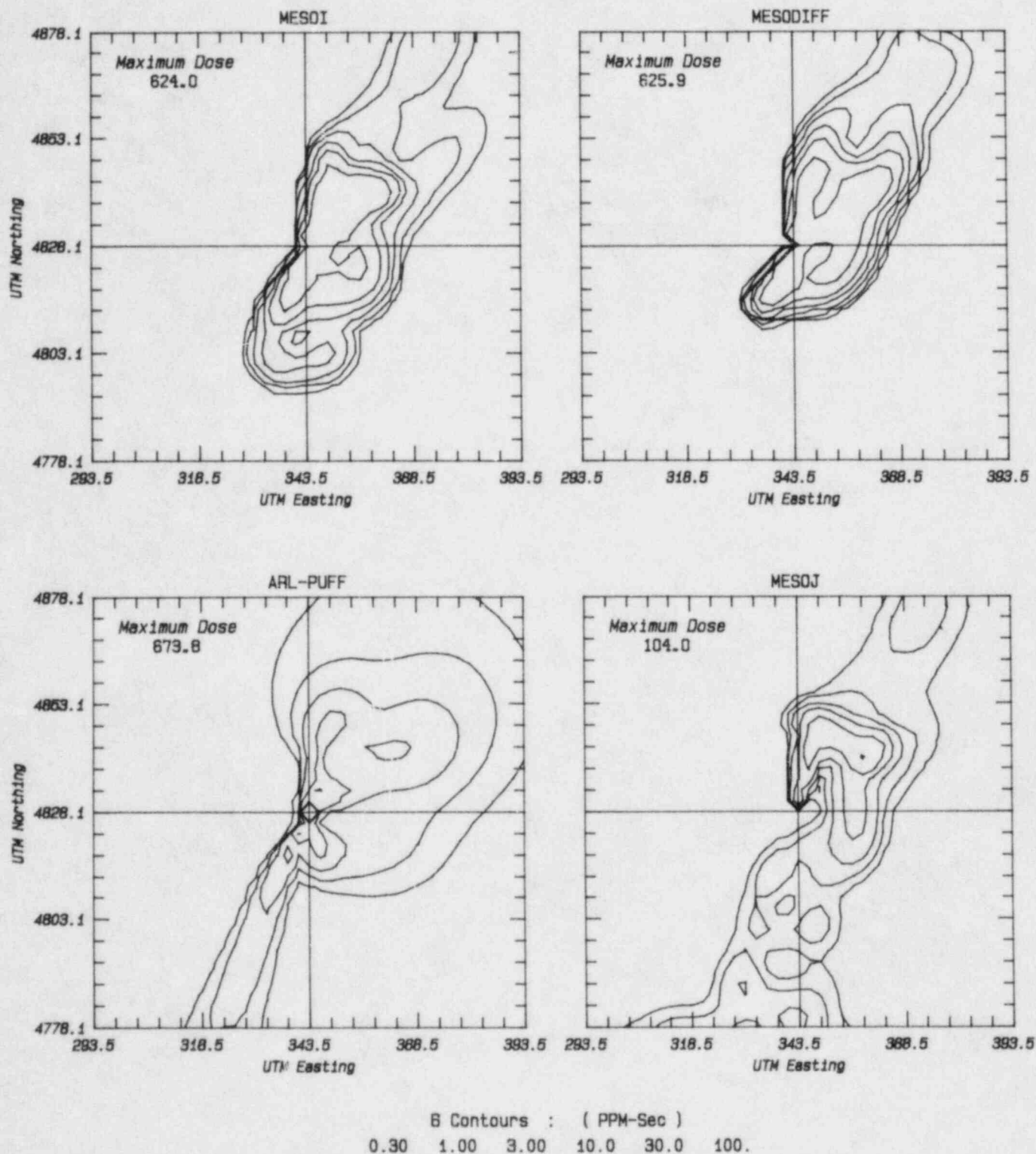


Figure B23



July 1981 INEL Field Experiment : Test 3  
Model Predictions : Total Surface Dose

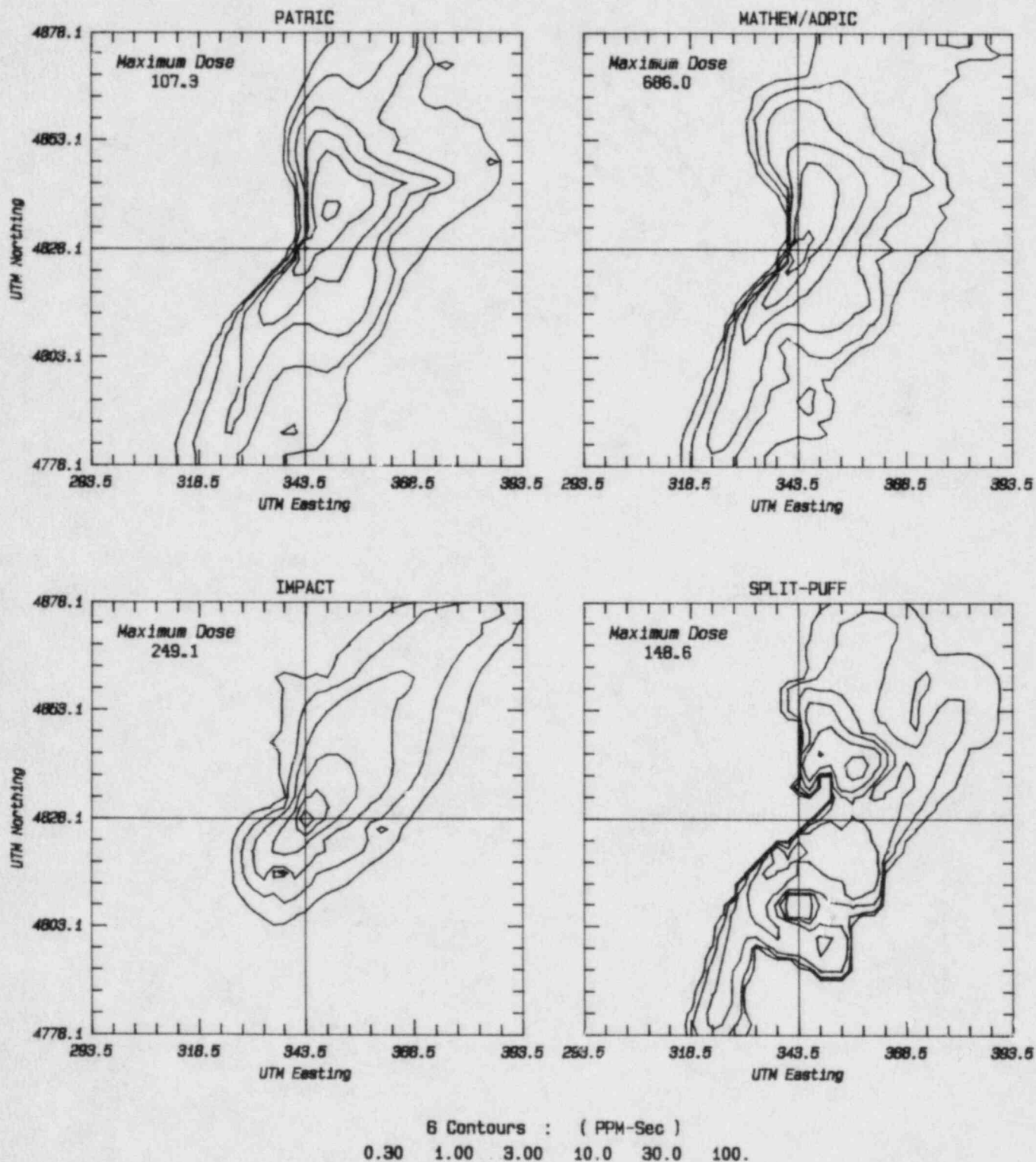


Figure 4.24



July 1981 INEL Field Experiment : Test 4  
Model Predictions : Total Surface Dose

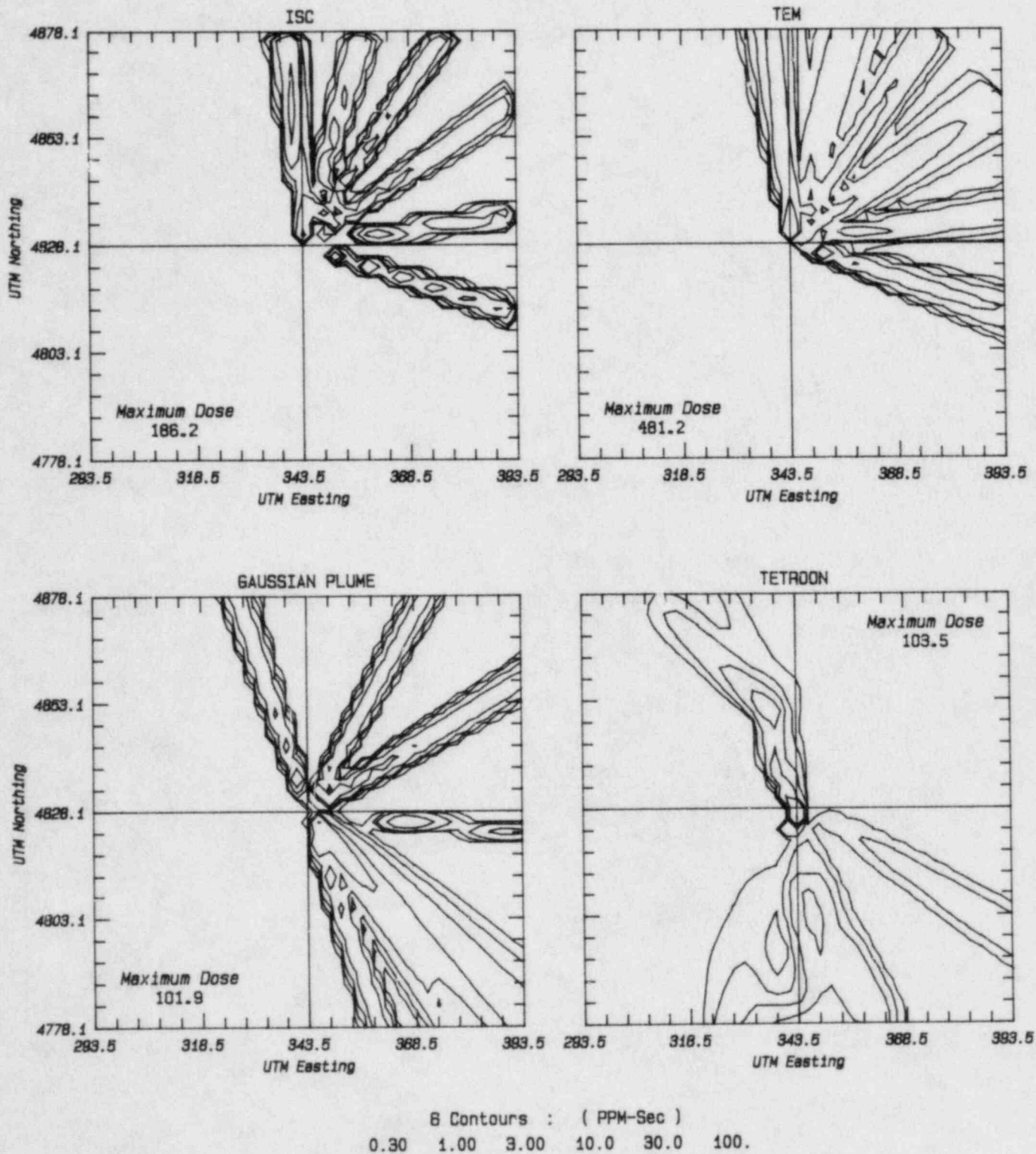


Figure B25

July 1981 INEL Field Experiment : Test 4  
Model Predictions : Total Surface Dose

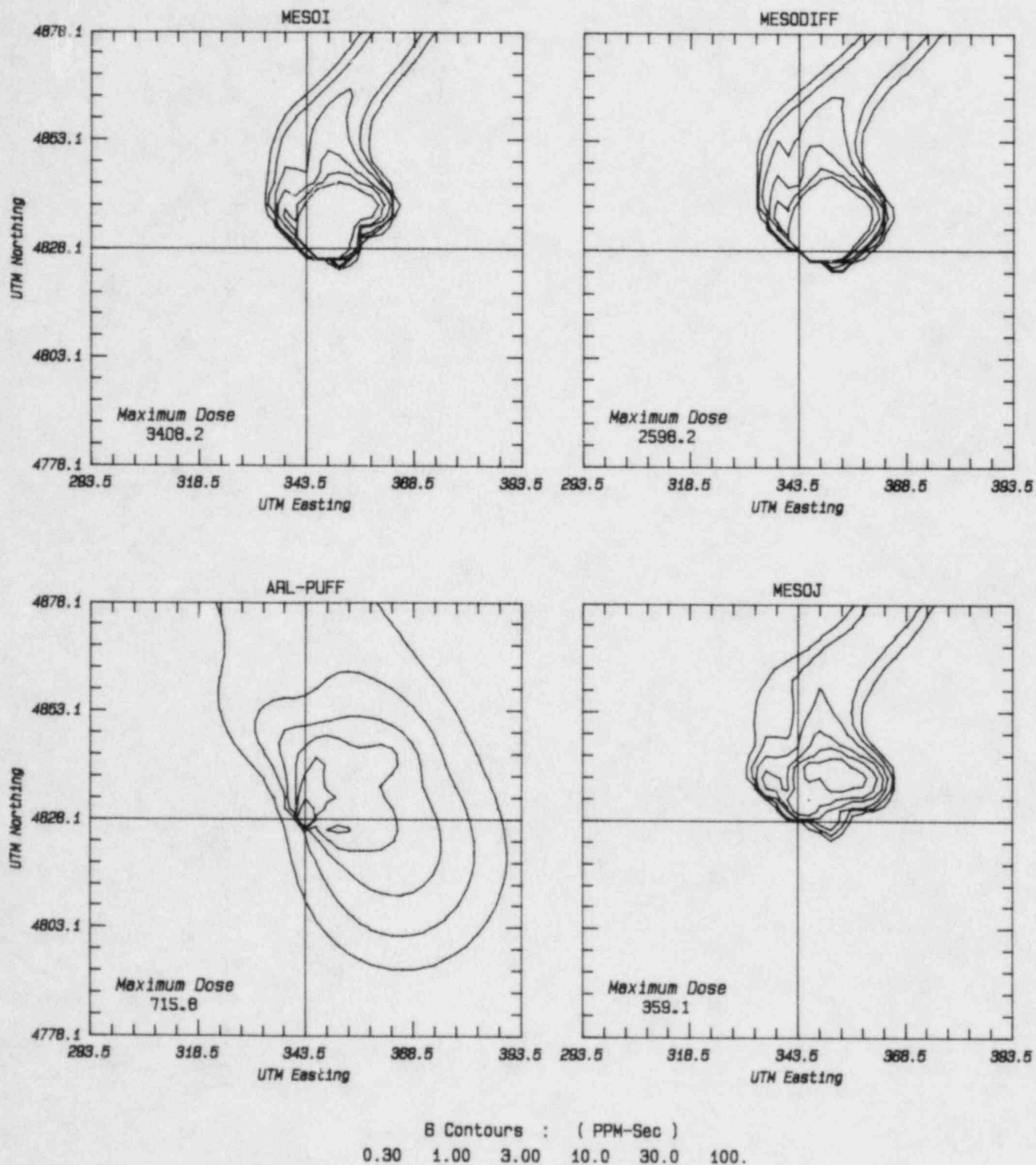


Figure B26

July 1981 INEL Field Experiment : Test 4  
Model Predictions : Total Surface Dose

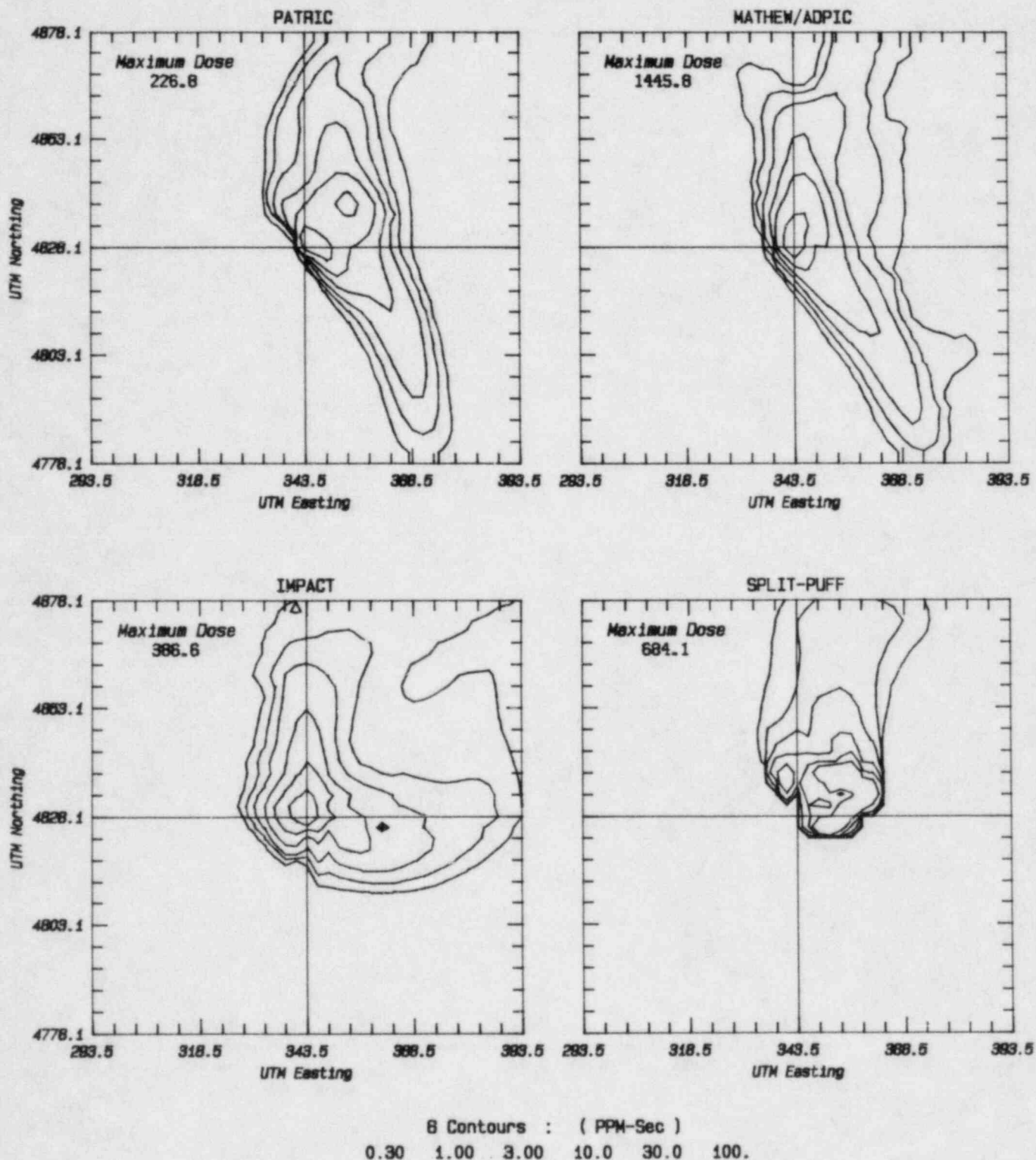


Figure B27

July 1981 INEL Field Experiment : Test 5  
Model Predictions : Total Surface Dose

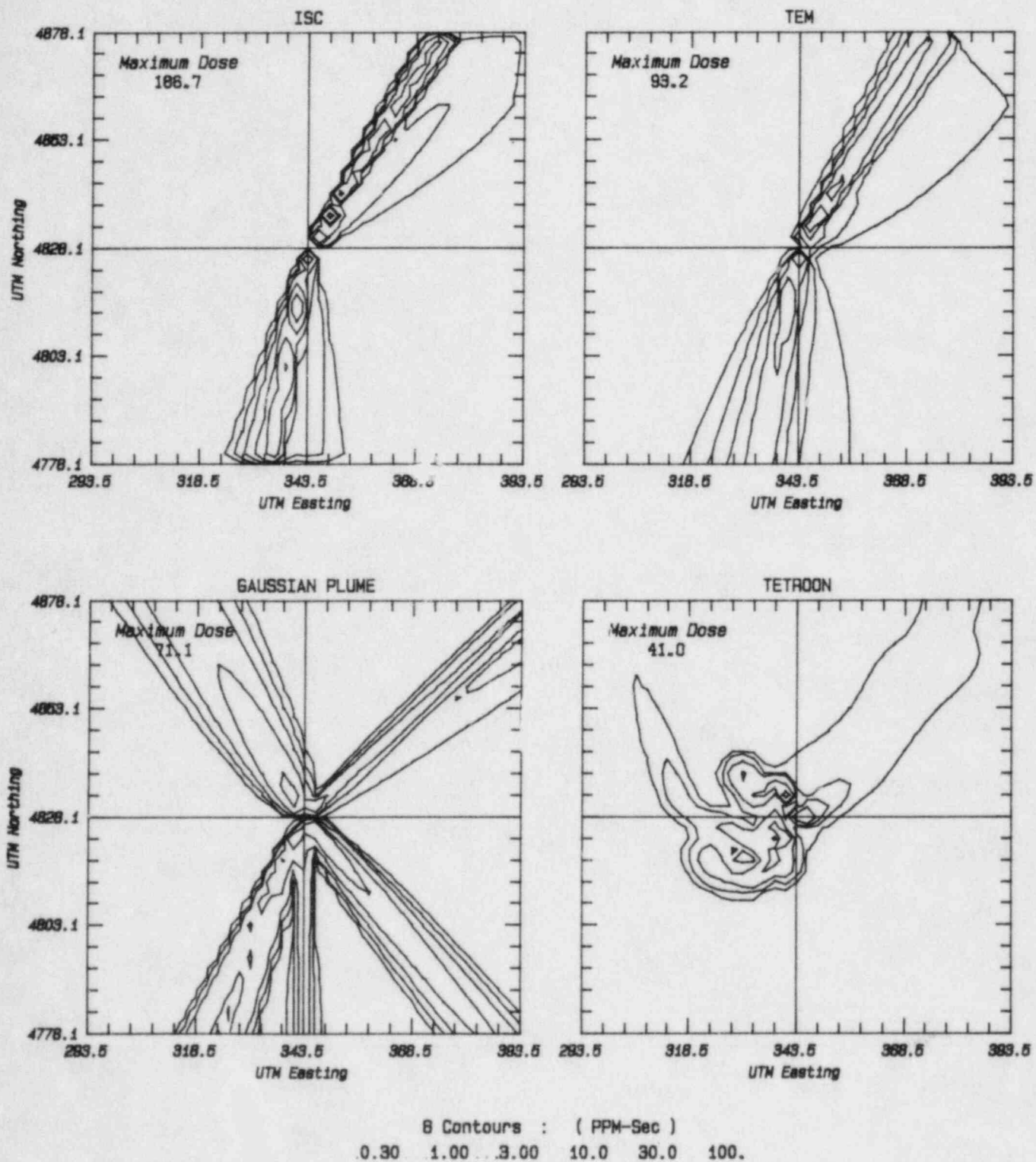


Figure B28

July 1981 INEL Field Experiment : Test 5  
Model Predictions : Total Surface Dose

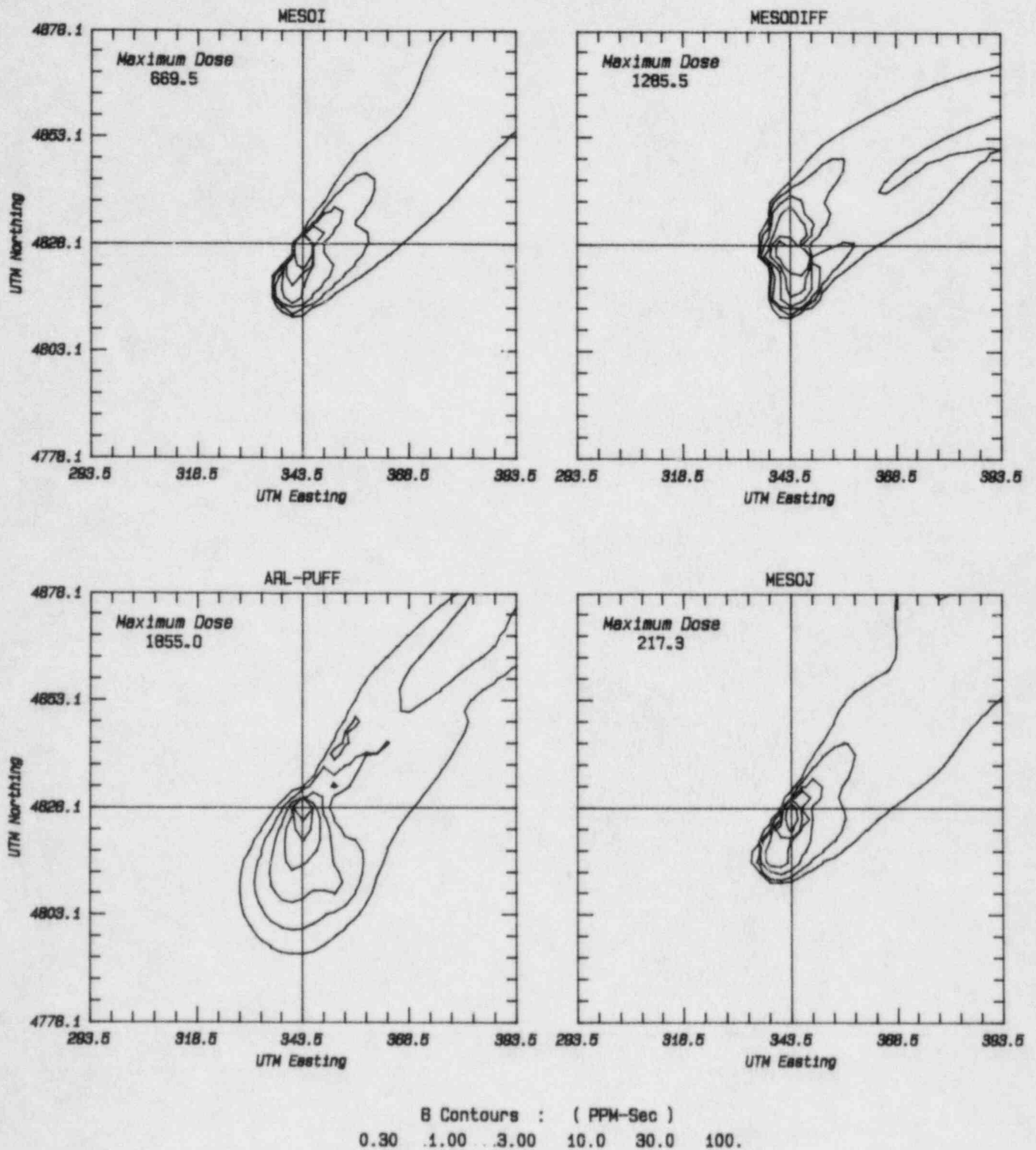


Figure B29



July 1981 INEL Field Experiment : Test 5  
Model Predictions : Total Surface Dose

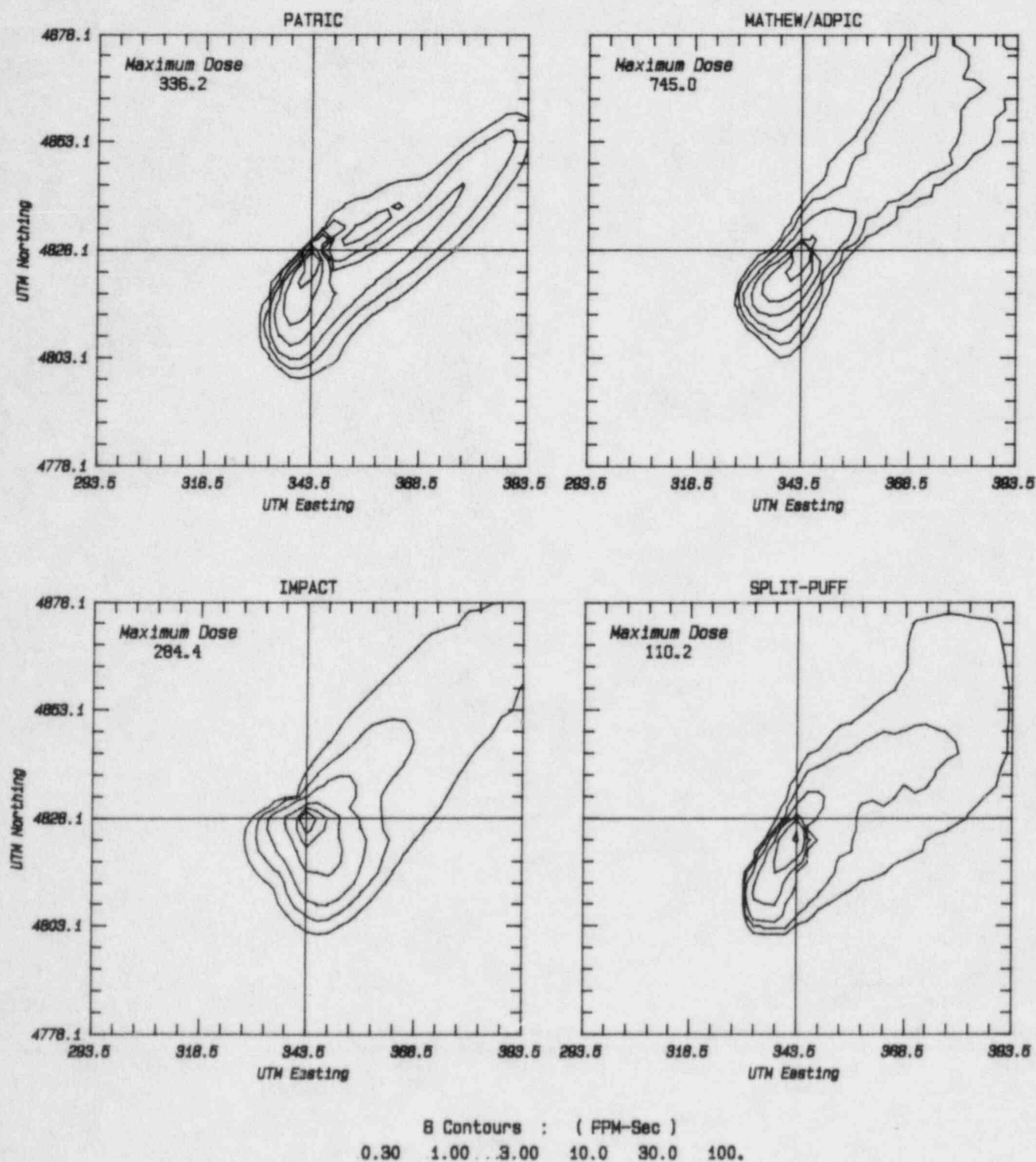


Figure B30



July 1981 INEL Field Experiment : Test 6  
Model Predictions : Total Surface Dose

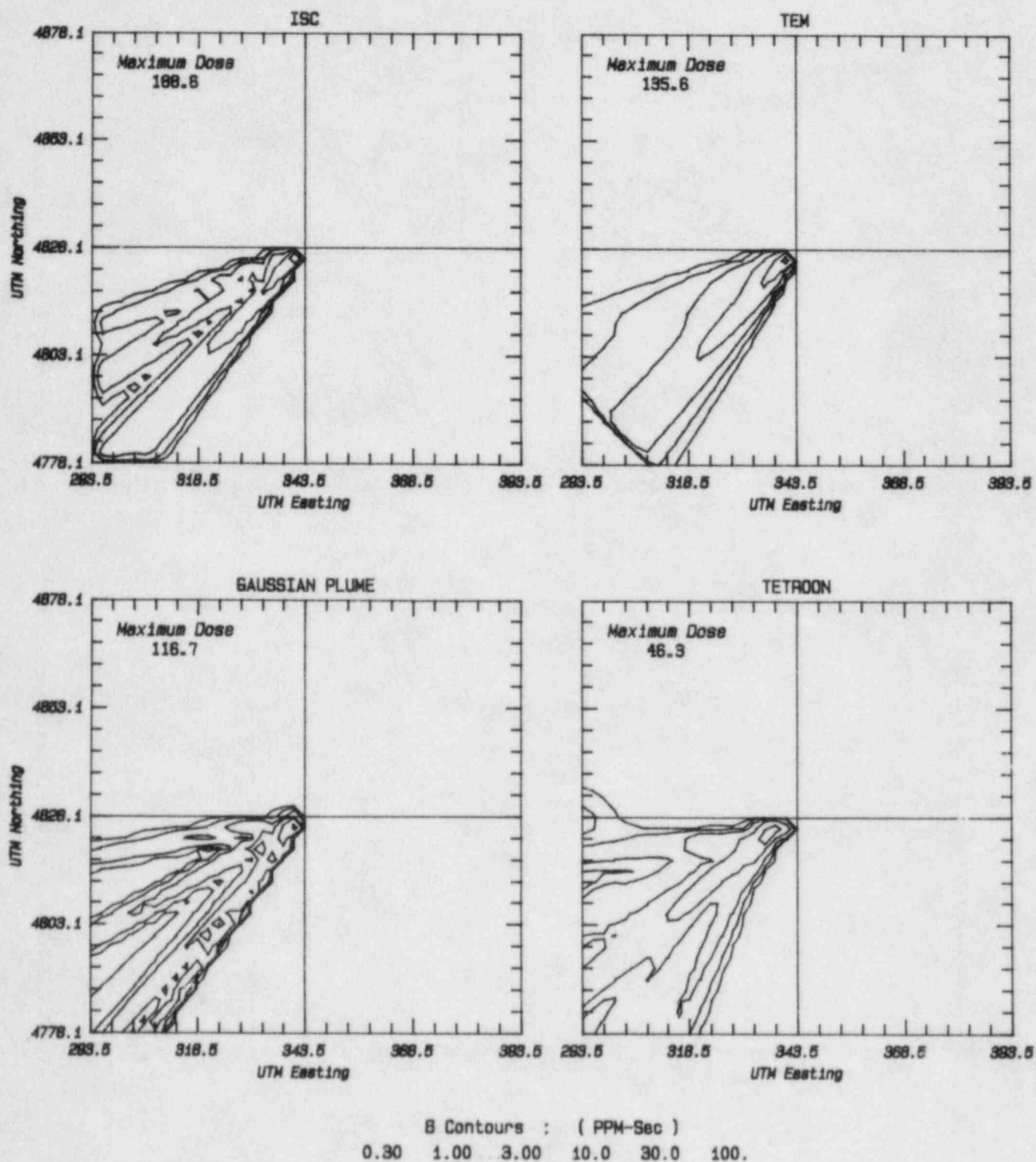


Figure B31

July 1981 INEL Field Experiment : Test 6  
Model Predictions : Total Surface Dose

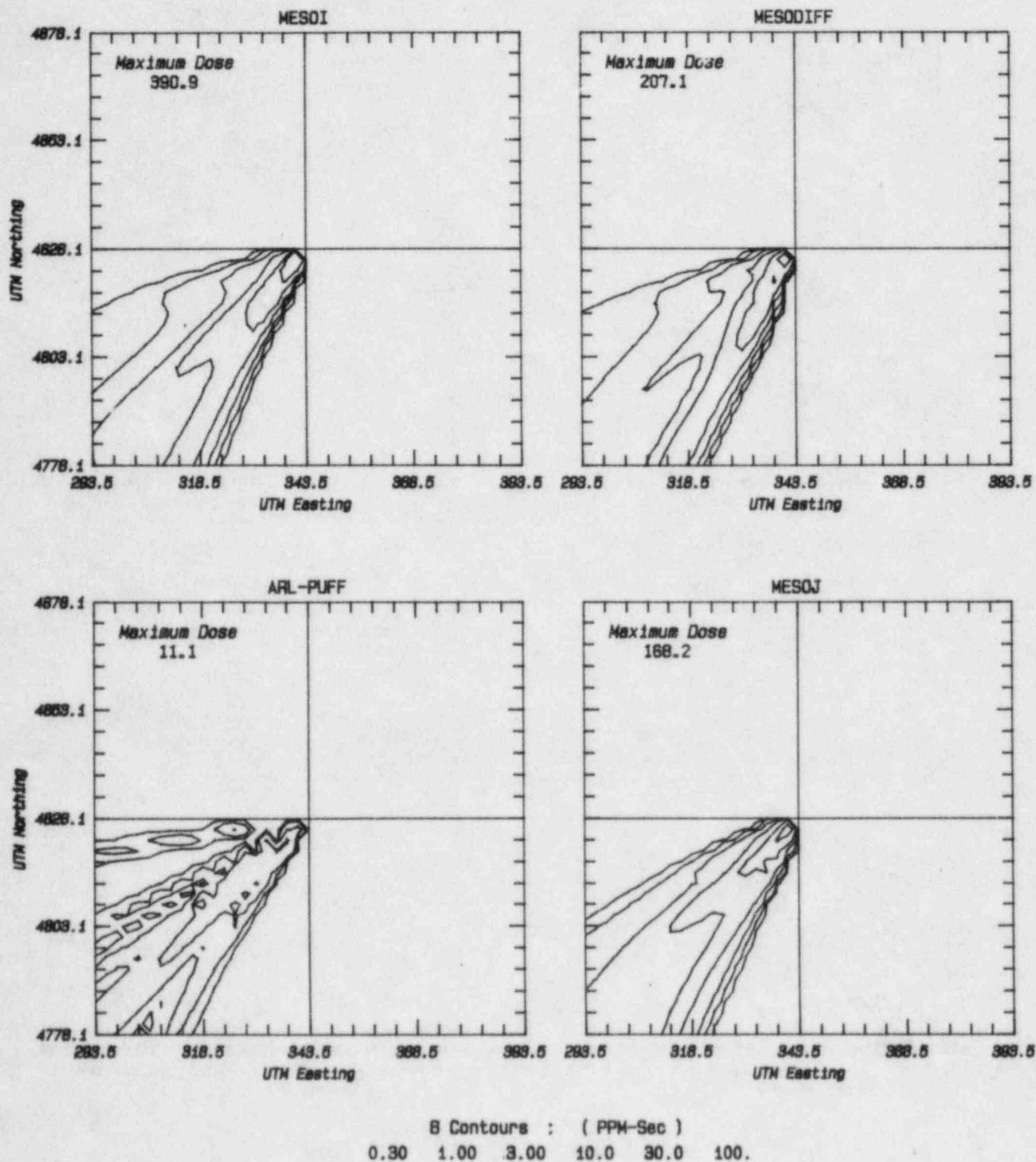


Figure B32

July 1981 INEL Field Experiment : Test 6  
Model Predictions : Total Surface Dose

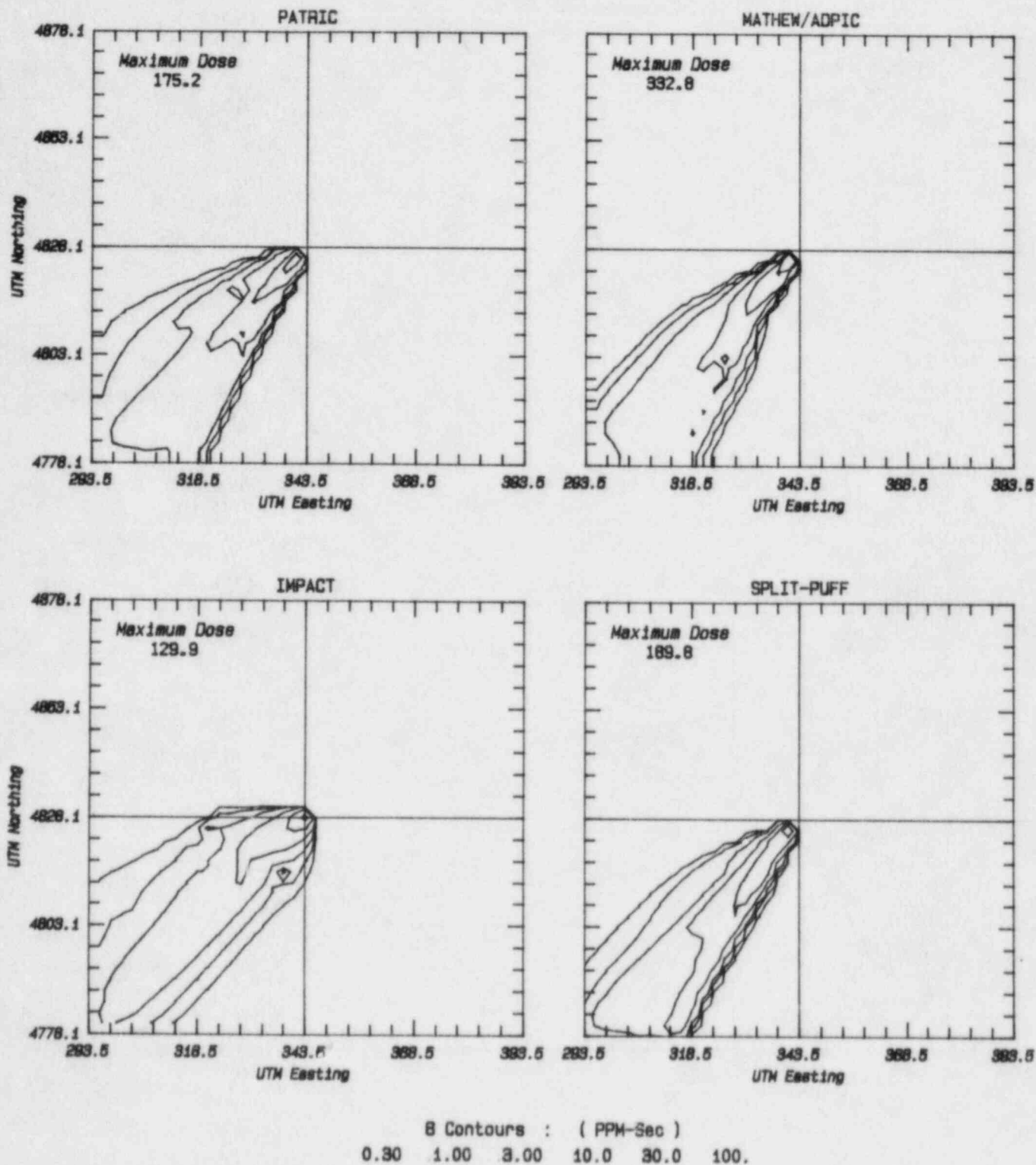


Figure B33

July 1981 INEL Field Experiment : Test 7  
Model Predictions : Total Surface Dose

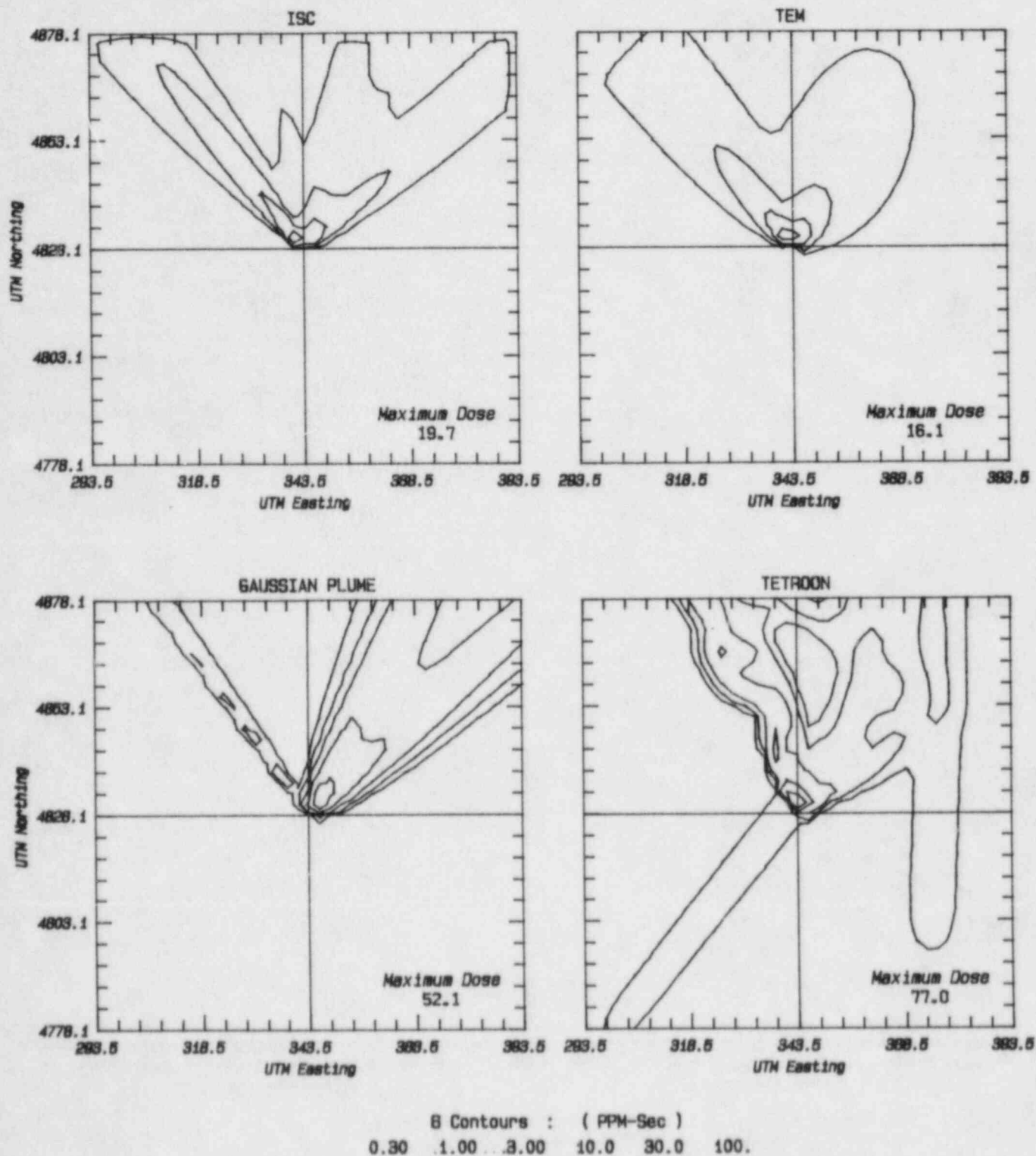


Figure B34

July 1981 INEL Field Experiment : Test 7  
Model Predictions : Total Surface Dose

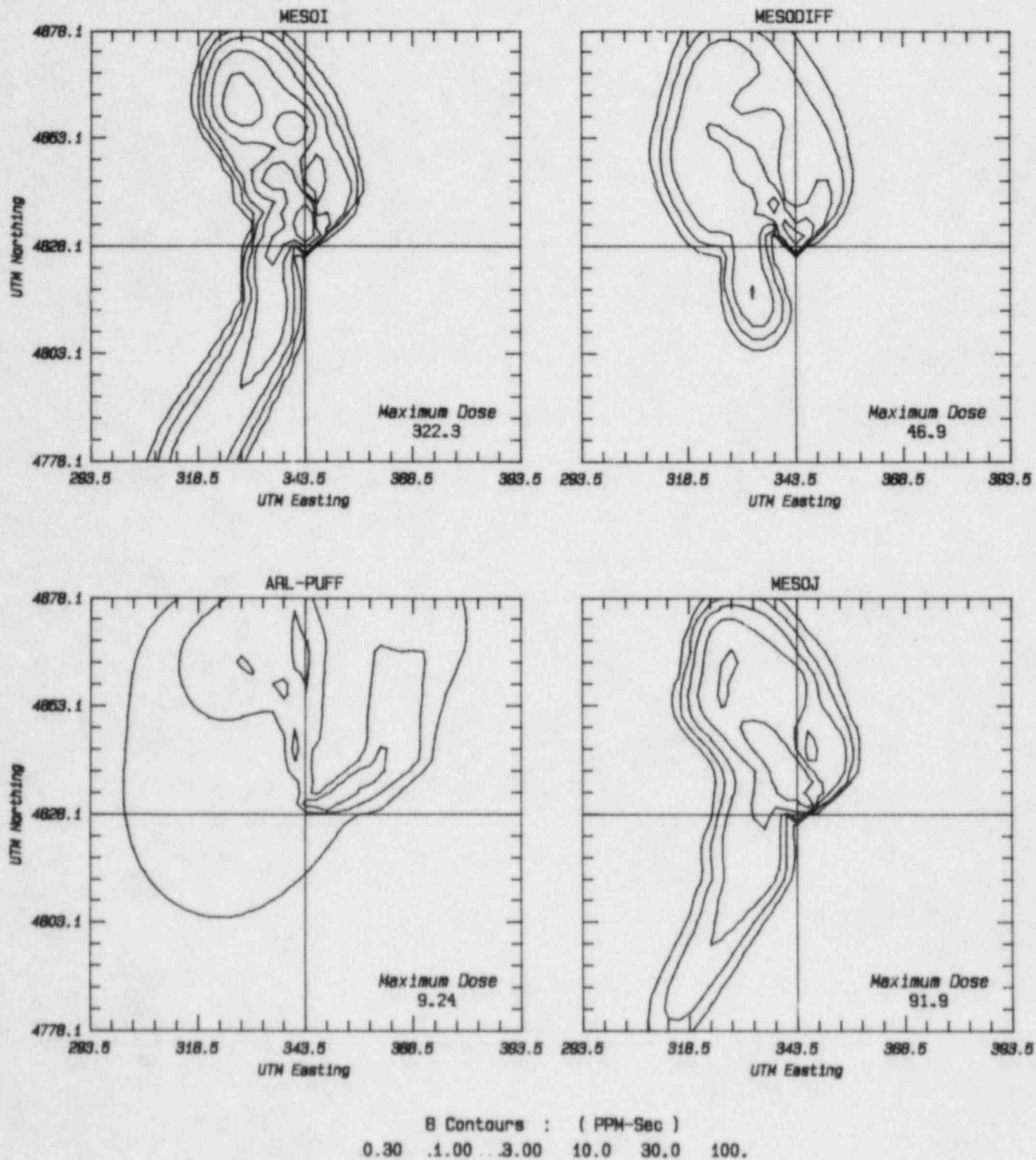


Figure B35



July 1981 INEL Field Experiment : Test 7  
Model Predictions : Total Surface Dose

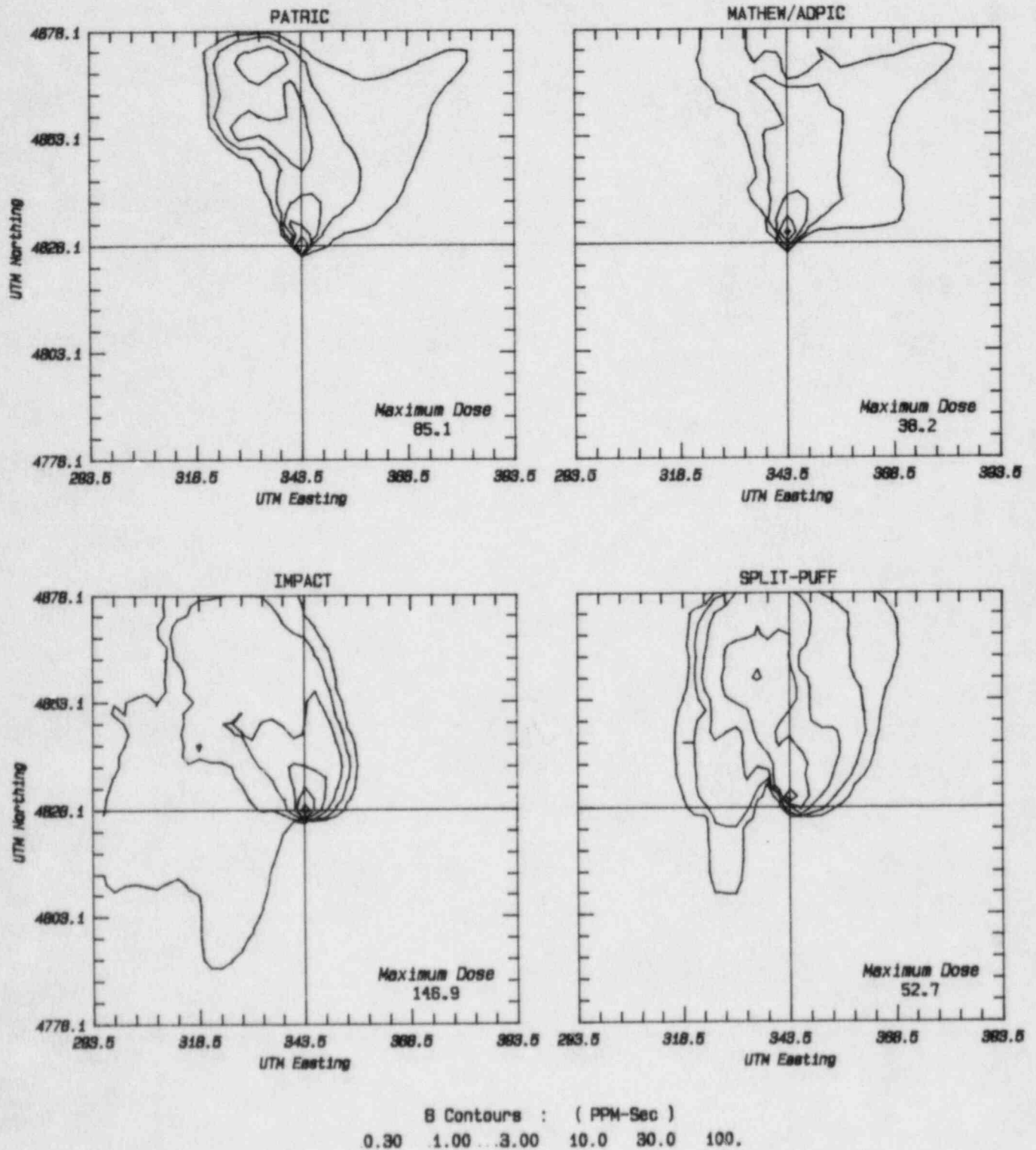


Figure B36



July 1981 INEL Field Experiment : Test 8  
Model Predictions : Total Surface Dose

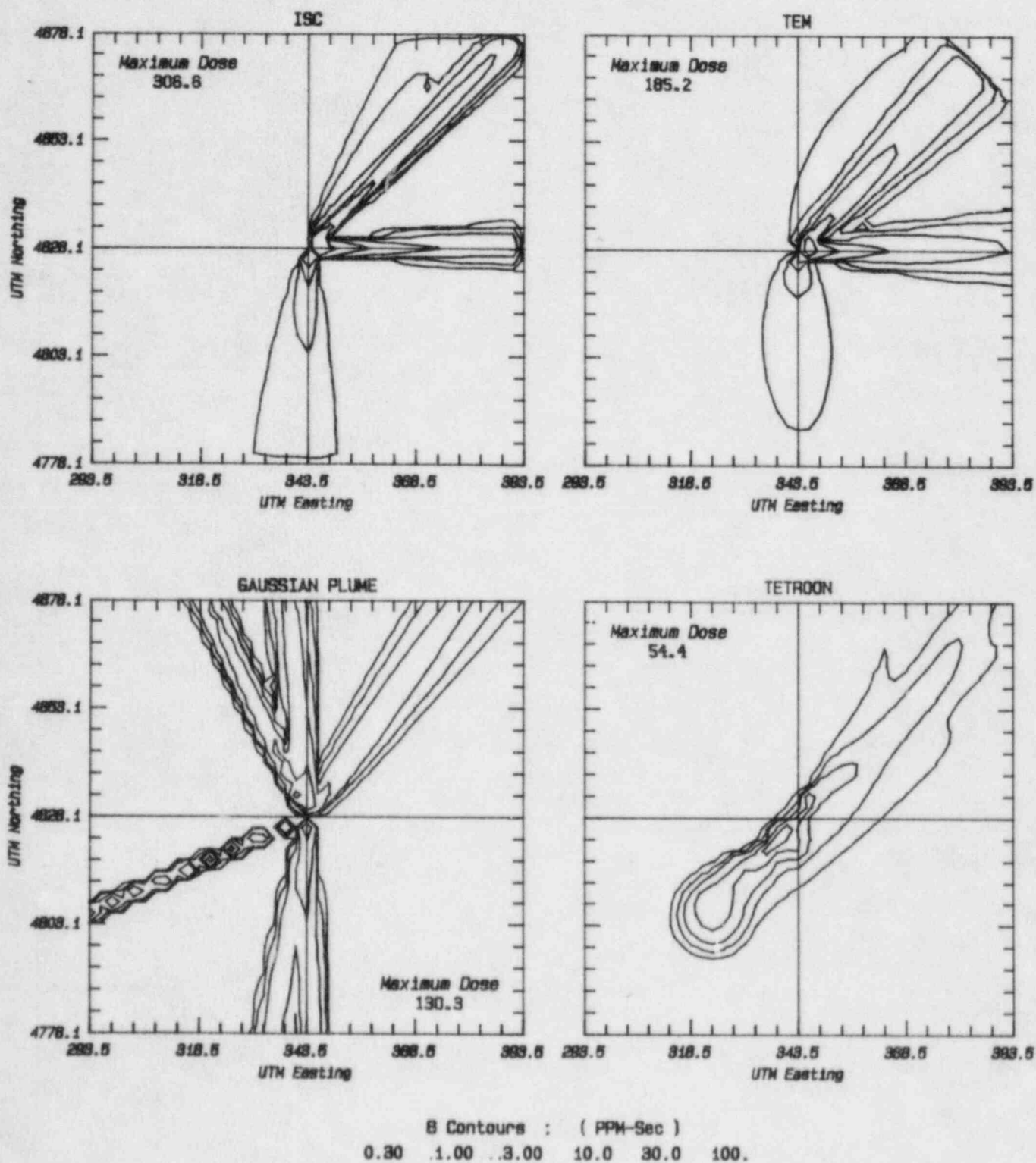


Figure B37

July 1981 INEL Field Experiment : Test 8  
Model Predictions : Total Surface Dose

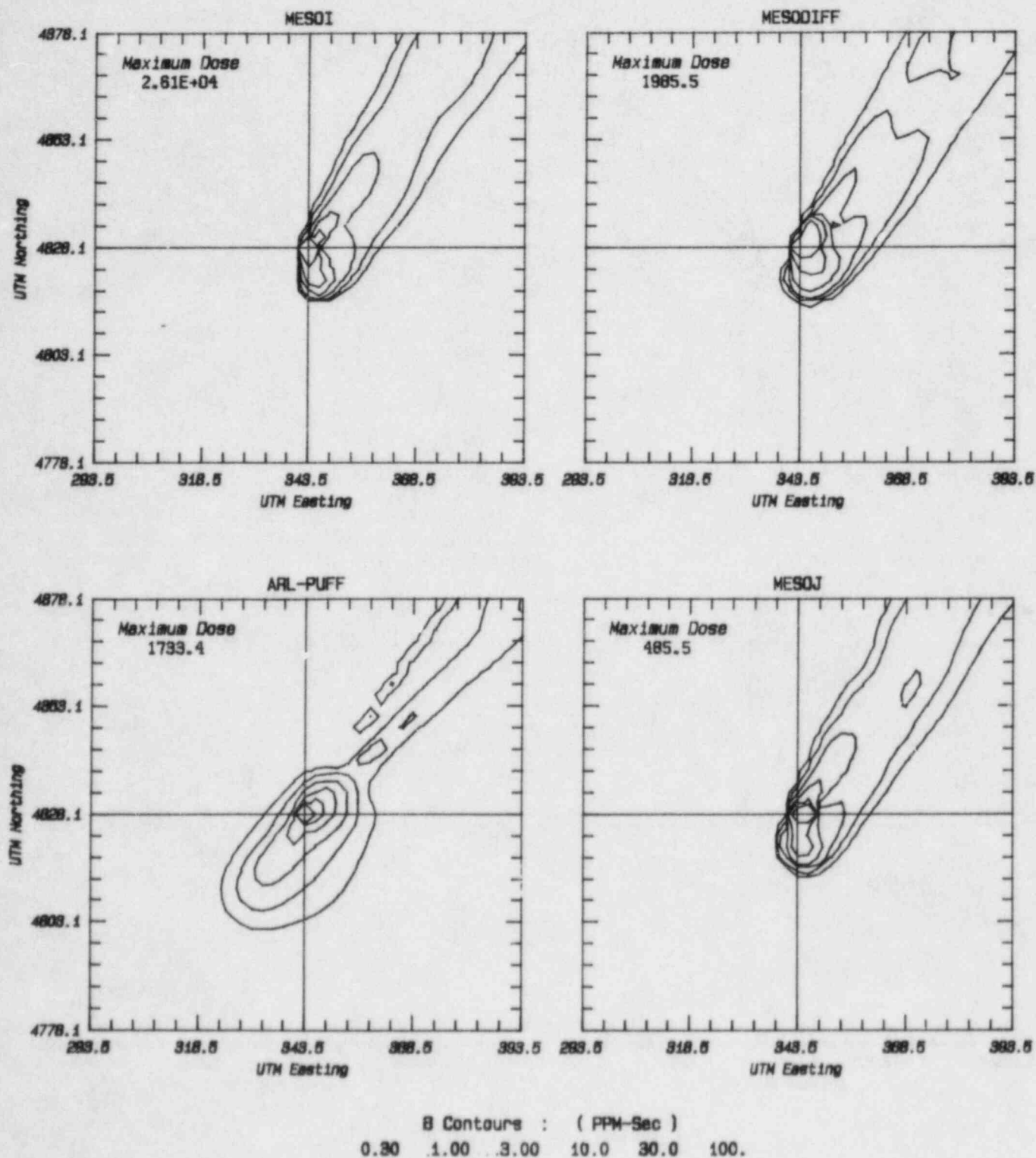


Figure B38

July 1981 INEL Field Experiment : Test 8  
Model Predictions : Total Surface Dose

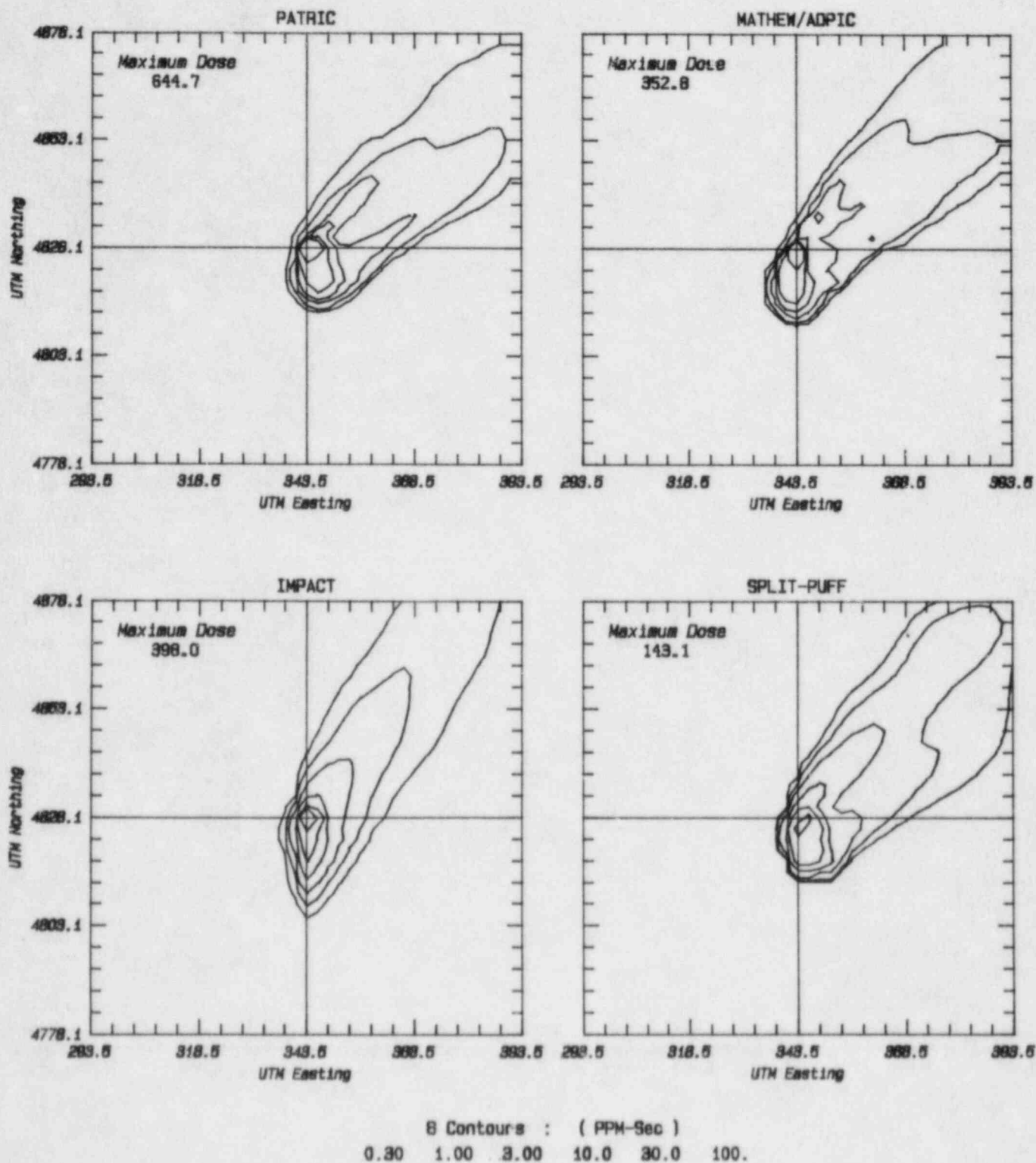


Figure B39

July 1981 INEL Field Experiment : Test 9  
Model Predictions : Total Surface Dose

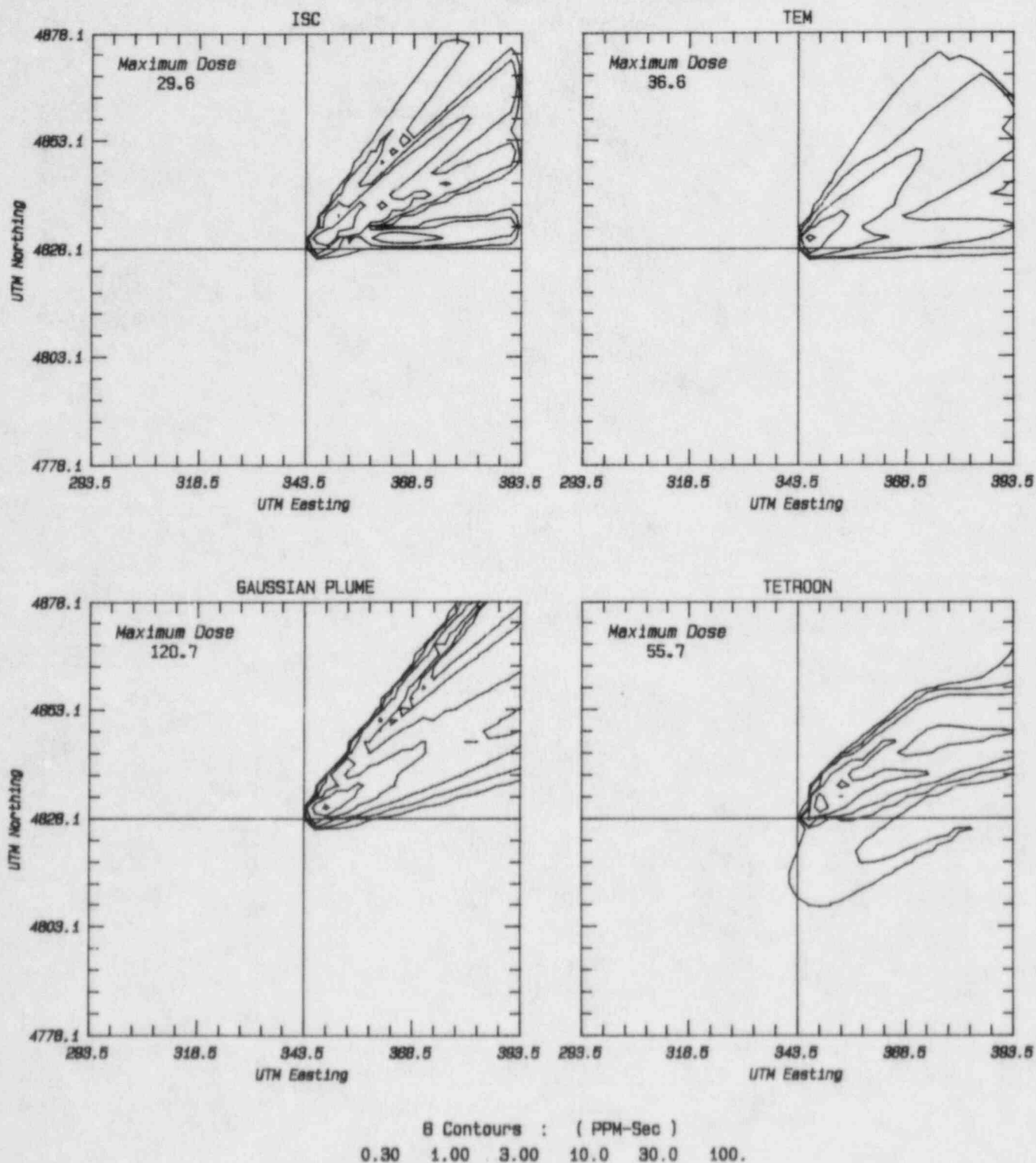


Figure B40

July 1981 INEL Field Experiment : Test 9  
Model Predictions : Total Surface Dose

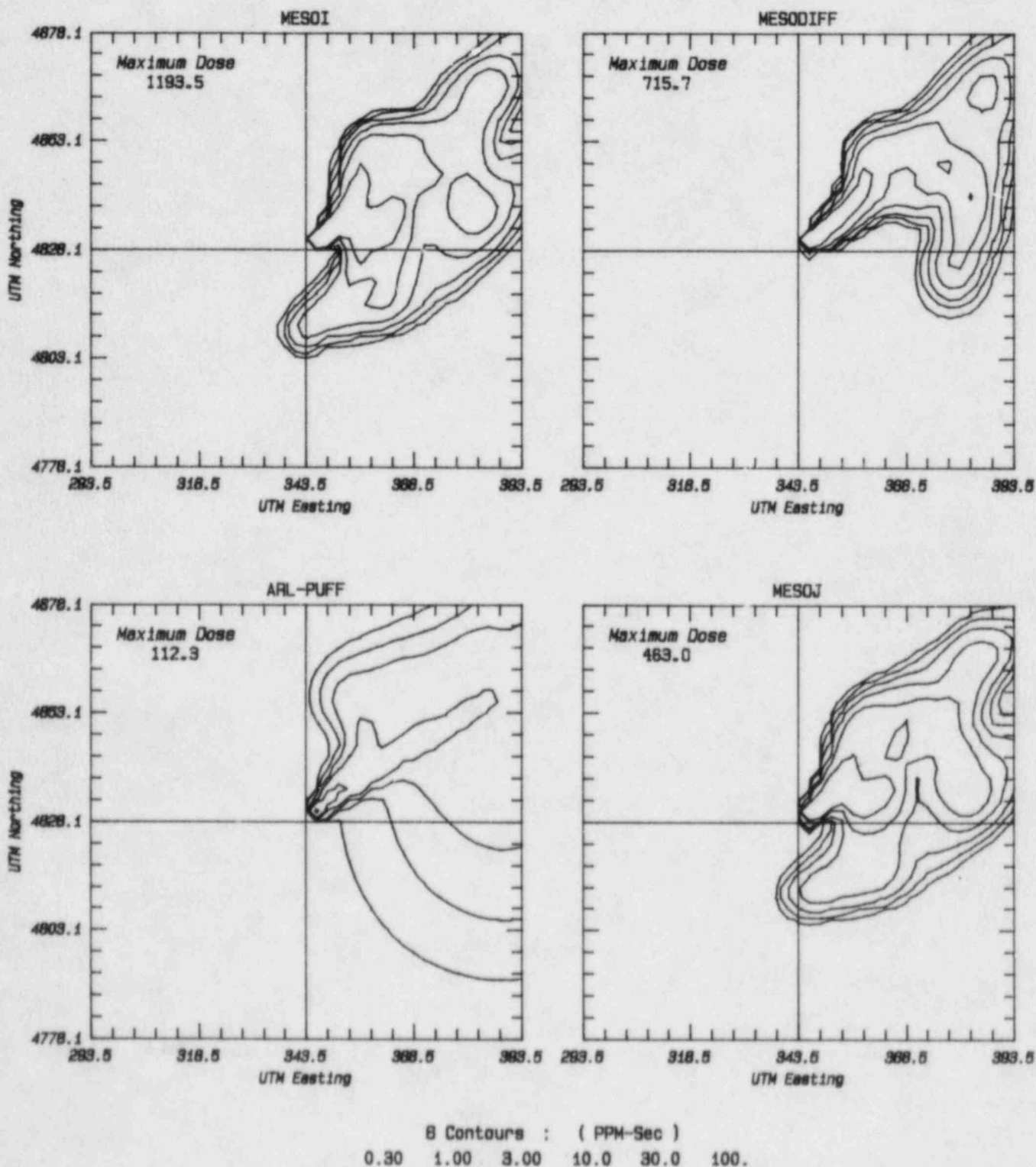


Figure B41



July 1981 INEL Field Experiment : Test 9  
Model Predictions : Total Surface Dose

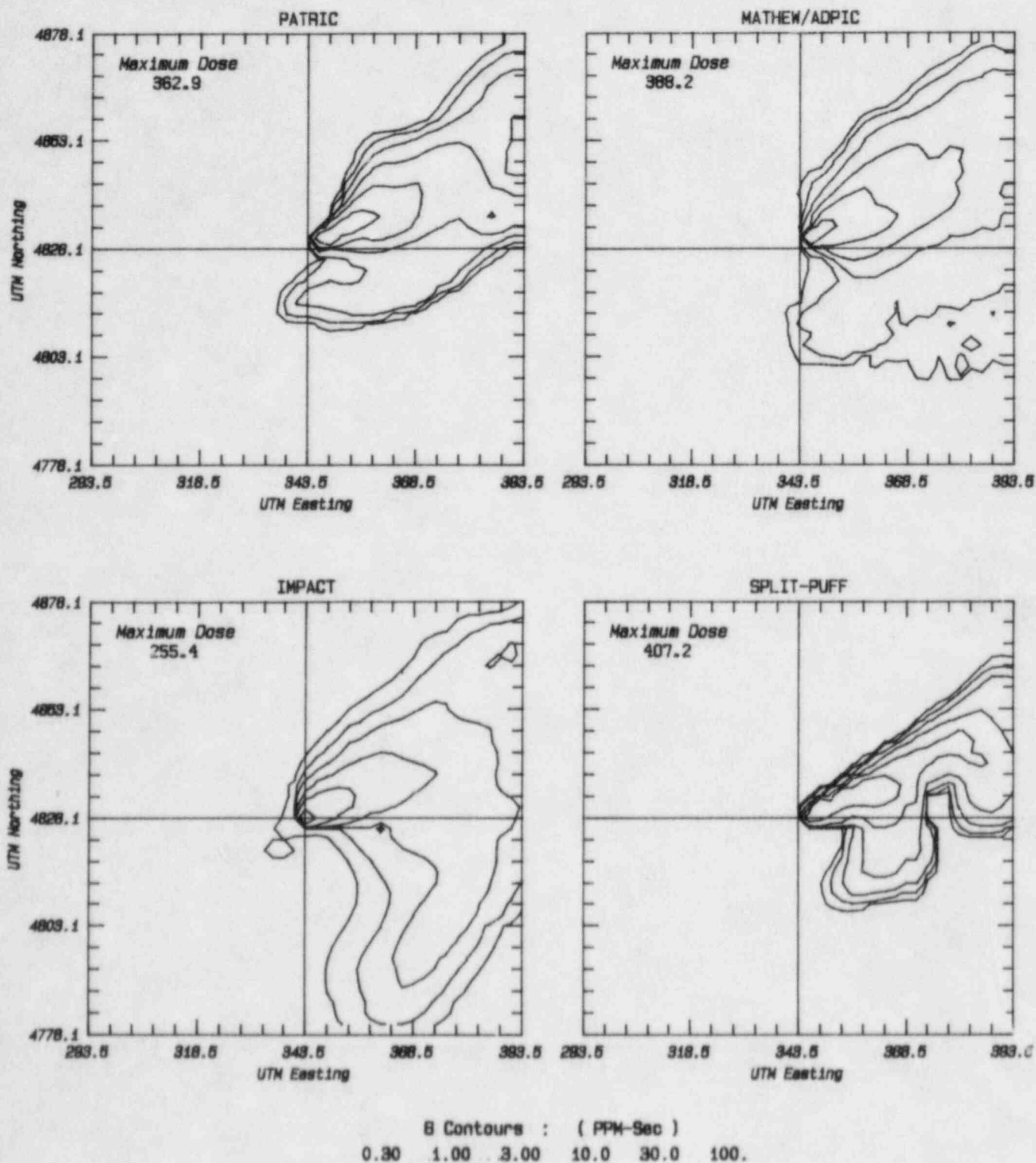


Figure B42



## Appendix C

### Analysis of the Lidar Data

The ALPHA-1 lidar system provides a virtually instantaneous vertical cross-section of the plume since the aircraft traverses at speeds of roughly  $100 \text{ ms}^{-1}$ , i.e. much faster than the wind speed. An estimate of the average concentration is generally obtained by averaging together a number of these cross-sections, taken over a period of an hour. This is the basis of the lidar measurements of  $\sigma_y$  and  $\sigma_z$  which were used for model evaluation in this report. However, the lidar cross-sections provide a large amount of detailed information about the plume, and in this Appendix we examine some methods for extracting more from the data than the two numbers,  $\sigma_y$  and  $\sigma_z$ .

The most obvious quantity to examine is the mean concentration field,  $\bar{c}(y,z)$ , as obtained from the cross-sections. An example of this field is shown in Figure C.1; this represents the average of 10 cross-sections taken between 0700 and 0800 on July 23rd, 1980. The section is transverse to the mean wind, and is made about 5 km downstream of the source; the boundary layer was stable at this time, so that the vertical spread of the plume is very limited.

It is clear that the estimate of the mean in Figure C.1 is very rough, and although the general size and shape of the plume is determined, we do not have a good estimate of a smooth ensemble mean. If we try to use the basic data to obtain higher-order statistics such as variance estimates and confidence limits, then we find that the rapid spatial variations are so erratic as to completely mask any overall structure. The problem here is that the plume is meandering a good deal, and 10 cross-sections are not large enough sample to give good statistics for this intermittent variable. In order to get more information from the data, we need to increase our effective sample size.

INEL : ALPHA1 : JULY 23 : 0700 - 0800  
AVERAGE CONCENTRATION

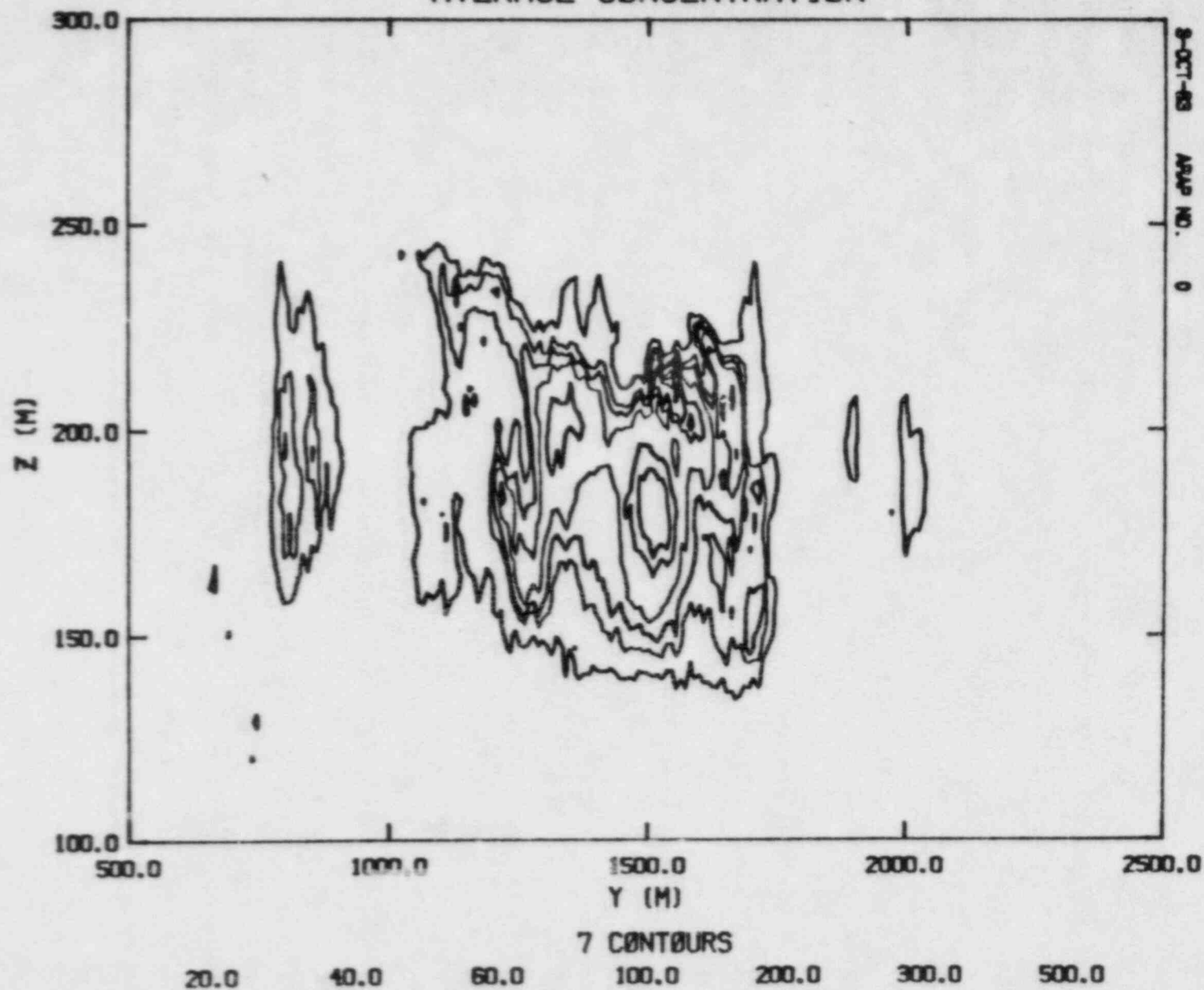


Figure C1

An increase in the sample size requires some kind of hypothesis about the data, since the actual amount of real data is fixed. One could, for example, assume a Gaussian shape and fit such a function to the data as was done to obtain  $\sigma_y$  and  $\sigma_z$ . However, this is a very strong assumption, and seems to impose unnecessary restrictions on the shape of the plume which we would prefer to determine from the data. An hypothesis which is much weaker, but still gives sufficient data, is that the shape of the instantaneous plume is uncorrelated with its centroid positions. The assumption seems reasonable, because the centroid will be determined by large-scale wind fluctuations, while the detailed shape is controlled by smaller-scale eddies. This hypothesis allows one to generate 100 cross-sections by shifting each cross-section of the plume onto all 10 centroids.

Figure C.2 shows the mean concentration obtained from these 100 samples. It is very much smoother than Figure C.1; most of the small-scale variations have been eliminated by shifting the centroids. Using 100 sections, we can now calculate an r.m.s. concentration fluctuation,  $\sigma_c$ , and this field is shown in Figure C.3. It is rougher than the mean concentration, but the structure is still evident, and it is clearly wider than the  $\bar{c}$ -field. The maximum  $\sigma_c$  is roughly 500 in the center of the plume, compared to a maximum  $\bar{c}$  of about 100. The units here are arbitrary since the lidar detects smoke particles, not  $\text{SF}_6$  concentration.

To illustrate the structure of the concentration fluctuations field, Figures C.4 and C.5 show cross-sections of the ratio  $\sigma_c/\bar{c}$  through the centroid of the plume in both vertical and horizontal directions. We see a distinct minimum in the ratio in the center of the plume, with a value of about 2-2.5. There is still a significant amount of rapid spatial variation, but the larger structure is evident. This ratio of  $\sigma_c/\bar{c}$  is consistent with the fact that 100 cross-sections gave very poor estimates of  $\bar{c}$ , since a ratio of 2.5 indicates a highly variable plume.

We can also obtain confidence limits on our derived quantities using the "bootstrap" technique (Effron, 1982). This is a non-parametric statistical method, and is useful here because it avoids the assumption of Gaussian

INEL : ALPHA1 : JULY 23 : 0700 - 0800  
AVERAGE CONCENTRATION

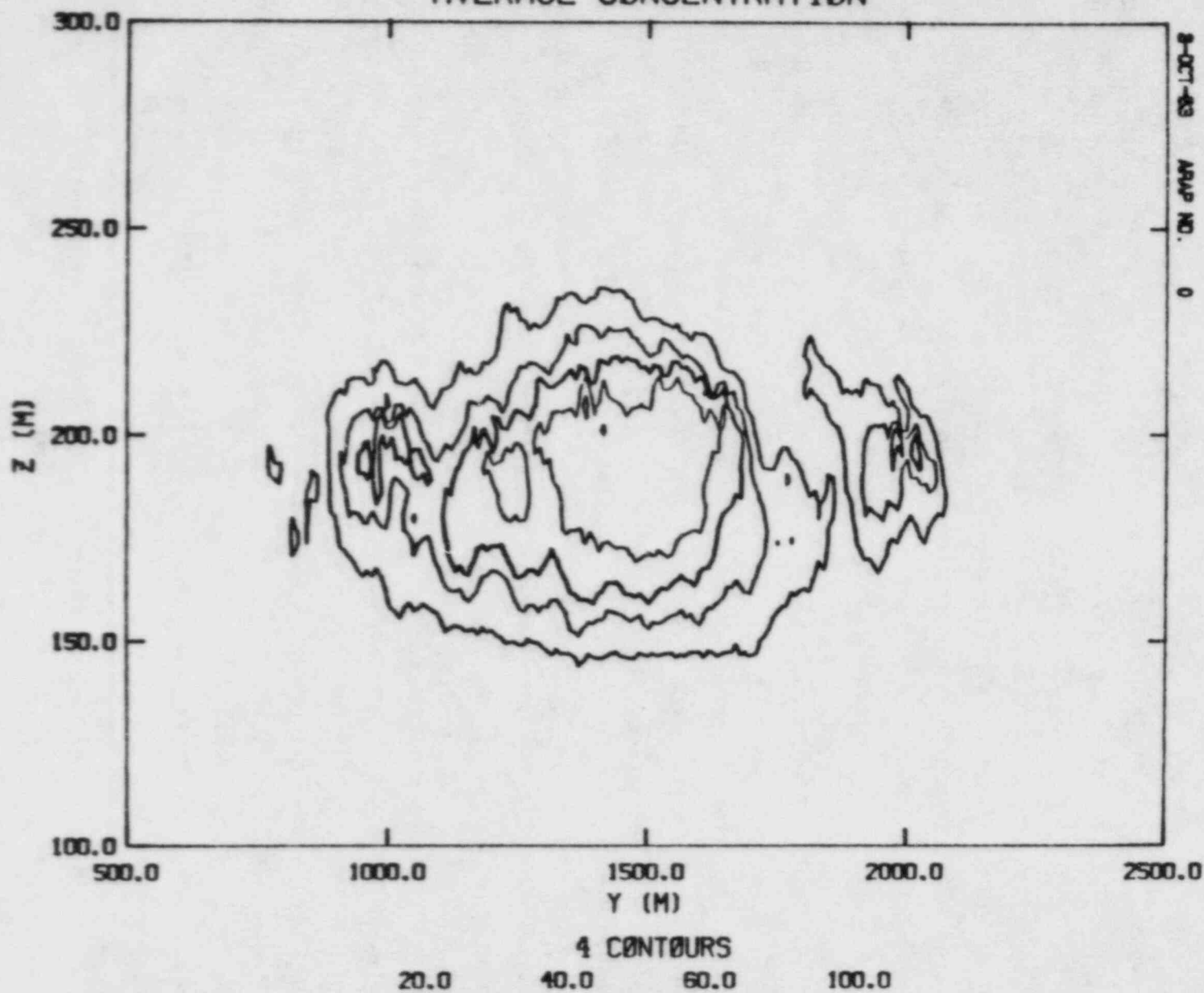


Figure C2

INEL : ALPHA1 : JULY 23 : 0700 - 0800  
SIGMA(C)

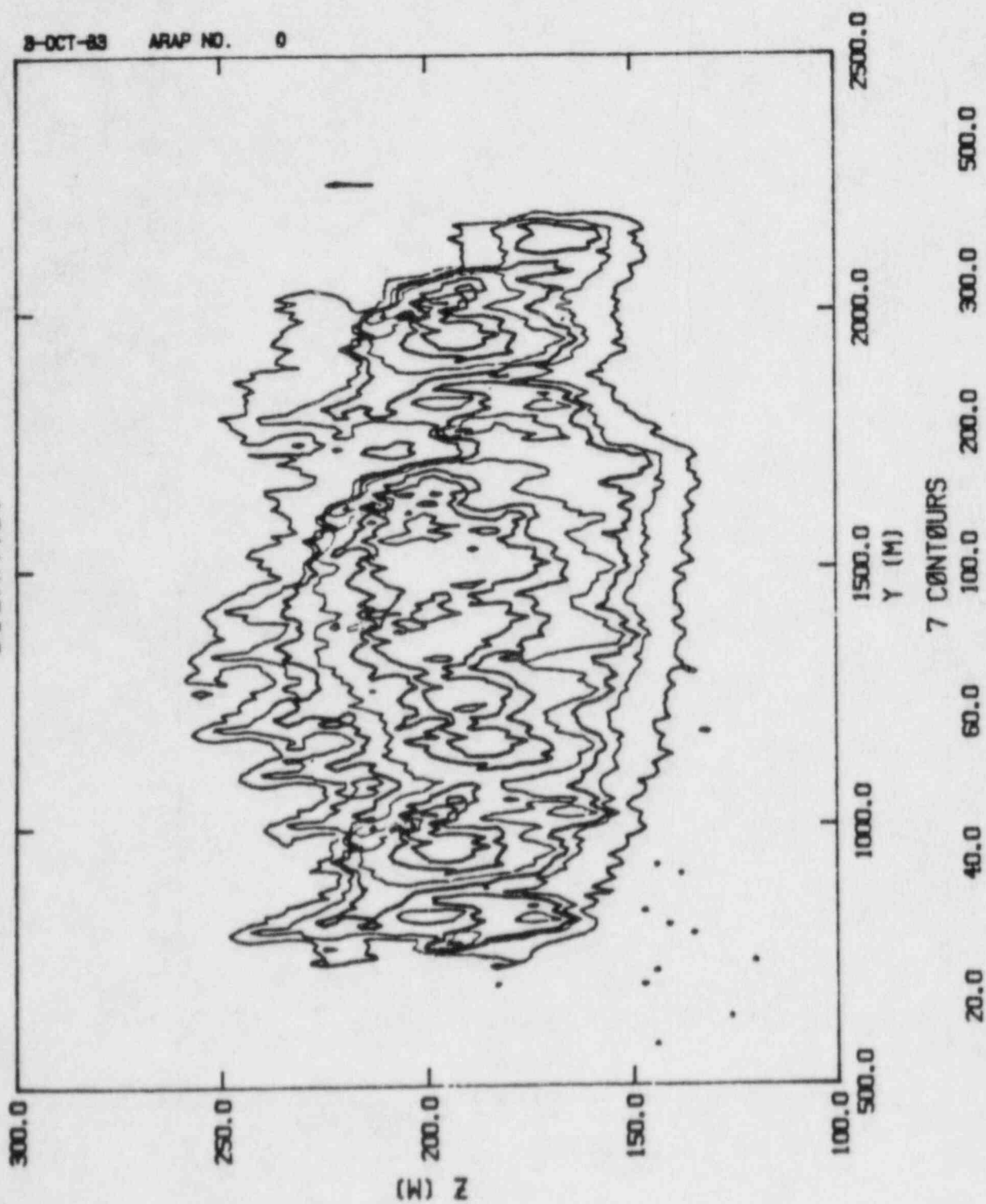


Figure C3

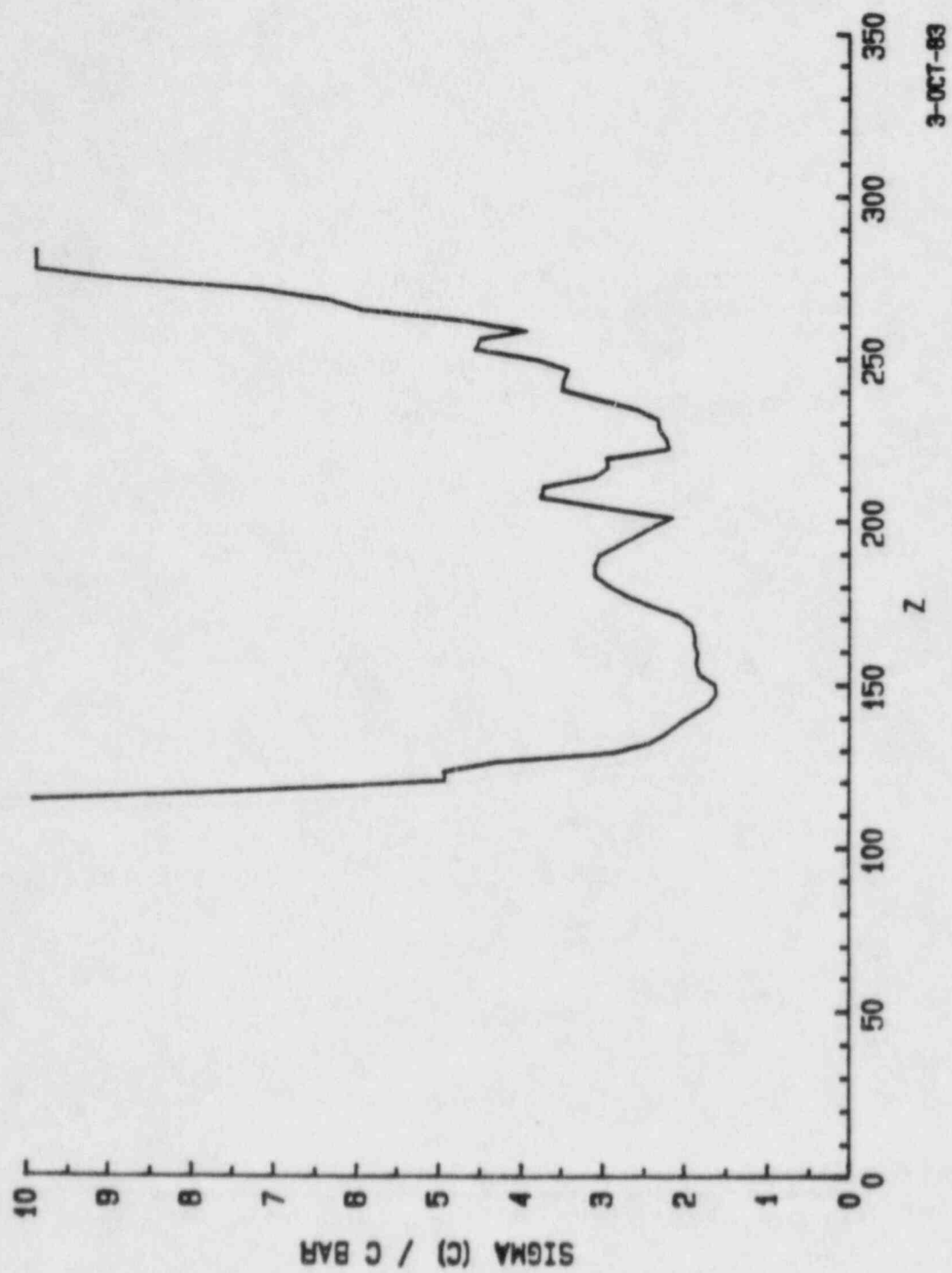
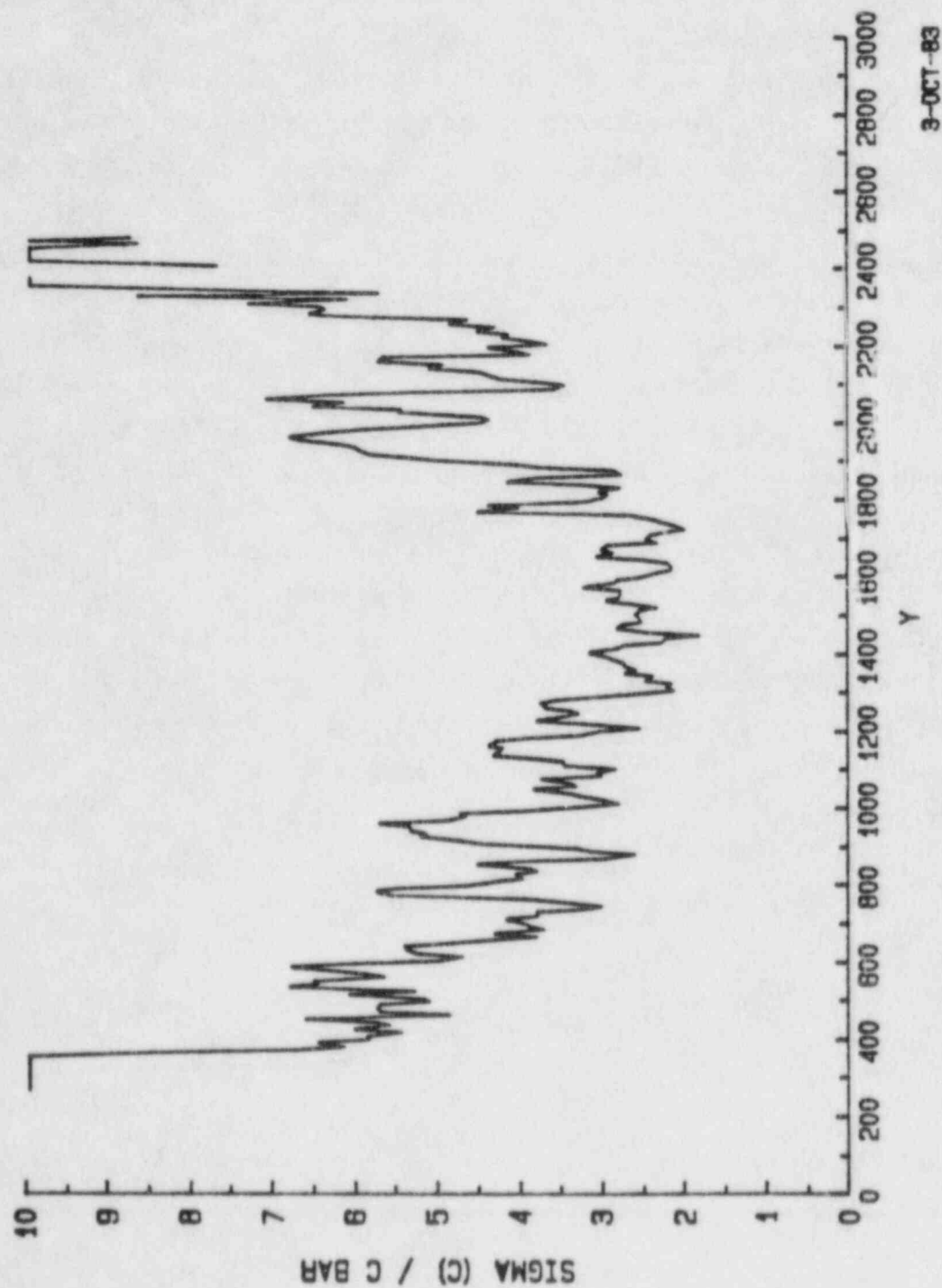


Figure C4

3-OCT-83



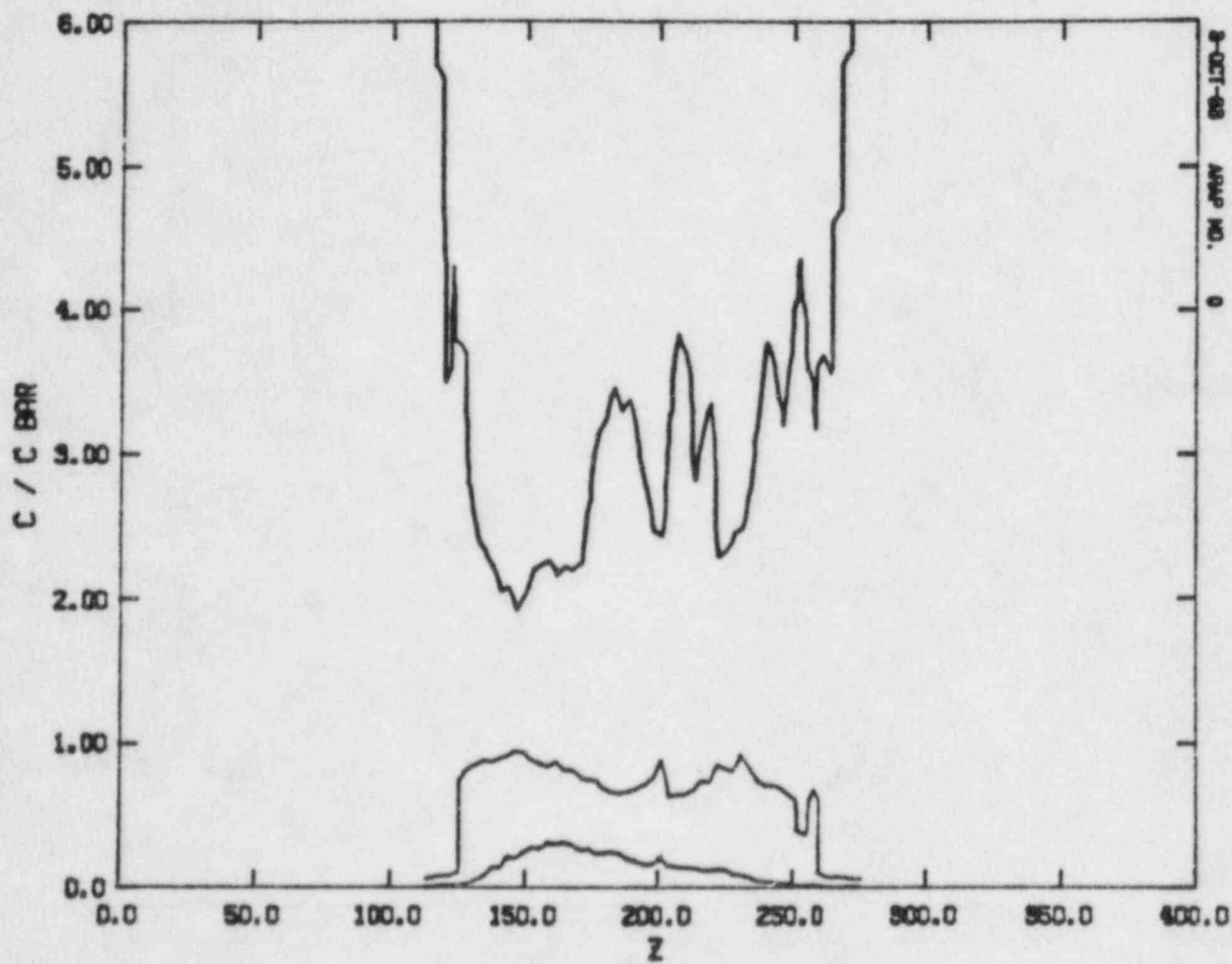


3-OCT-83

Figure C5

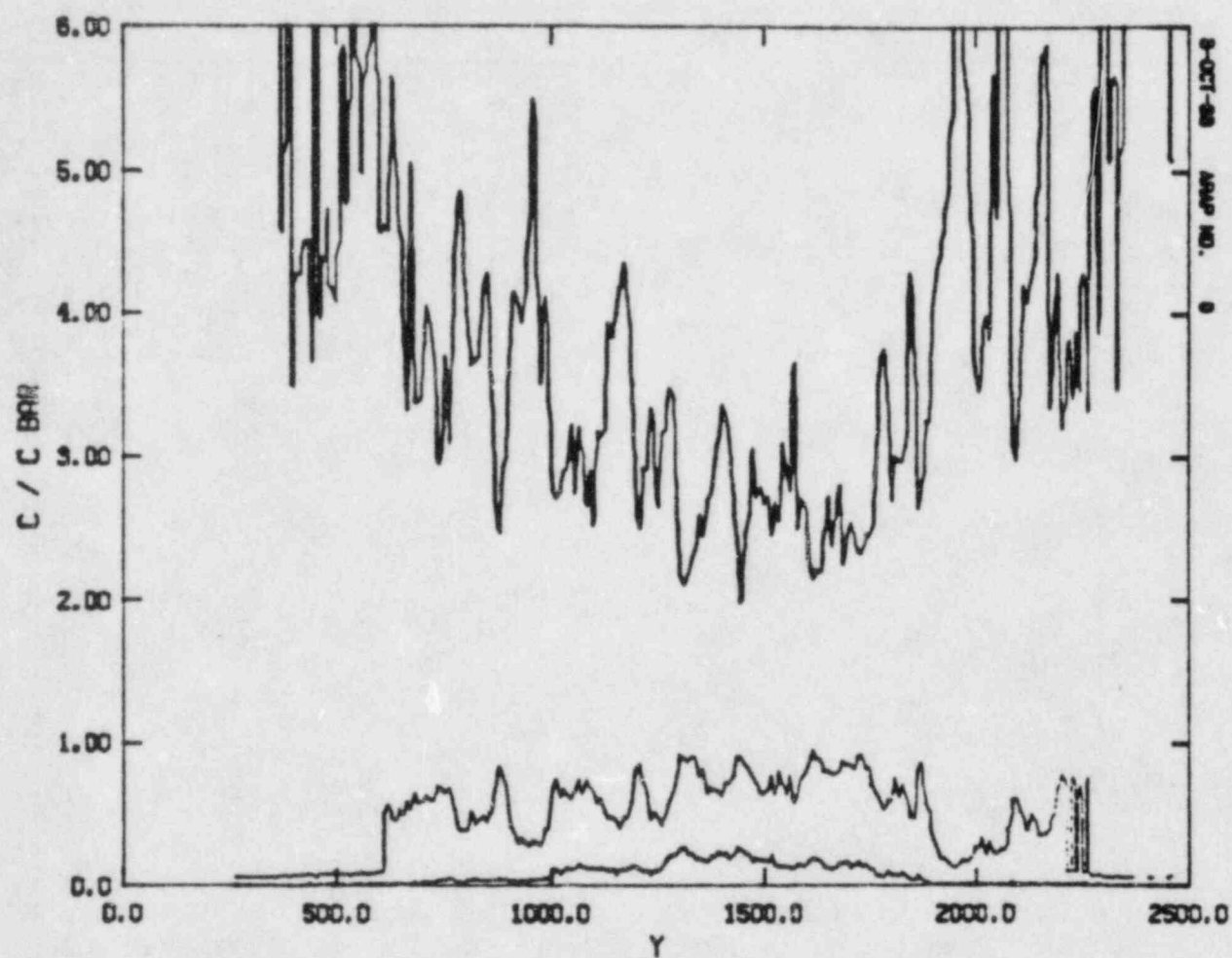
probability density functions (pdf's). Instead, a "real" pdf can be generated by resampling the data itself. Thus, to obtain confidence limits on the value of  $\bar{c}$  obtained by averaging the 10 lidar cross-sections, we generate a pdf for  $\bar{c}$  by randomly selecting 10 fields from the data to calculate  $\bar{c}$  many times. The selection is performed with replacement, i.e., we are free to select a particular field more than once. This could be done by sampling the original 10 fields, but the spatial variation is much too rough. If we sample from our 100 pseudo data fields, then we get confidence limits as illustrated in Figures C.6 and C.7. These figures show 5%, 50%, and 95% probability levels for  $c/\bar{c}$  in vertical and horizontal cross-sections through the plume centroid. They show that there is a 90% confidence that the value obtained by averaging 10 fields will be between about  $0.3\bar{c}$  and  $2.5\bar{c}$  in the center of the plume, i.e., 90% confidence of being within a factor of 3 of the mean. However, this range widens considerably as one moves toward the edges of the plume.

The same type of "bootstrap" analysis gives the cumulative probability functions for  $\sigma_y$  and  $\sigma_z$  as estimated from averaging 10 data fields, the bootstrap samples were taken from the full 100 data fields again. Figures C.8 and C.9 show that 90% confidence limits on  $\sigma_y$  extend from 210m to 380m, while those of  $\sigma_z$  are from 18m to 26m. The corresponding values quoted in Table 1 of Section IV from SRI's analysis of this same data are 344 and 22 m respectively.



9 CONTOURS  
CONTOUR LEVELS FROM .0500 TO .950  
CONTOUR INTERVAL OF .450

Figure C6



3 CONTOURS  
CONTOUR LEVELS FROM .0500 TO .950  
CONTOUR INTERVAL OF .450

Figure C7

PDF FOR INEL TEST5 - 0700-0800

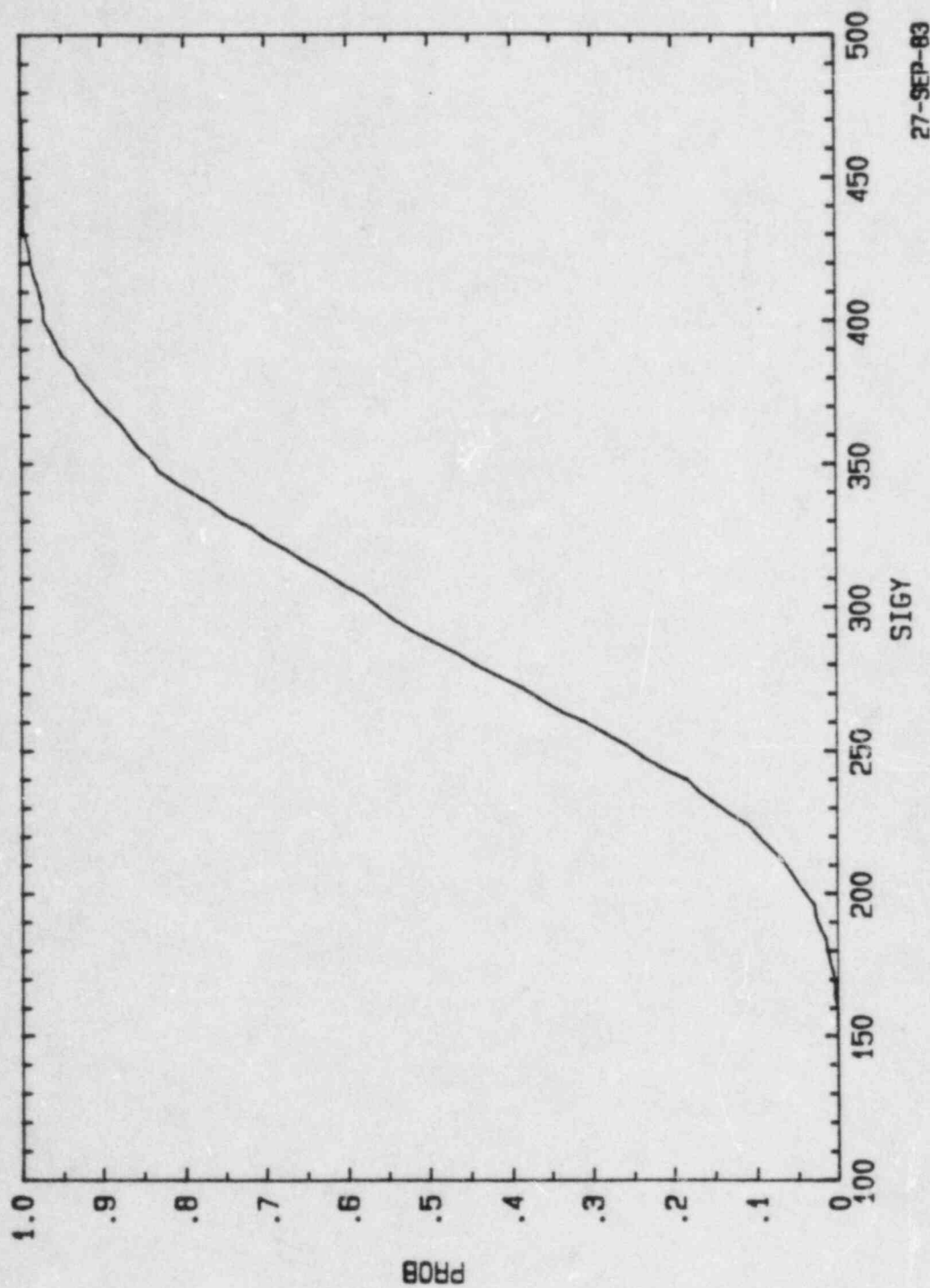
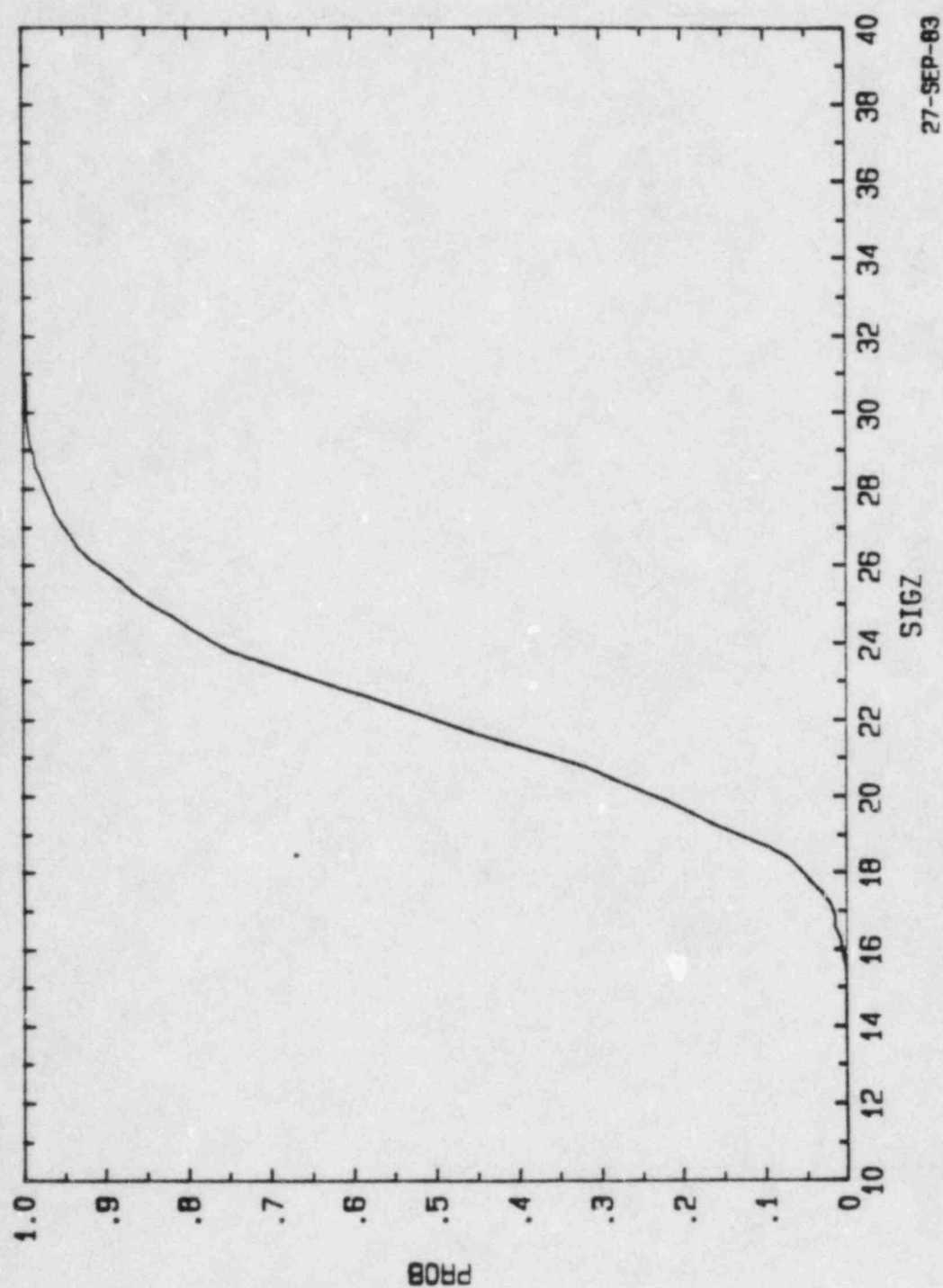


Figure C8

27-SEP-83



PDF FOR INEL TEST5 - 0700-0800



27-SEP-83

Figure C9



### References

Effron, B. (1982), "The Jackknife, the Bootstrap and Other Resampling Plans", Soc. Ind. Appl. Math., Philadelphia.

<b>NRC FORM 335</b> <small>(11-81)</small>		<b>U.S. NUCLEAR REGULATORY COMMISSION</b> <b>BIBLIOGRAPHIC DATA SHEET</b>		<b>1. REPORT NUMBER (Assigned by DDC)</b> NUREG/CR-4159 ARAP Report No. 505	
<b>4. TITLE AND SUBTITLE (Add Volume No., if appropriate)</b> Comparison of the 1981 INEL Dispersion Data with Results from a Number of Different Models				<b>2. (Leave blank)</b>	
<b>7. AUTHOR(S)</b> W.S. Lewellen, R.I. Sykes and S.F. Parker				<b>3. RECIPIENT'S ACCESSION NO.</b>	
<b>9. PERFORMING ORGANIZATION NAME AND MAILING ADDRESS (Include Zip Code)</b> Aeronautical Research Associates of Princeton, Inc. 50 Washington Road Post Office Box 2229 Princeton, New Jersey 08540				<b>5. DATE REPORT COMPLETED</b> MONTH January YEAR 1985	
<b>12. SPONSORING ORGANIZATION NAME AND MAILING ADDRESS (Include Zip Code)</b> Division of Radiation Programs and Earth Sciences Office of Nuclear Regulatory Research U.S. Nuclear Regulatory Commission Washington, D.C. 20555				<b>DATE REPORT ISSUED</b> MONTH May YEAR 1985	
<b>13. TYPE OF REPORT</b> Technical				<b>PERIOD COVERED (Inclusive dates)</b>	
<b>15. SUPPLEMENTARY NOTES</b>				<b>10. PROJECT/TASK/WORK UNIT NO.</b>	
<b>16. ABSTRACT (200 words or less)</b> Results from simulations by 12 different dispersion models are compared with observations from an extensive field experiment at the Idaho National Engineering Laboratory in July, 1981. Comparisons were made based on hourly ground-level SF <sub>6</sub> samples, out to approximately 10 km from the 46 m release tower, both during and following 7 different 8-hour releases. Comparisons are also made for total integrated doses collected out to approximately 40 km. Within the limited range appropriate for Class A models this data comparison shows that neither the puff models or the transport and diffusion models agree with the data any better than the simple Gaussian plume models. The puff and transport and diffusion models do show a slight edge in performance in comparison with the total dose over the extended range appropriate for Class B models. The best model results for the hourly samples show approximately 40% calculated within a factor of two when a 15° uncertainty in plume position is permitted, and it is assumed that higher data samples may occur at stations between the actual sample sites. This is increased to 60% for the 12 hour integrated dose and 70% for the total integrated dose. None of the models reproduce the observed patchy dose patterns. This patchiness appears to be consistent with the inherent uncertainty associated with time averaged plume observations.				<b>11. FIN NO.</b> B0446	
<b>17. KEY WORDS AND DOCUMENT ANALYSIS</b> atmospheric dispersion concentration patterns dispersion models Gaussian plume models model evaluations puff models				<b>17a. DESCRIPTORS</b>	
<b>17b. IDENTIFIERS: OPEN-ENDED TERMS</b>					
<b>18. AVAILABILITY STATEMENT</b> UNLIMITED		<b>19. SECURITY CLASS (This report)</b> Unclassified		<b>21. NO. OF PAGES</b>	
		<b>20. SECURITY CLASS (This page)</b> Unclassified		<b>22. PRICE</b> \$	

UNITED STATES  
NUCLEAR REGULATORY COMMISSION  
WASHINGTON, D.C. 20555

OFFICIAL BUSINESS  
PENALTY FOR PRIVATE USE, \$300

FOURTH CLASS MAIL  
POSTAGE & FEES PAID  
USNRC  
WASH. D.C.  
PERMIT No. G-67

120555078877 1 1A1RB  
US NRC  
ADM-DIV OF TIDC  
POLICY & PUB MGT BR-PDR NUREG  
W-501  
WASHINGTON DC 20555